FDL-TDR-64-10

STATIC AERODYNAMIC CHARACTERISTICS AT MACH 5 AND 8 OF AN AERODYNAMICALLY CONTROLLABLE WINGED RE-ENTRY CONFIGURATION

PART OF AN INVESTIGATION OF HYPERSONIC FLOW SEPARATION AND CONTROL CHARACTERISTICS

TECHNICAL DOCUMENTARY REPORT FDL-TDR-64-10

SEPTEMBER 1963

AF FLIGHT DYNAMICS LABORATORY
RESEARCH AND TECHNOLOGY DIVISION
AIR FORCE SYSTEMS COMMAND
WRIGHT-PATTERSON AIR FORCE BASE, OHIO

Project No. 8219, Task No. 821902

(Prepared under Contract No. AF 33(616)-8130 by the Research Department, Grumman Aircraft Engineering Corporation, Bethpage, New York; Author: Lawrence Meckler)

NOTICES

When Government drawings, specifications, or other data are used for any purpose other than in connection with a definitely related Government procurement operation, the United States Government thereby incurs no responsibility nor any obligation whatsoever; and the fact that the Government may have formulated, furnished, or in any way supplied the said drawings, specifications, or other data, is not to be regarded by implication or otherwise as in any manner licensing the holder or any other person or corporation, or conveying any rights or permission to manufacture, use, or sell any patented invention that may in any way be related thereto.

Qualified requesters may obtain copies of this report from the Defense Documentation Center (DDC), (formerly ASTIA), Cameron Station, Bldg. 5, 5010 Duke Street, Alexandria, Virginia, 22314.

This report has been released to the Office of Technical Services, U.S. Department of Commerce, Washington 25, D. C., in stock quantities for sale to the general public.

Copies of this report should not be returned to the Research and Technology Division, Wright-Patterson Air Force Base, Ohio, unless return is required by security considerations, contractual obligations, or notice on a specific document.

500 - November 1964 - 448-12-321

CLEARINGHOUSE FOR FEDERAL SCIENTIFIC AND TECHNICAL INFORMATION CFSTI
DOCUMENT MANAGEMENT BRANCH 410.11

LIMITATIONS IN REPRODUCTION QUALITY

ACCESSION # AD608304

☒ 1. WE REGRET THAT LEGIBILITY OF THIS DOCUMENT IS IN PART UNSATISFACTORY. REPRODUCTION HAS BEEN MADE FROM BEST AVAILABLE COPY.

☐ 2. A PORTION OF THE ORIGINAL DOCUMENT CONTAINS FINE DETAIL WHICH MAY MAKE READING OF PHOTOCOPY DIFFICULT.

☐ 3. THE ORIGINAL DOCUMENT CONTAINS COLOR, BUT DISTRIBUTION COPIES ARE AVAILABLE IN BLACK-AND-WHITE REPRODUCTION ONLY.

☐ 4. THE INITIAL DISTRIBUTION COPIES CONTAIN COLOR WHICH WILL BE SHOWN IN BLACK-AND-WHITE WHEN IT IS NECESSARY TO REPRINT.

☐ 5. LIMITED SUPPLY ON HAND: WHEN EXHAUSTED, DOCUMENT WILL BE AVAILABLE IN MICROFICHE ONLY.

☐ 6. LIMITED SUPPLY ON HAND: WHEN EXHAUSTED DOCUMENT WILL NOT BE AVAILABLE.

☐ 7. DOCUMENT IS AVAILABLE IN MICROFICHE ONLY.

☐ 8. DOCUMENT AVAILABLE ON LOAN FROM CFSTI (TT DOCUMENTS ONLY).

☐ 9.

PROCESSOR: J McLean

TSL-107-10/64

FOREWORD

This report presents the results of one segment of an experimental program for the investigation of hypersonic flow separation and control characteristics being conducted by the Research Department of Grumman Aircraft Engineering Corporation, Bethpage, New York. Mr. Donald E. Hoak of the Flight Control Laboratory, Research and Technology Division, located at Wright-Patterson Air Force Base, Ohio, is the Air Force Project Engineer for the program, which is being supported primarily under Contract AF33(616)-8130, Air Force Task 821902.

The experimental data to be obtained, pressure distributions, heat transfer, and six-component aerodynamic force data, are extensive and must be presented in a series of data reports, of which this is one. These data reports are presented without analysis for the purpose of disseminating all the experimental information as rapidly as possible.

The author wishes to express his appreciation to the staff of the von Karman Facility for their helpfulness in conducting the tests and particularly to Messrs. Schueler, Donaldson, and Uselton for providing the machine plotted graphs of the experimental data included in this report. The tabulated data, not included herein, are available to qualified Air Force requestors as an Appendix to this report. These Appendices can be obtained on loan from the Flight Control Laboratory, Research and Technology Division, Air Force Systems Command, Wright-Patterson Air Force Base, Ohio.

ABSTRACT

Six-component aerodynamic data were obtained at Mach 5 and 8 for a winged re-entry configuration having aerodynamic controls. The basic model consisted of a clipped delta wing with an overslung body. The main controls tested were a deflected apex and partial-span trailing-edge flaps. Data were also obtained on the effect of tip fins, full-span trailing-edge flap, and trailing-edge spoiler. At Mach number 5 the data were obtained over an angle of attack range from $-30°$ to $+45°$ at a unit Reynolds number of 2.26×10^6. At Mach number 8 the angle of attack range was $-54°$ to $+54°$ at the same unit Reynolds number.

This report has been reviewed and is approved.

C. R. Bryan

for W. A. SLOAN, Jr.
Colonel, USAF
Chief, Flight Control Division
AF Flight Dynamics Laboratory

TABLE OF CONTENTS

LIST OF ILLUSTRATIONS

LIST OF TABLES

LIST OF SYMBOLS

C_A	axial force coefficient (= C_{A_T})
C_{A_T}	total axial force coefficient (defined on p.7)
C_ℓ	rolling moment coefficient (defined on p.8)
C_m	pitching moment coefficient (defined on p. 7) taken about moment center 60% of virtual root chord aft of theoretical wing apex
C_n	yawing moment coefficient (defined on p. 8) taken about same moment center as C_m
C_N	normal force coefficient (defined on p.7)
C_{p_b}	base pressure coefficient (defined on p.7)
C_y	side force coefficient (defined on p.7)
CG	center of gravity (% virtual root chord)
F_{A_T}	axial force (lbs)
F_N	normal force (lbs)
F_Y	side force (lbs)
L	virtual root chord (in.)
M_ℓ	rolling moment (in.-lb)
M_m	pitching moment (in.-lb) taken about moment center 60% of virtual root chord aft of theoretical wing apex
M_n	yawing moment (in.-lb) taken about the same moment center as M_m

M_∞	free stream Mach number
p_b	base static pressure psi
p_∞	free stream static pressure psi
q_∞	free stream dynamic pressure psi
Re_∞/ft	free stream unit Reynolds number $\frac{p_\infty U_\infty}{\mu_\infty}$
S	wing planform area (based on virtual root chord) $in.^2$
U_∞	free stream velocity ft/sec
x	longitudinal coordinate } body axes
y	lateral coordinate } body axes
z	vertical coordinate } body axes
Z	height of CG above wing-chord plane (in.)
α	angle of attack (degrees)
γ	ratio of specific heats (= 1.4 for air)
δ_1	apex deflection (degrees)
δ_2	left rear flap deflection (degrees)
δ_3	right rear flap deflection (degrees)
δ_c	central flap section deflection (degrees)
ρ_∞	free stream density ($slugs/ft^3$)
μ_∞	free stream viscosity (slugs/ft sec)

INTRODUCTION

The Fluid Mechanics Section of the Grumman Research Department is currently engaged in a research program directed at determining flow separation effects, and the effectiveness of aerodynamic controls, on hypersonic flight vehicles. The program consists of theoretical and experimental research on "basic" configurations, flat plates with various flow separators (flap and wedge type), and "typical" hypersonic glide vehicles, a clipped delta wing-body combination and a pyramidal body. The configurations to be investigated in the over-all program are shown in Fig. 1a.

This report presents the results of one segment of the experimental program. It treats a winged hypersonic glider configuration consisting, in basic form, of a clipped delta wing with an overslung body. This configuration was used for obtaining the data required to determine the effectiveness of various aerodynamic controls at supersonic and hypersonic Mach numbers. The controls investigated were a deflectable apex, with a travel of $\pm 20°$, partial-span trailing-edge flaps, with deflections of ± 40, a full-span flap, with a deflection of $+20$, a full-span plug-type trailing-edge spoiler and tip fins.

The experimental work was done at the AEDC 40-inch Supersonic Wind Tunnel, at Mach 5, and the AEDC 50-inch Mach 8 Hypersonic Wind Tunnel during November and December of 1962. Descriptions of these test facilities can be found in Ref. 1. Six-component force data were obtained for all configurations at both Mach numbers at a unit Reynolds number of 2.26×10^6 with selected points at Reynolds numbers of 0.79×10^6 and 5×10^6. A geometrically similar model, instrumented to obtain pressure and heat transfer data, will be tested in these facilities at a later date. Another geometrically similar model, with limited pressure instrumentation, was tested in AEDC Hotshot 2 Hypervelocity Tunnel and the results are reported in Ref. 2.

Manuscript released by the author 10 January 1964 for publication as an FDL Technical Documentary Report.

DESCRIPTION OF MODELS

General

Six test configurations were built up from a basic model that consisted of a clipped delta wing with an overslung body. The clipped delta wing had a spherically blunted apex, cylindrically blunted leading edges and a blunt base. The control surfaces to be tested, a deflectable apex and partial-span trailing-edge flaps, were built into the wing and were remotely actuated. Three-view drawings of all six test configurations are presented in Fig. 1b through 1g. The dimensions of the basic configuration are shown in Fig. 1b and are the same for all other configurations. The other configuration drawings show dimensions only for the components added to the basic configuration.

Controls and Sign Convention

Each control was driven by a 27 volt dc, gear reduced, water cooled, electrical motor through a 1/2 inch-10 acme thread leadscrew. This type of actuation produced a deflection rate of 1 degree/sec. Control deflection read-outs were obtained through a calibrated linear potentiometer. The control surfaces were calibrated cold, that is, when the model was installed in the tunnel, and checked regularly. The calibrating was done with precut templates varying, in 5-degree increments, from 0 degrees to 40 degrees. The potentiometer outputs were recorded visually from Leeds and Northrup Midget Model D indicators for use in setting flap angles during the test. This calibration was also recorded into the digital computing equipment at AEDC for use of the computer during the print-out procedure. This design procedure provided for the independent operation of each control surface. We were thus able to test asymmetric, as well as symmetric, control configurations.

The sign convention for denoting the angle of attack and the control deflection angle can be obtained from the basic model, namely, a flat plate clipped delta wing with an overslung body. This definition fixes the flat plate surface of the wing as the lower surface. Thus, the angle of attack is positive when the flat plate surface is the windward surface and negative when the flat plate surface is the leeward surface of the model. The control deflection angles are also defined with respect to the lower (flat plate) surface of model. If we consider our model at zero angle

of attack (flow parallel to the lower [flat-plate] surface), then positive trailing-edge flap deflections are obtained by deflecting the trailing edge down and negative deflections are obtained by deflecting the trailing edge up. The sign convention for the deflectable apex is positive when the nose is deflected up and negative when deflected down. These definitions are illustrated in Fig. 2.

The deflectable apex was designed for a maximum travel of ±20 degrees and can be calibrated to obtain any deflection angle in this range. Similarly, the partial-span trailing-edge flaps, designed to operate independently of each other as well as of the apex, had a maximum travel angle of ±40 degrees and could be calibrated to yield any deflection angle in this range.

Model Designations

The first major configuration consisted of a clipped delta wing with an overslung body. The overslung body consisted of a half-conical foresection and a half-cylindrical aftersection joined together at the shoulder by a spherical fairing. This wing-body combination was one of two major configurations of this test program and is referred to as Configuration I. The second major configuration was obtained by adding a set of tip fins to Configuration I and is referred to as Configuration IV. These tip fins were clipped deltas in elevation and were attached in such a way as not to alter the aspect ratio (of the configuration).

Each of these major configurations was expanded into two additional control models thus yielding six test configurations for the evaluation of control effectiveness.

Configurations I and IV provide the data for determining the control effectiveness of a deflectable apex and partial span trailing edge flaps. In order to determine whether these controls have any comparative advantage over other types of aerodynamic controls it was decided to compare their effectiveness to that of a full-span flap and a full-span spoiler. It was also decided that an adequate comparison point would be at a flap deflection angle of +20 degrees. In line with this reasoning a 20-degree wedge section was designed to fit between the partial-span flaps to form a full-span flap when the partial span flaps were deflected +20 degrees. When this wedge section was fitted to Configuration I the resulting model, Configuration II, was a clipped delta wing-body combination with a full-span 20-degree flap. When the wedge

section was fitted to Configuration IV the resulting model, Configuration III, was a clipped delta wing-body combination with a full-span 20-degree flap and tip fins. The design condition for the full-span, plug-type, trailing-edge spoiler was that its height be equal to the vertical displacement of the trailing-edge flaps when they are deflected +20 degrees. This spoiler was attached to the lower, flat plate, surface at the trailing edge. When the spoiler was attached to Configuration I, we obtained Configuration VI, which was a clipped delta wing-body combination with a full-span spoiler, and when attached to Configuration IV we obtained Configuration V, which was a clipped delta wing-body combination with tip fins and a full-span trailing-edge spoiler.

The basic model and all the attachments, fins, spoiler, and central flap section, were fabricated out of No. 416 stainless steel and the balance mount was made of Inconel X.

The center of gravity (CG) location of each configuration was determined at AEDC. These CG locations are given in Table 1. The same models were used in both wind tunnels.

DESCRIPTION OF WIND TUNNELS AND EQUIPMENT

This segment of the experimental program was conducted in the 40 in. by 40 in. Supersonic Wind Tunnel, at $M_\infty = 5.0$, and the 50-in. Mach 8 Hypersonic Wind Tunnel located at Arnold Engineering Development Center's von Karman Facility. A complete description of the wind tunnels and their associated measuring, recording and tabulating equipment is given in Ref. 1.

The yaw actuator, designed and built at the von Karman facility for use in the 40 in. by 40 in. Supersonic Wind Tunnel, was used in the supersonic test program. The yaw actuator, which is mounted in the plane of the sector, increases the sting throw from 20 degrees to 70 degrees, substantially reduces the number of tunnel openings required in the program and allowed for the program completion in a minimum amount of time. It provided an angle of attack range from -5 degrees to +45 degrees. Negative angles of attack were obtained by inverting the model.

In the 50-in. Mach 8 Hypersonic tunnel the angle of attack range was obtained by using two different pre-bend angles on the water- cooled split sting that is standard tunnel equipment. The two pre-bend angles used were 12 degrees and 39 degrees and between them provided an angle of attack range of -3 degrees to +54 degrees. Again, the negative angles of attack were obtained by inverting the model.

The dimensions and mounting specifications of the water-cooled, six component, balance used in these tests are presented in AEDC drawing No. 330 2103 R-A. This same balance was used in both wind tunnels. The measuring capabilities of this balance are: normal force ±700 lbs, axial force ±150 lbs, side force ±700 lbs, pitching moment ±3600 in.-lbs, yawing moment ±1800 in.-lbs, rolling moment ±300 in.-lbs. Additional information on this balance can be obtained from the von Karman Facility at AEDC.

EXPERIMENTAL DATA

Test Conditions

The supersonic test program was conducted at a nominal test section Mach number of 5.0 and test section unit Reynolds numbers of 2.26×10^6 per foot and 5.0×10^6, per foot. Most of the program was run at the lower Reynolds number and data were obtained at the higher Reynolds number for comparative purposes only. Due to tunnel operating conditions, the actual test Mach number was 5.01. The low range Reynolds number ranged from 2.20×10^6 per foot, to 2.28×10^6 per foot while the higher range of Reynolds numbers varied from 4.98×10^6 per foot to 5.73×10^6 per foot.

The two main configurations (I and IV) were tested through an angle of attack range of -30 degrees to +44.5 degrees. Included in these tests were trailing-edge flap deflections of -40 degrees to +40 degrees and apex deflections of -20 degrees to +20 degrees. In addition to the symmetric conditions, a set of asymmetric conditions were tested. These included using both trailing-edge flaps as ailerons, i.e., deflecting one positively and the other negatively, and also deflecting one flap only and determining their effectiveness as roll devices.

The hypersonic test program was conducted at a nominal test section Mach number of 8.0 and test section unit Reynolds numbers of 2.26×10^6 per foot and 0.79×10^6 per foot. As before, most of the program was conducted at a Reynolds number of 2.26×10^6 per foot and the lower Reynolds number data were used for comparative purposes only. Due to the tunnel operating conditions the actual test Mach number was 8.08. Where a nominal Reynolds number of 2.26×10^6 per foot was called for the actual test Reynolds number varied from 2.24×10^6 per foot to 2.34×10^6 per foot and where the nominal Reynolds number was 0.79×10^6 per foot the actual test Reynolds number varied from 0.765×10^6 per foot to 0.822×10^6 per foot.

As in the supersonic case, the two main configurations (I and IV) were tested most extensively while the tests on the other configurations were restricted and are used only to provide comparison data with the main configurations. Configurations I and IV were tested through an angle of attack range from -54 degrees to +54 degrees, for symmetric, partial-span, flap deflections of -40 degrees to +40 degrees and apex deflections of -20 degrees to +20 degrees. Asymmetric flap deflection conditions using both

flaps and a single flap were also tested to determine the effectiveness of partial span flaps as rolling devices.

A complete tabulation of the test program showing the angle of attack range, control deflection and flow conditions, is presented in Table 2.

Six component force and moment data, as well as base pressure coefficients, were obtained for all the test configurations. The six component data were obtained, and are presented, for a body axis system and in coefficient form. For the symmetric conditions only, the longitudinal aerodynamic characteristics are presented while for the asymmetric conditions the six aerodynamic components are presented. For convenience these data are presented in graphical form.

Data Reduction and Accuracy

Forces, moments, base, and balance cavity pressures were measured and reduced to standard coefficient form using the following equations:

$$\text{Base pressure coefficient} = C_{p_b} = \frac{p_b - p_\infty}{q_\infty}$$

$$\text{Normal force coefficient} = C_N = \frac{F_N}{q_\infty S}$$

$$\text{Total axial force coefficient} = C_{A_T} = \frac{F_{A_T}}{q_\infty S}$$

$$\text{Side force coefficient} = C_y = \frac{F_Y}{q_\infty S}$$

$$\text{Pitching moment coefficient} = C_m = \frac{M_m}{q_\infty SL}$$

$$\text{Yawing moment coefficient} = C_n = \frac{M_n}{q_\infty SL}$$

$$\text{Rolling moment coefficient} = C_\ell = \frac{M_\ell}{q_\infty SL}$$

The reference lengths and areas used in nondimensionalizing these equations, namely, the wing planform area, S, and the root chord, L, were calculated for a sharp apex clipped delta wing. Thus, the reference properties are based on the virtual root chord. On this basis it was found that $S = 191.2$ in.^{2} and $L = 18.2$ in. (The actual planform area and root chord are presented in Table 3 along with other pertinent geometric parameters.)

For convenience the data are presented in the body-oriented coordinate system in which it was obtained, and the moment center was taken at 60 per cent of the virtual root chord aft of the theoretical apex of the wing. The longitudinal axis of this coordinate system is the axis of symmetry of the force balance and thus is slightly displaced from a parallel axis that would pass through the center of gravity of the model. The error in the pitching moment coefficients, due to this vertical displacement of the longitudinal axis, is negligible and no effort was made to correct it. It was also found that, at the low and intermediate angles of attack the base pressure correction to the total axial force coefficient was generally on the order of 0.5 per cent to 1.5 per cent. At the higher angles of attack attained in the 50-in. Mach 8 Hypersonic Wind Tunnel the indicated base pressure corrections were slightly higher but in neither case were these corrections sufficiently large to warrant alteration of the measured force data. We therefore use the measured and corrected data interchangeably, i.e., C_{A_T} and C_A. There was no need to correct the data for variations in dynamic pressure during a run since the tunnel conditions were recorded along with the data, at each angle of attack, and the data were reduced on the basis of the tunnel dynamic pressure existing at the instant the data were recorded. The preceding discussion was applicable to the data taken from both tunnels.

The major error in the data is due to the basic recording limitations of the balance, which are known. This type of inaccuracy is most pronounced at the low angles of attack and becomes insignifi-

cant at the high angles of attack. The inaccuracy of the data measurements due to balance error have been converted to coefficient form and are presented in Table 4.

RESULTS AND DISCUSSION

This program was designed to provide controls information on one basic type of hypersonic flight vehicle, namely, a clipped delta wing-body combination. Data are presented at positive and negative angles of attack for the case of an overslung body. This configuration was tested with tip fins on and off, with partial-span trailing-edge flaps, with a full-span trailing-edge flap, with a full-span trailing-edge spoiler, and with a deflectable apex. The experiments were conducted at two Mach numbers, 5.01 and 8.08, and with limited Reynolds number comparisons.

For the symmetric cases only three component force data are presented whereas for the asymmetric conditions six-component data are presented.

The data are presented in two major sets according to the Mach number at which they were obtained. Each set is then subdivided into two groups, the symmetric cases where both trailing-edge flaps are deflected together and in the same direction and the asymmetric cases where the trailing-edge flaps are deflected individually or in opposite directions (roll conditions). Those cases that include tests of the full-span trailing-edge flap, full-span trailing-edge spoiler, and apex deflection are included in the first group, the symmetric cases. Those conditions that were tested fins on and fins off are included in the appropriate group.

The basic wing-body combination was designed to provide controls information for configurations having either overslung or underslung bodies. For convenience we have chosen the overslung body configuration as our reference and we have defined the coordinate system and control deflection angles with reference to this basic configuration. Thus the positive angle of attack regime for the overslung body provides the aerodynamic data for the underslung body at negative angles of attack. The sign of the flap deflection angles, for the underslung body case, must be reversed in order that both cases be viewed in the same reference system. The complete test program is tabulated in Table 2 and the specific conditions presented in each figure are noted in the List of Illustrations on pages v through ix.

Mach 5 Data

The static longitudinal aerodynamic data for Configuration I, covering the range of angles of attack and symmetric trailing edge

flap deflections, are presented in Fig. 3. The corresponding data for Configuration IV are presented in Fig. 7. The Reynolds number comparisons for Configurations I and IV are presented in Figs. 4 and 8, respectively. The data for Configurations II, III, V, and VI are presented in Figs. 5 and 6. The aerodynamic characteristics of Configurations I and IV with apex deflections as well as three possible trim conditions are presented in Figs. 9 and 10. The data for the asymmetric conditions of Configurations I and IV, for which six component data are plotted, are presented in Figs. 11 and 12.

Mach 8 Data

The data for Configurations I and IV, covering the symmetric trailing edge flap deflection conditions, are presented in Figs. 13 and 15. The effect of Reynolds number on the aerodynamic characteristics of Configurations I and IV is presented in Figs. 14 and 16. The data for Configurations II, III, V, and VI are presented in Figs. 17 and 19. Figure 18 presents a comparison between Configurations III and IV for two different Reynolds numbers. Figures 20 and 21 present the aerodynamic characteristic of Configurations I and IV with the apex deflected and the trailing-edge flaps undeflected as well as several possible trim conditions. The data for the asymmetric conditions for Configurations I and IV, obtained to determine the rolling effectiveness of the partial-span trailing-edge flaps when used as ailerons, are presented in Figs. 22 and 23.

The side force data at both Mach numbers are erratic and are shown only to maintain the completeness of the data presentation. The 4-9 minute roll angles caused by repeated inverting of the model, to obtain various positive and negative angle of attack ranges, are not sufficient to explain this erratic behavior. Since the other data do not indicate the presence of any flow instability, it is concluded that the erratic behavior of the particular data component is caused by the side forces being so small that the measuring instrument is more sensitive to the random tunnel oscillations than to the generated side force.

REFERENCES

1. Arnold Center Test Facilities Handbook, AEDC, Arnold Air Force Station, Tennessee, January 1961.

2. Hartofilis, Stavros A., Pressure Measurements at Mach 19 for a Winged Re-entry Configuration, ASD TDR 63-319, March 1963.

3. Evans, William J., and Kaufman, Louis G. II, Pretest Report on Hypersonic Flow Separation and Control Models for AEDC Tunnels A, B, Hotshot 2, and Grumman Hypersonic Shock Tunnel, Grumman Research Department Memorandum RM-209, July 1962.

TABLE 1

MODEL CG LOCATION

Config-uration	Weight ~ lbs	Axial ~ % Virtual Root Chord from Apex	Vertical -Z- Distance Above Wing Chord Plane ~ in.	Definition
I	75.27	64.2	0.126	Basic Wing-Body (Basic)
II	76.5	64.7	0.104	Basic + Full Span Flap
III	82.18	66.6	0.092	Basic + Full Span Flap + Tip Fins
IV	80.77	66.15	0.114	Basic + Tip Fins
V	83.93	67.25	0.064	Basic + Spoiler + Tip Fins
VI	78.39	65.5	0.068	Basic + Spoiler

TABLE 2

TEST SCHEDULE

40" x 40" SUPERSONIC WIND TUNNEL

MACH 5.01

CONF.	CONTROL					Angle Attack Range	Re_∞/ft x 10^{-6}
	Apex	Trailing Edge Flap			Spoiler		
		Partial Span		Central			
	δ_1	δ_2	δ_3	δ_c		$\alpha_{min} \rightarrow \alpha_{max}$	
I	0	0	0	NA*	NA	-29.9 → 45.1	2.26
	0	+10	+10			-30 → 14.7	
	0	+20	+20			-30 → 45	
	0	+30	+30			-30 → 14.6	
	0	+40	+40			-30 → 14.6, 25.6 → 45.1	
	0	-10	-10			-4.5 → 45.1	
	0	-20	-20			-29.9 → 45.1	
	0	-30	-30			-4.5 → 45.1	
	0	-40	-40			-29.9 → 45.1	
	0	+20	0			-4.6 → 14.6	
	0	+40	0			-4.6 → 14.6	
	0	-20	0			-4.5 → 14.7	
	0	-40	0			-4.5 → 14.7	
	0	+20	-20			-4.6 → 14.7	
	0	+40	-40			-4.6 → 14.7	
	+10	0	0			-4.5 → 45	
	+20	0	0			-4.5 → 45.1	
	-10	0	0			-29.9 → 14.7	
	-20	0	0			-29.9 → 14.7	
	-20	+20	+20			-30 → 4.5	
	+20	-20	-20			-4.5 → 45.1	
	+20	-40	-40			-4.5 → 14.7	
	0	+20	+20			-4.6 → 14.7	5.0
II	0	+20	+20	+20		-4.6 → 29.8	2.26
	0	+20	+20	+20		-4.6 → 14.7	5.0
III	0	+20	+20	+20		-4.6 → 14.6	2.26
	0	+20	+20	+20		-4.7 → 14.7	5.0

*NA - Not Applicable.

TABLE 2 (Cont.)

TEST SCHEDULE

40" x 40" SUPERSONIC WIND TUNNEL

MACH 5.01

CONF.	CONTROL				Spoiler	Angle Attack Range	Re_∞/ft x 10^{-6}
	Apex	Trailing Edge Flap					
		Partial Span		Central			
	δ_1	δ_2	δ_3	δ_c		$\alpha_{min} \rightarrow \alpha_{max}$	
IV	0	0	0	NA	NA	-29.9 → 45.1	2.26
	0	+10	+10			-29.9 → 14.6	
	0	+20	+20			-29.9 → 45	
	0	+30	+30			-29.9 → 14.6	
	0	+40	+40			-29.9 → 14.6	
	0	-10	-10			-4.6 → 45.1	
	0	-20	-20			-29.8 → 45.1	
	0	-30	-30			-4.5 → 45.1	
	0	-40	-40			-4.5 → 45.1	
	0	+20	0			-4.6 → 14.6	
	0	+40	0			-4.6 → 14.6	
	0	-35.5	0			-4.5 → 14.7	
	0	+20	-20			-4.5 → 14.6	
	0	+40	-40			-4.6 → 14.6	
	+10	0	0			-4.5 → 45.1	
	+20	0	0			-4.5 → 45.1	
	-10	0	0			-29.9 → 14.6	
	-20	0	0			-29.9 → 14.6	
	-20	+20	+20			-29.9 → 14.6	
	+20	-20	-20			-4.5 → 45.1	
	+20	-35.5	-35.5			-4.5 → 45.1	
	0	0	0			-4.6 → 14.8	5.0
	0	+20	+20			-4.7 → 14.7	5.0
V	NA	NA	NA	NA	YES	-4.5 → 14.6	2.26
	NA	NA	NA	NA	YES	-4.6 → 14.7	5.0
VI	NA	NA	NA	NA	YES	-4.5 → 29.8	2.26
	NA	NA	NA	NA	YES	-4.6 → 14.7	5.0

TABLE 2 (Cont.)

TEST SCHEDULE

50" HYPERSONIC WIND TUNNEL

MACH 8.08

CONF.	CONTROL					Angle Attack Range	Re_x/ft x 10^{-6}
	Trailing Edge Flap				Spoiler		
	Apex	Partial Span		Central			
	δ_1	δ_2	δ_3	δ_c		$\alpha_{min} \rightarrow \alpha_{max}$	
I	0	0	0	NA	NA	-54.8 → 54.8	2.26
	0	+10	+10			-54.9 → 3.7	
	0	+20	+20			-54.8 → 54.8	
	0	+30	+30			-54.9 → 3.7	
	0	+39	+39			-54.9 → 54.8	
	0	-10	-10			-54.8 → -24.3, -3 → 54.8	
	0	-20	-20			-54.8 → 54.9	
	0	-30	-30			-3 → 54.9	
	0	-39	-39			-54.9 → 54.9	
	0	+10	0			-3 → 27	
	0	+20	0			-26.7 → 27	
	0	+30	0			-3 → 27	
	0	+39	0			-26.7 → 27	
	0	0	-10			-3 → 27	
	0	0	-20			-26.6 → 27	
	0	0	-39			-26.5 → 27	
	0	+10	-10			-26.6 → 27	
	0	+20	-20			-26.6 → 27	
	0	+30	-30			-26.6 → 27	
	0	+39	-39			-26.6 → 27	
	+10	0	0			-3 → 54.7	
	+20	0	0			-3 → 54.8	
	-10	0	0			-54.8 → 3.5	
	-20	0	0			-54.8 → 3.7	
	+10	-20	-20			-3 → 54.8	
	+10	-39	-39			-3 → 54.8	
	+20	-20	-20			-3 → 54.9	
	+20	-39	-39			-3 → 54.9	
	-10	+20	+20			-54.9 → 3.7	
	-10	+39	+39			-54.9 → 3.6	
	-20	20	+20			-54.8 → 3.6	
	-20	+39	+39			-54.9 → 3.6	
	0	0	0			-24.5 → 27	0.79
	0	-20	-20			-3 → 27	0.79
II	0	+20	+20	+20	NA	-3 → 27	2.26

TABLE 2 (Cont.)

TEST SCHEDULE

50" HYPERSONIC WIND TUNNEL

MACH 8.08

CONF.	CONTROL					Angle Attack Range	Re_∞/ft x 10^{-6}
	Apex	Trailing Edge Flap			Spoiler		
		Partial Span		Central			
	ξ_1	ξ_2	ξ_3	ξ_c		$\alpha_{min} \rightarrow \alpha_{max}$	
III	0	+20	+20	+20	NA	-3 → 27	2.26
	0	+20	+20	+20		-3 → 27	5.0
IV	0	0	0	NA	NA	-54.6 → 54.6	2.26
	0	+10	+10			-54.6 → 3.7	
	0	+20	+20			-54.8 → 54.8	
	0	+30	+30			-54.8 → 3.7	
	0	+39	+39			-54.8 → 54.8	
	0	-10	-10			-3 → 54.7	
	0	-20	-20			-26.4 → 54.8	
	0	-30	-30			-3 → 54.8	
	0	-39	-39			-26.4 → 54.7	
	0	+10	0			-3 → 27	
	0	+20	0			-26.5 → 27	
	0	+30	0			-3 → 27	
	0	+39	0			-26.5 → 27	
	0	0	-10			-3 → 27	
	0	0	-20			-26.4 → 27	
	0	0	-39			-26.4 → 27	
	0	+10	-10			-26.5 → 27	
	0	+20	-20			-26.5 → 27	
	0	+30	-30			-26.5 → 27	
	0	+39	-39			-26.4 → 27	
	+10	0	0			-3 → 27	
	+20	0	0			-3 → 54.6	
	-10	0	0			-26.5 → 3.7	
	-20	0	0			-54.8 → 3.7	
	+10	-20	-20			-3 → 27	
	+10	-39	-39			-3 → 27	
	+10	+39	+39			-3 → 27	
	+20	-20	-20			-3 → 54.7	
	+20	-39	-39			-3 → 54.7	
	+20	+39	+39			-3 → 27	
	-10	+20	+20			-26.6 → 3.7	
	-10	+39	+39			-26.6 → 3.6	
	-20	+20	+20			-26.6 → 3.6	
	-20	+39	+39			-26.6 → 3.6	
	0	0	0			-26.2 → 27	0.79
	0	-20	-20			-3 → 27	
V	0	0	0	NA	YES	-3 → 27	0.79
	0	0	0			-3 → 27	2.26
VI	0	0	0	NA	YES	-3 → 27	0.79
	0	0	0			-3 → 27	2.26

TABLE 3

GEOMETRIC CHARACTERISTICS

Wing:	
Clipped Delta Wing with Blunt Apex, Leading Edges and Base	
Root Chord	17.29 inches actual, 18.2 inches virtual
Tip Chord	3.651 inches
Span	16.8 inches
Apex Radius	0.910 inches
Leading Edge Sweep	60 degrees
Leading Edge Radius	0.910 inches
Wing Thickness (Constant)	1.820 inches
Planform Area	182.91 inches^2 actual, 191.3 inches^2 virtual
Aspect Ratio	1.542
Taper Ratio	0.211
Thickness Ratio (Root)	0.1052
Control Area - Partial Span Flaps	25 inches^2
- Apex	6.722 inches^2
Body:	
Half Cone - Cylinder (Base Mounted Flush with Wing Trailing Edge)	
Cone Angle	13 degrees
Cone Length	7.682 inches
Cone Radius (Maximum at Tangency Point)	1.773 inches
Cylinder Length	6.188 inches
Cylinder Radius	1.820 inches
Fairing (Cone to Cylinder)	
Length	0.409 inches
Radius	1.820 inches
Included Angle	13 degrees
Total Body Length	14.279 inches
Planform Area	34.9 inches^2
Tip Fin:	
Clipped Delta Wing with Blunt Leading Edge	
Root Chord	4.584 inches
Tip Chord	1.384 inches
Span	5.824 inches
Leading Edge Sweep	50 degrees
Leading Edge Radius	0.455 inches
Thickness (Constant)	0.91 inches
Area	18.17 inches^2
Aspect Ratio	1.862
Taper Ratio	0.3025
Thickness Ratio (Fin Root-Wing Center Plane)	0.199

TABLE 3 (Cont.)

GEOMETRIC CHARACTERISTICS

Central Flap:	
Wedge Section - Central Section of Full Span Trailing Edge Flap	
Chord (Constant)	2.414 inches
Span	3.640 inches
Wedge Angle	20 degrees
Planform Area	8.787 inches^2
Spoiler:	
Full Span, Plug Type with Cylindrical Lower Edge	
Chord (Constant)	0.910 inches
Span	14.980 inches
Height	0.855 inches
Planform Area	13.632 inches^2
Bottom Cylinder Radius	0.455 inches

TABLE 4

COEFFICIENTS OF BALANCE ERROR INACCURACIES

		F_N	F_A	F_y	M_m	M_n	M_ℓ
Balance Limit		±700#	±150#	±700#	±3600 in#	±1800 in#	±300 in#
Balance Accuracy		±1.062#	±.564#	±.733#	±8.55 in#	±4.925 in#	±1.396 in#
	Re_∞/ft x 10^{-6}	C_N	C_{A_T}	C_y	C_m	C_n	C_ℓ
Data Accuracy M = 5.01	2.26	±.0039	±.0021	±.0029	±.0016	±.001	±.0003
	5.0	±.0016	±.0008	±.0012	±.0007	±.0004	±.0001
Data Accuracy M = 8.08	2.26	±.0024	±.0013	±.0018	±.001	±.0006	±.0002
	0.79	±.0074	±.0039	±.0054	±.0031	±.0019	±.0005

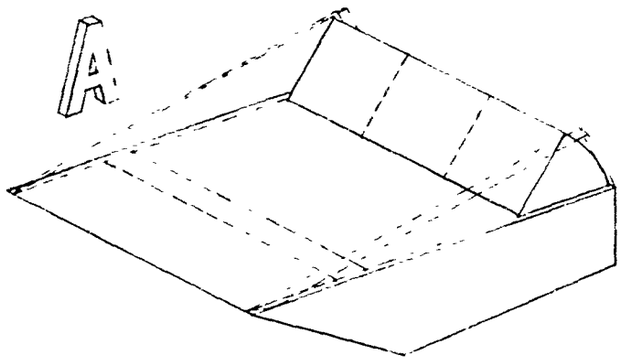

Separated Flows ahead of a Ramp
Fore and aft flaps, end plates
3 separate models:

1) Pressure and heat transfer, AEDC Tunnels A & B, M = 5 & 8

2) Controlled wall temperature, pressure, AEDC Tunnel B, M = 8

3) Pressure and heat transfer, Grumman Shock Tunnel, M ≈ 13 & 19

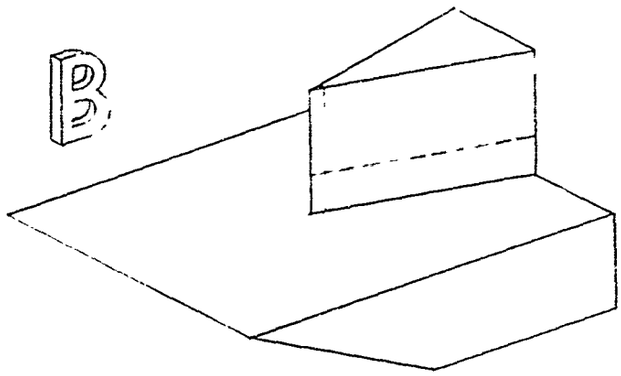

Wedge - Plate Interaction
Small and large fins with sharp and blunt leading edges
2 separate models:

1) Pressure and heat transfer, AEDC Tunnels A & B, M = 5 & 8

2) Pressure and heat transfer, Grumman Shock Tunnel, M ≈ 13 & 19

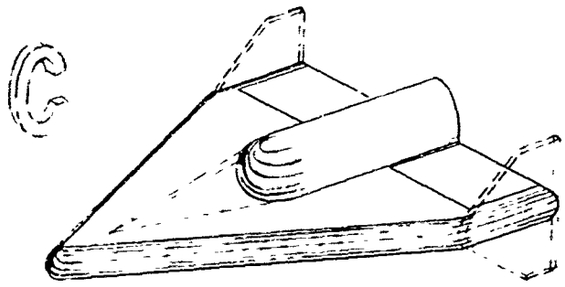

Clipped Delta, Blunt L.E.
Center body, T.E. flaps, drooped nose, spoiler, tip fins
3 separate models:

1) Pressure and heat transfer, AEDC Tunnels A & B, M = 5 & 8

2) Pressure, AEDC Hotshot 2, M ≈ 19

3) Six component force, AEDC Tunnels A & B, M = 5 & 8

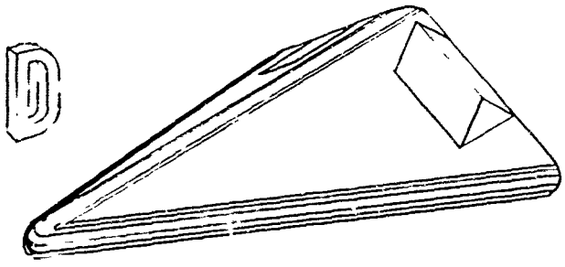

Delta, Blunt L.E., Dihedral
T.E. flaps, canard, ventral fin
3 separate models:

1) Pressure and heat transfer, AEDC Tunnels A & B, M = 5 & 8

2) Pressure and heat transfer, Grumman Shock Tunnel, M ~ 19

3) Six component force, AEDC Tunnels A & B, M = 5 & 8

Fig. 1a General Outline of Models and Remarks for Over-all Program

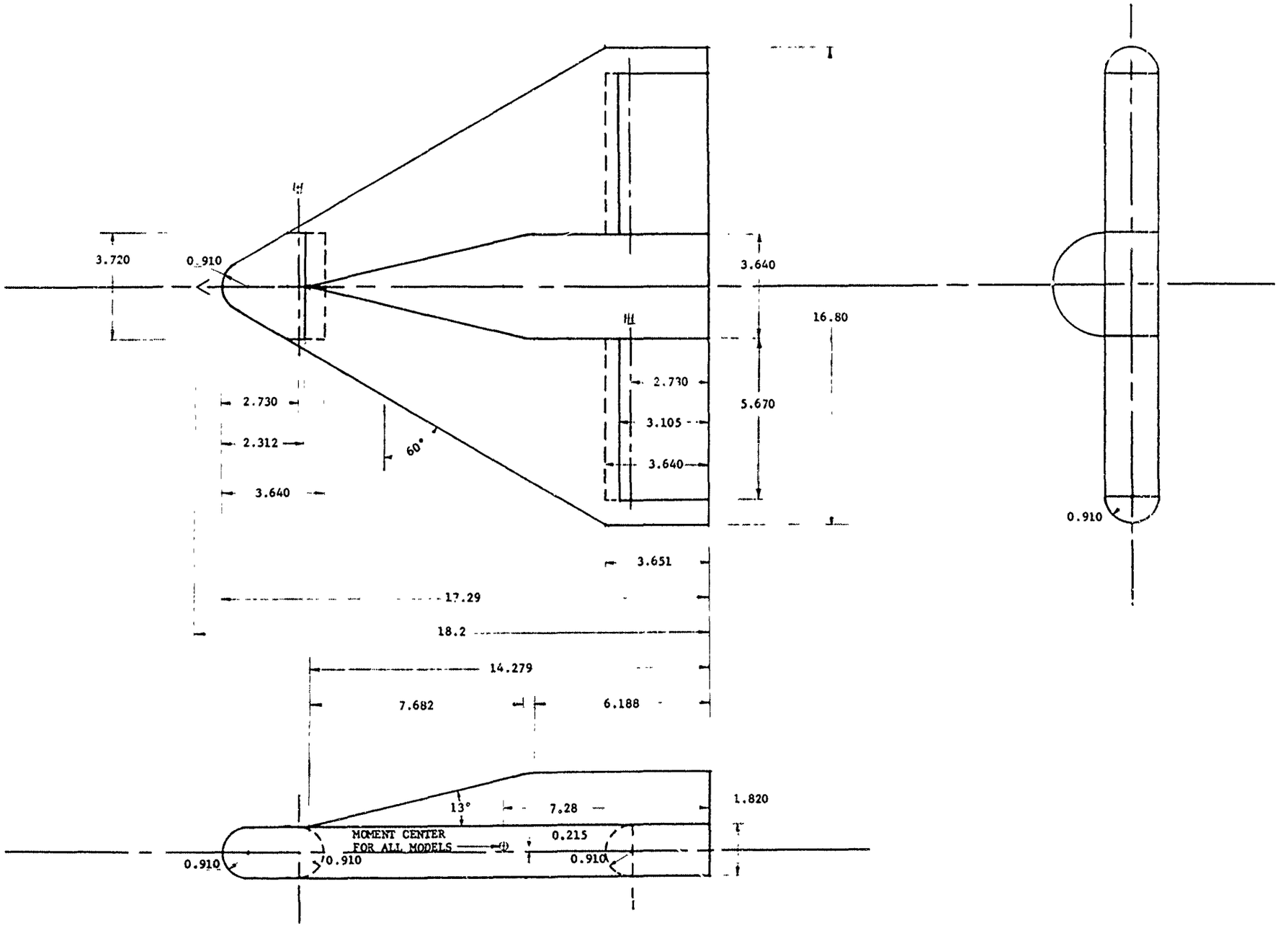

Fig. 1b Basic Configuration (Configuration I) - Clipped Delta Wing-Body Combination

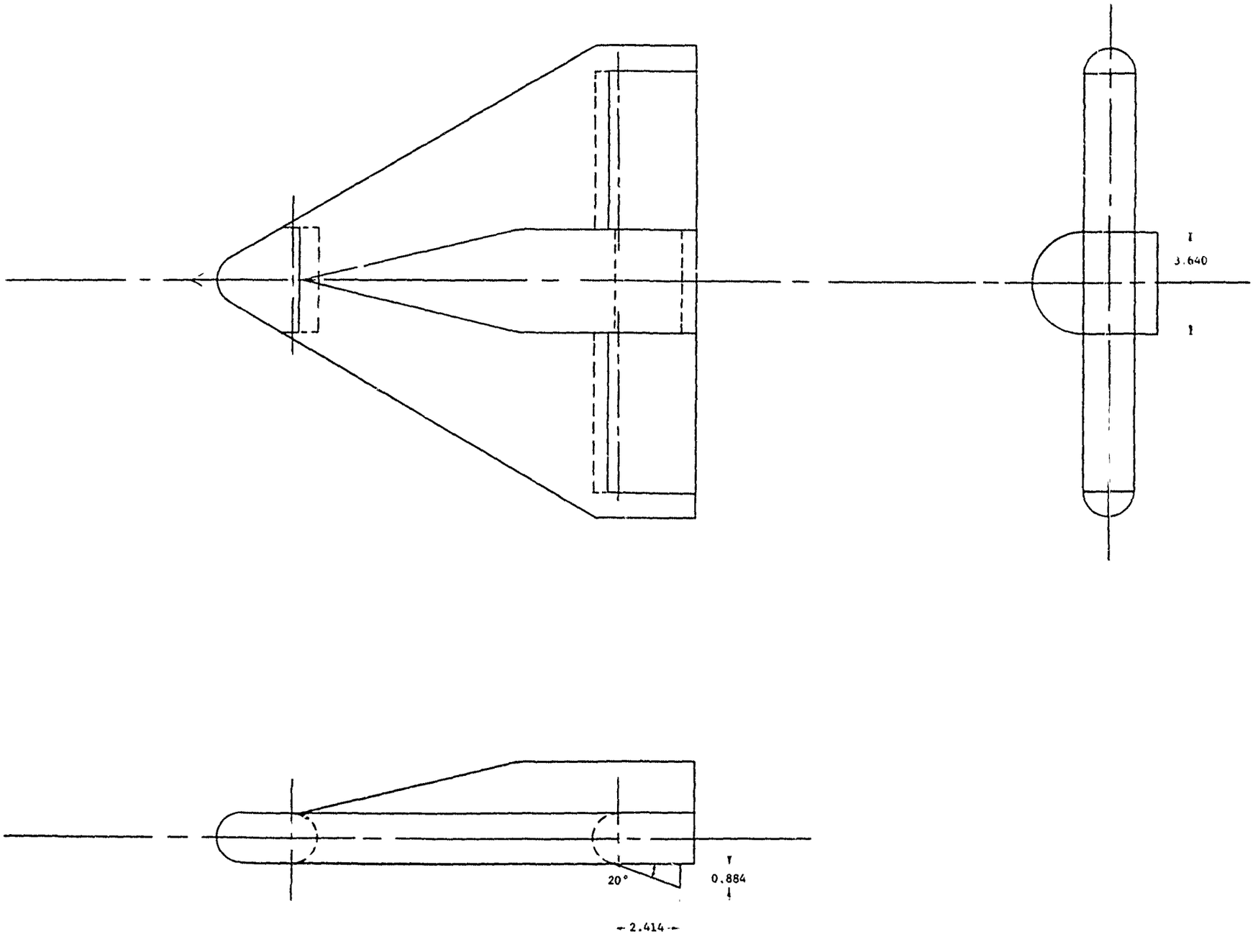

Fig. 1c Configuration II - Basic + Central Flap section (for other dimensions see Fig. 1b)

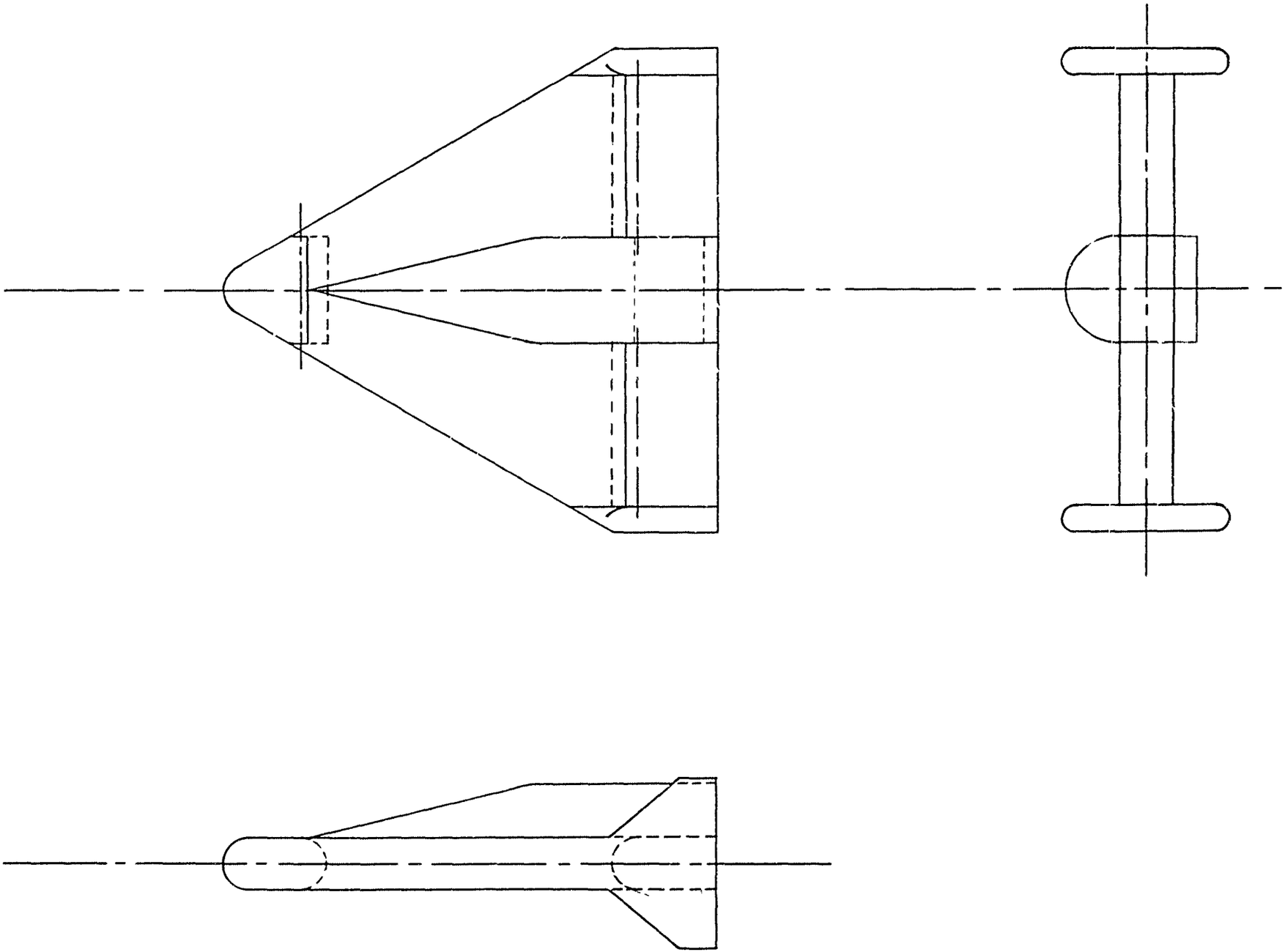

Fig. 1d Configuration III - Basic + Fins + Central Flap section
(for dimensions see Figs. 1b, 1c, and 1e)

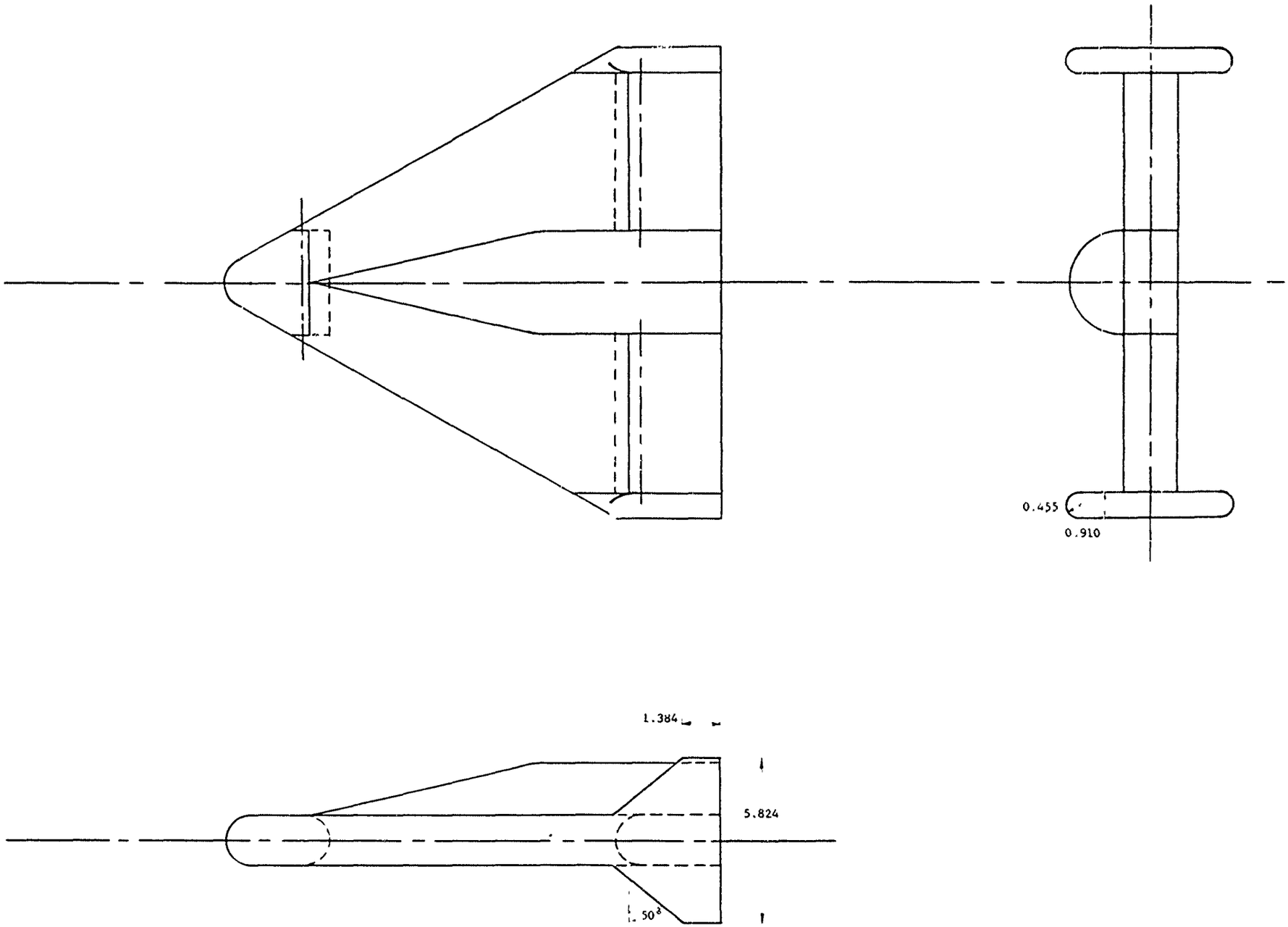

Fig. 1e Configuration IV - Basic + Tip Fins (for other dimensions see Fig. 1b)

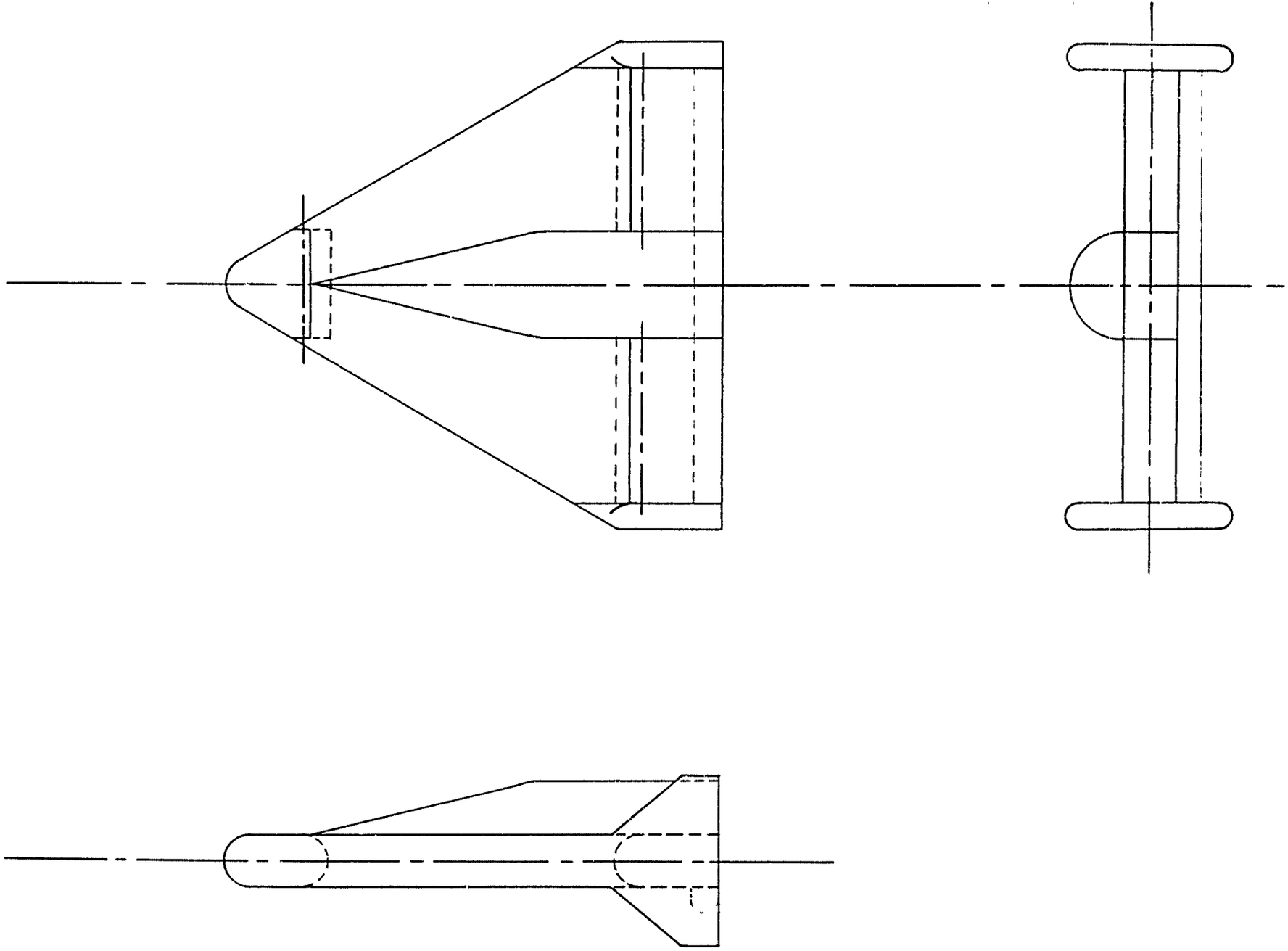

Fig. 1f Configuration V - Basic + Tip Fins + Full Span Plug Spoiler (for other dimensions see Fig. 1b and 1g)

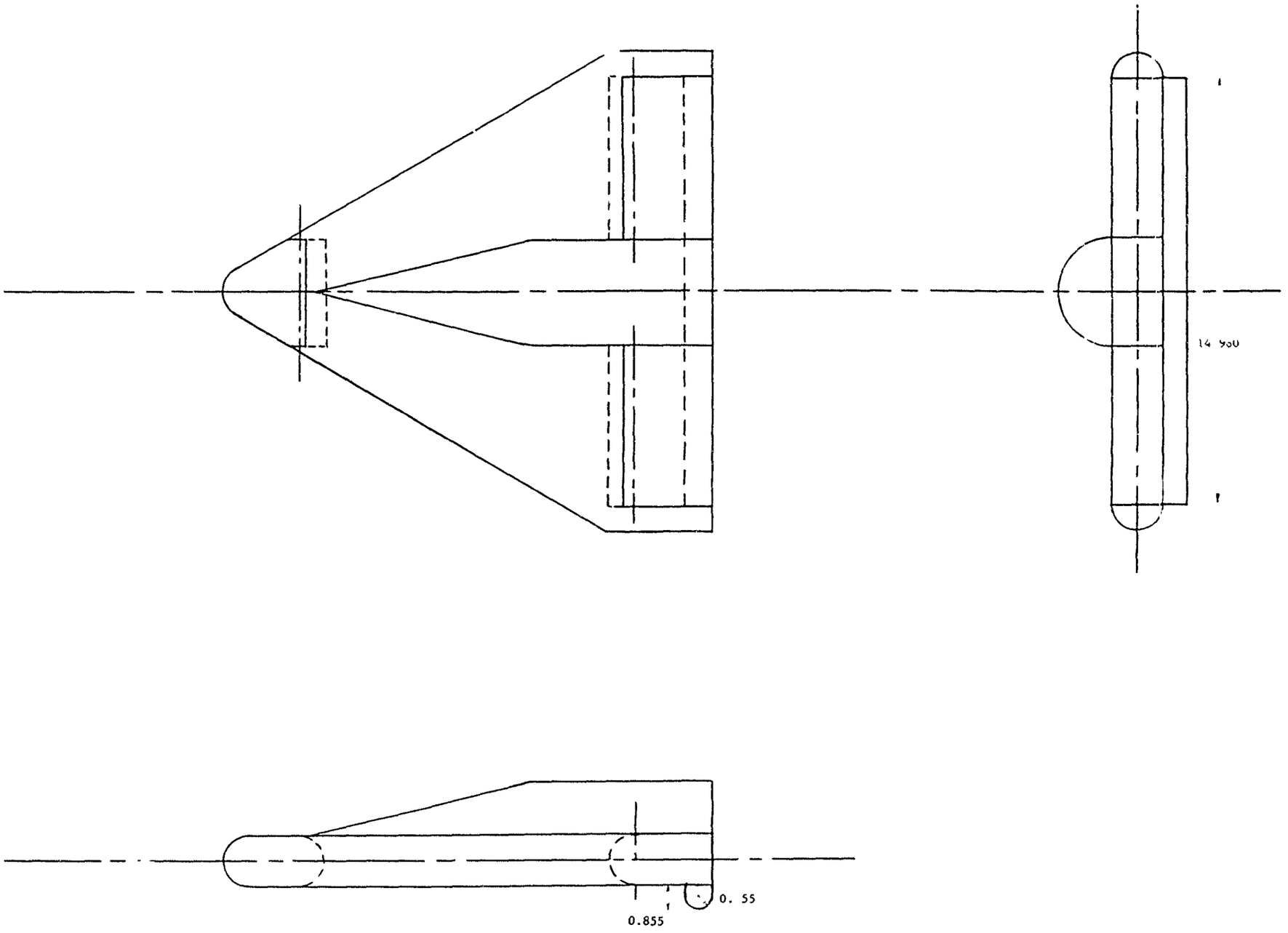

Fig. 1g Configuration VI - Basic + Full Span Plug (for other dimensions see Fig. 1b)

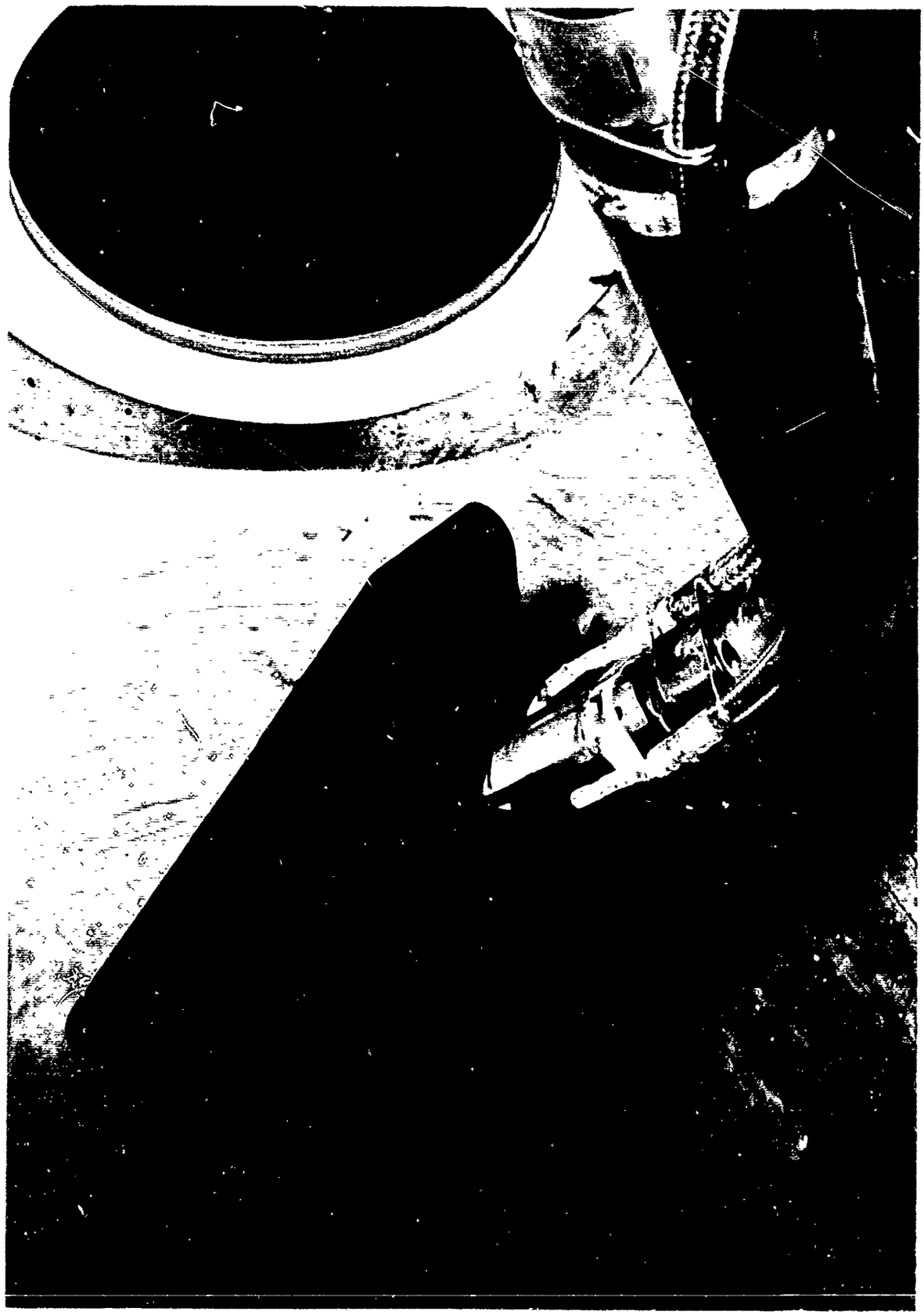

Fig. 1h Rear View Photograph - Configuration I in the 50" Mach 8 Hypersonic Wind Tunnel - Mounted for Negative Angles of Attack

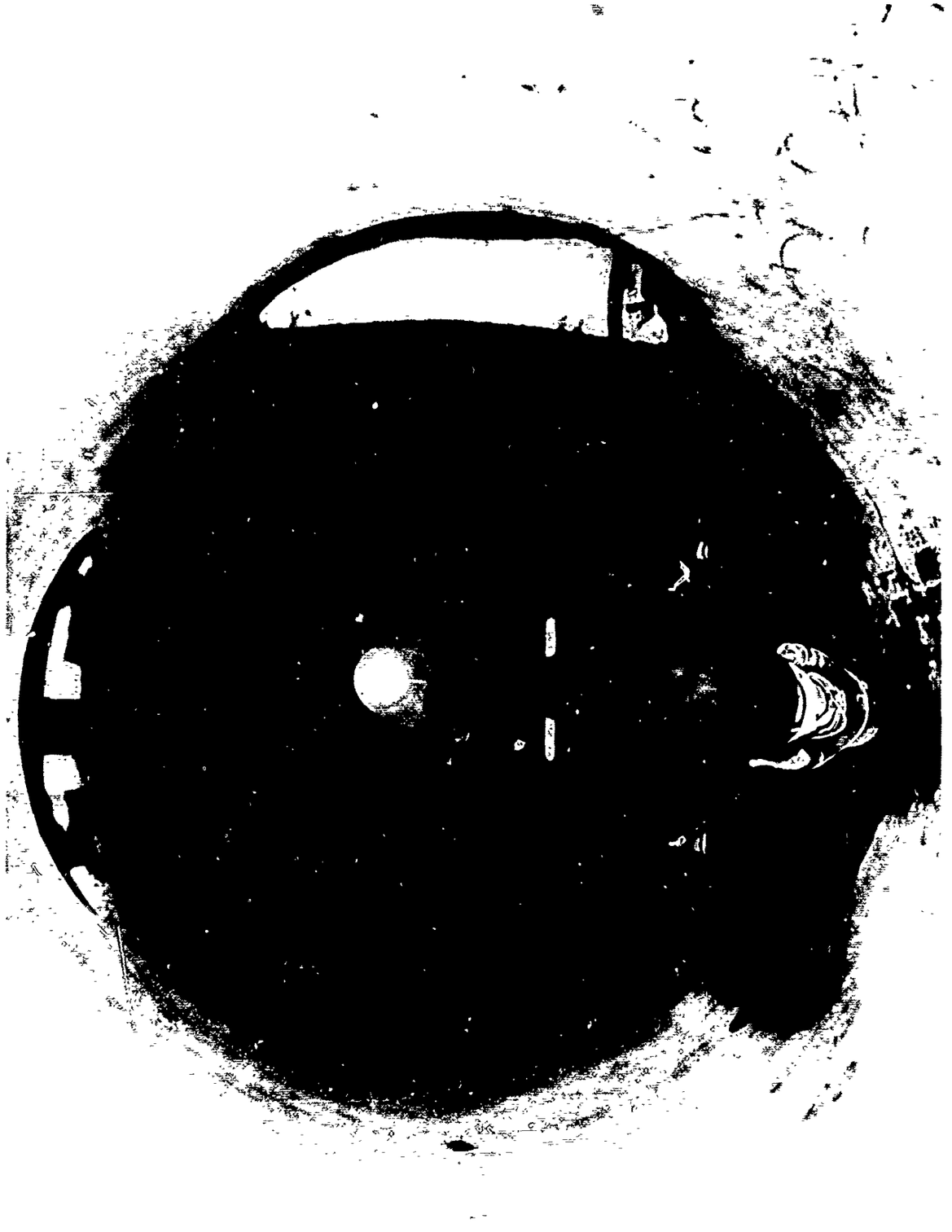

Fig. 1i Front View Photograph - Configuration I in the 50" Mach 8 Wind Tunnel - Mounted for Negative Angle of Attack

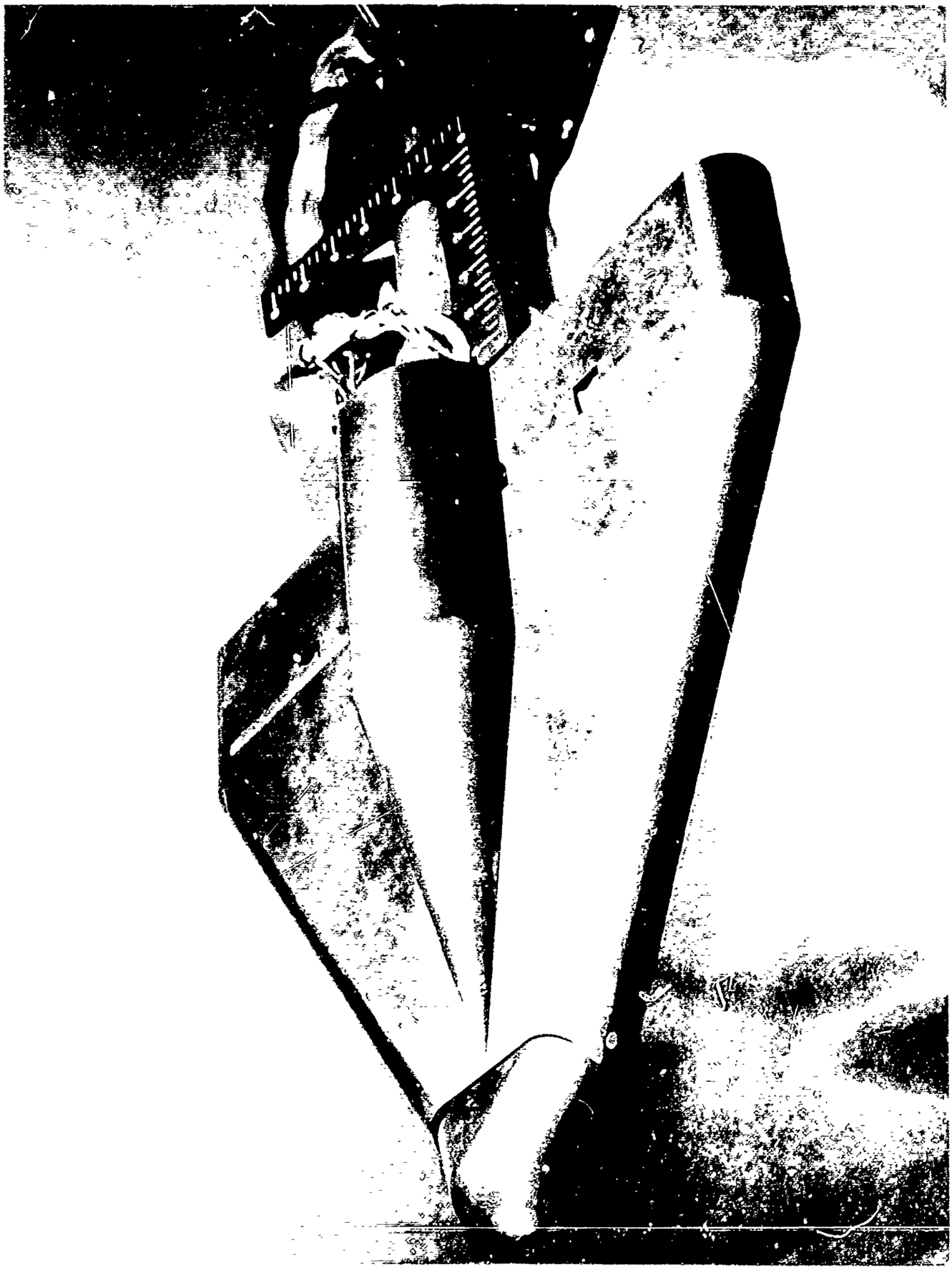

Fig. 1j Photograph - Configuration I with Positive Apex Deflection

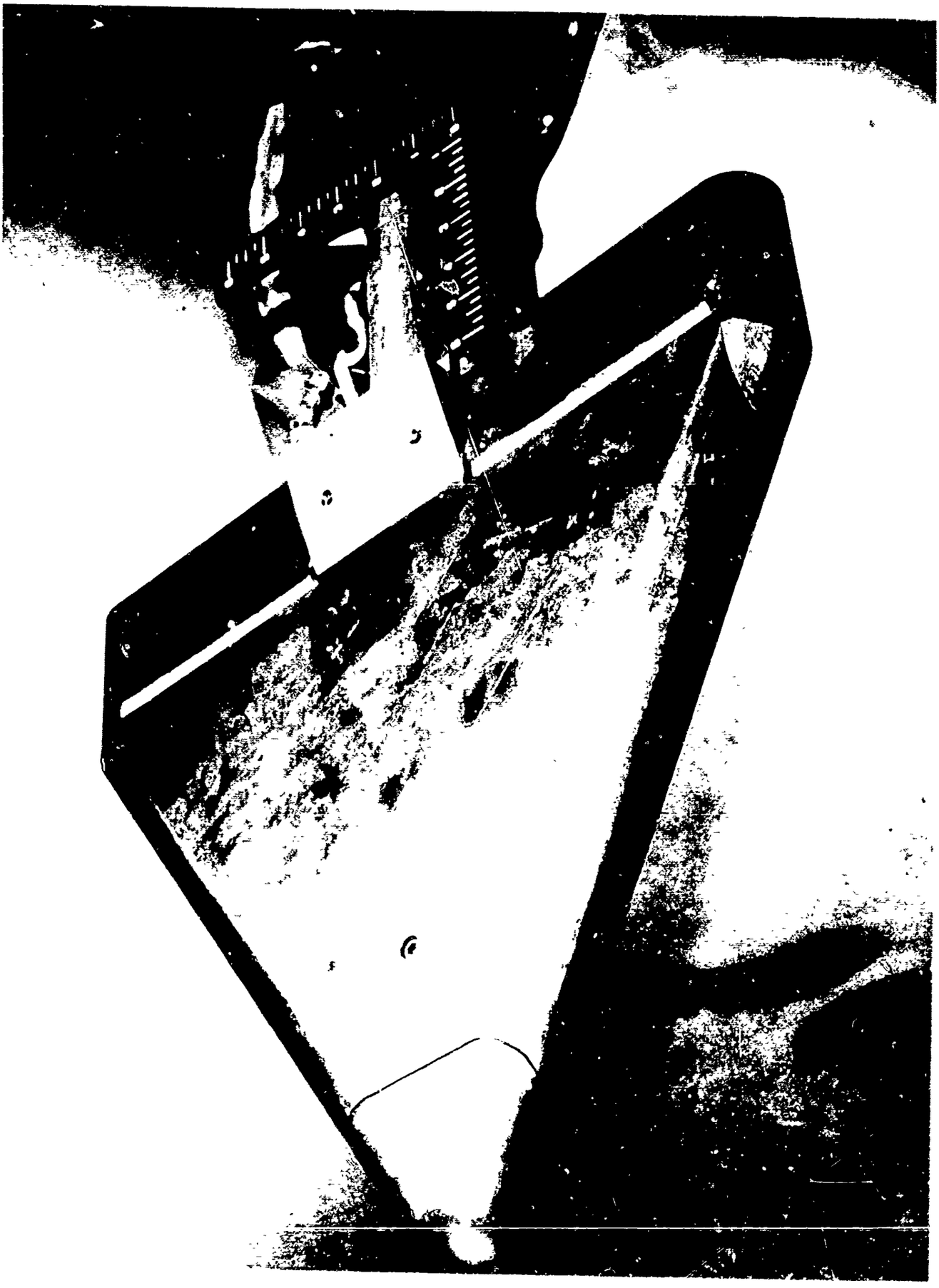

Fig. 1k Photograph - Configuration II with Central Flap Section Installed

Fig. 1ℓ Photograph - Configuration II with Full Span Flap

Fig. 1m Photograph - Configuration IV

Fig. 1n Photograph - Configuration IV with Partial Span Trailing Edge Flaps Deflected

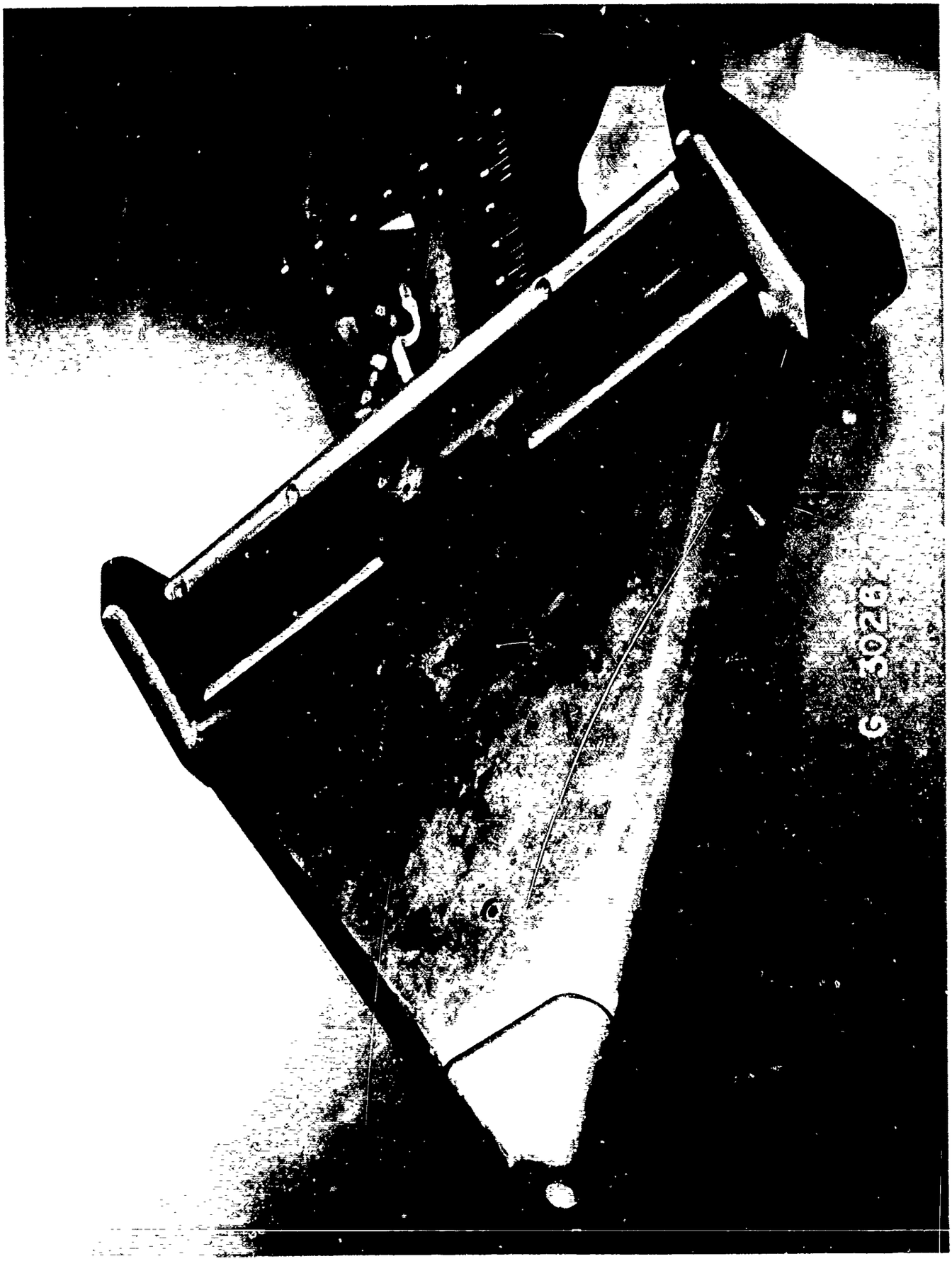

Fig. 1o Photograph - Configuration V

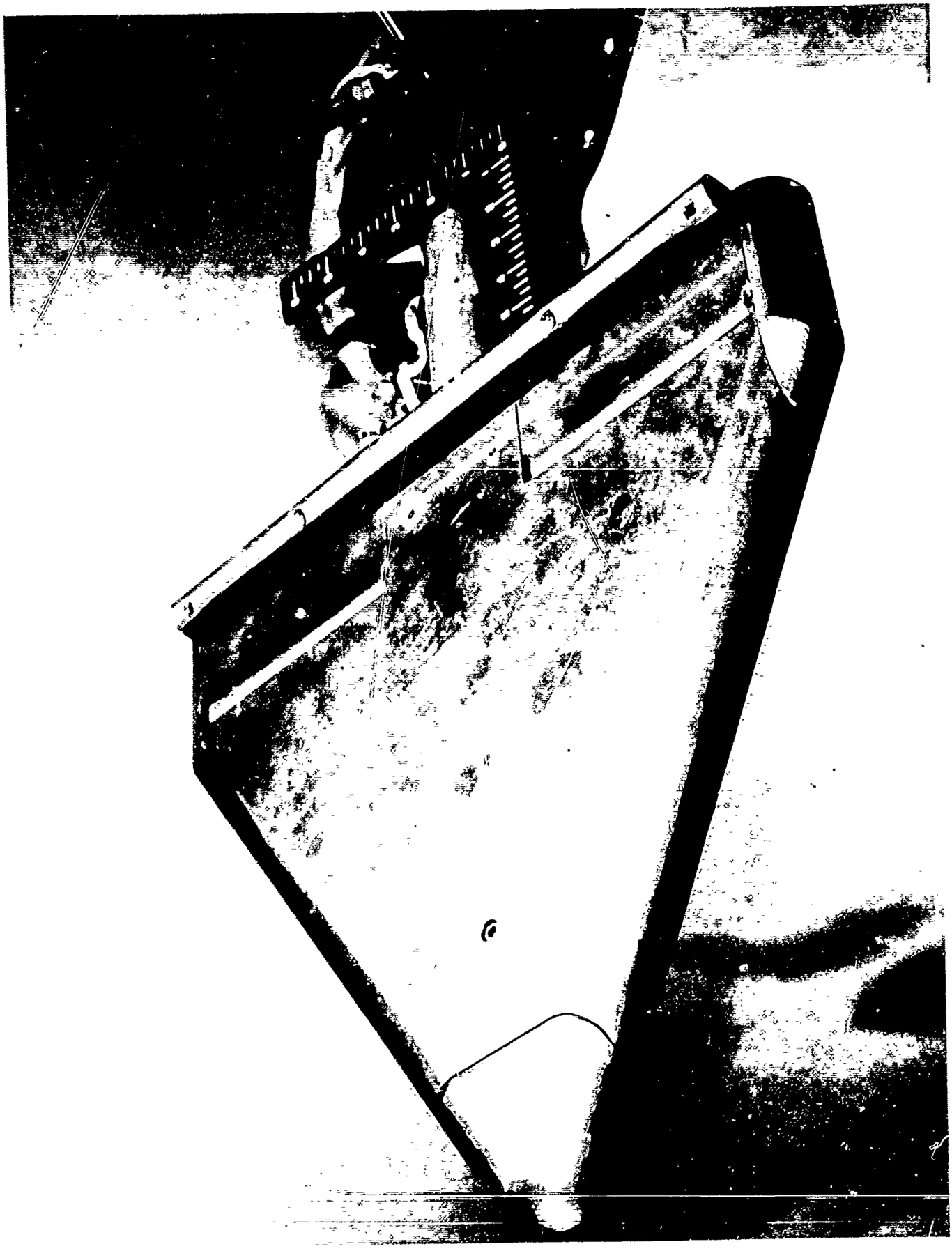

Fig. 1p Photograph - Configuration VI

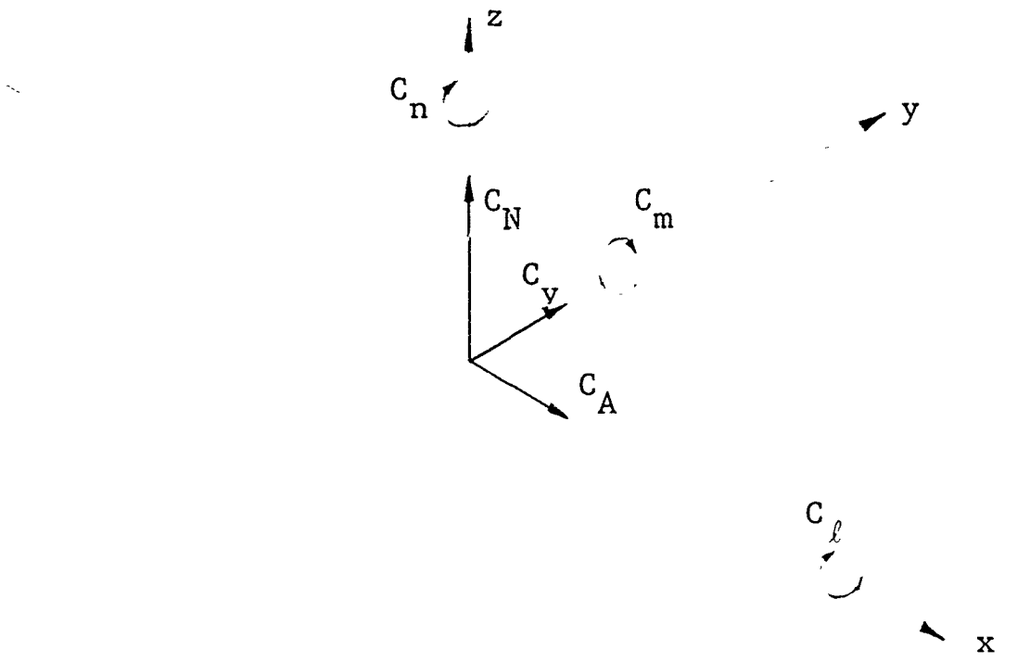

Fig. 2a Body Oriented Coordinate System

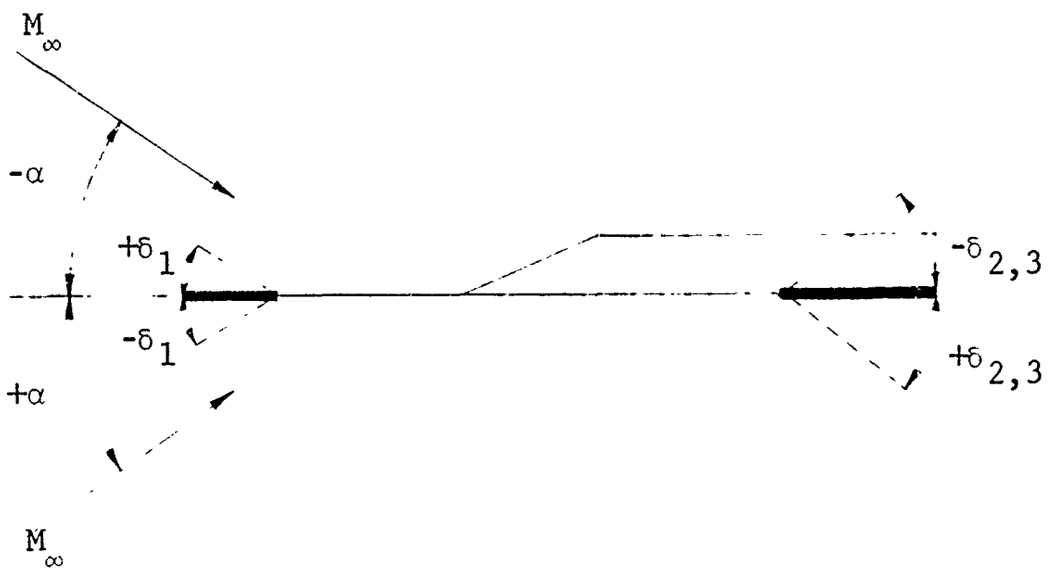

Fig. 2b Sign Convention for Control Deflection Angles

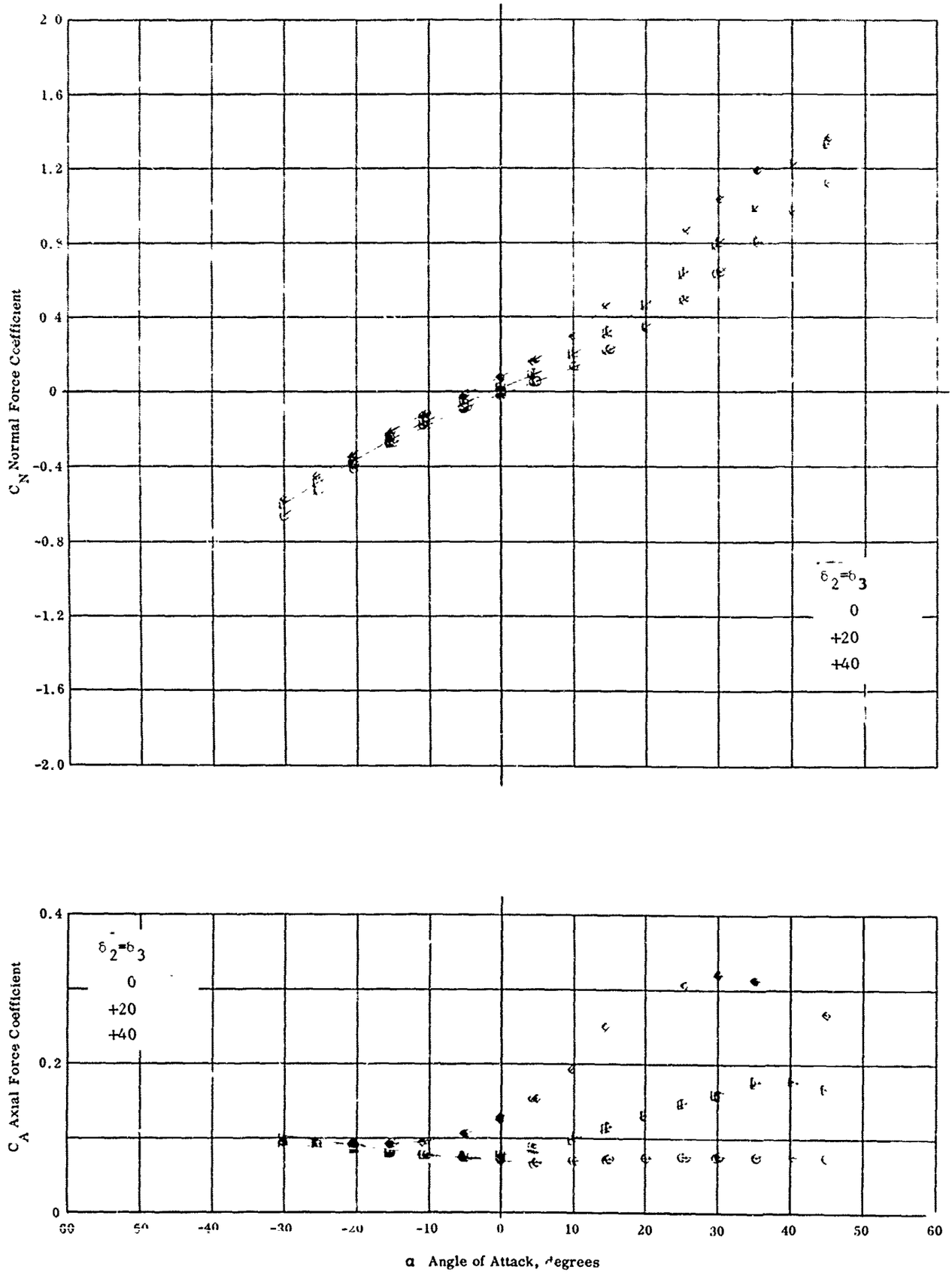

Fig. 3a Configuration I - M_∞=5.01, C_N & C_A vs. α
$Re_\infty/ft \times 10^{-6}$ = 2.26, δ_1=0 $\delta_2=\delta_3$=0, +20, +40

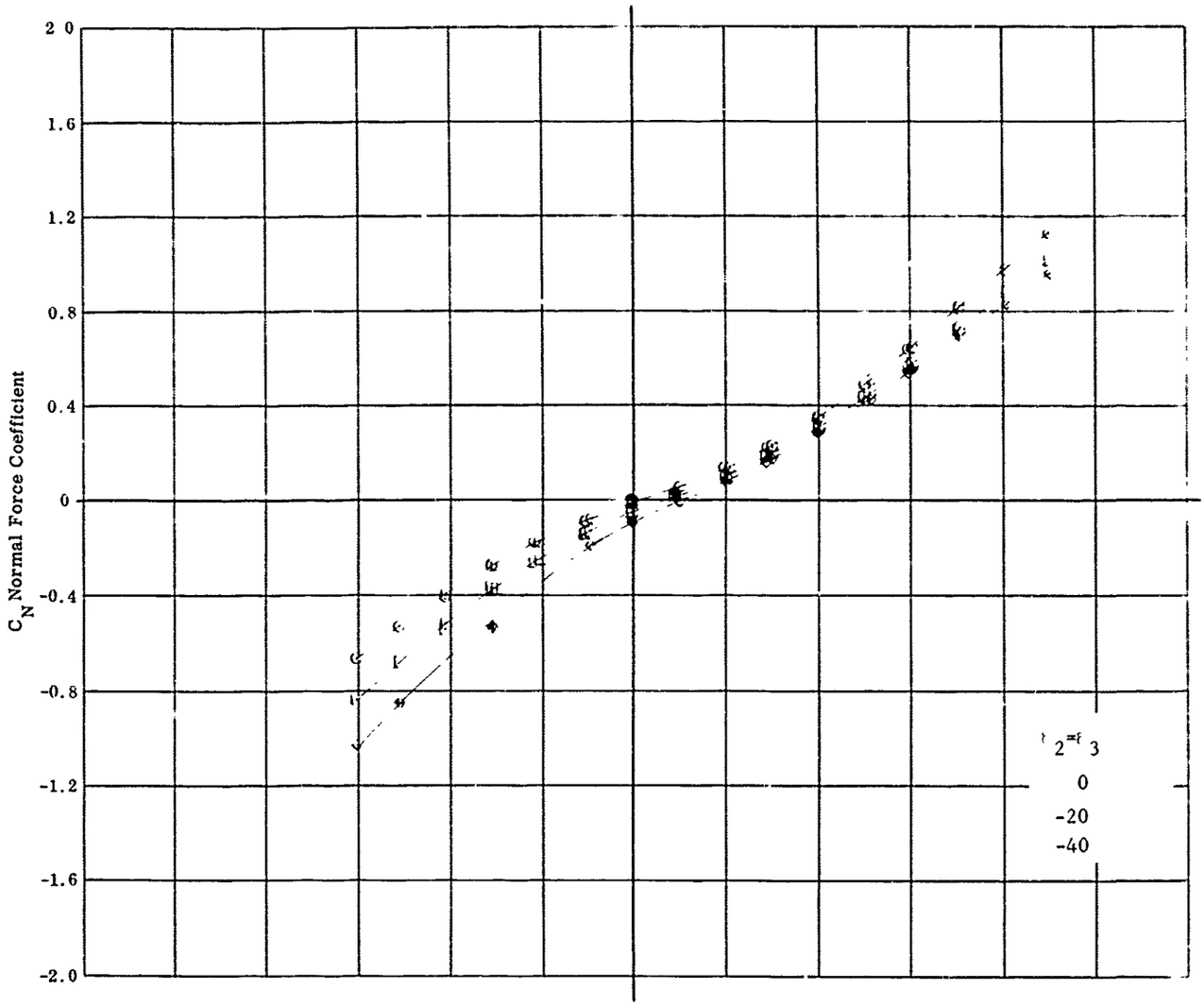

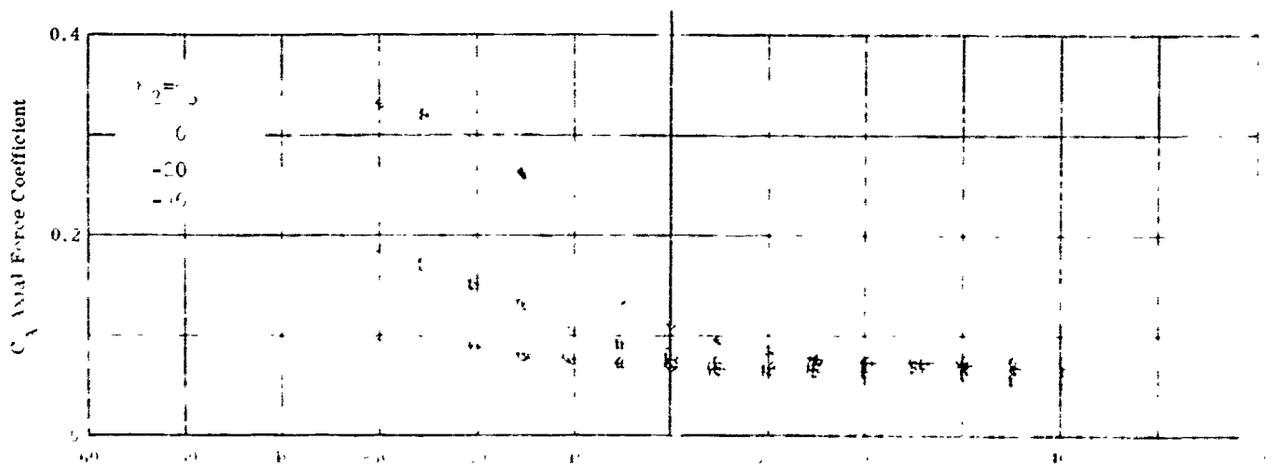

α Angle of Attack, deg

Fig. 6b Continued. M = 2.01, [illegible]

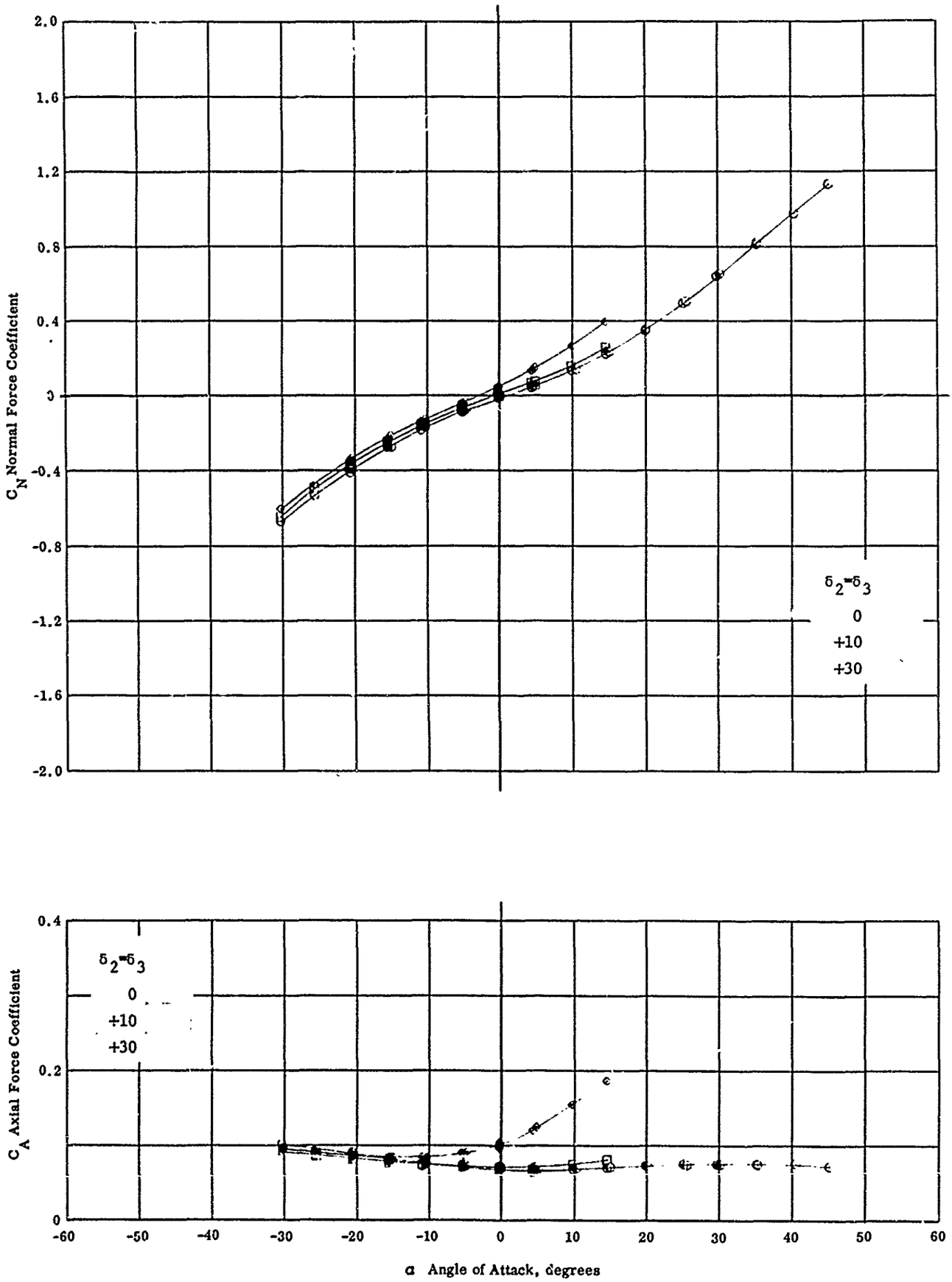

Fig. 3c Configuration I - M_∞=5.01, C_N & C_A vs. α
$Re_\infty/ft \times 10^{-6}$ = 2.26, δ_1=0 $\delta_2=\delta_3$=0, +10, +30

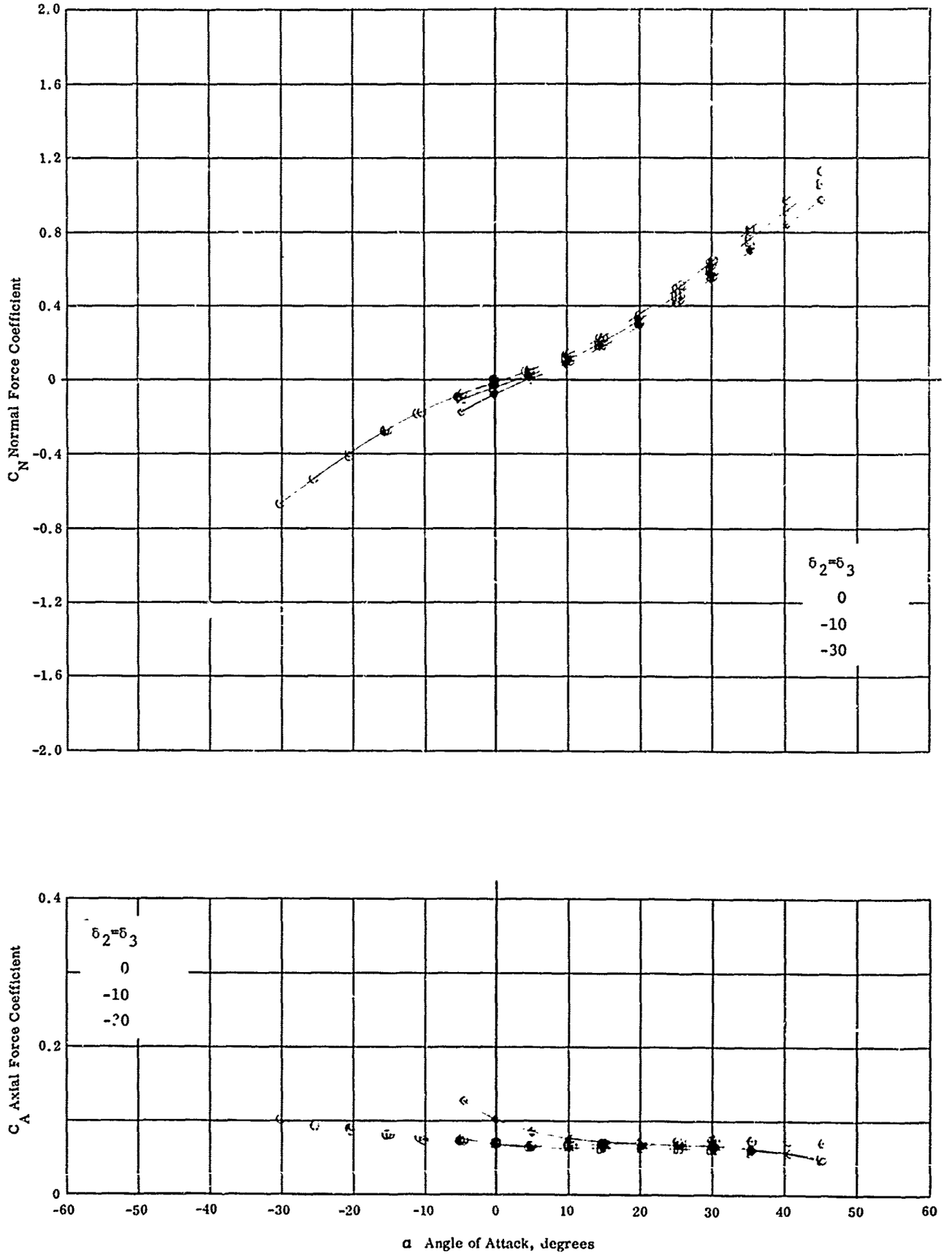

Fig. 3d Configuration I - M_∞=5.01, C_N & C_A vs. α
Re_∞/ft x 10^{-6} = 2.26, δ_1=0 $\delta_2=\delta_3$=0, -10, -30

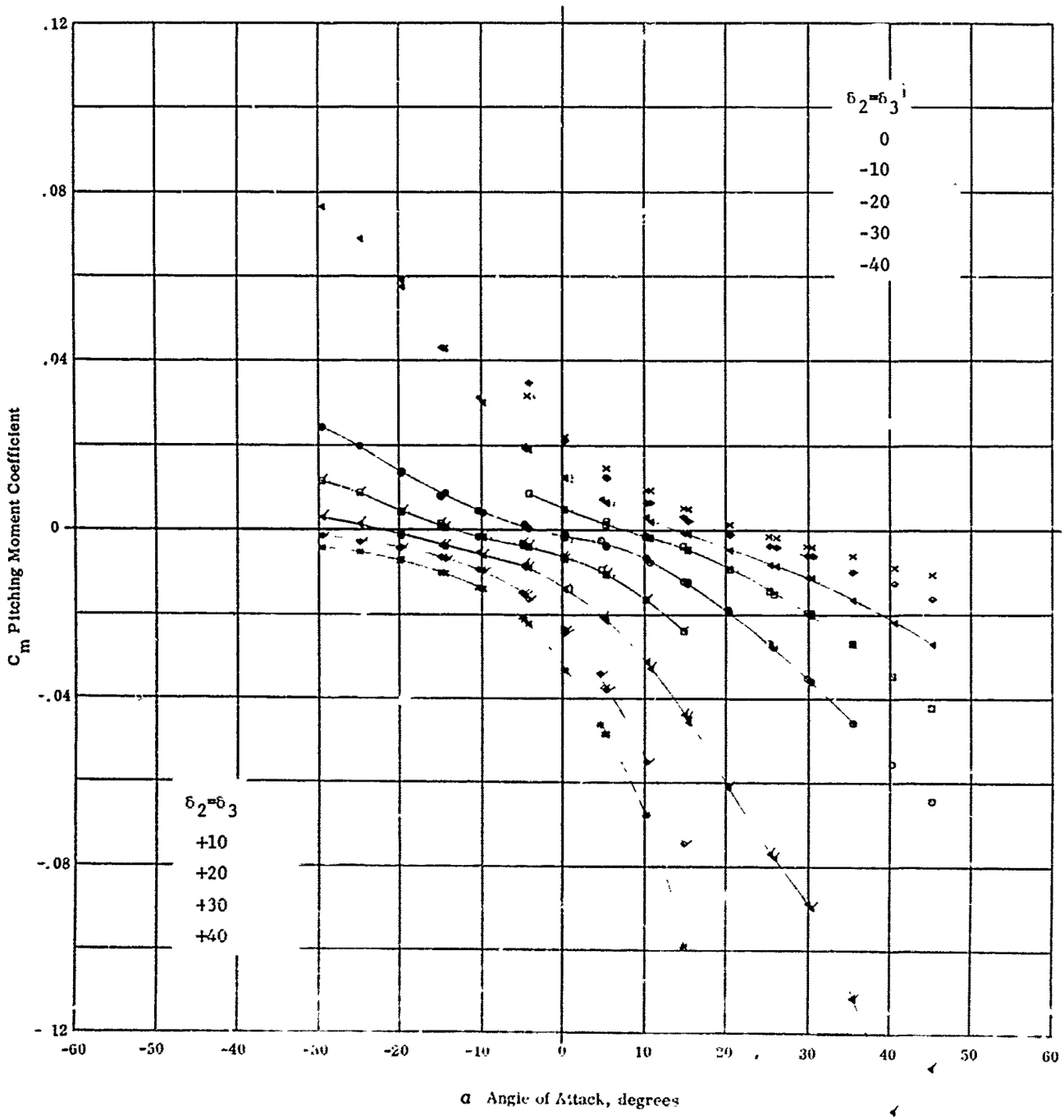

Fig. 3e Configuration I - M_∞=5.01, C_m vs. α Re /ft x 10^{-6} = 2.26

δ_1=0 $\delta_2=\delta_3$=0, ±10, 20, 30, 40

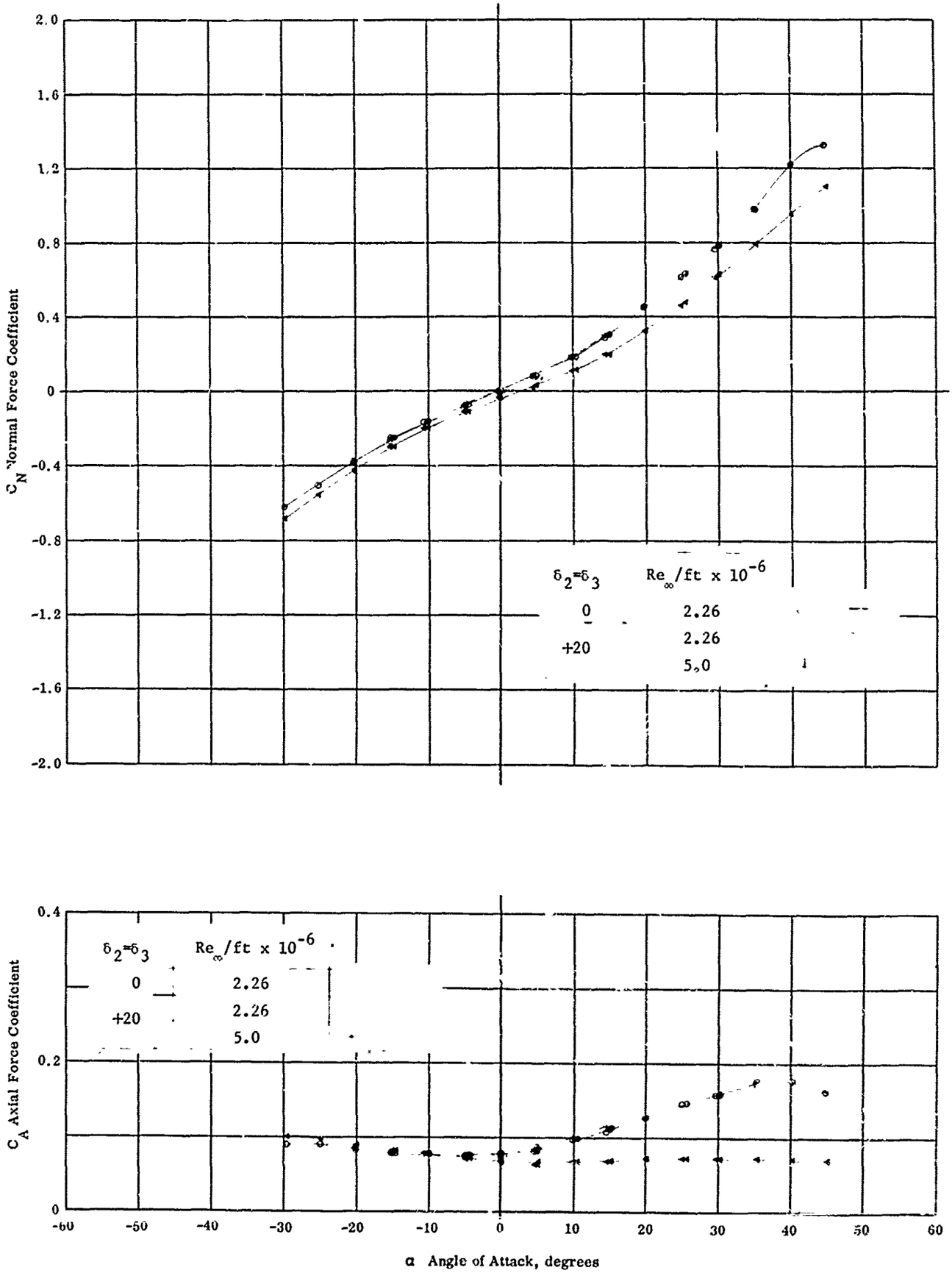

Fig. 4a Configuration I - M_∞=5.01, C_N & C_A vs. α
Re_∞/ft x 10^{-6} = 2.26, 5.0, δ_1=0 $\delta_2=\delta_3$=0, +20

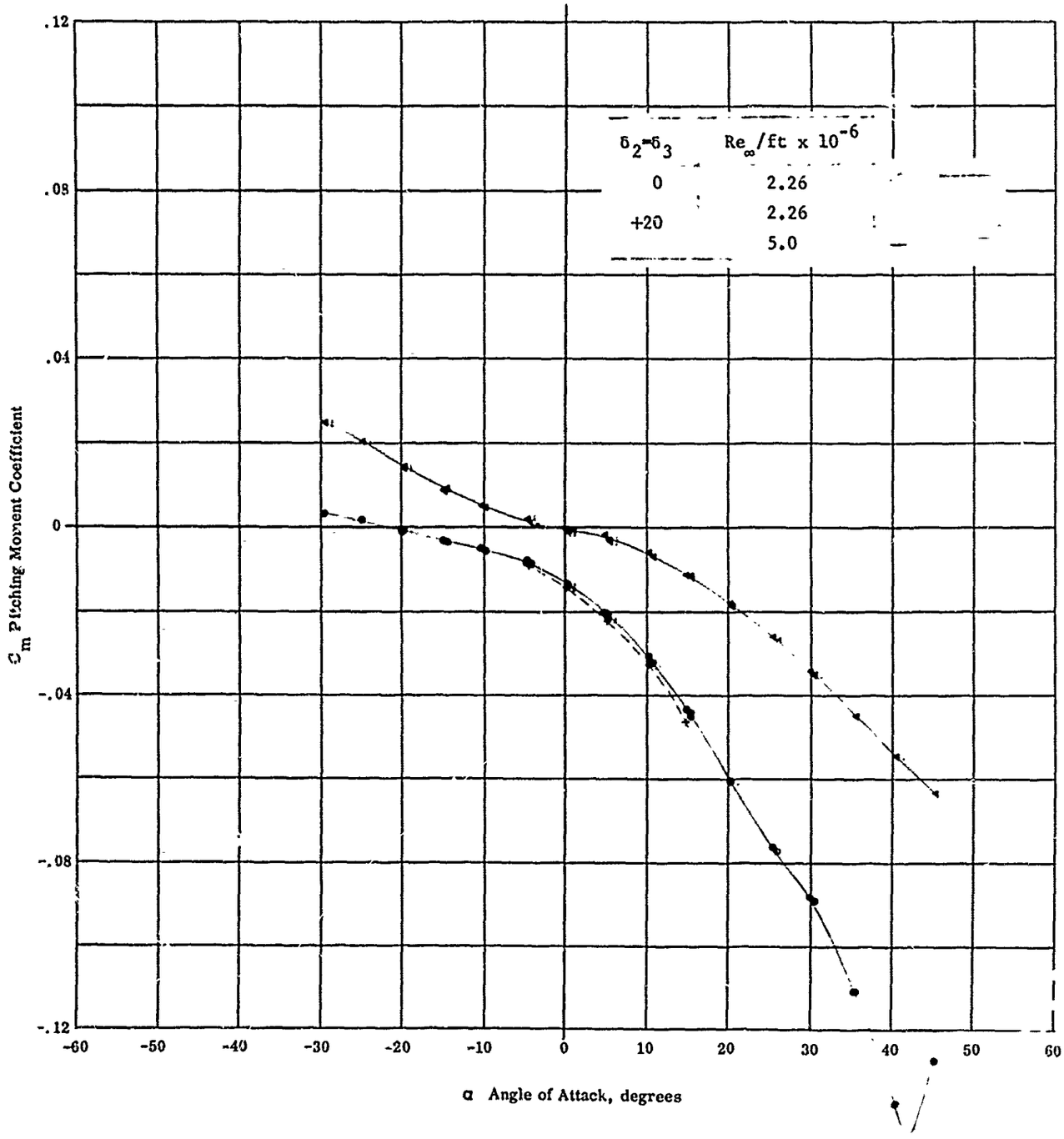

Fig. 4b Configuration I - M_∞=5.01, C_m vs α
Re_∞/ft x 10^{-6} = 2.26, 5.0, δ_1=0 $\delta_2=\delta_3$=0, +20

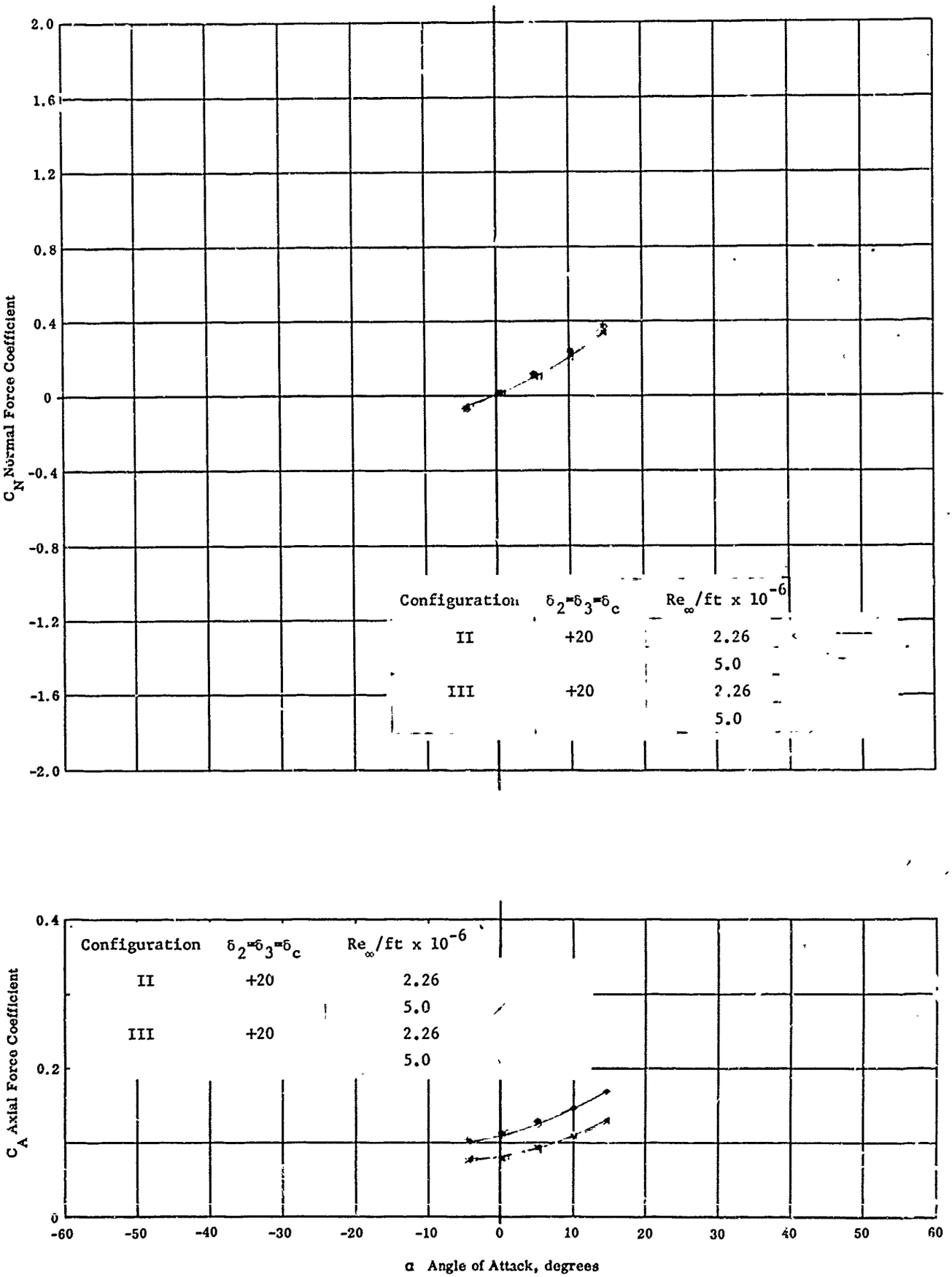

Fig. 5a Configuration II & III - $M_\infty=5.01$, C_N & C_A vs. α
$Re_\infty/ft \times 10^{-6} = 2.26, 5.0,$ $\delta_1=0$ $\delta_2=\delta_3=\delta_c=+20$

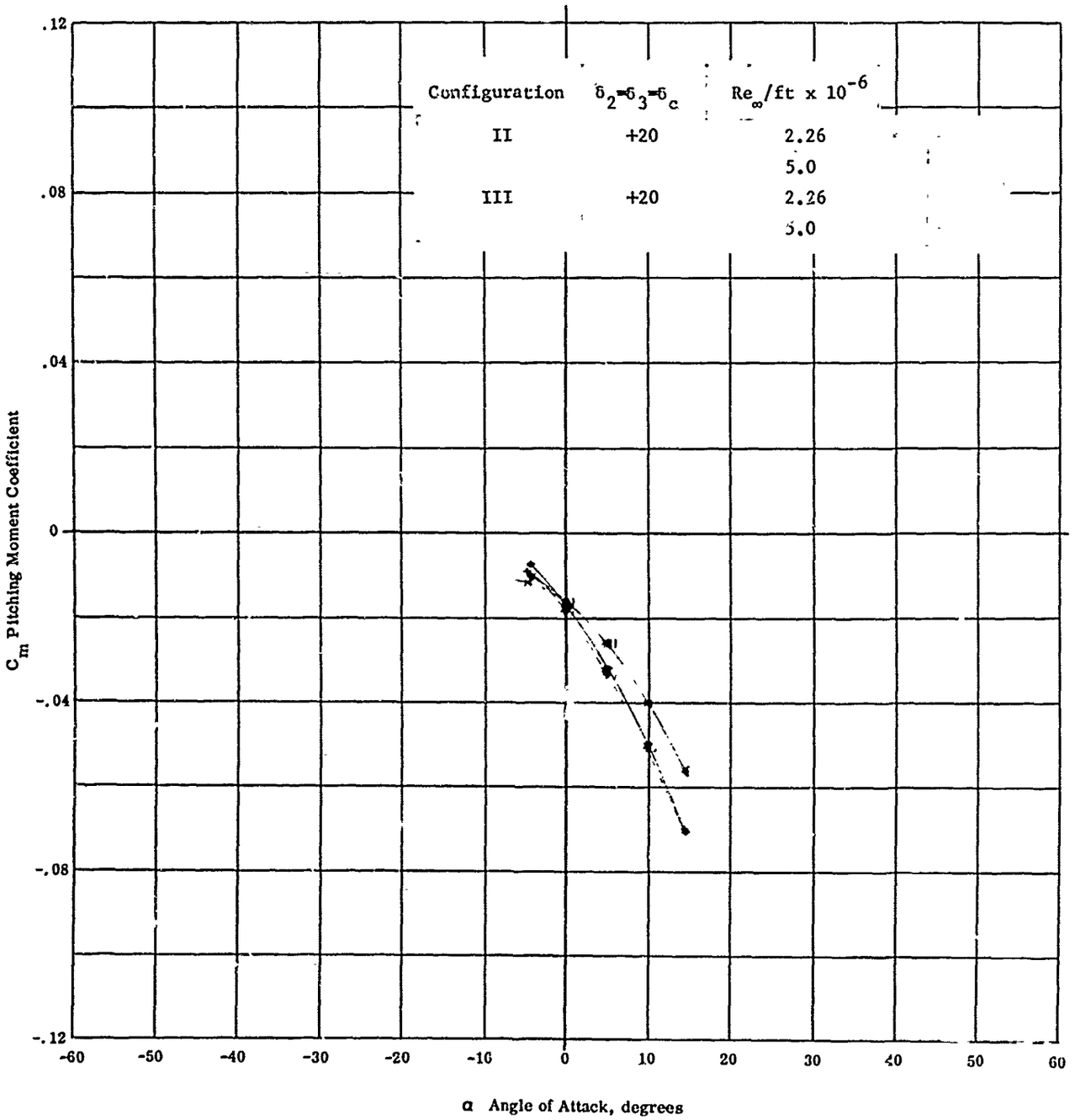

Fig. 5b Configuration II & III - M_∞=5.01, C_m vs. α
Re_∞/ft x 10^{-6} = 2.26, 5.0 δ_1=0 $\delta_2=\delta_3=\delta_c$=+20

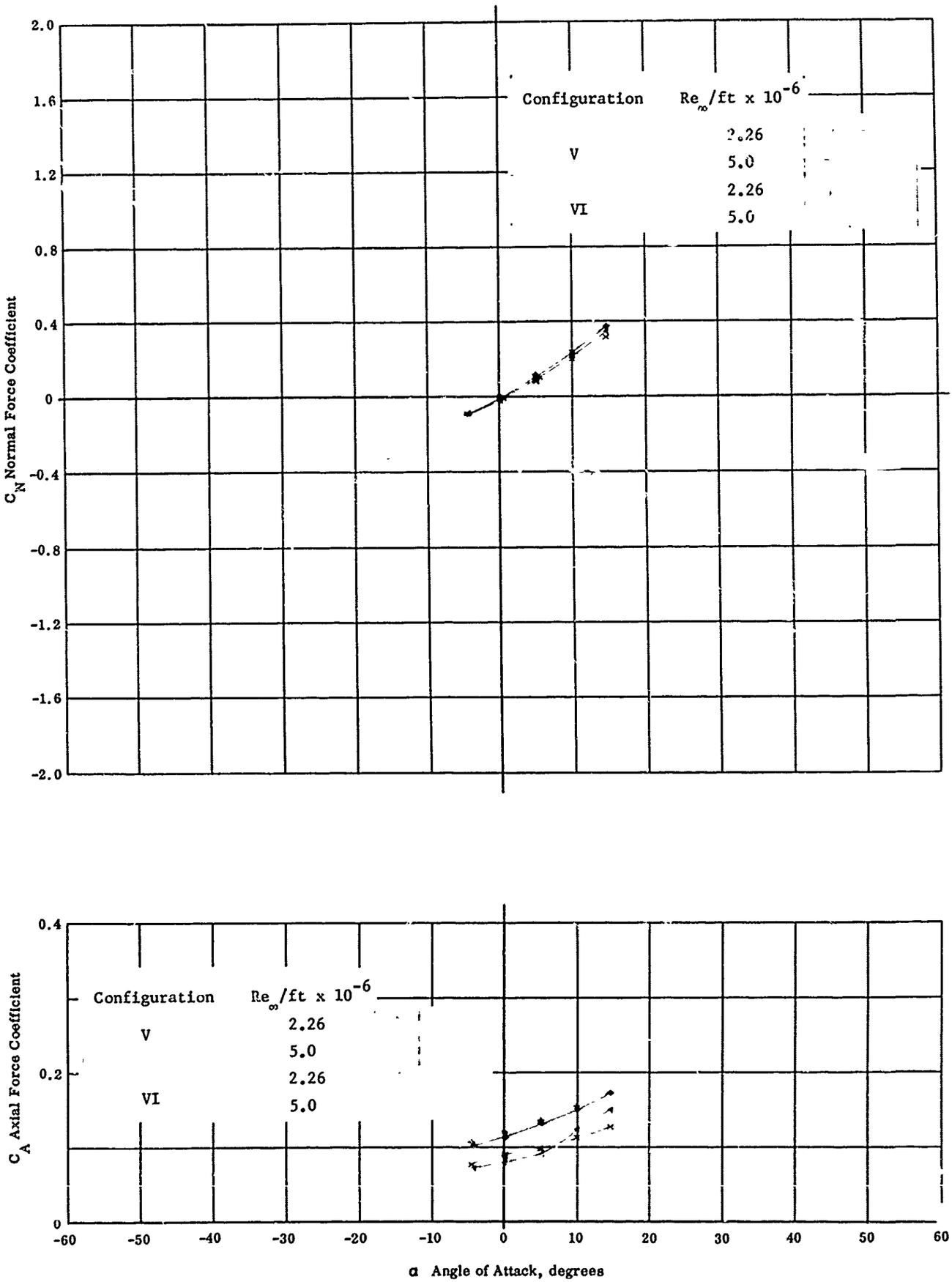

Fig. 6a Configuration V & VI - M_∞=5.01 C_N & C_A vs. α
Re_∞/ft x 10^{-6} = 2.26, 5.0 $\delta_1=\delta_2=\delta_3=0$, Spoiler On

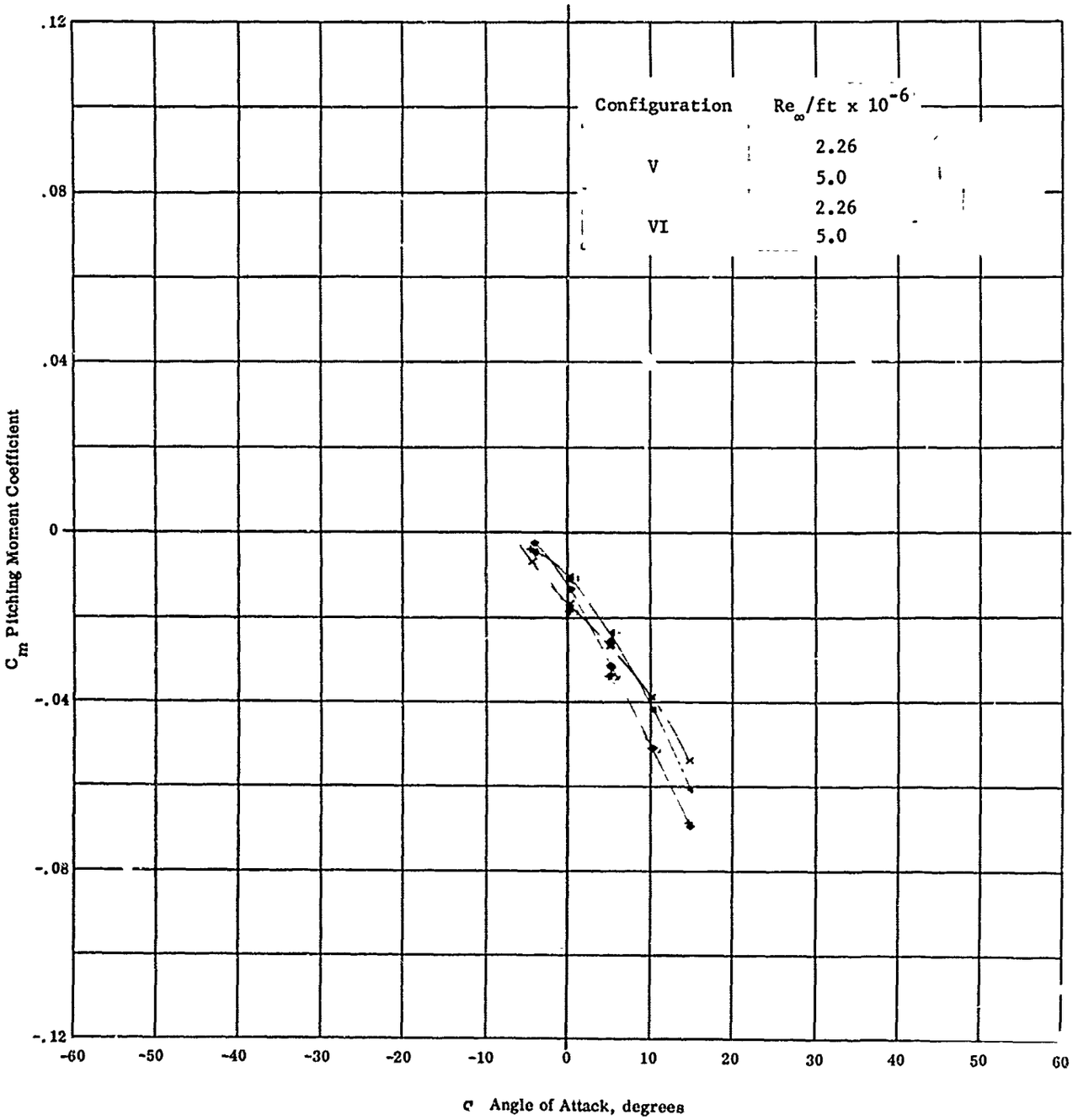

Fig. 6b Configuration V & VI - M_∞=5.01 C_m vs. α
Re_∞/ft x 10^{-6} = 2.26, 5.0 $\delta_1=\delta_2=\delta_3=0$, Spoiler On

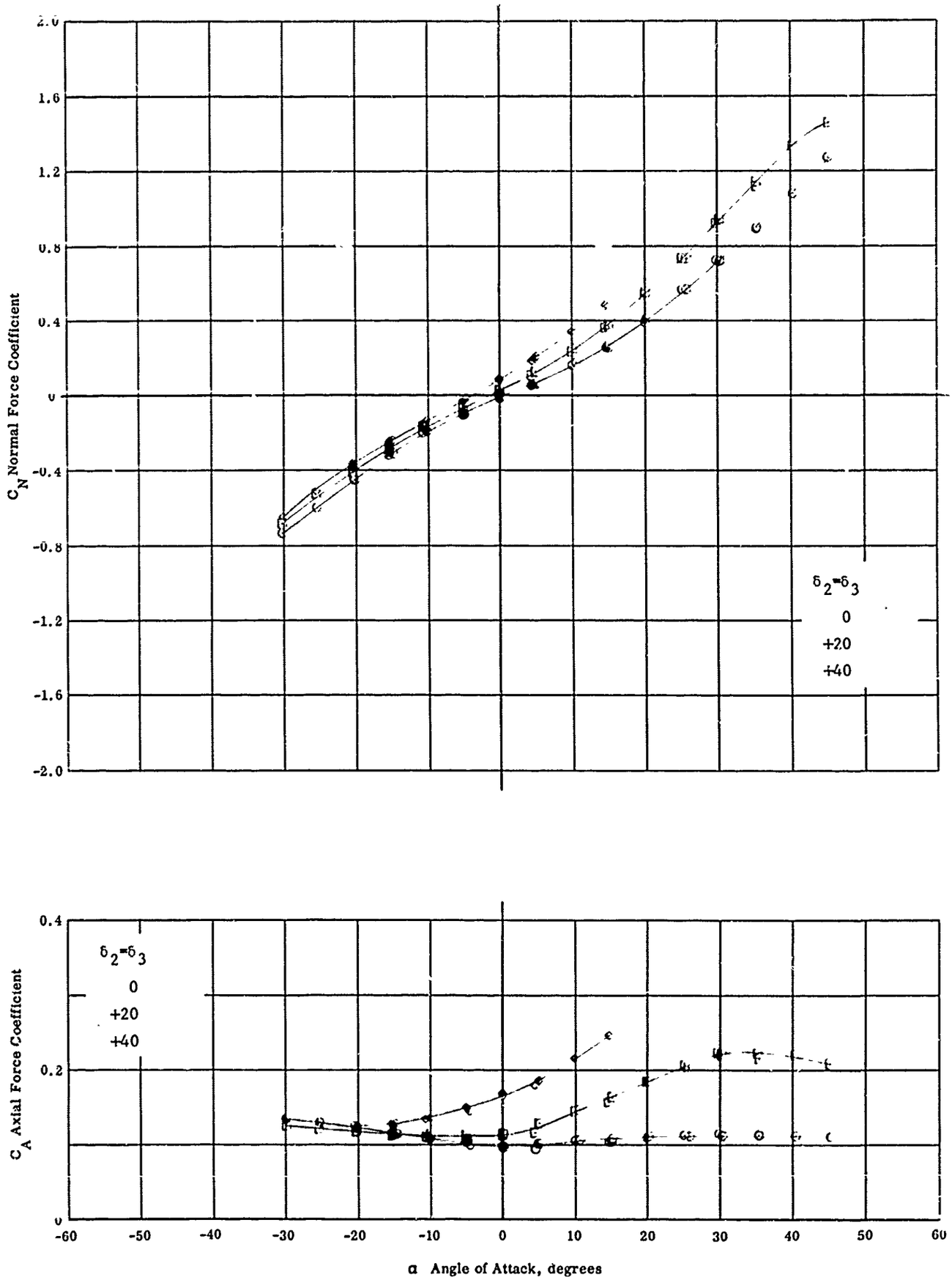

Fig. 7a Configuration IV - M_∞=5.01, C_N & C_A vs. α
$Re_\infty/ft \times 10^{-6}$ = 2.26 δ_1=0 $\delta_2=\delta_3$=0, +20, +40

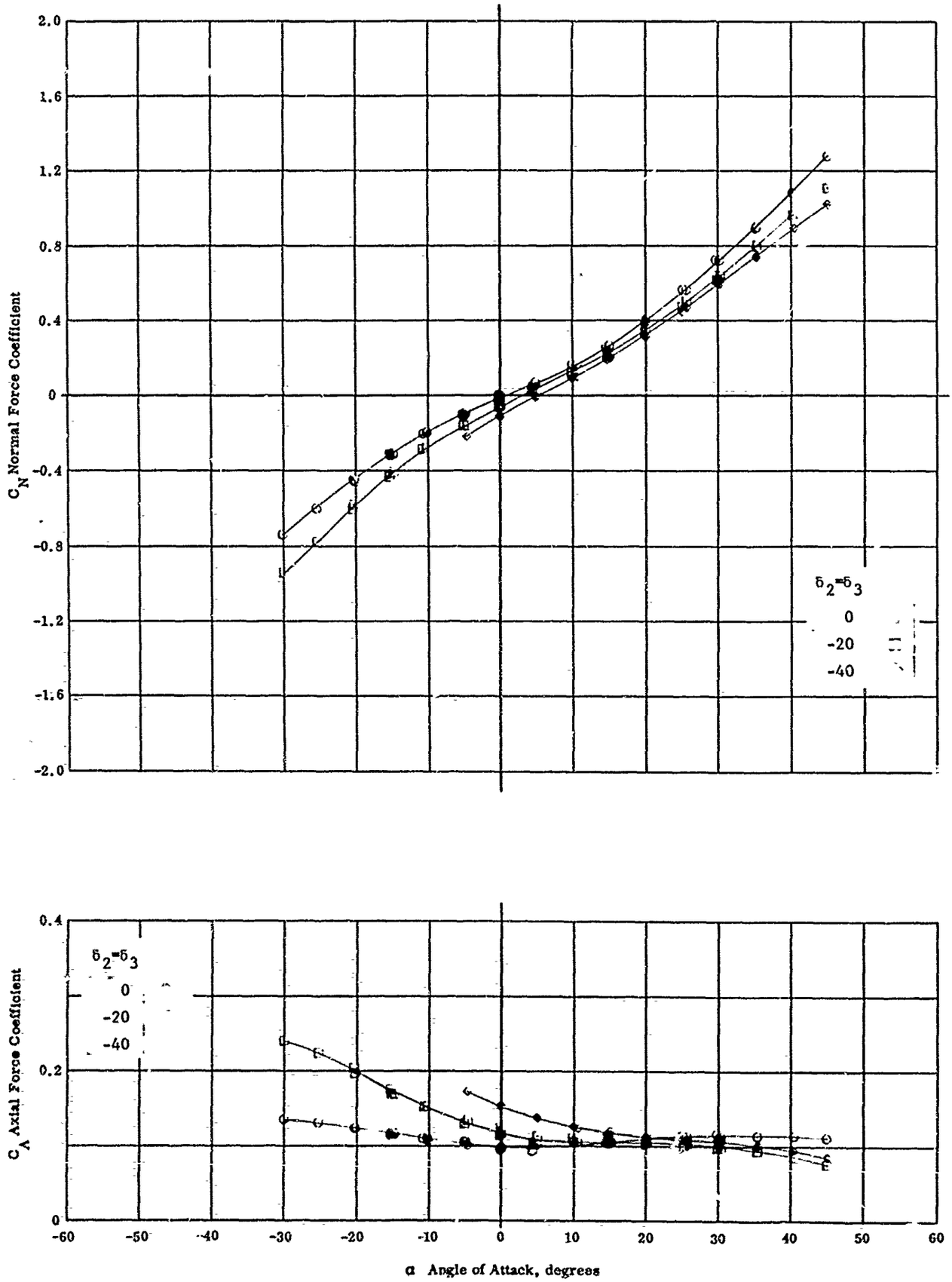

Fig. 7b Configuration IV - M_∞=5.01, C_N & C_A vs. α
$Re_\infty/ft \times 10^{-6}$ = 2.26 δ_1=0 $\delta_2=\delta_3$=0,+20,+40

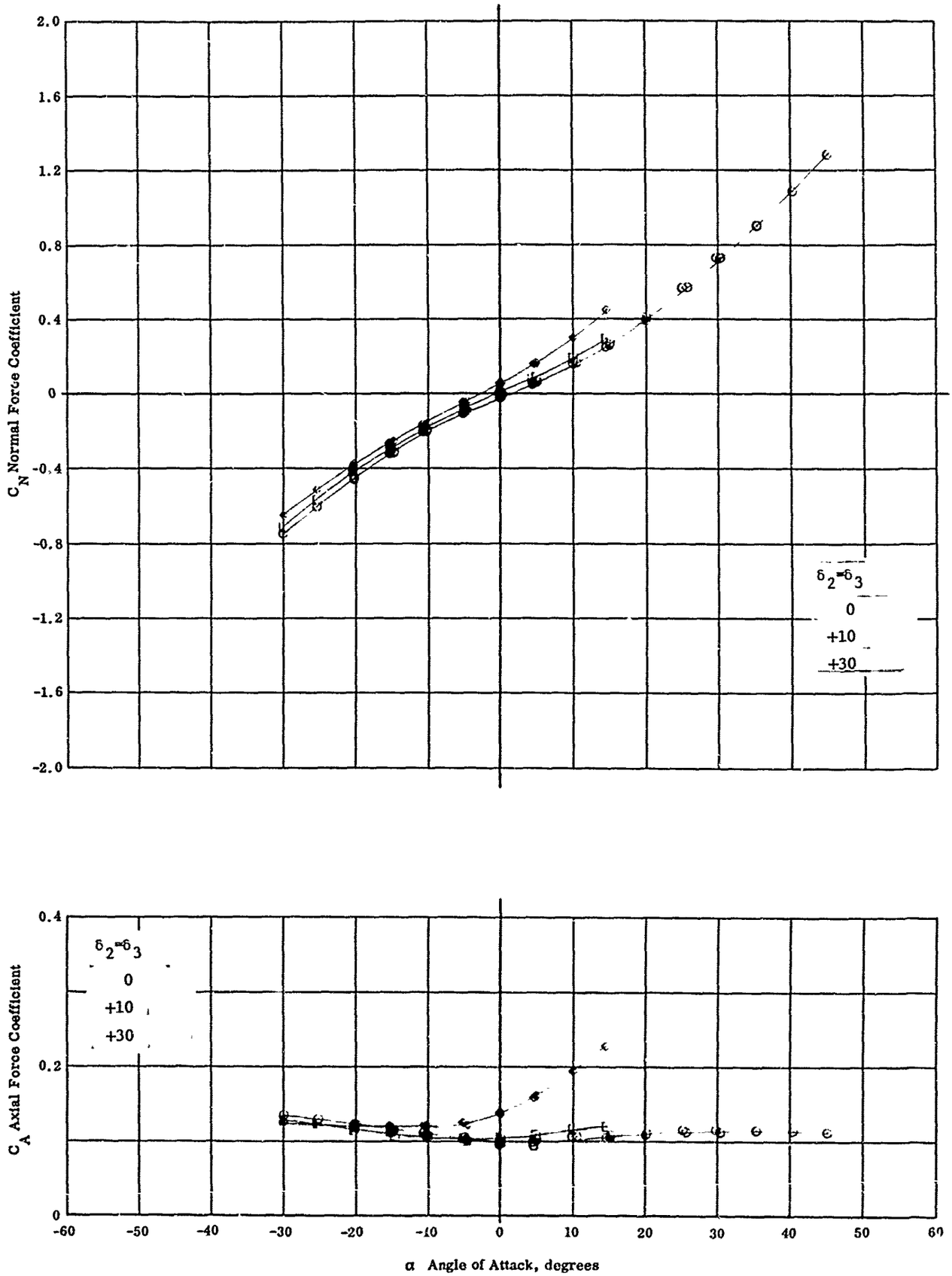

Fig. 7c Configuration IV - M_∞=5.01, C_N& C_A vs. α
Re_∞/ft x 10^{-6} = 2.26 δ_1=0 $\delta_2=\delta_3$=0, +10, +30

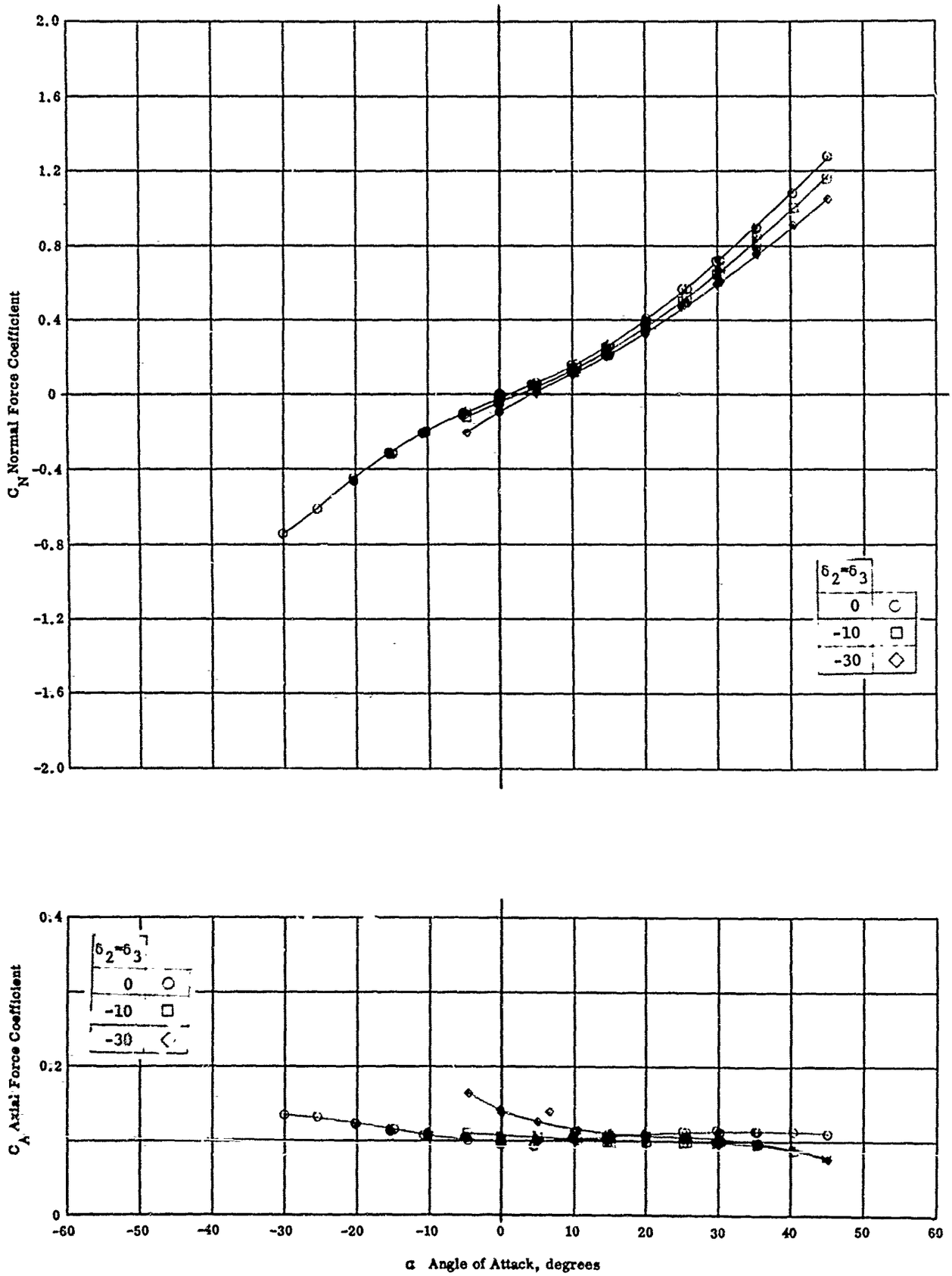

Fig. 7d Configuration IV - M_∞=5.01, C_N & C_A vs. α
$Re_\infty/ft \times 10^{-6}$ = 2.26 δ_1=0 $\delta_2=\delta_3$=0, -10, -30

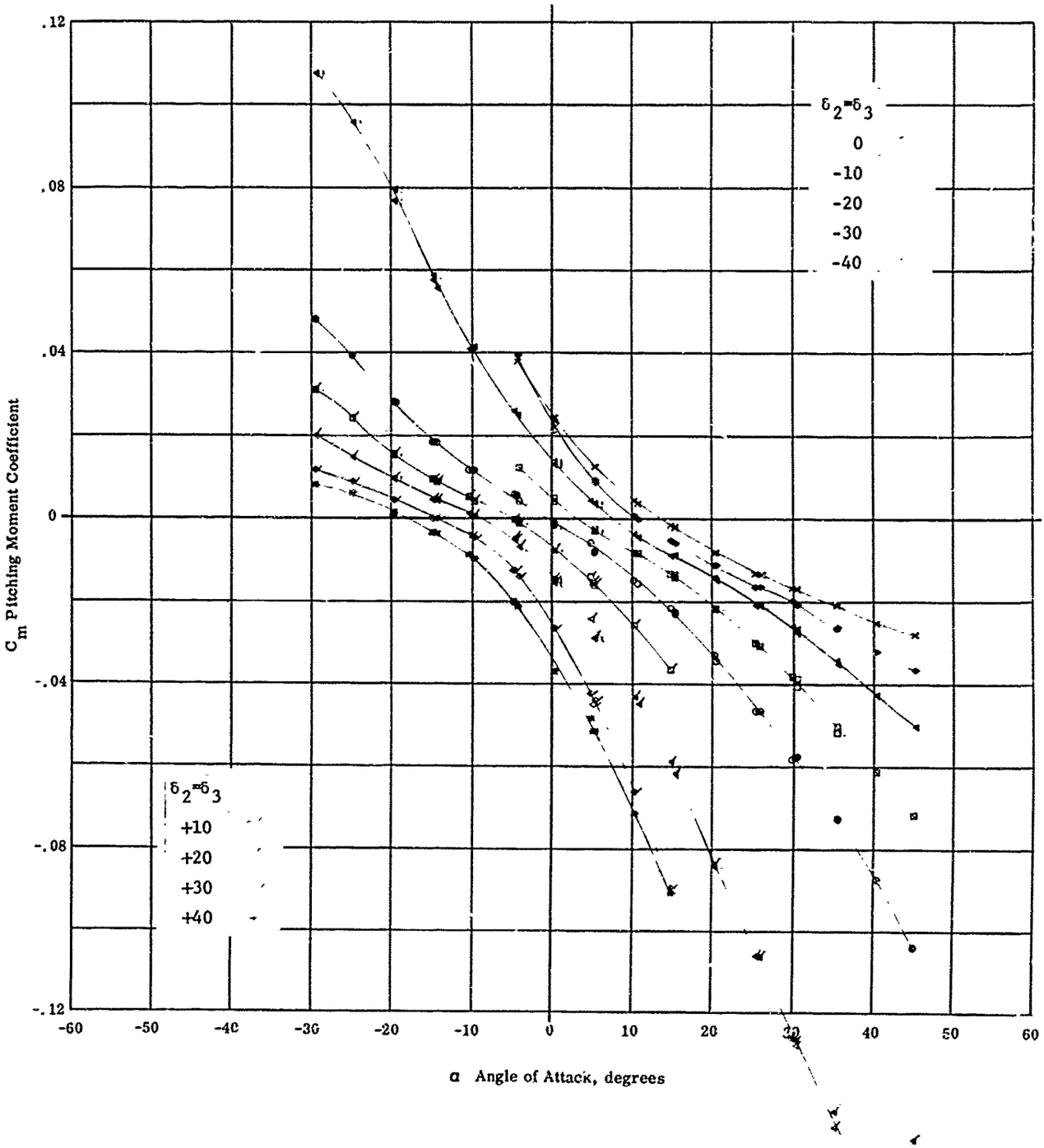

Fig. 7e Configuration IV - M_∞=5.01, C_m vs. α
Re_∞/ft x 10^{-6} = 2.26 δ_1=0 $\delta_2=\delta_3$=0, ±10, +20. +30, +40

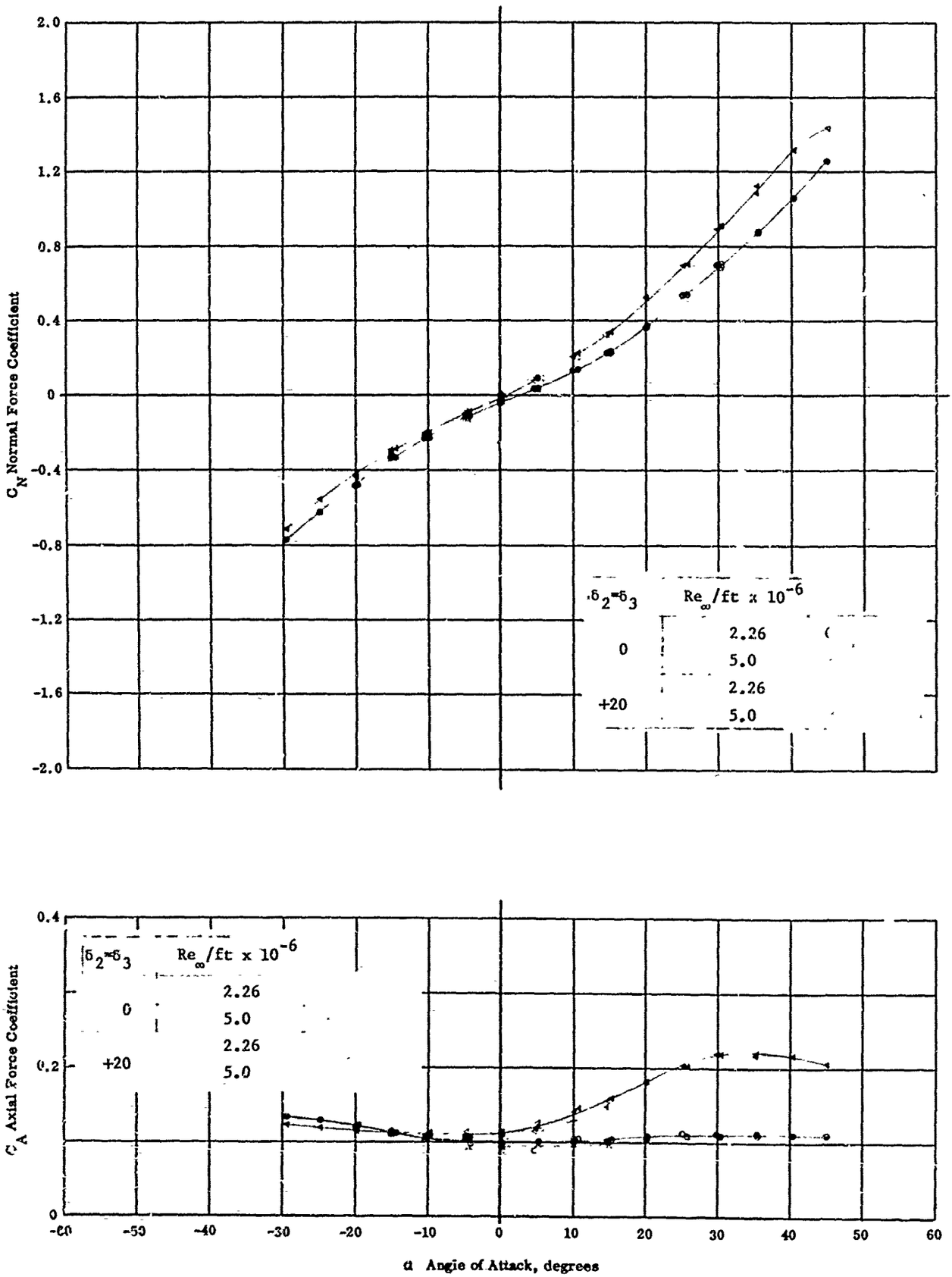

Fig. 8a Configuration IV - M=5.01, C_N & C_A vs. α
$Re_\infty/ft \times 10^{-6}$ = 2.26, 5.0 $\delta_1=0$ $\delta_2=\delta_3=0$, +20

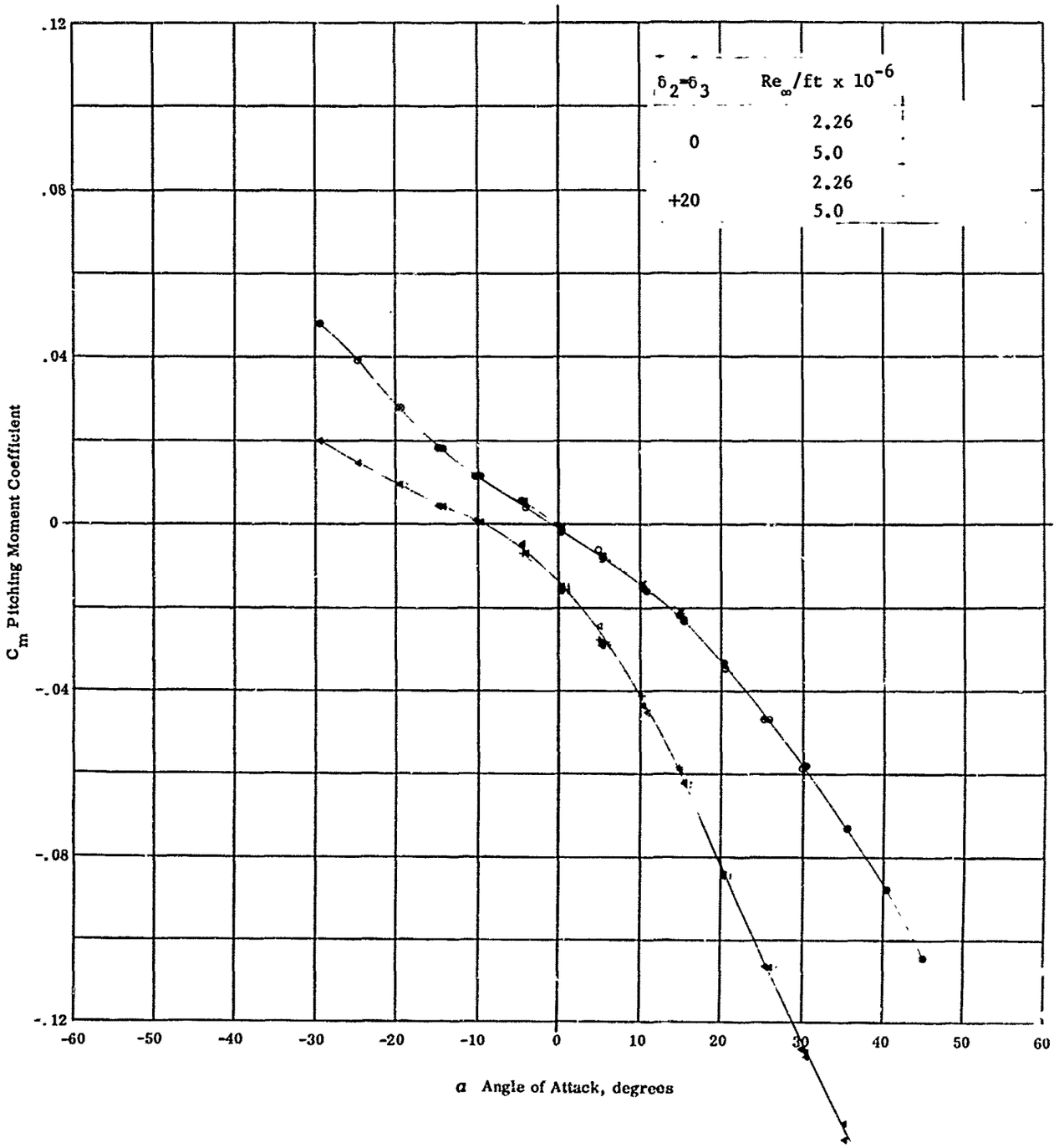

Fig. 8b Configuration IV - M=5.01, C_m vs. α
$Re_\infty/ft \times 10^{-6}$ = 2.26, 5.0 $\delta_1=0$ $\delta_2=\delta_3=0$, +20

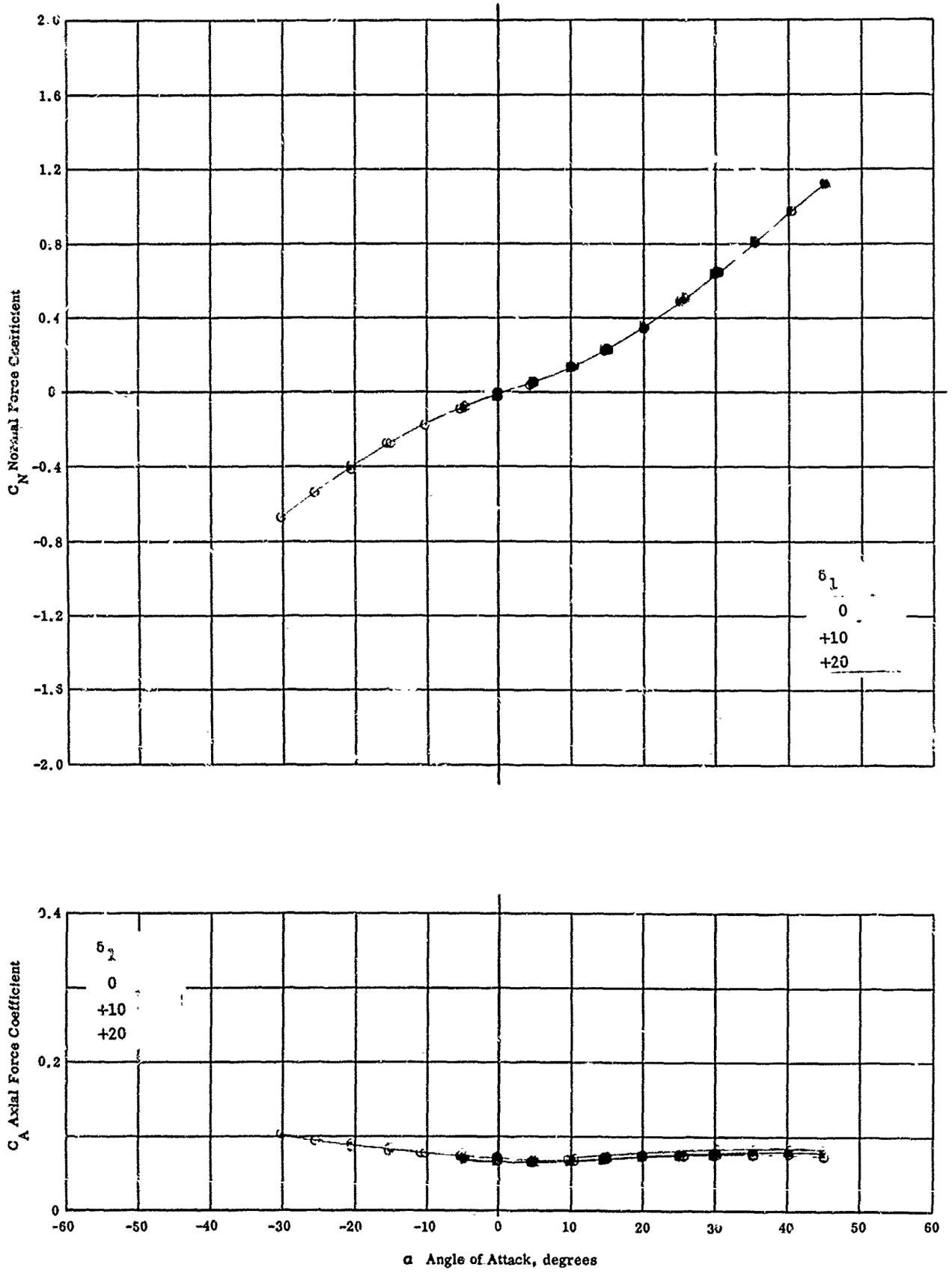

Fig. 9a Configuration I - M_∞=5.01, C_N & C_A vs. α
$Re_\infty/ft \times 10^{-6}$ = 2.26 δ_1=0, +10, +20 δ_2=δ_3=0

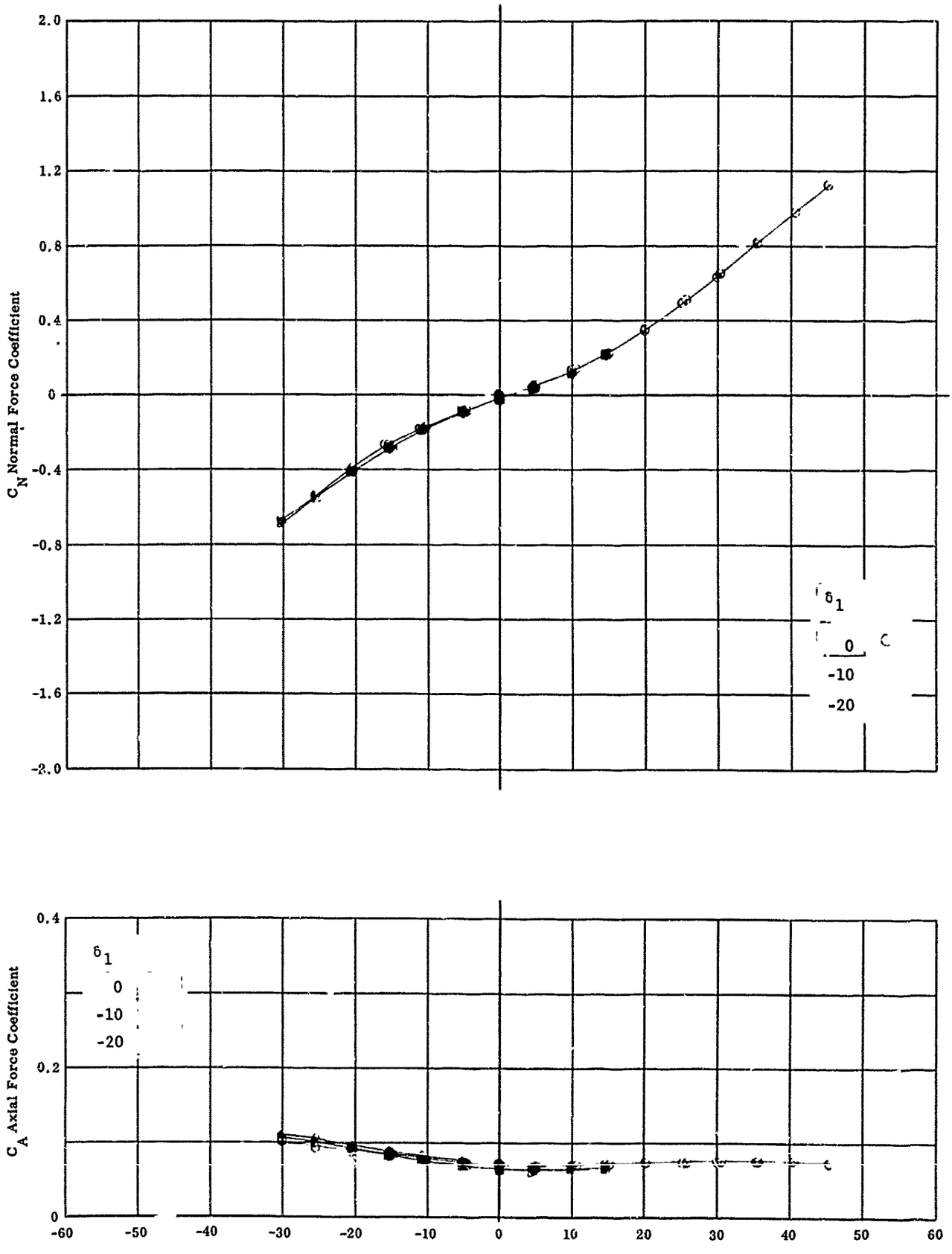

Fig. 9b Configuration I - M_∞=5.01 C_N & C_A vs. α
Re_∞/ft x 10^{-6} = 2.26 δ_1=0, -10, -20 δ_2=δ_3=0

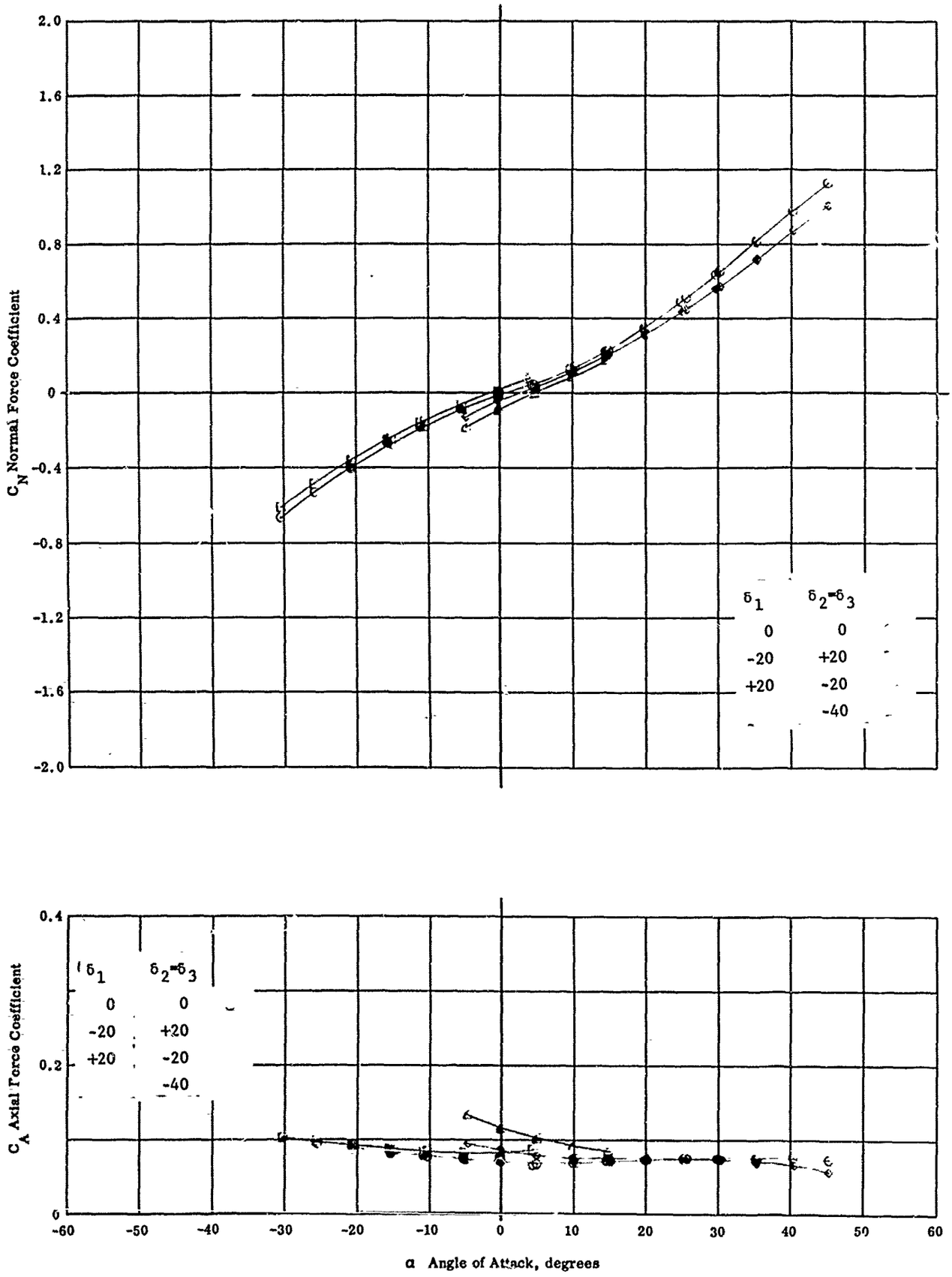

Fig. 9c Configuration I - M_∞=5.01, C_N & C_A vs. α
$Re_\infty/ft \times 10^{-6}$ = 2.26 $\delta_1=\delta_2=\delta_3=0$, δ_1= -20 $\delta_2=\delta_3$= +20,
δ_1= +20 $\delta_2=\delta_3$= -20, -40

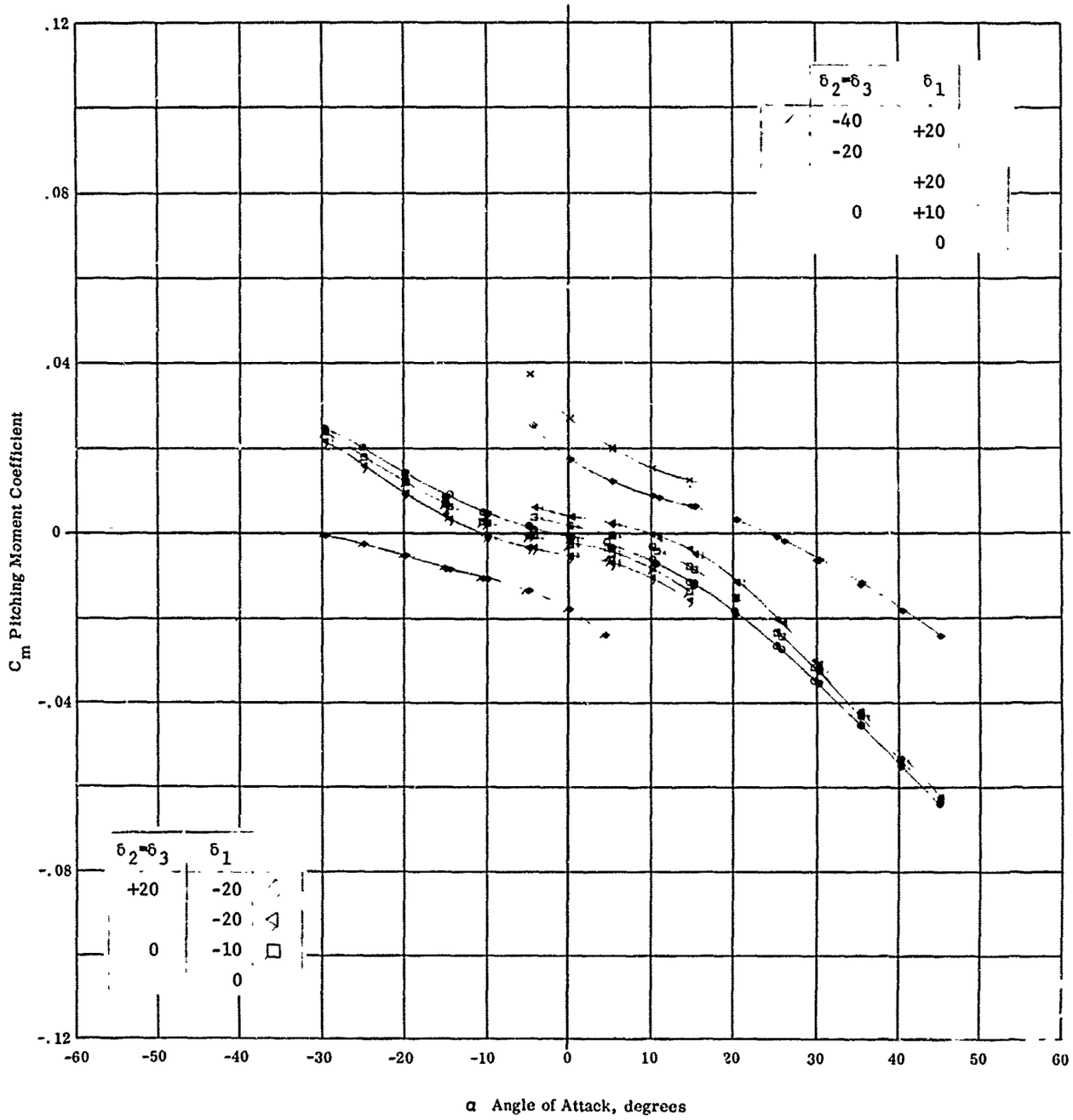

Fig. 9d Configuration I - M_∞=5.01, C_m vs. α

Re_∞/ft x 10^{-6} = 2.26 δ_1=0, ±10, ±20 $\delta_2=\delta_3$=0

δ_1= -20 $\delta_2=\delta_3$= +20

δ_1= +20 $\delta_2=\delta_3$=-20, -40

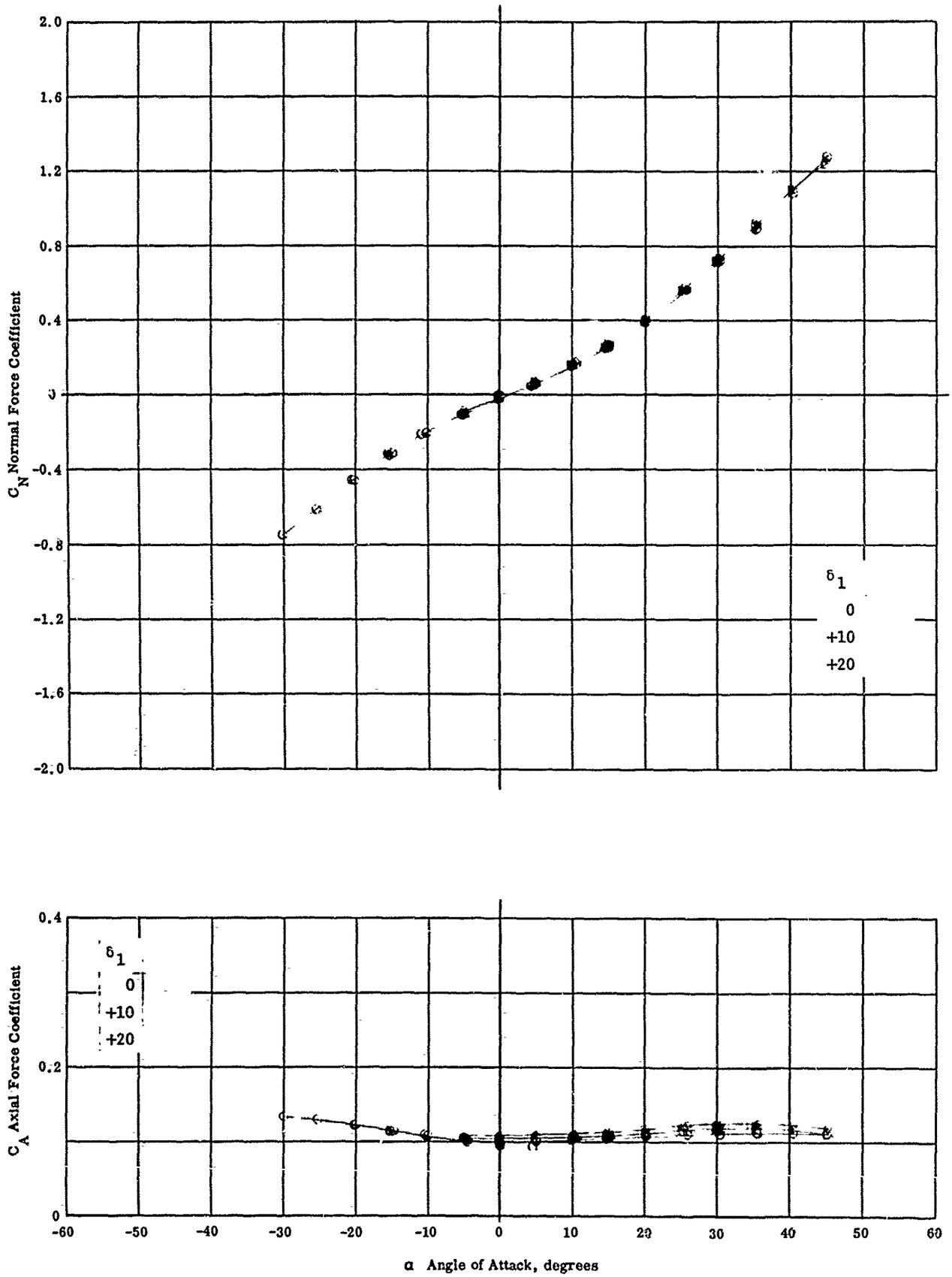

Fig. 10a Configuration IV - M_∞=5.01, C_N & C_A vs. α
Re_∞/ft x 10^{-6} δ_1=0, +10, +20 δ_2=δ_3=0

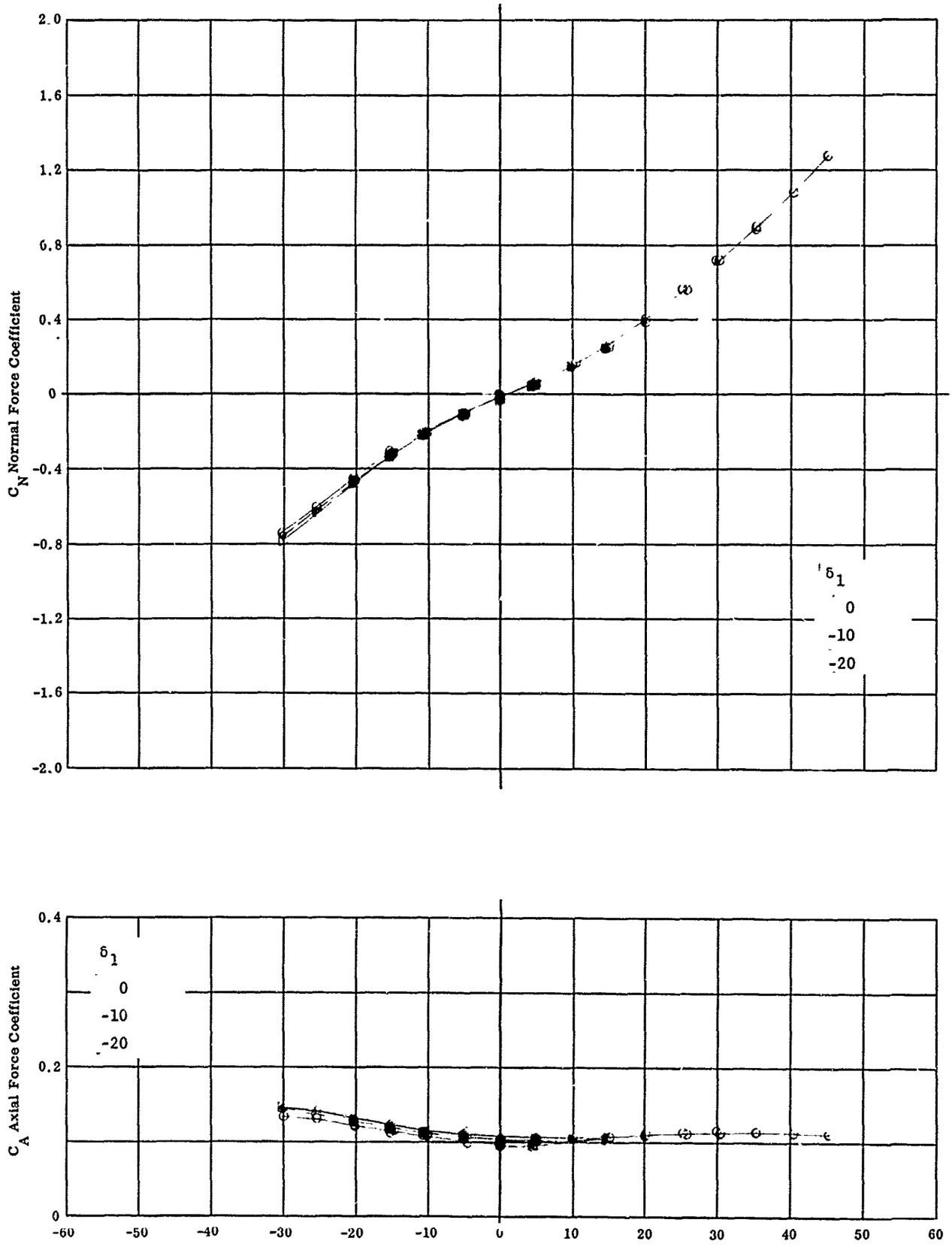

Fig. 10b Configuration IV - M_∞=5.01, C_N & C_A bs. α
Re_∞/ft x 10^{-6} δ_1=0, -10, -20 δ_2=δ_3=0

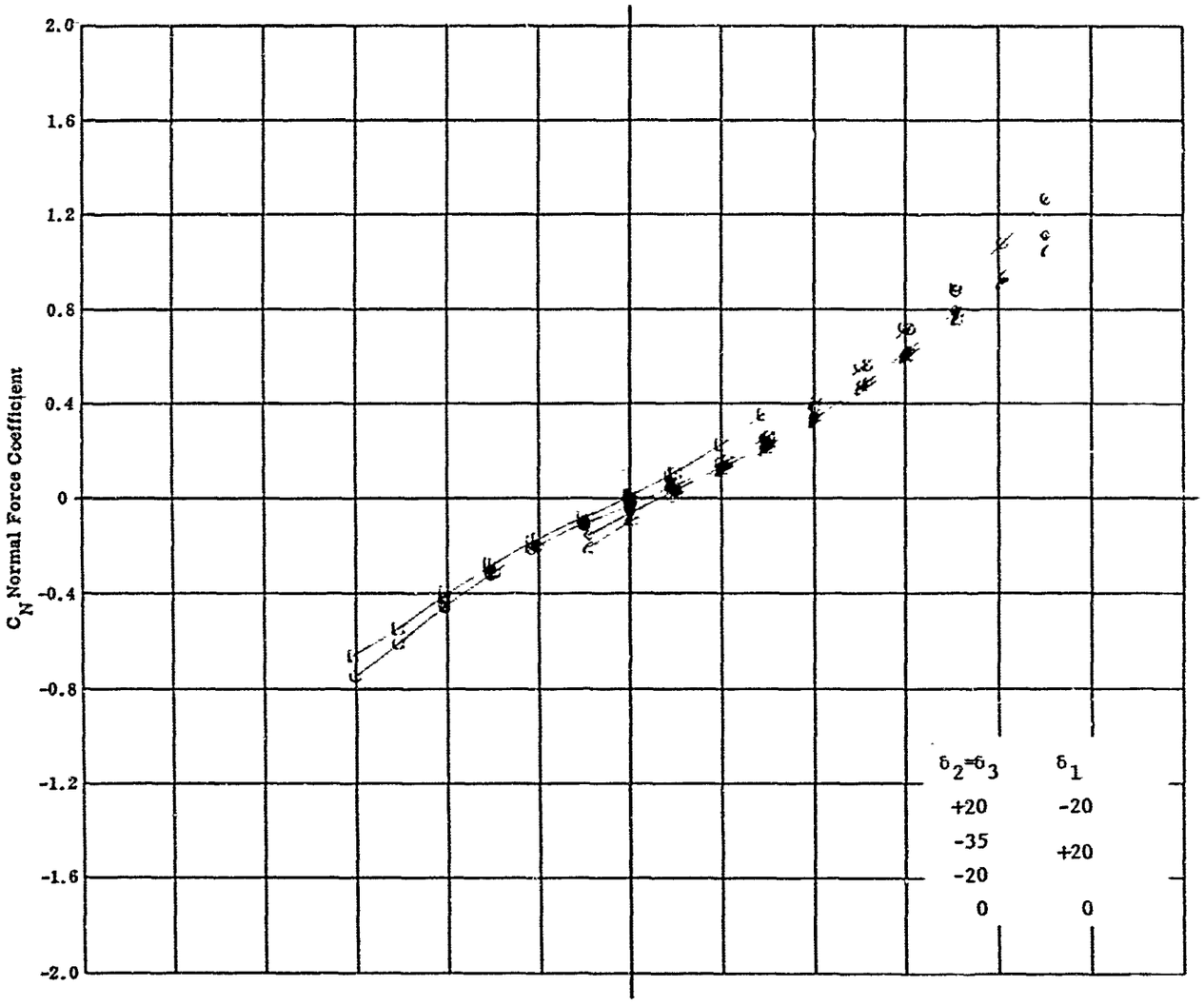

Fig. 10c Configuration IV - M_∞=5.01, C_N & C_A vs. α
$Re_\infty/ft \times 10^{-6}$=2.26 $\delta_1=\delta_2=\delta_3=0$
δ_1=-20 $\delta_2=\delta_3$= +20
δ_1=+20 $\delta_2=\delta_3$=-20, -35

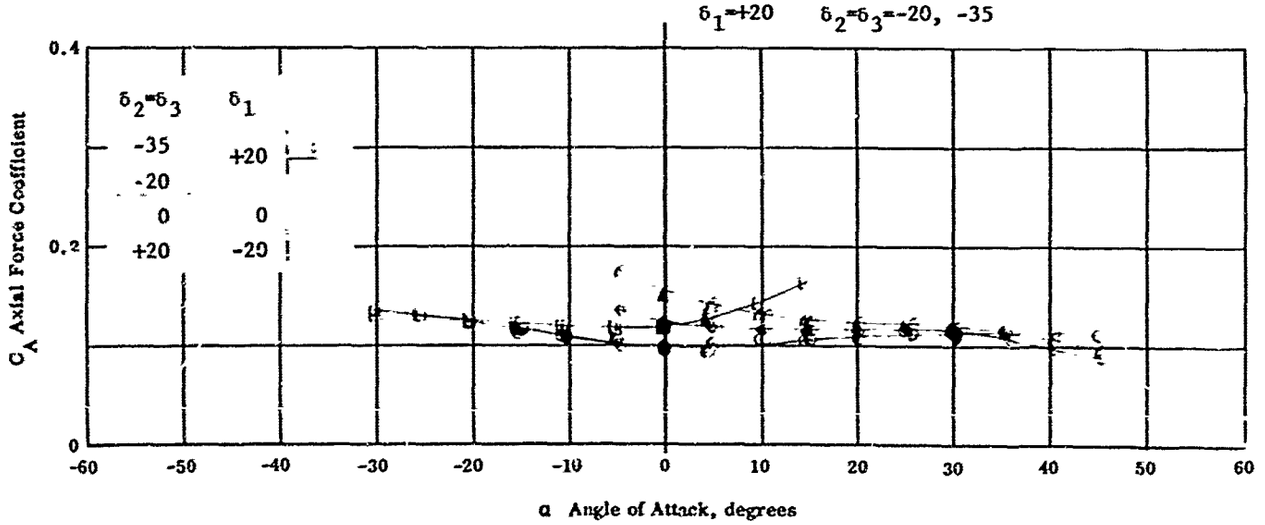

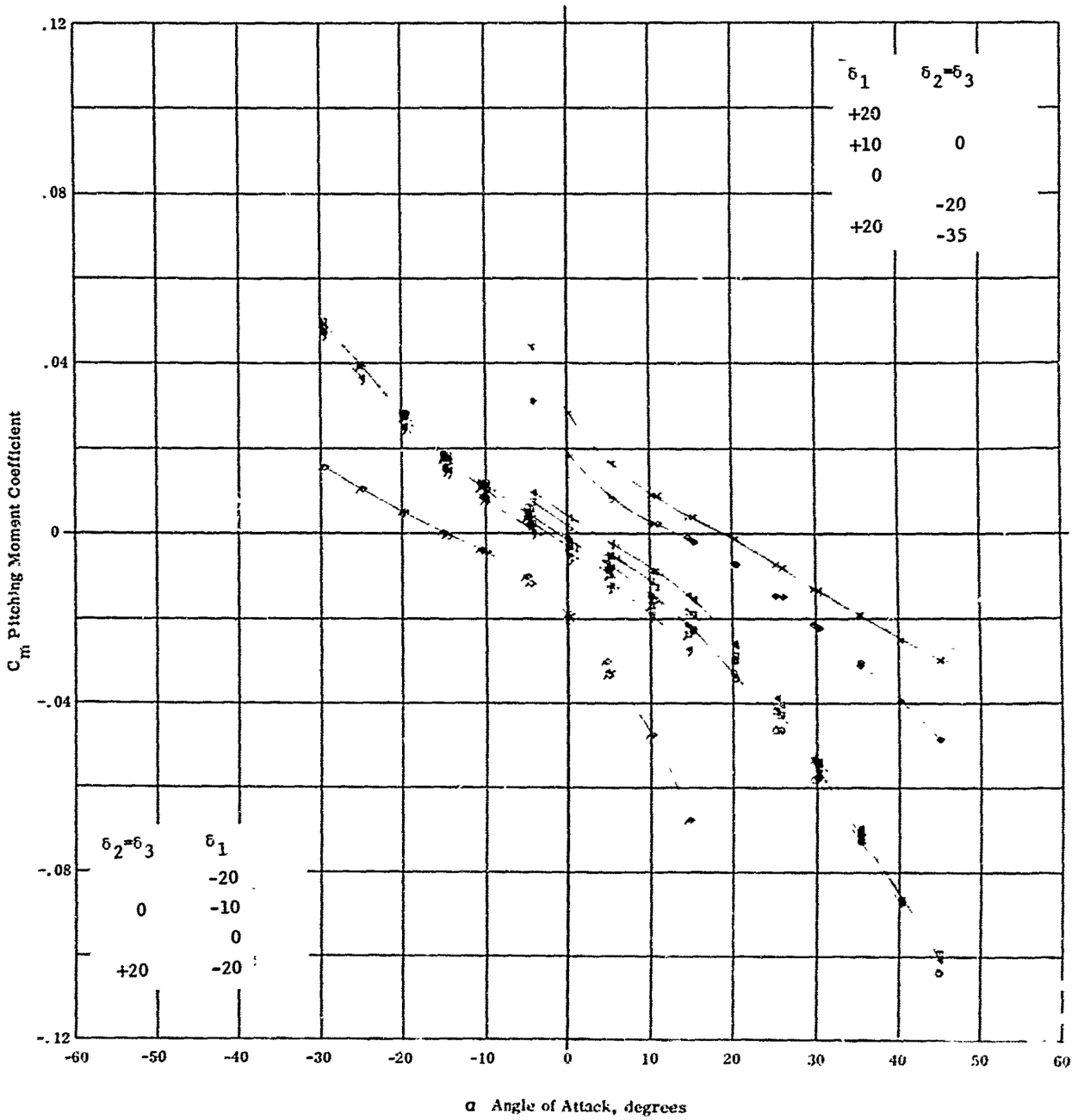

Fig. 10d Configuration IV - M =5.01, C_m vs.
Re_∞ / ft x 10^{-6} = 2.26 δ_1=0, ±10, -20, δ_2=δ_3=0
δ_1=-20 δ_2=δ_3= +20
δ_1=+20 δ_2=δ_3= -20, -35

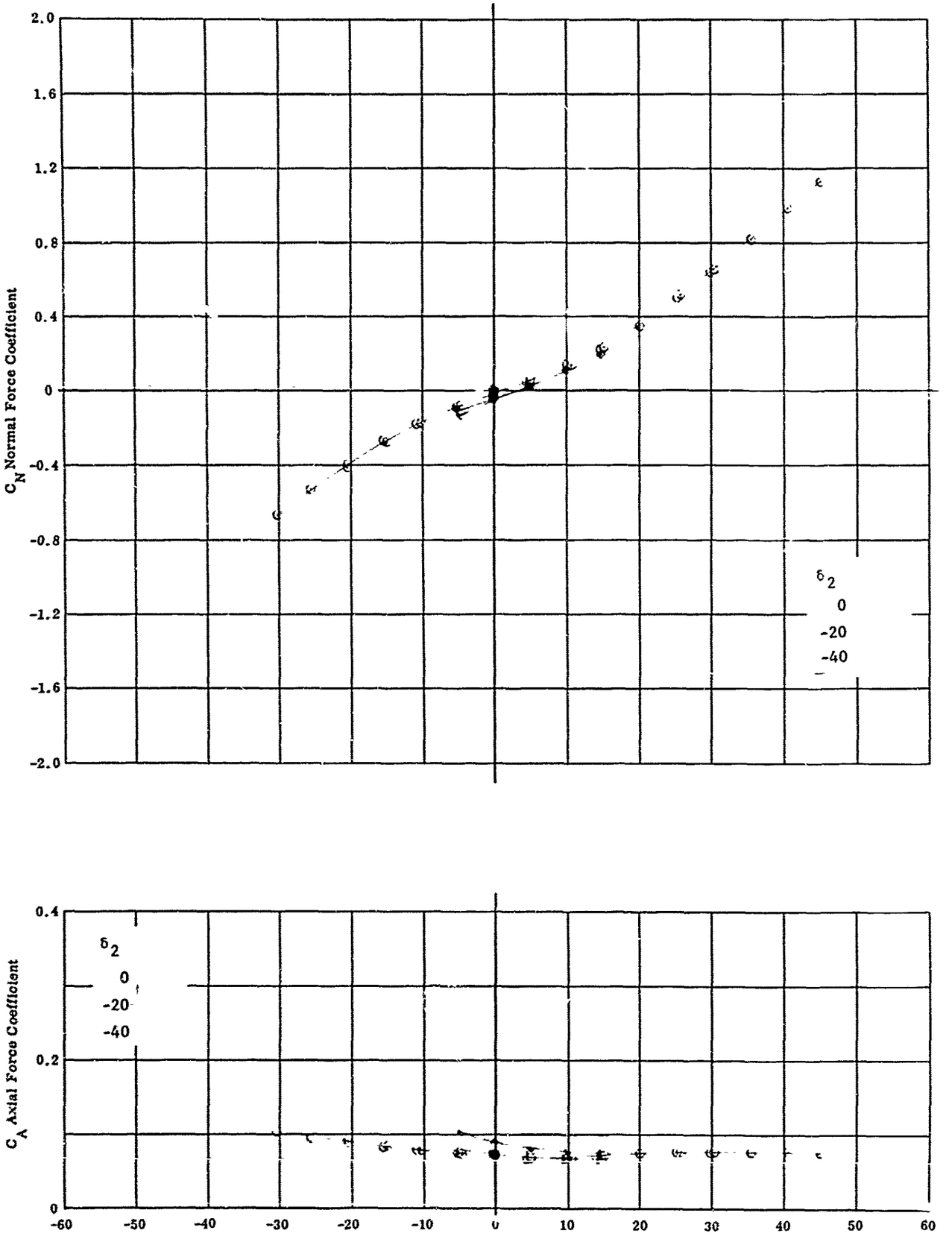

Fig. 11a Configuration I - M_∞=5.01 C_N & C_A vs. α
$Re_\infty/ft \times 10^{-6}$ = 2.26 $\delta_1=\delta_3=0$ δ_2=0,-20,-40

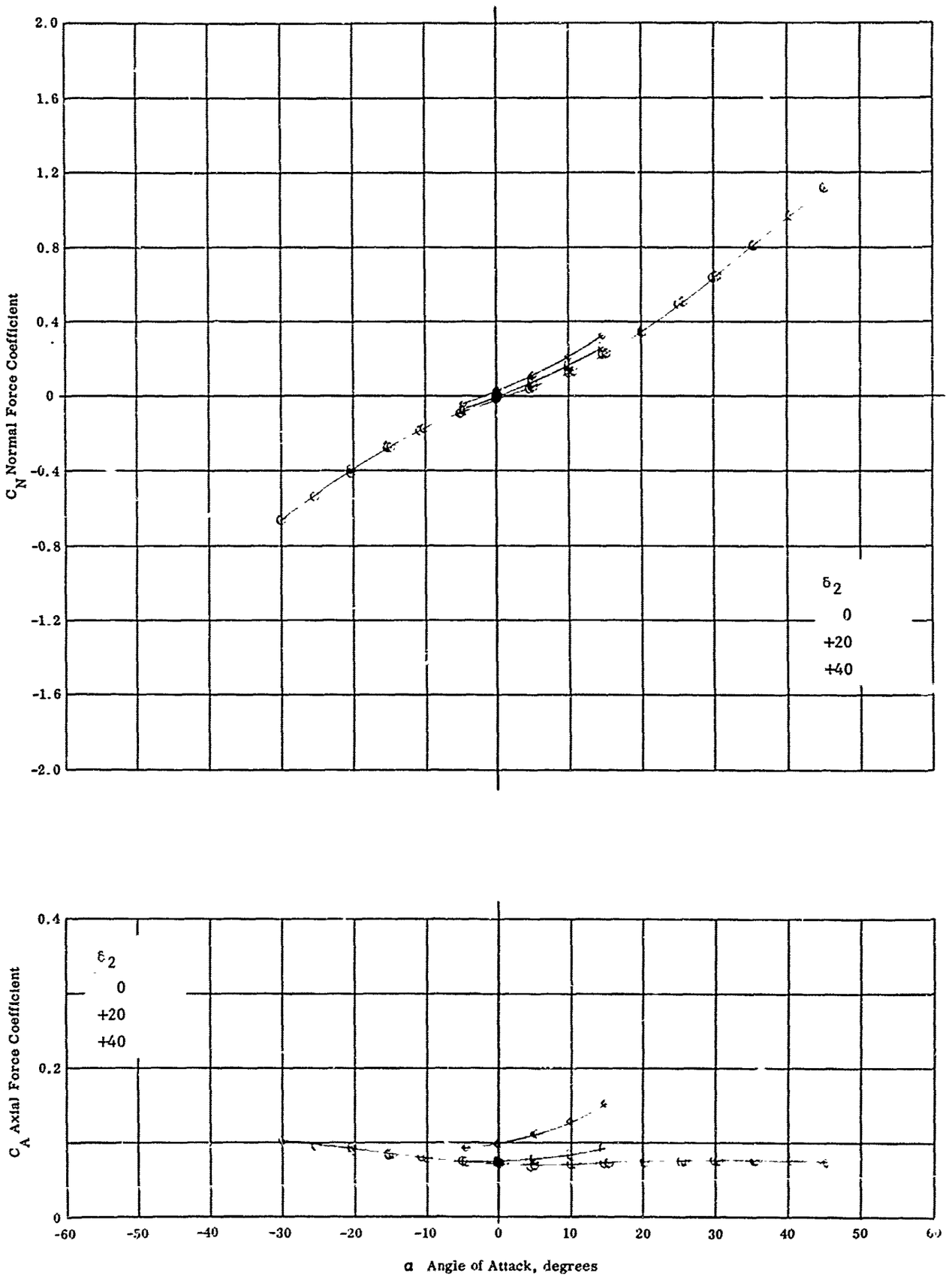

Fig. 11b Configuration I - M_∞=5.01 C_N & C_A vs. α
Re/ft x 10^{-6} $\delta_1=\delta_3=0$ $\delta_2=0,+20,+40$

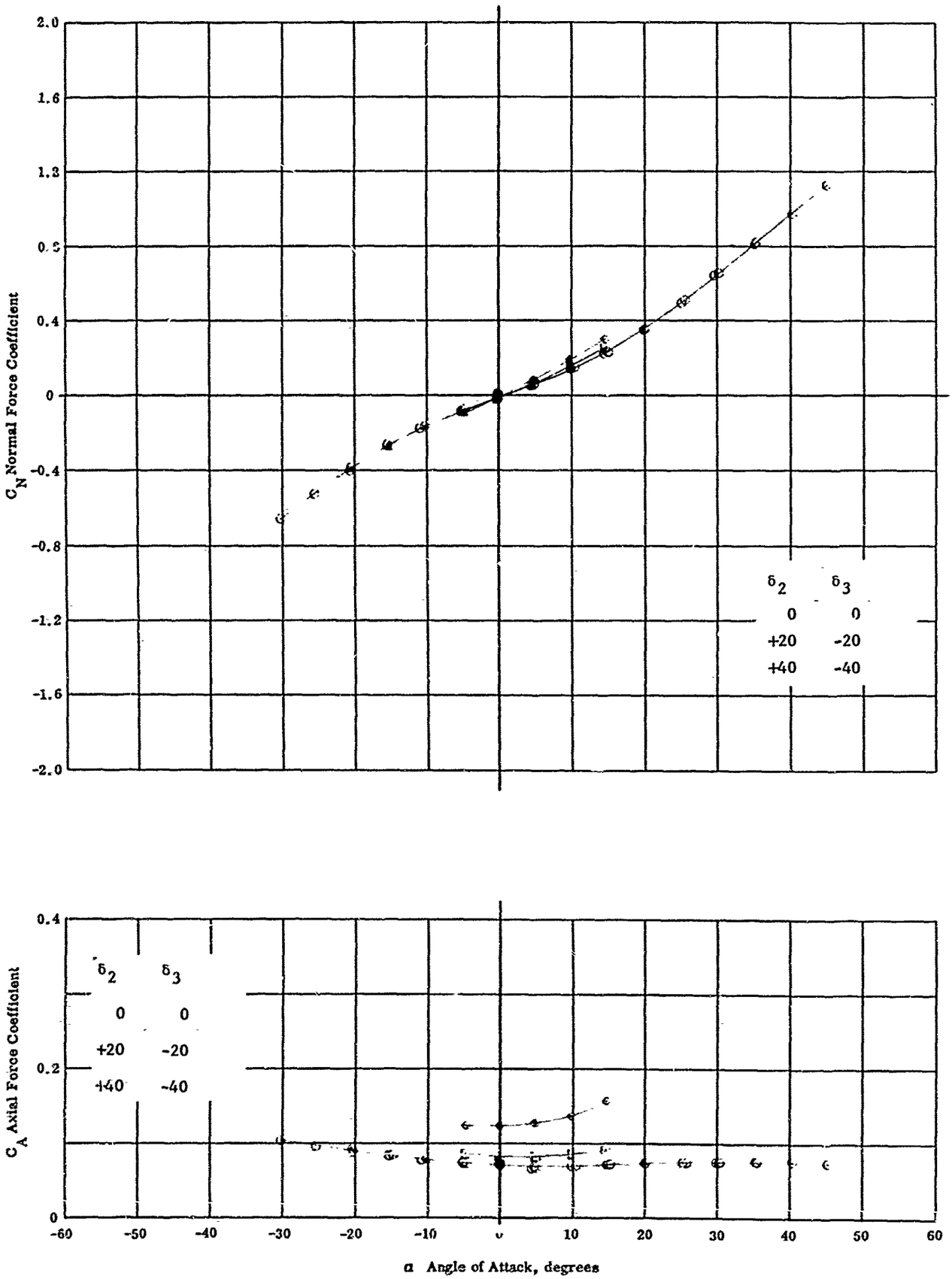

Fig. 11c Configuration I - M_∞=5.01 C_N & C_A vs. α
$Re_\infty/ft \times 10^{-6}$ = 2.26 δ_1=0 δ_2=-δ_3=0, +20, +40

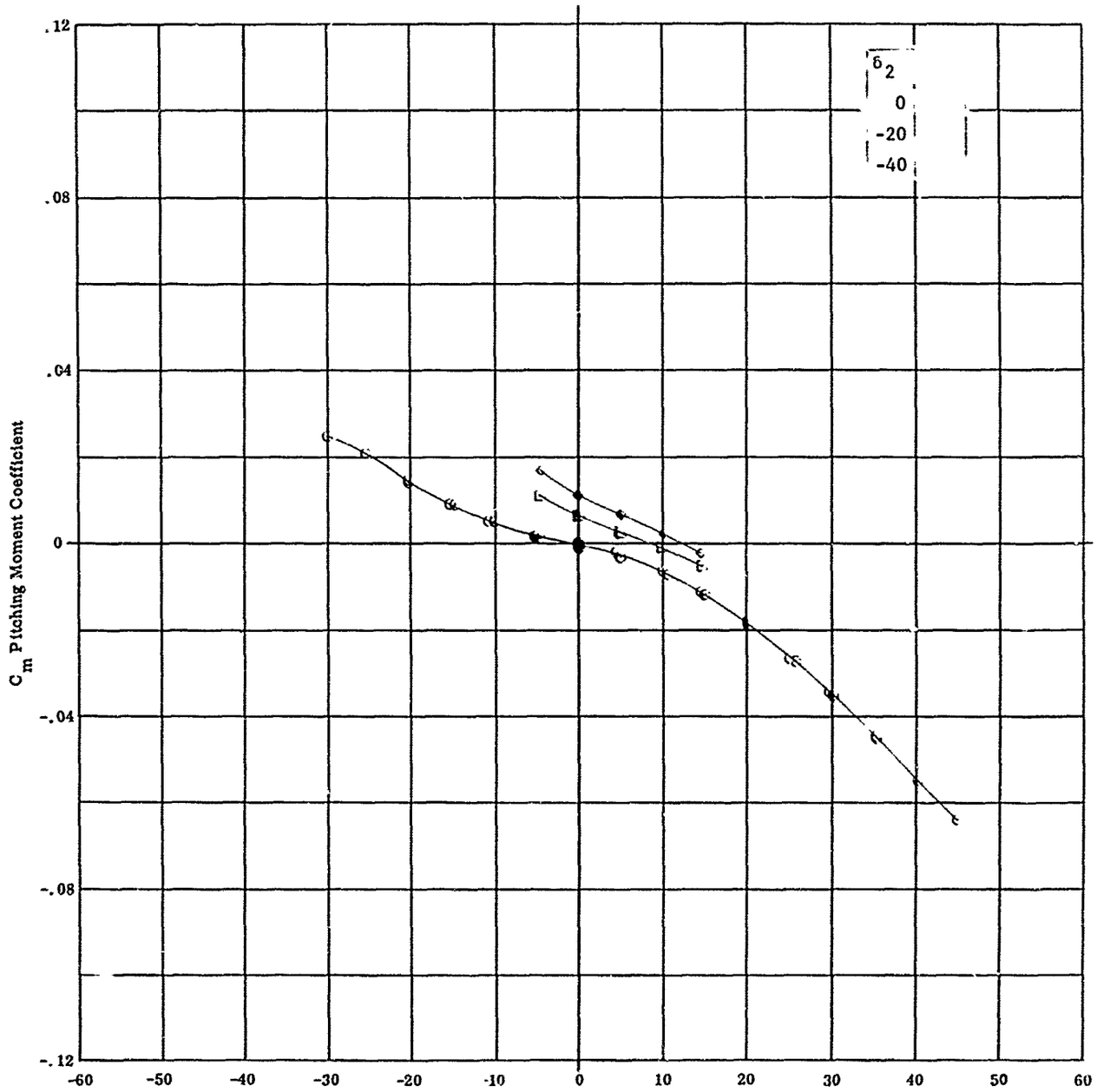

Fig. 11d Configuration I - M_∞=3.01 C_m vs. α
$Re_\infty/ft \times 10^{-6}$ = 2.26 $\delta_1=\delta_3=0$ δ_2=0, -20, -40

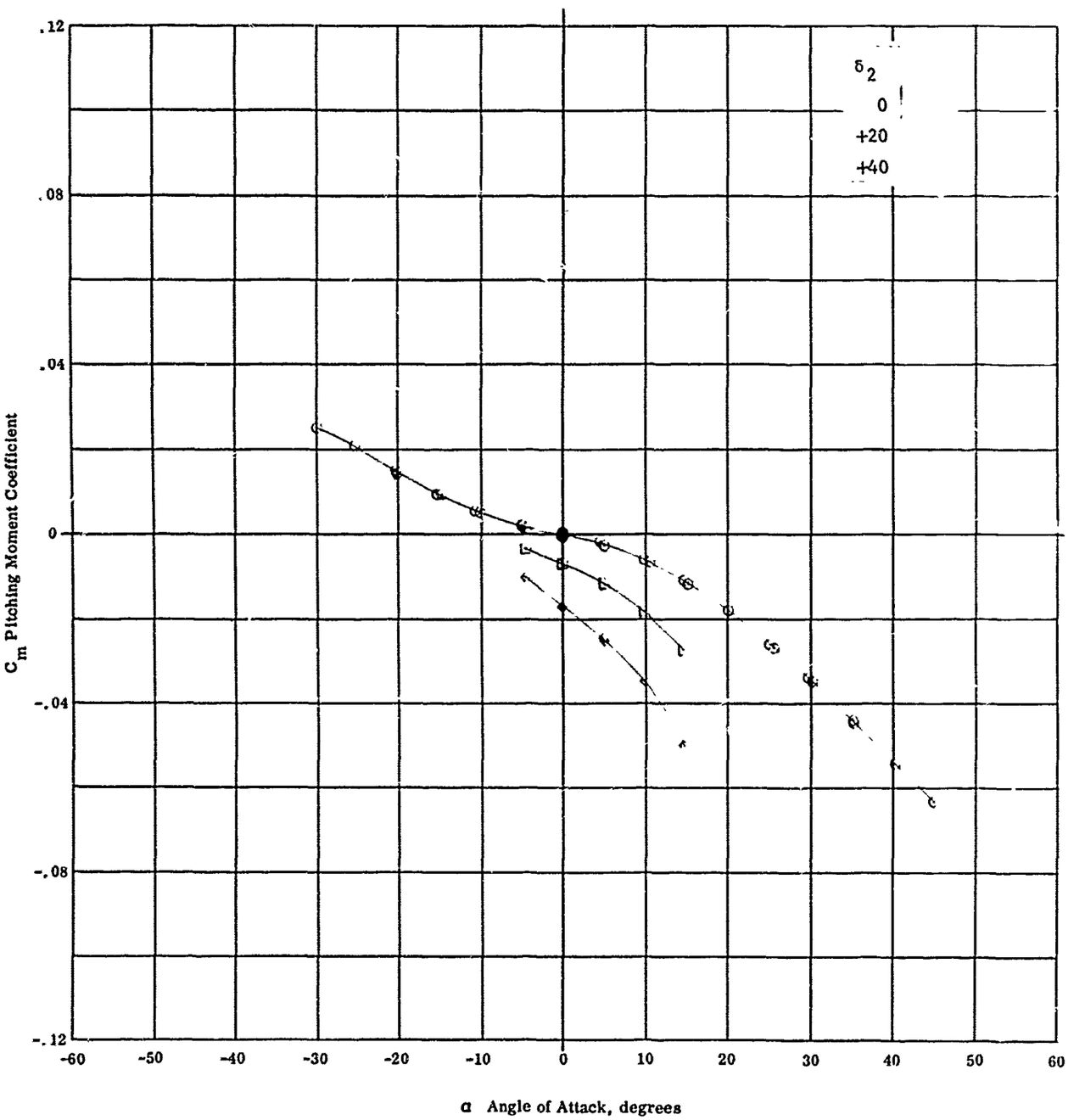

Fig. 11e Configuration I - M_∞=5.01 C_m vs. α
Re_∞/ft x 10^{-6}= 2.26 $\delta_1=\delta_3=0$ δ_2=0,+20,+40

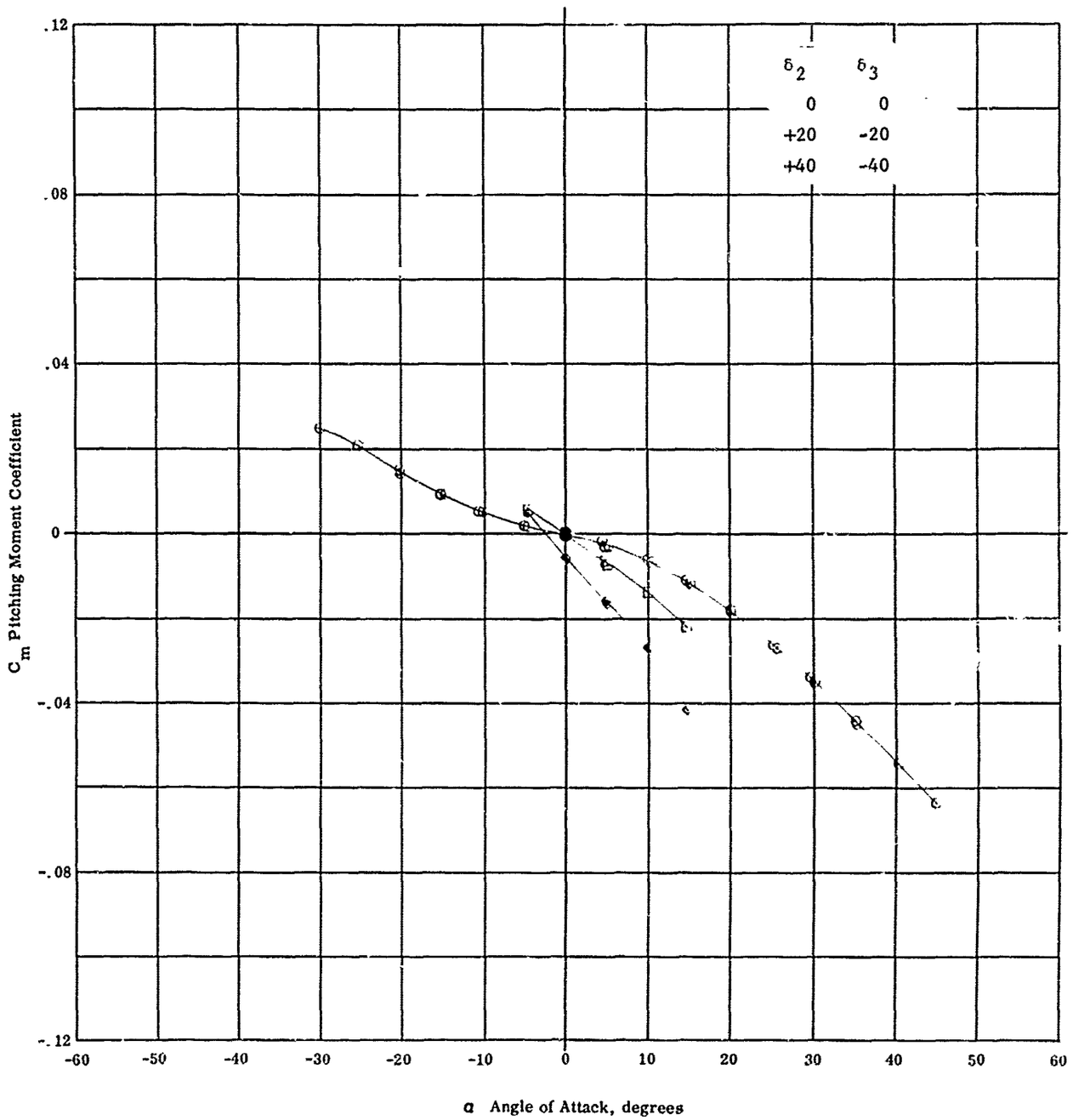

Fig. 11f Configuration I - M_∞=5.01 C_m vs. α
$Re_\infty/ft \times 10^{-6}$ = 2.26 δ_1=0 δ_2=-δ_3=0, +20, +40

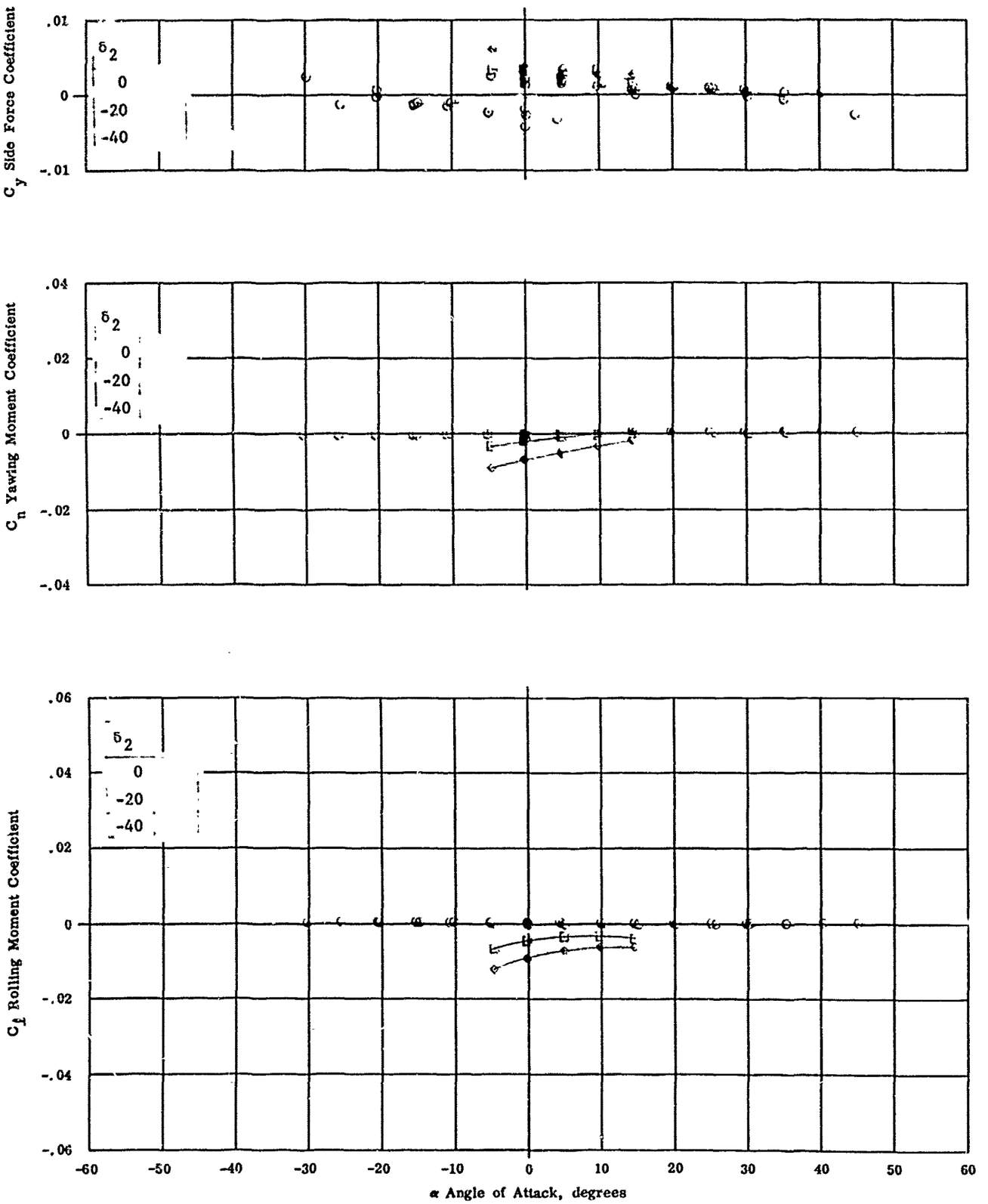

Fig. 11g Configuration I - M_∞=5.01 C_y, C_m, C_ℓ vs. α
$Re_\infty/ft \times 10^{-6}$ = 2.26 $\delta_1=\delta_3=0$ δ_2=0, -20, -40

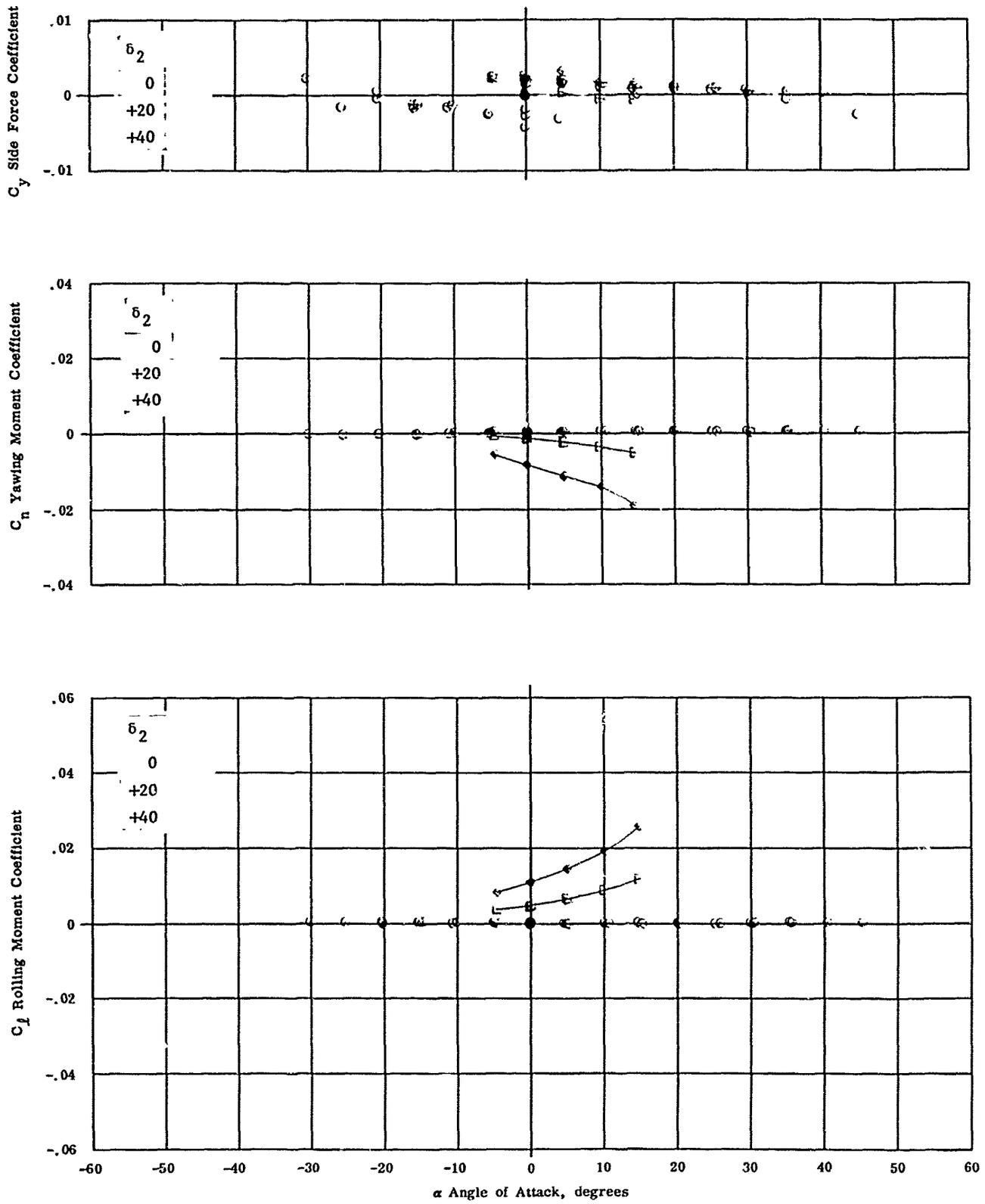

Fig. 11h Configuration I - M_∞=5.01 C_y, C_n, C_ℓ vs. α
$Re_\infty/f \times 10^{-6}$ = 2.26 $\delta_1=\delta_3=0$ δ_2=0, +20, +40

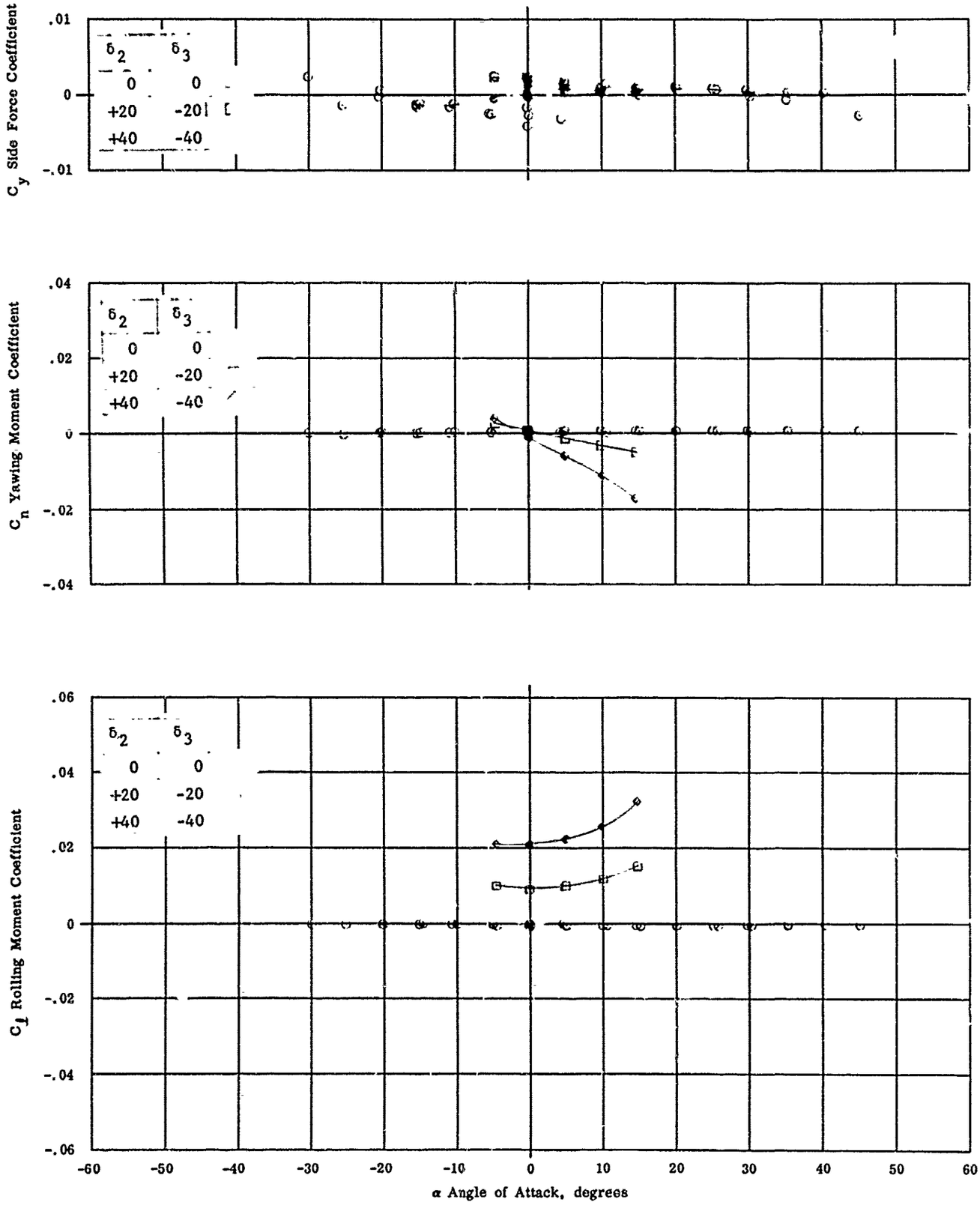

Fig. 111 Configuration I - M_∞=5.01, C_y, C_n, C_ℓ vs. α
$Re_\infty/ft \times 10^{-6}$ = 2.26 δ_1=0 δ_2=-δ_3=0,+20,+40

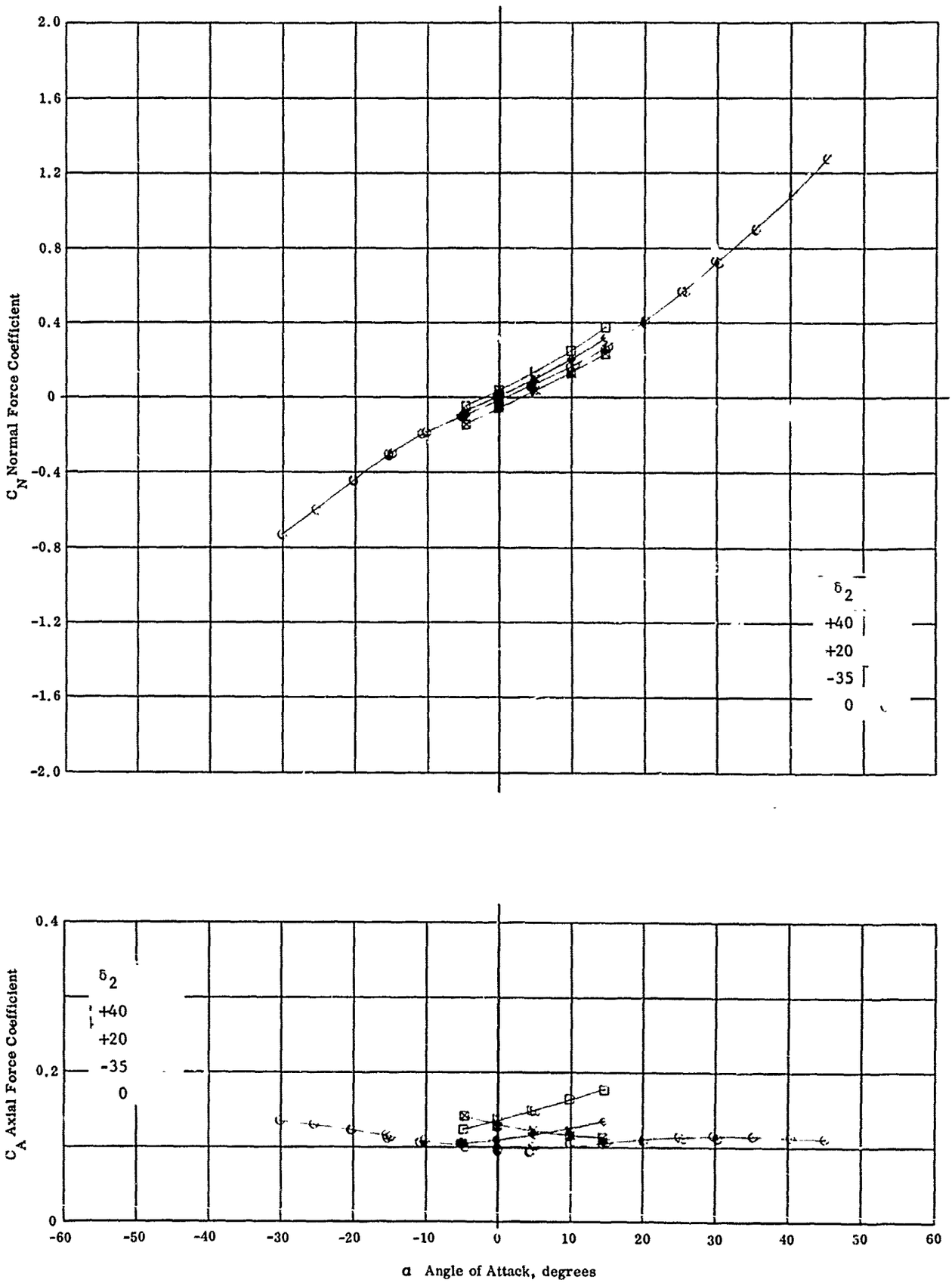

Fig. 12a Configuration IV - M_∞=5.01, C_N & C_A vs. α
Re_∞/ft x 10^{-6} = 2.26 $\delta_1=\delta_3=0$ δ_2=-35,0,+20,+40

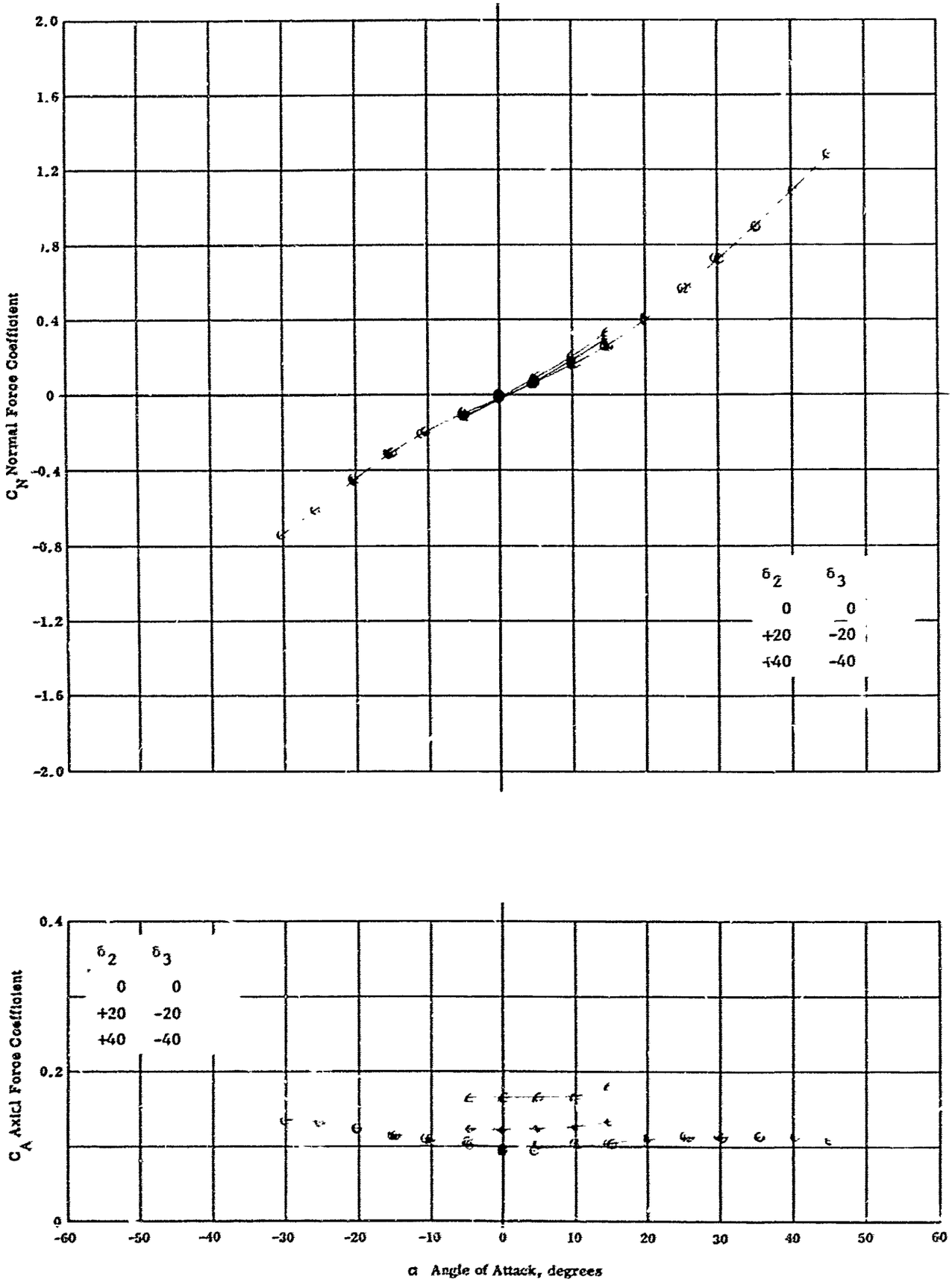

Fig. 12b Configuration IV - M_∞=5.01, C_N & C_A vs. α
$Re_\infty/ft \times 10^{-6}$ = 2.26 δ_1=0 δ_2=-δ_3=0,+20,+40

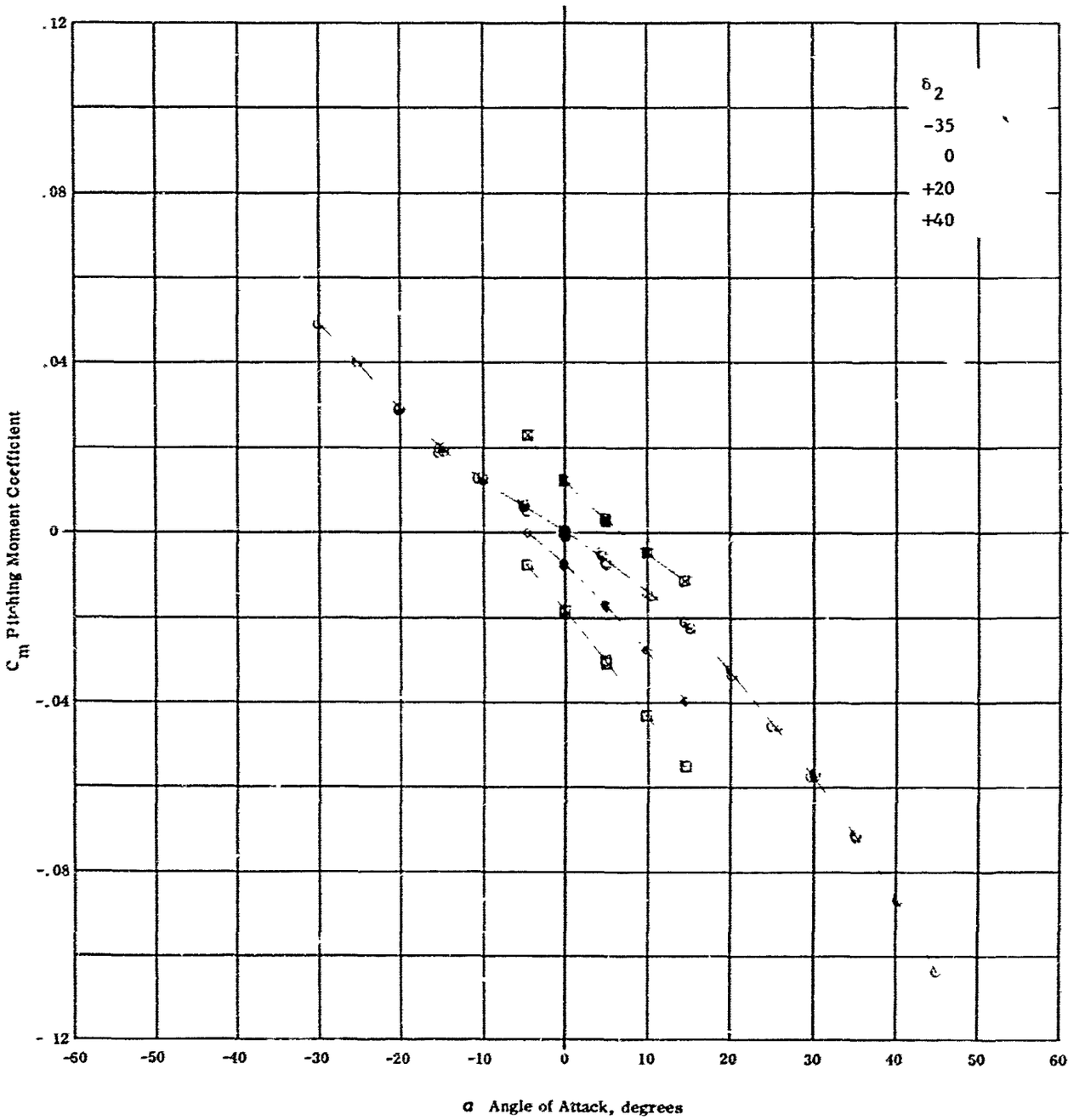

Fig. 12c Configuration IV - M_∞=5.01, C_m vs. α

Re_∞/ft x 10^{-6} = 2.26 δ_1=δ_3=0 δ_2=-35, 0, +20, +40

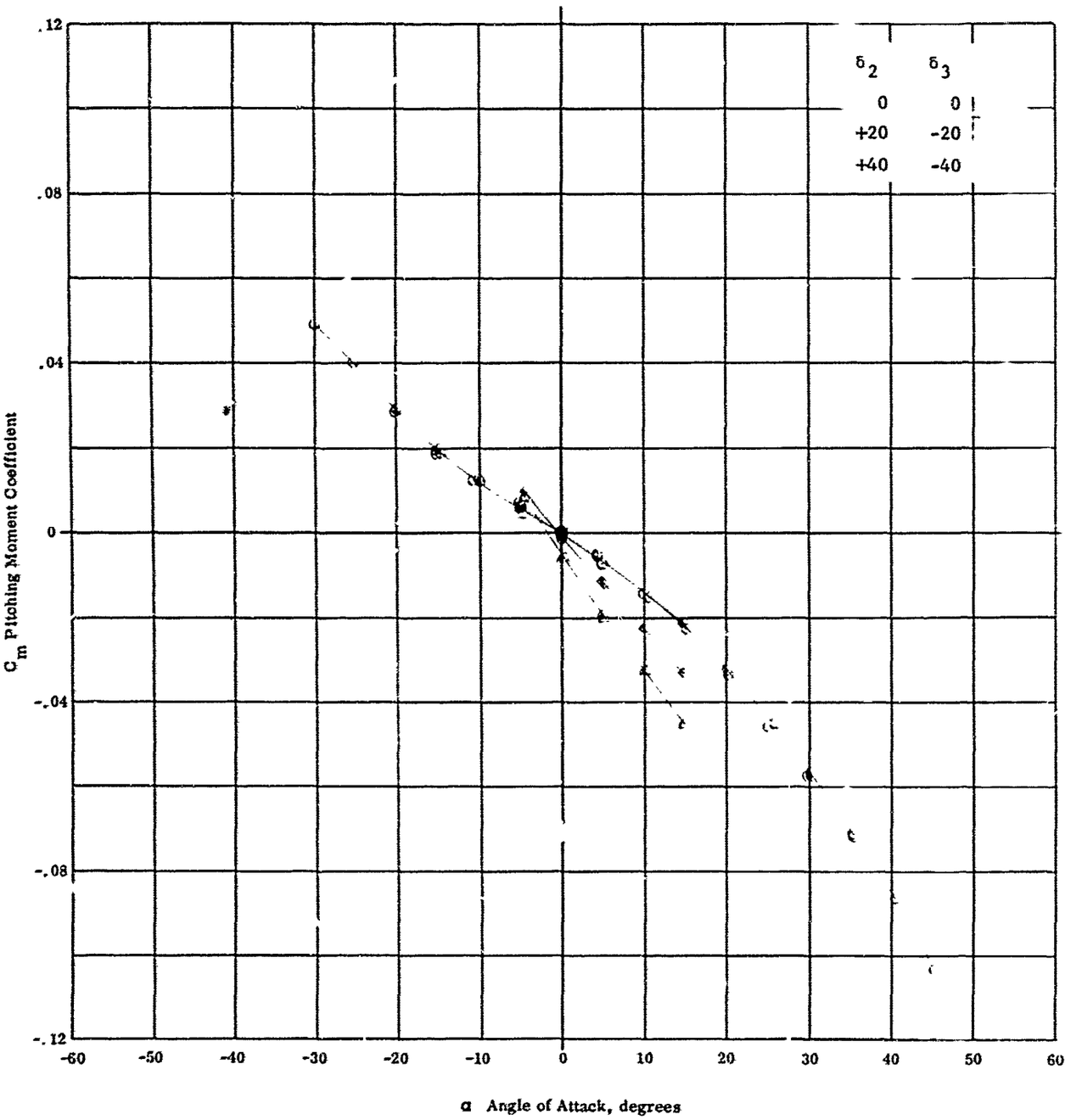

Fig. 12d Configuration IV - M_∞=5.01, C_m vs. α
$Re_\infty/ft \times 10^{-6}$ = 2.26 δ_1=0 δ_2=-δ_3=0, +20, +40

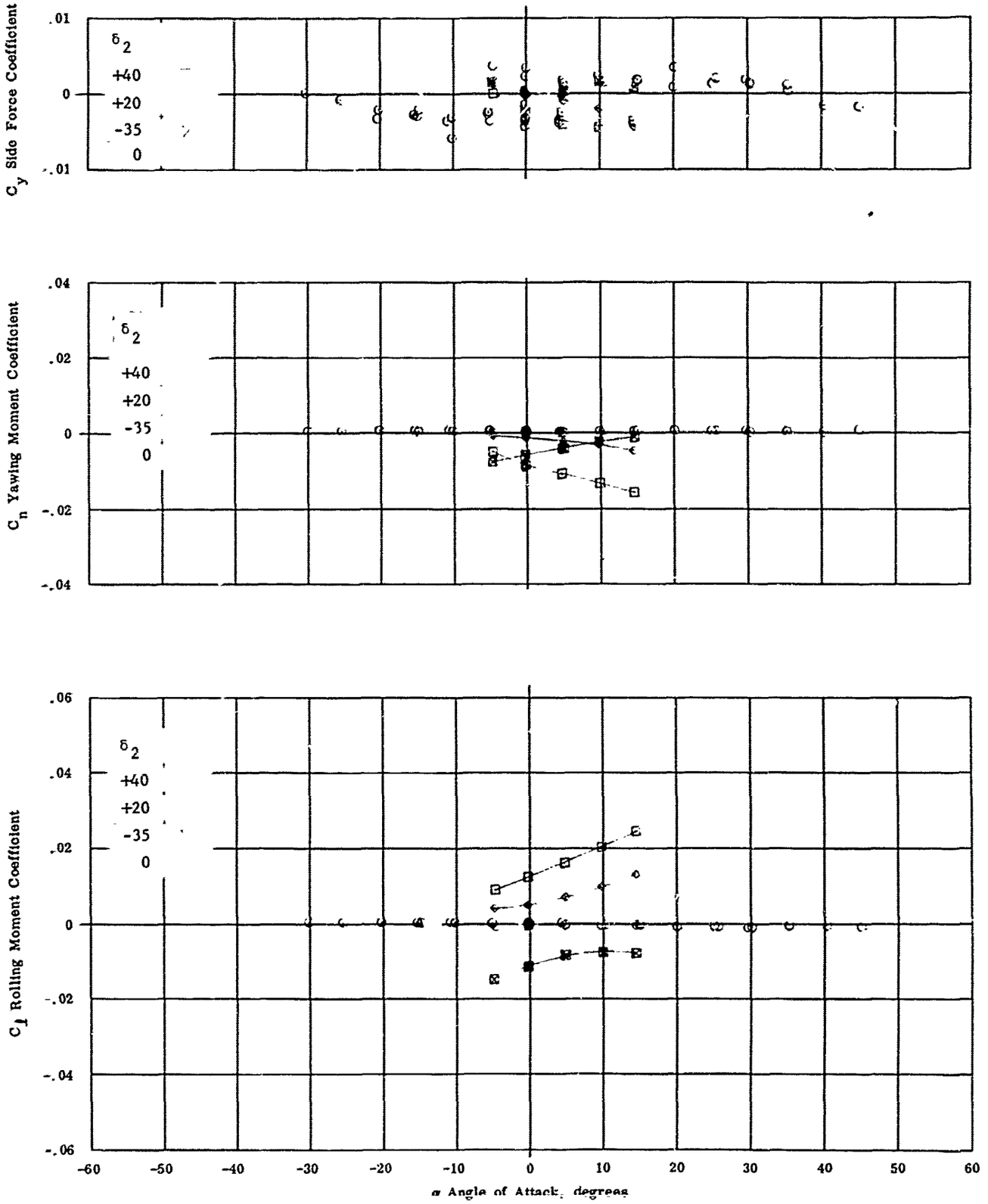

Fig. 12e Configuration IV - M_∞=5.01, C_y, C_n, C_ℓ vs. α
$Re_\infty/ft \times 10^{-6}$ = 2.26 $\delta_1=\delta_3=0$ δ_2=-35, 0, +20, +40

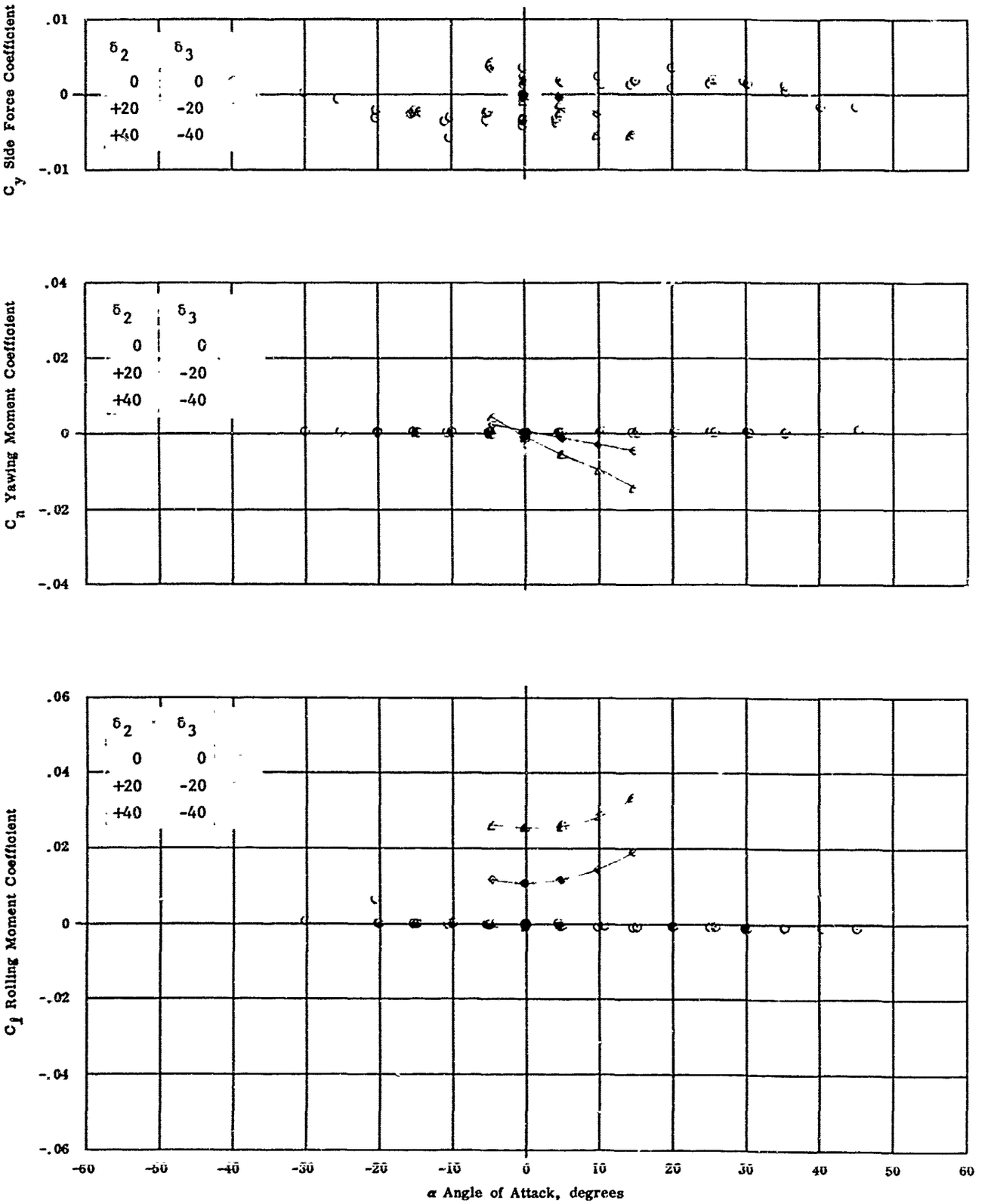

Fig. 12f Configuration IV - M_∞=5.01, C_y, C_n, C_ℓ vs. α
$Re_\infty/ft \times 10^{-6}$ = 2.26 δ_1=0 δ_2=-δ_3=0, +20, +40

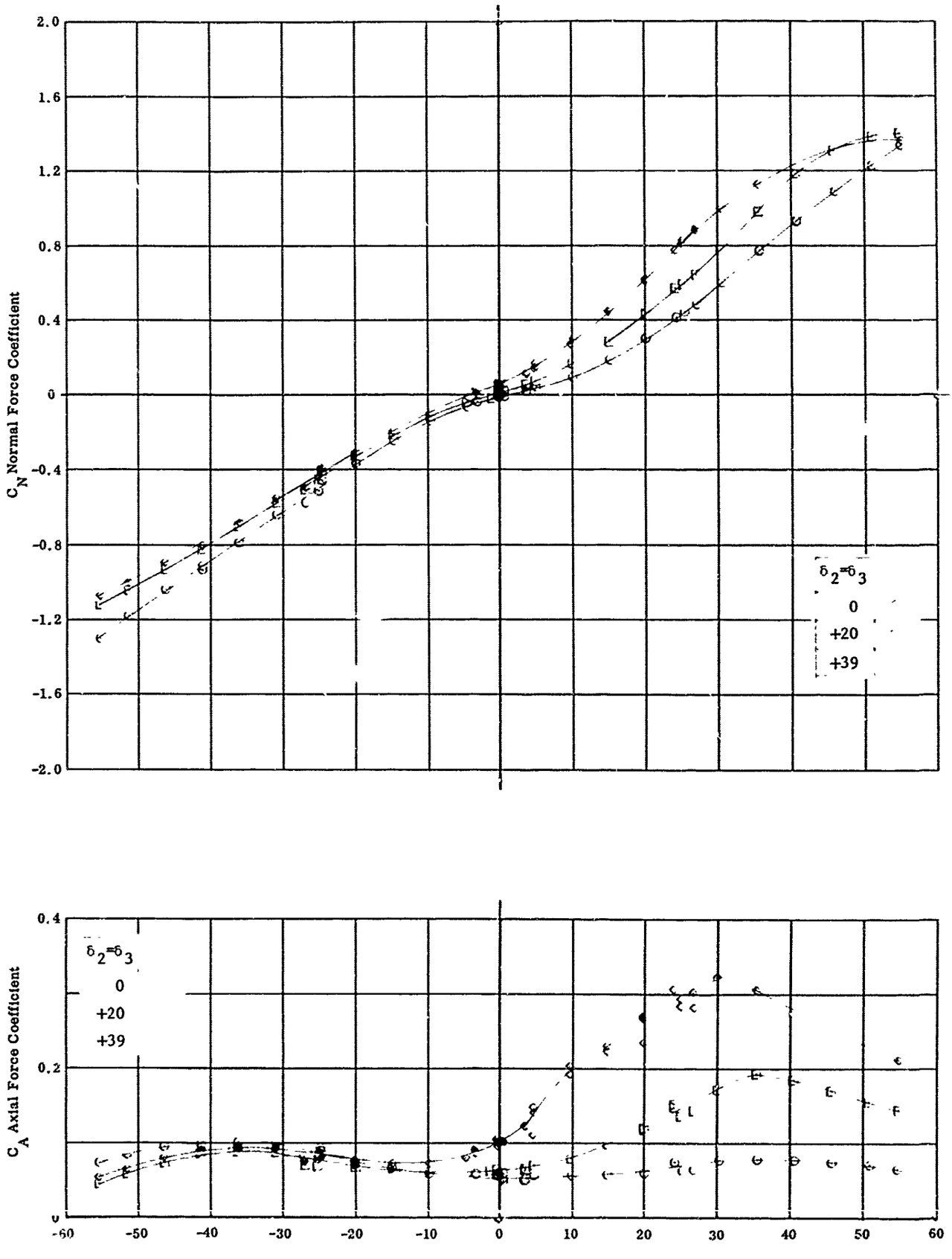

Fig. 13a Configuration I - M_∞=8.08, C_N & C_A vs. α
$Re_\infty/ft \times 10^{-6}$ = 2.26 δ_1=0 $\delta_2=\delta_3$=0, +20, +39

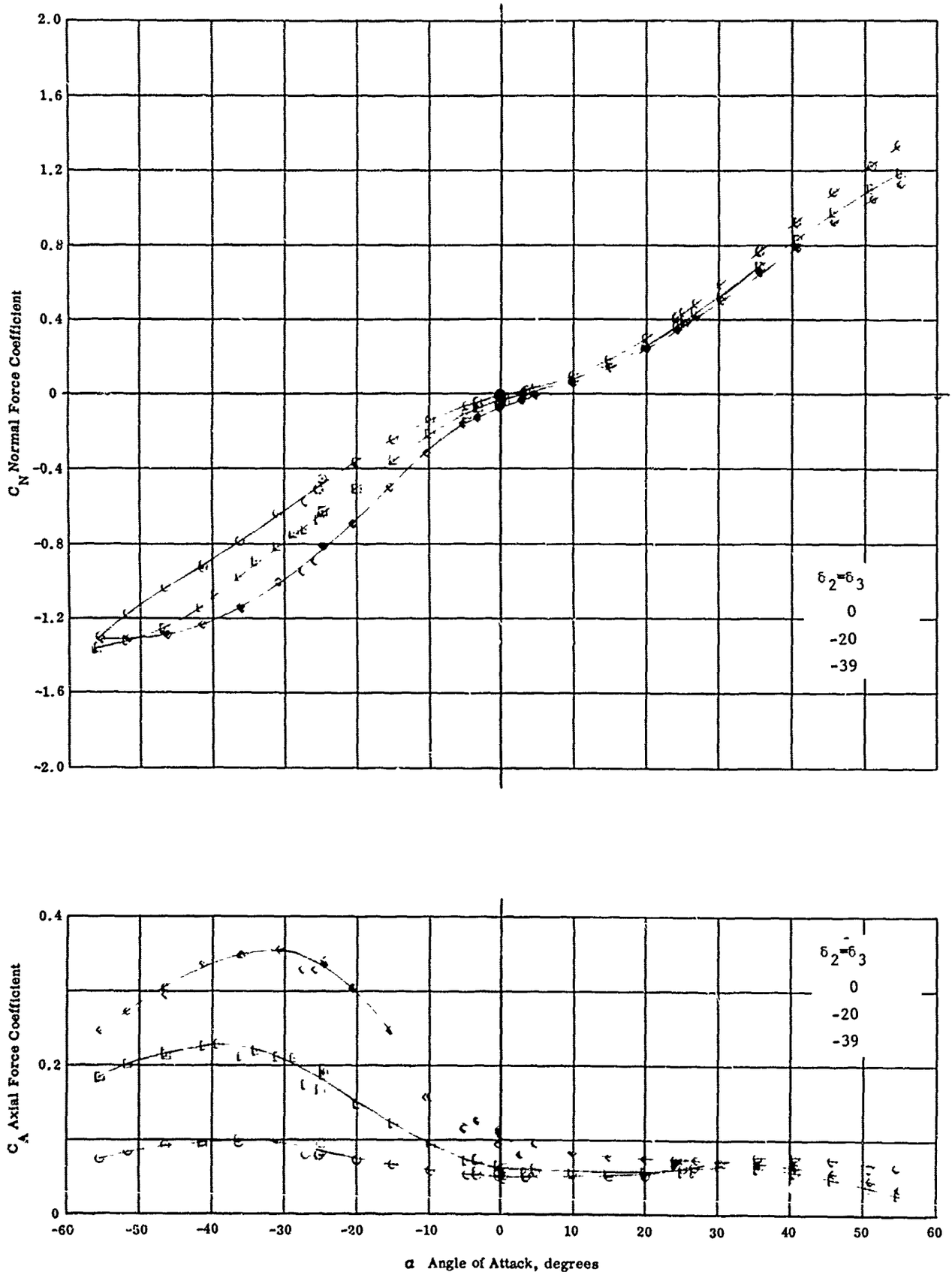

Fig. 13b Configuration I - M_∞=8.08, C_N & C_A vs. α
$Re_\infty/ft \times 10^{-6}$ = 2.26, δ_1=0 $\delta_2=\delta_3$=0, -20, -39

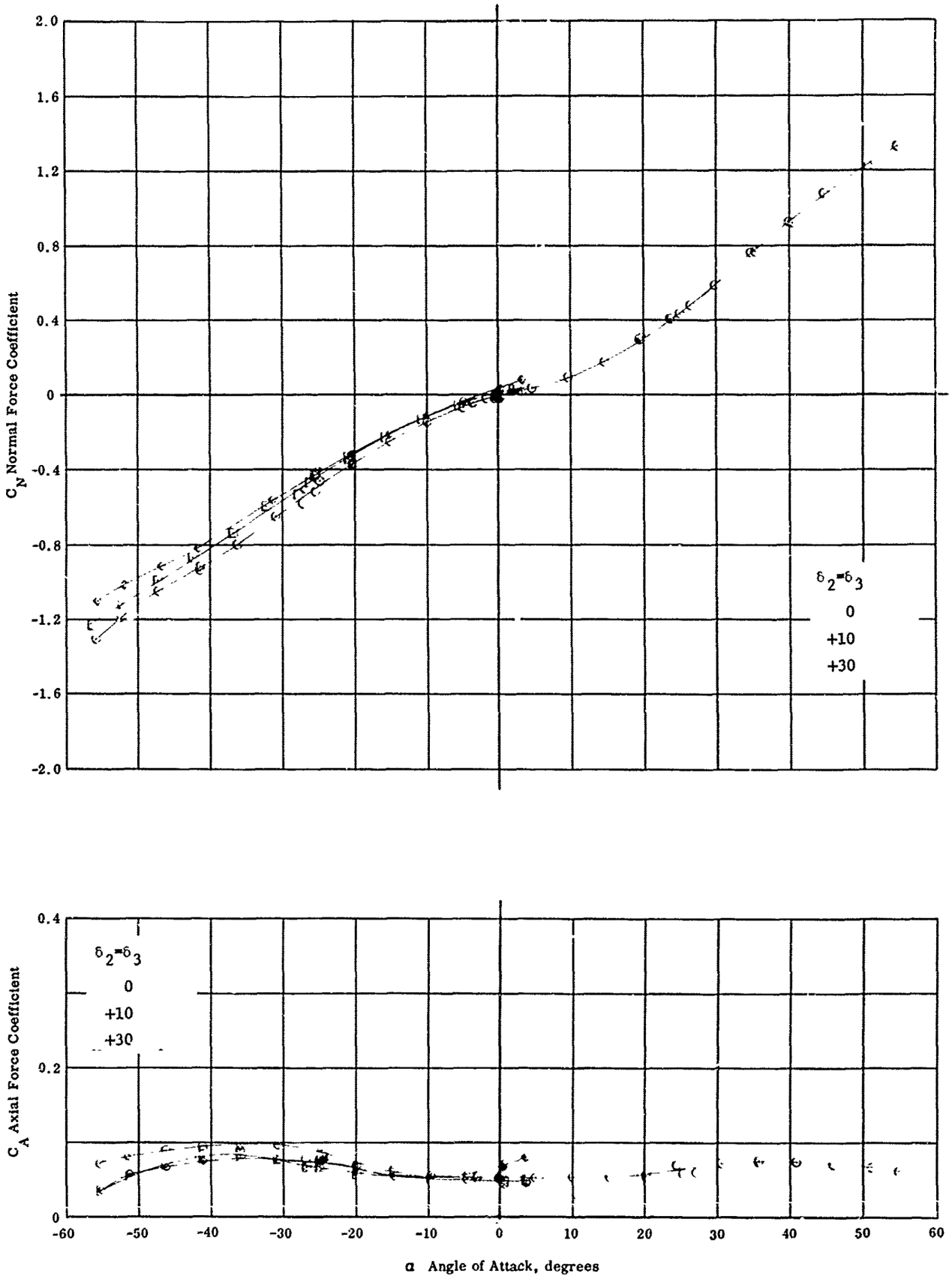

Fig. 13c Configuration I - M_∞=8.08, C_N & C_A vs. α
$Re_\infty/ft \times 10^{-6}$ = 2.26 δ_1=0 $\delta_2=\delta_3$=0, +10, +30

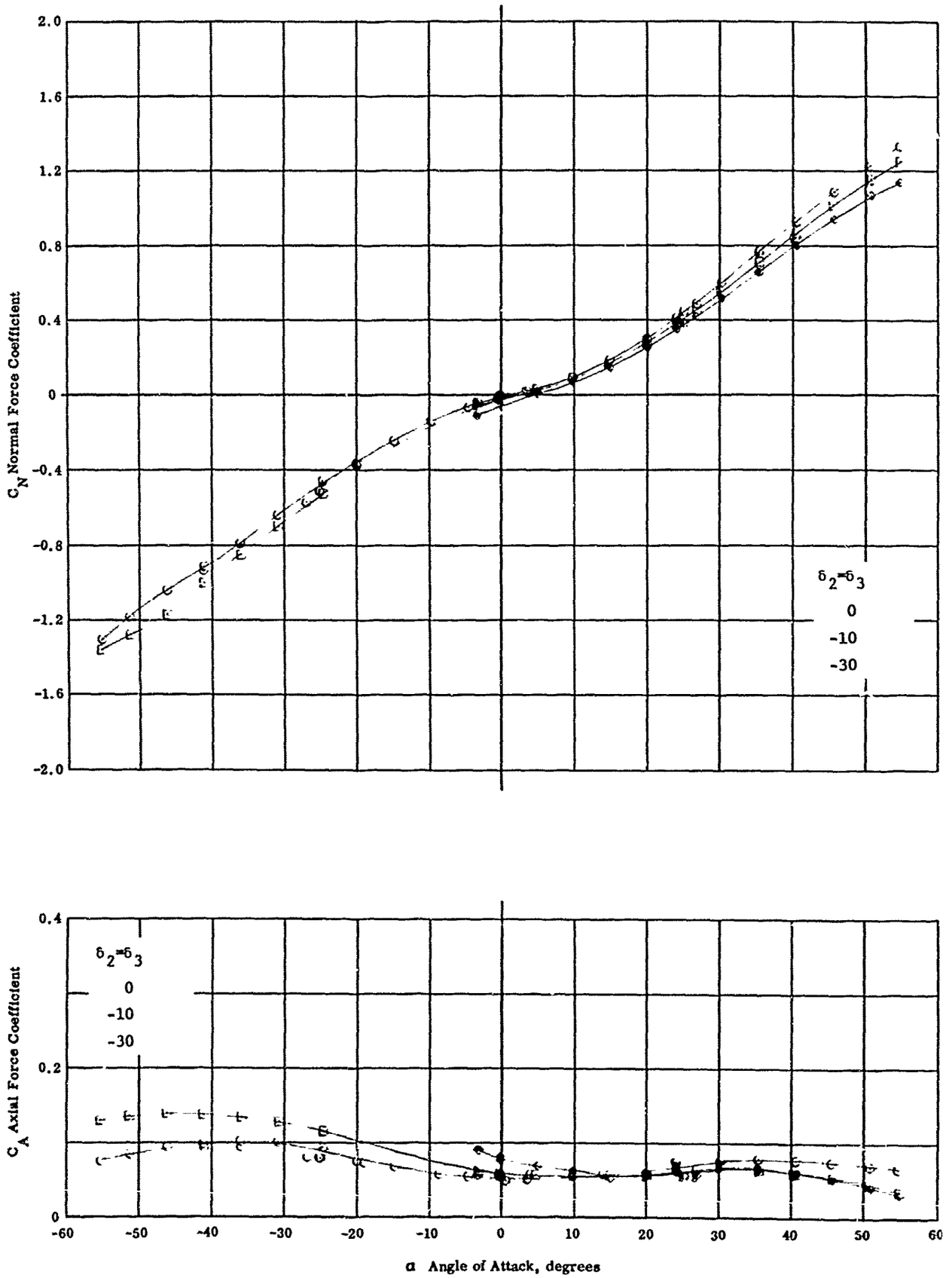

Fig. 13d Configuration I - M_∞=8.08, C_N & C_A vs. α
Re_∞/ft x 10^{-6} = 2.26 δ_1=0 δ_2=δ_3=0, -10, -30

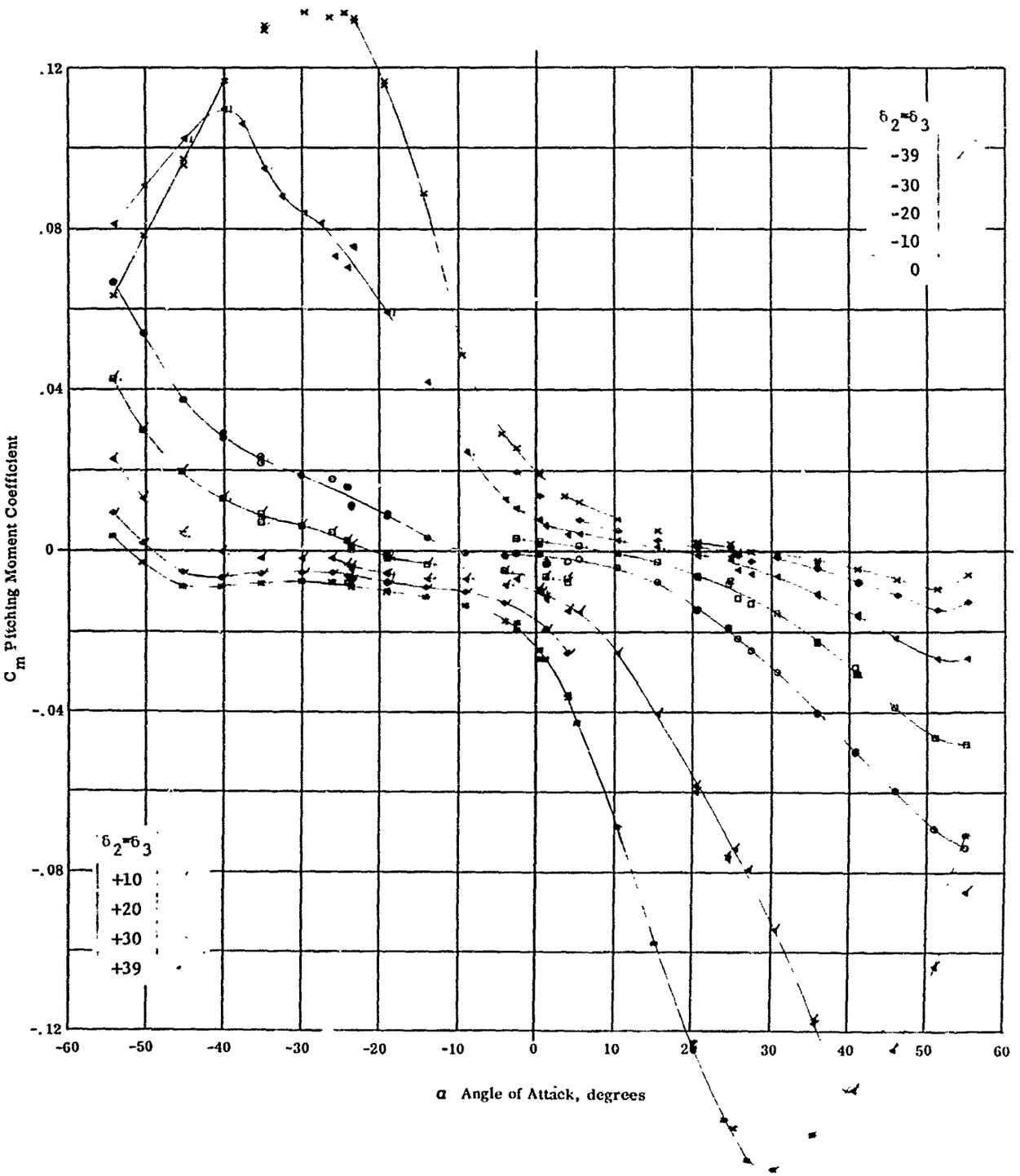

Fig. 13e Configuration I - M_∞=8.08, C_m vs. α
$Re_\infty/ft \times 10^{-6}$ = 2.26 δ_1=0 $\delta_2=\delta_3$=0, +10, +20, +30, +39

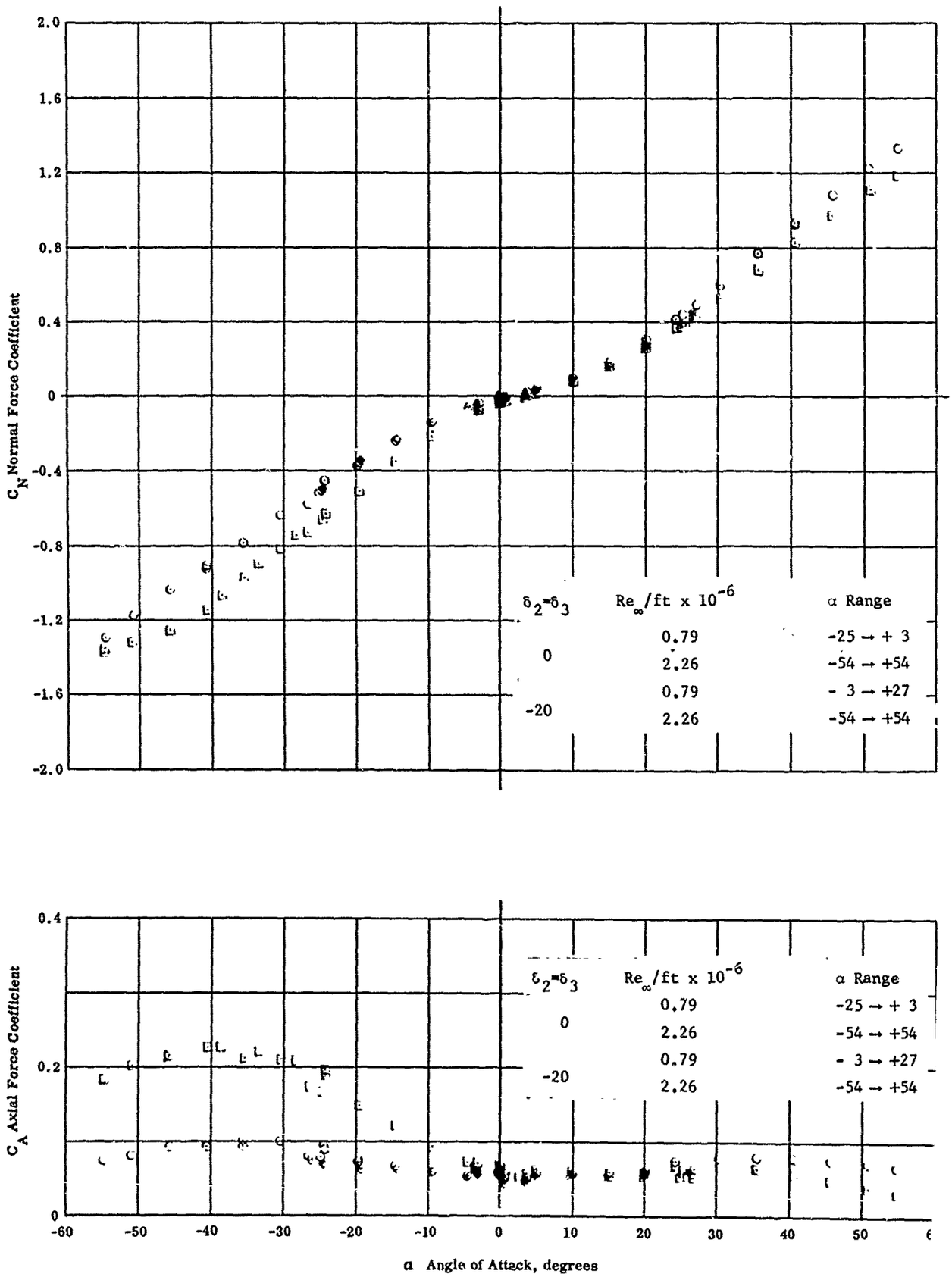

Fig. 14a Configuration I - M_∞=8.08, C_N & C_A vs. α
$Re_\infty/ft \times 10^{-6}$ = 0.79 & 2.26 δ_1=0 $\delta_2=\delta_3$=0, -20

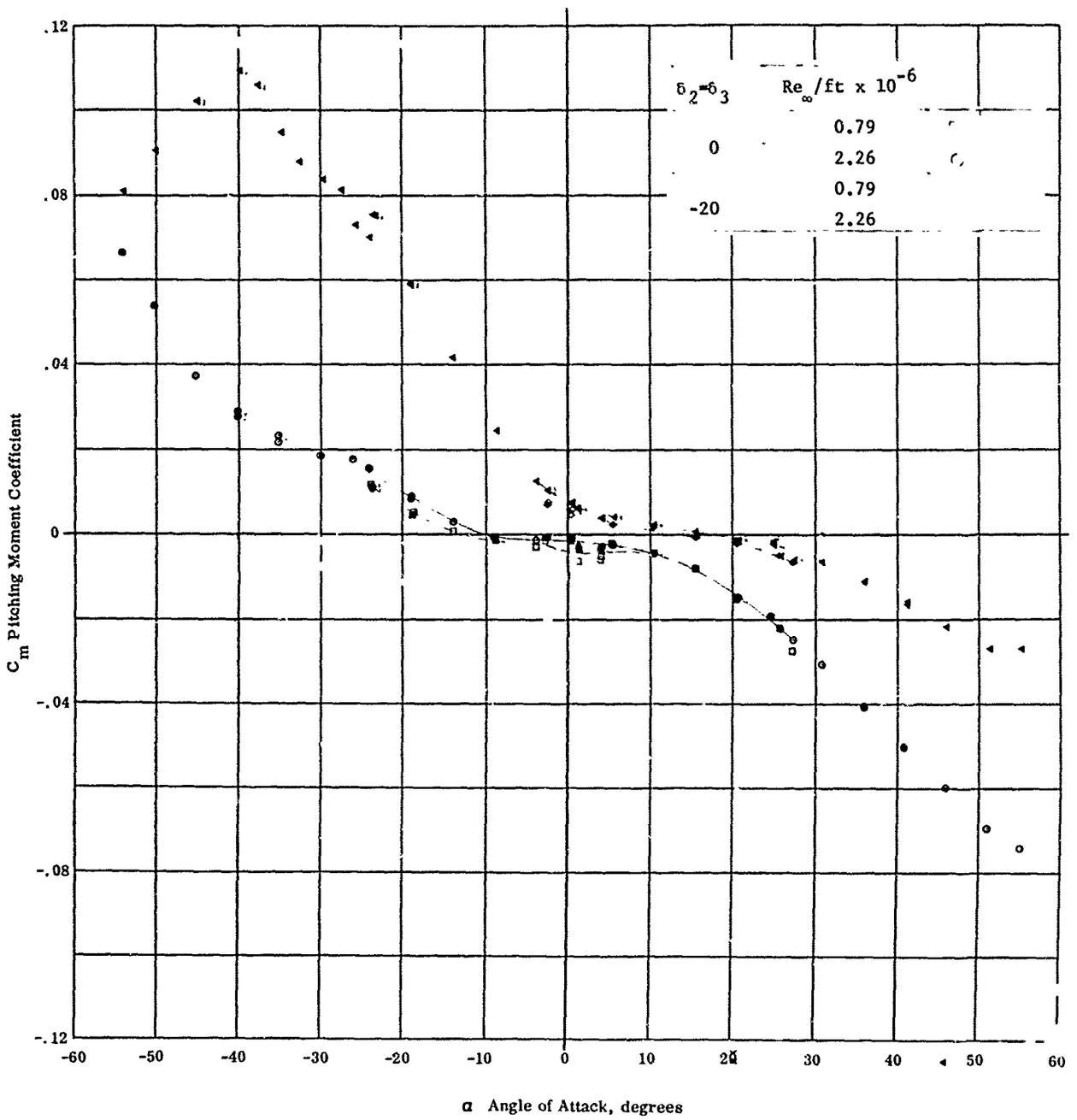

Fig. 14b Configuration I - M_∞=8.08, C_m vs. α
Re_∞/ft x 10^{-6} = 0.79 & 2.26 $\delta_1=0$ $\delta_2=\delta_3=0, -20$

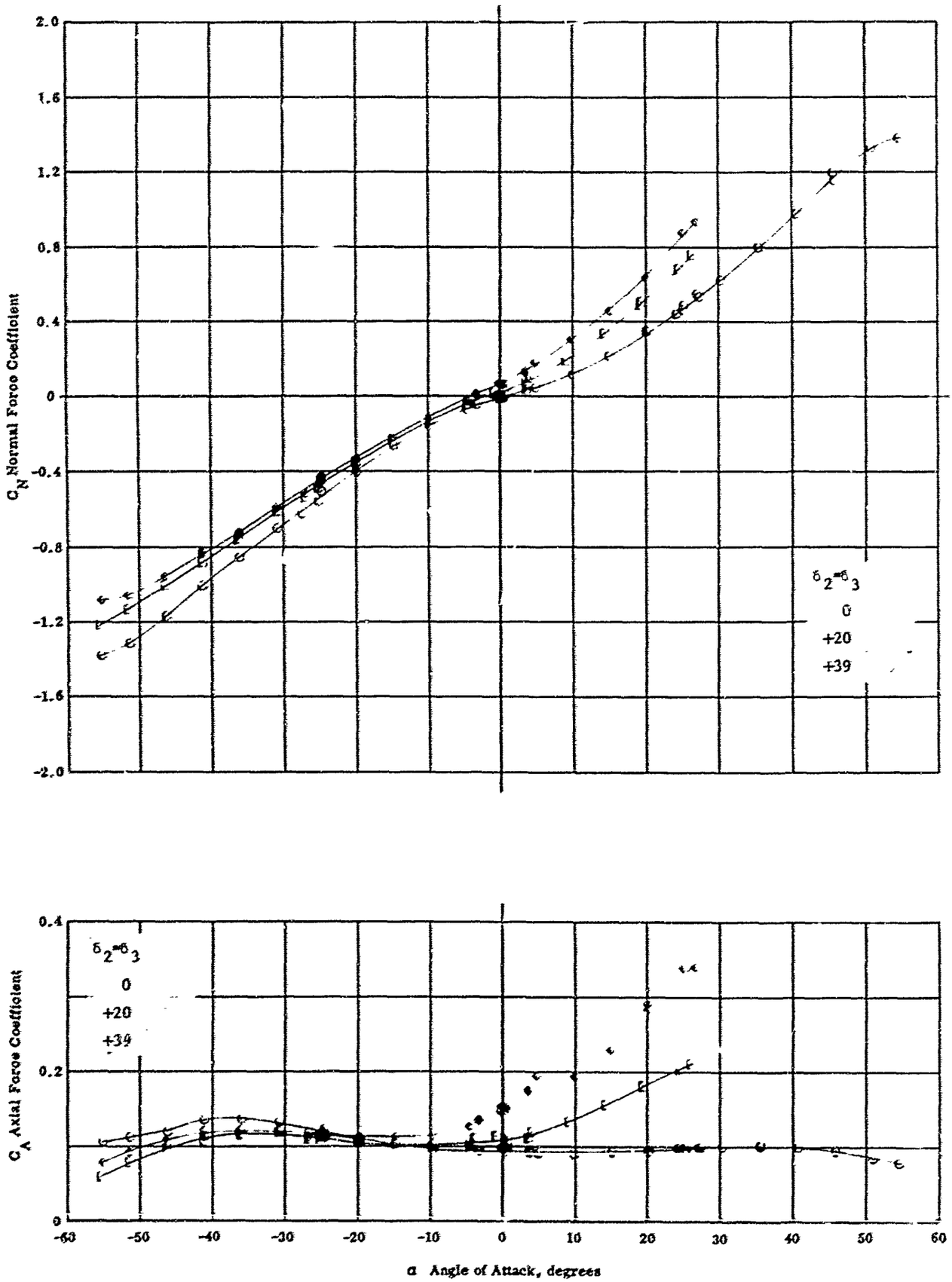

Fig. 15a Configuration IV - M_∞=8.08, C_N & C_A vs. α
$Re_\infty/ft \times 10^{-6}$ = 2.26 δ_1=0 $\delta_2=\delta_3$=0, +20, +39

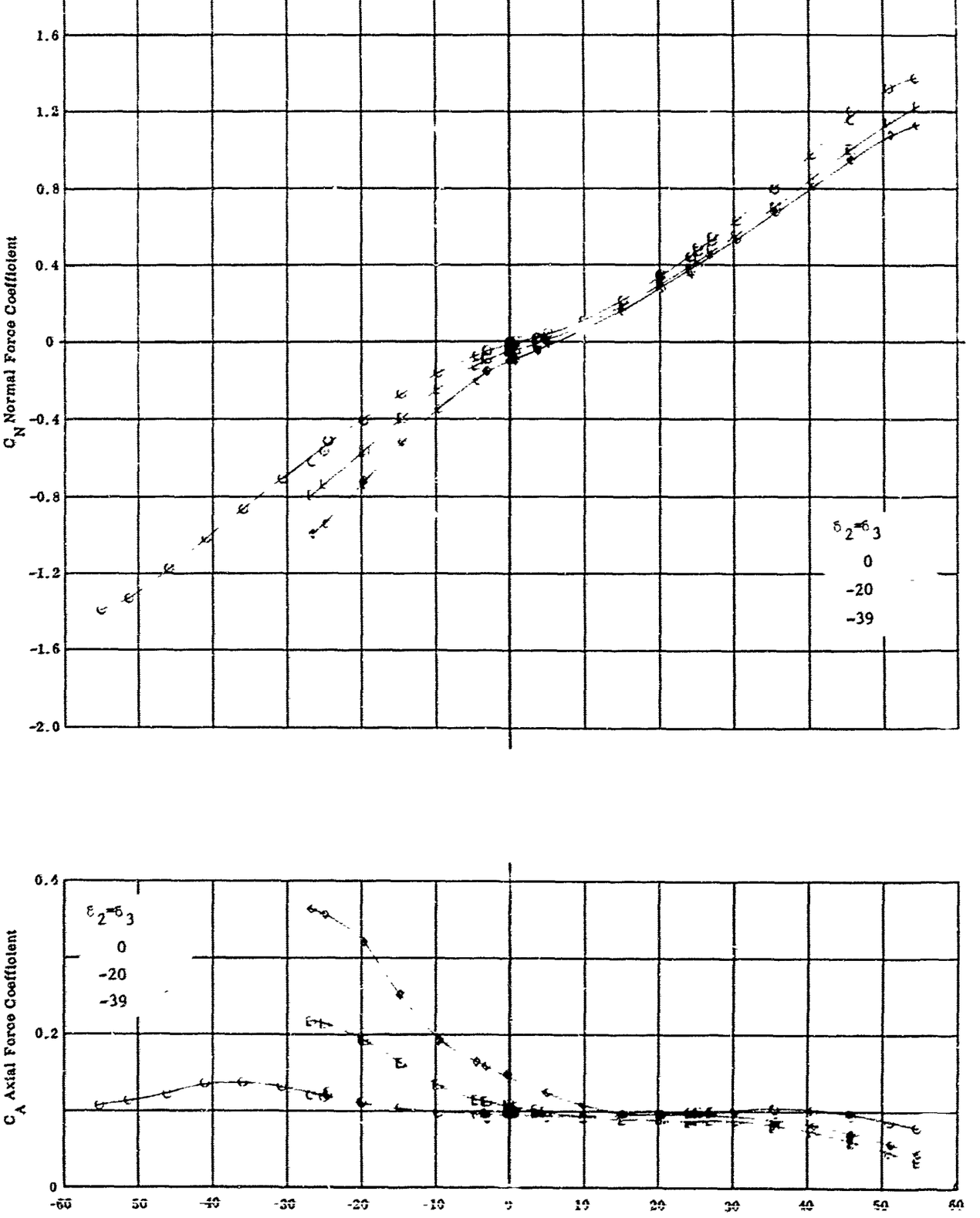

Fig. 15b Configuration IV - M_∞=8.08, C_N & C_A vs. α
$Re_\infty/ft \times 10^{-6}$ = 2.26 δ_1=0 $\delta_2=\delta_3$=0, -20,-39

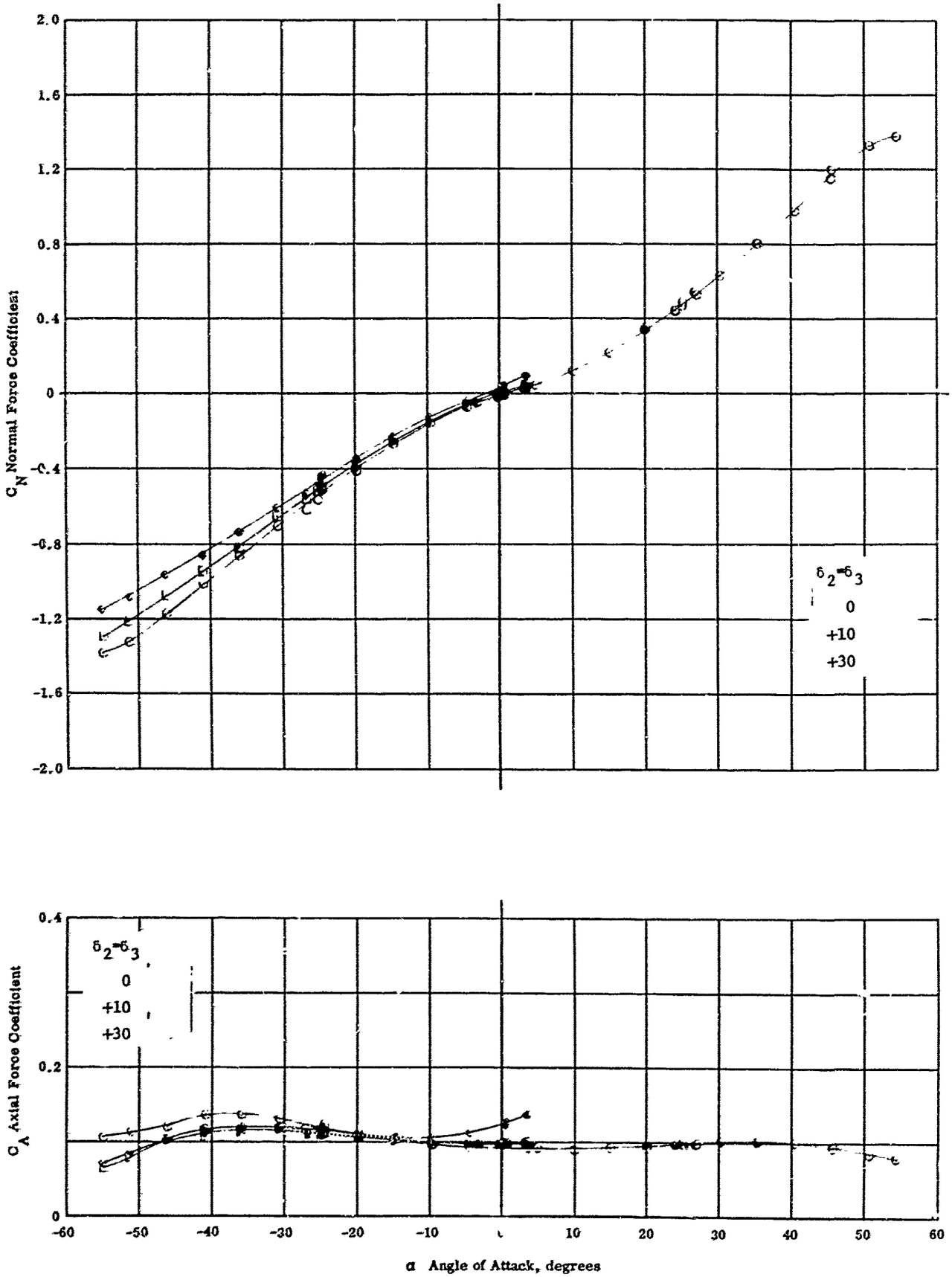

Fig. 15c Configuration IV - M_∞=8.08, C_N & C_A vs. α
$Re_\infty/ft \times 10^{-6}$ = 2.26 δ_1=0 $\delta_2=\delta_3$=0, +10, +30

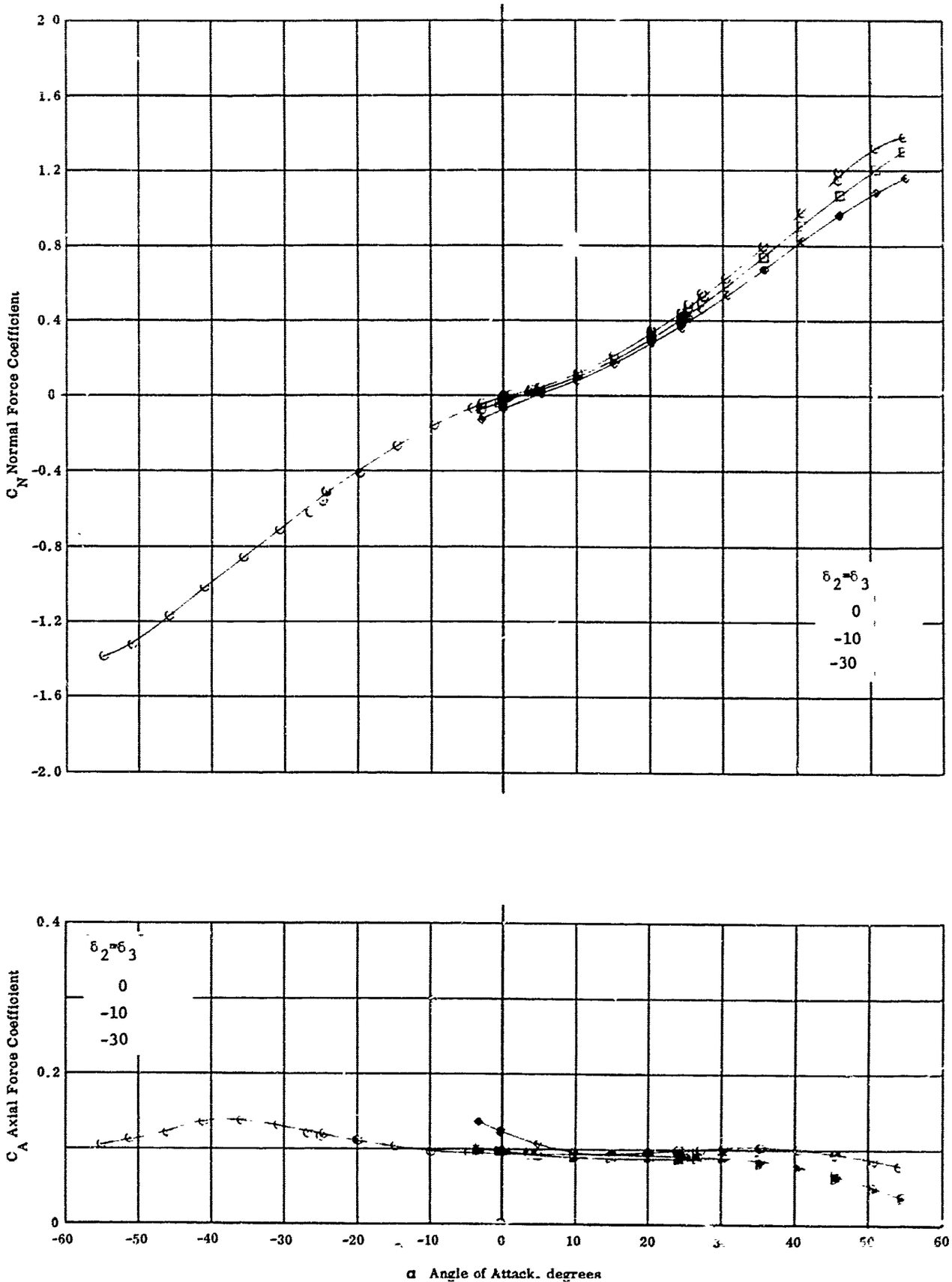

Fig. 15d Configuration IV - M_∞ = 8.08, C_N & C_A vs. α
$Re_\infty/ft \times 10^{-6}$ = 2.26 δ_1=0 $\delta_2=\delta_3$=0, -10, -30

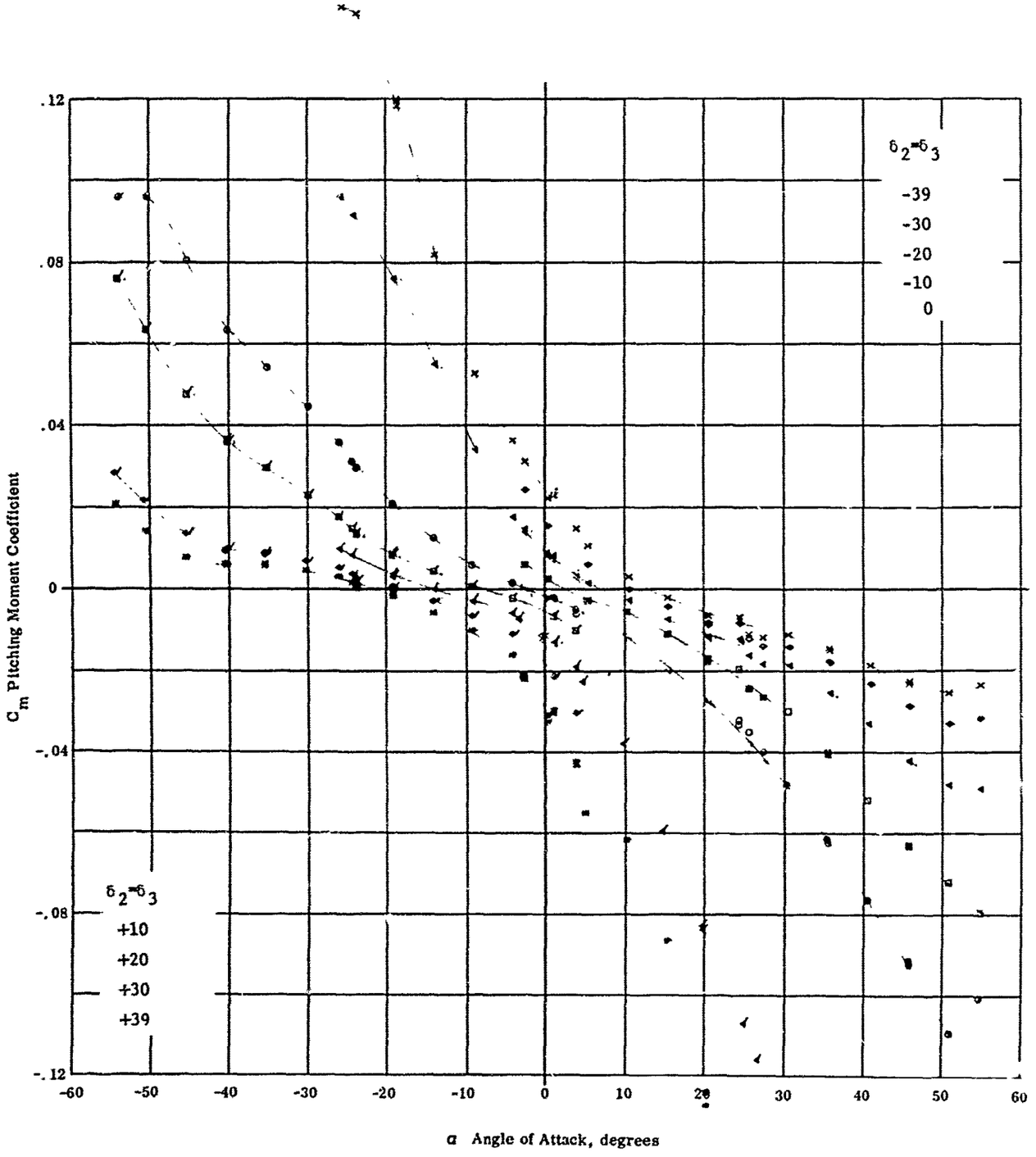

Fig. 15e Configuration IV - M_∞=8.08, C_m vs. α
$Re_L/ft \times 10^{-6}$ = 2.26 δ_1=0 $\delta_2=\delta_3$=0, ±10, ±20, ±30, ±39

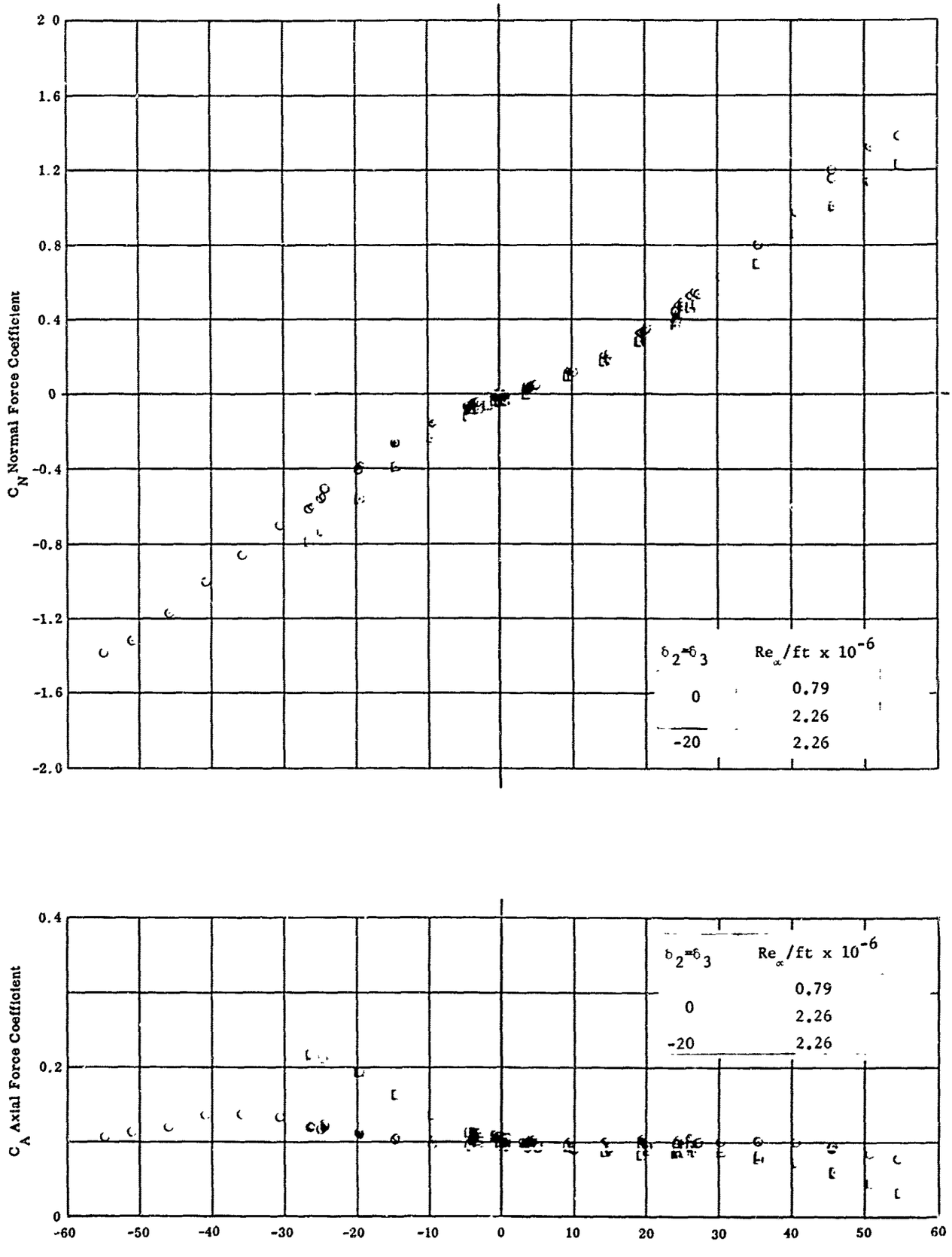

Fig. 16a Configuration IV - M_∞=8.08 C_N & C_A vs. α
Re_∞/ft x 10^{-6} = 0.79, 2.26 δ_1=0 $\delta_2=\delta_3$=0, -20

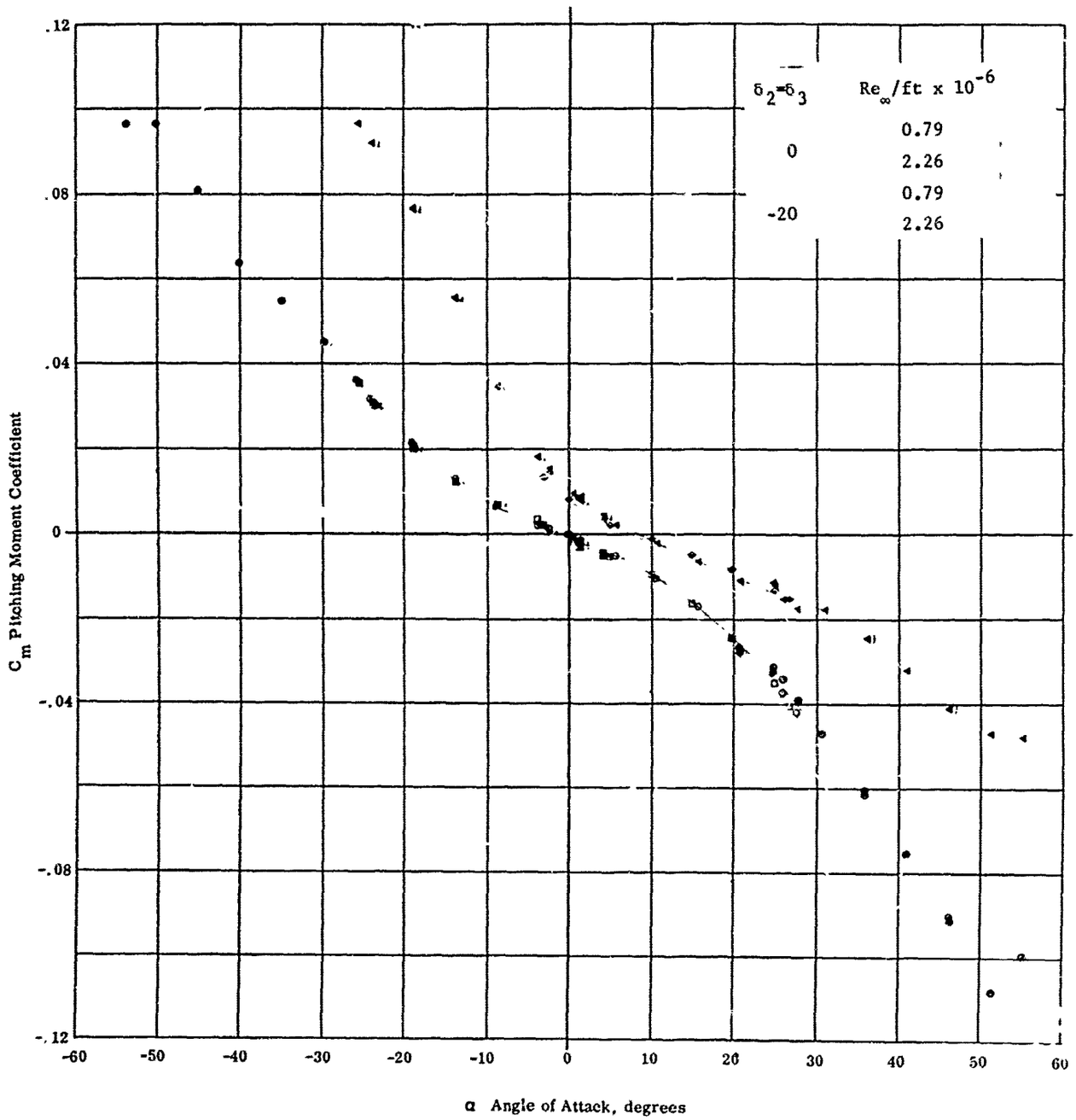

Fig. 16b Configuration IV - M_∞=8.08, C_m vs. α
$Re_\infty/ft \times 10^{-6}$ = 0.79, 2.26 δ_1=0 $\delta_2=\delta_3$=0, -20

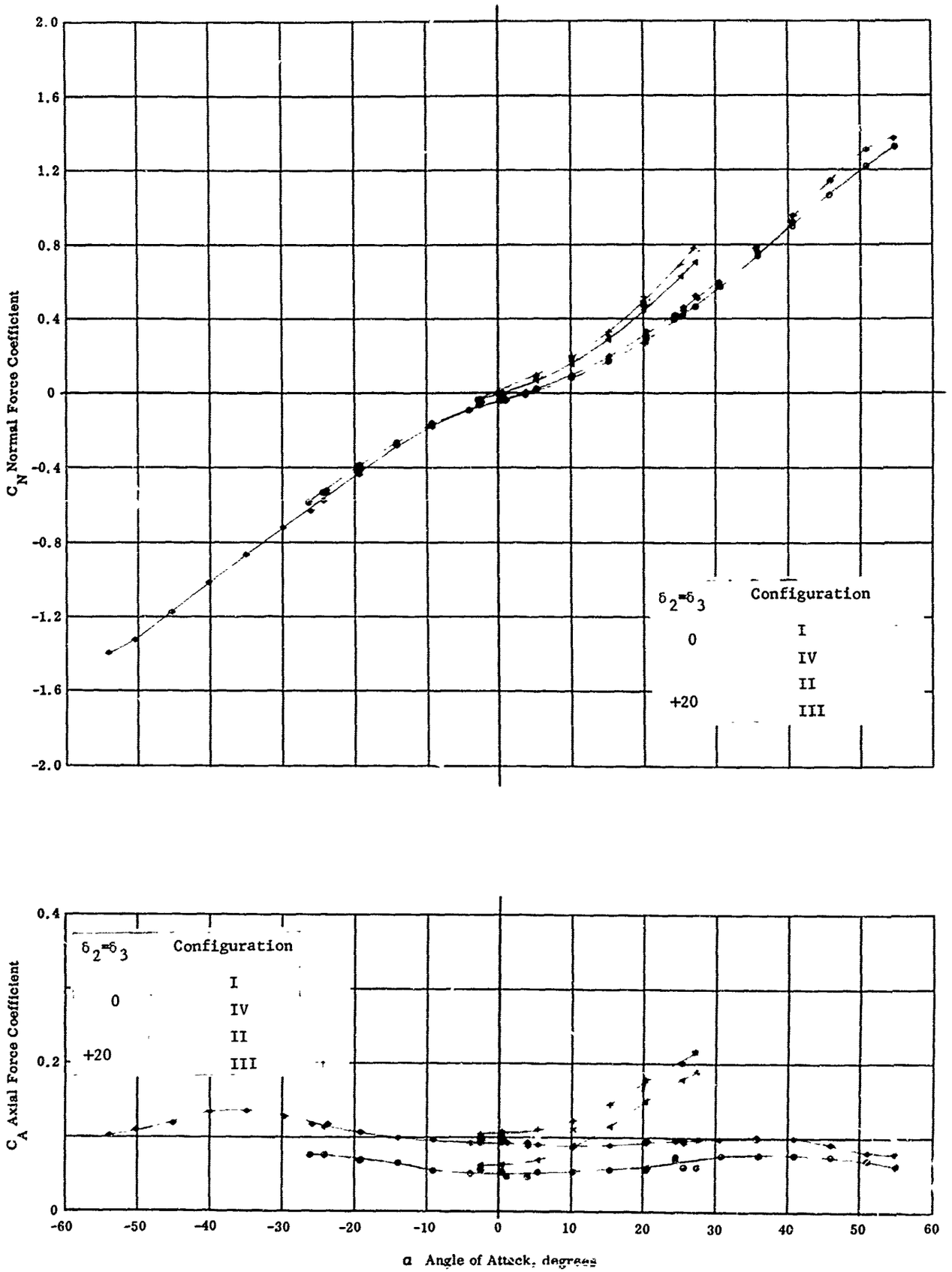

Fig. 17a Configuration II & III - M_∞=8.08, C_N & C_A vs. α
$Re_\infty/ft \times 10^{-6}$ = 2.26 δ_1=0 $\delta_c=\delta_2=\delta_3$=0, +20

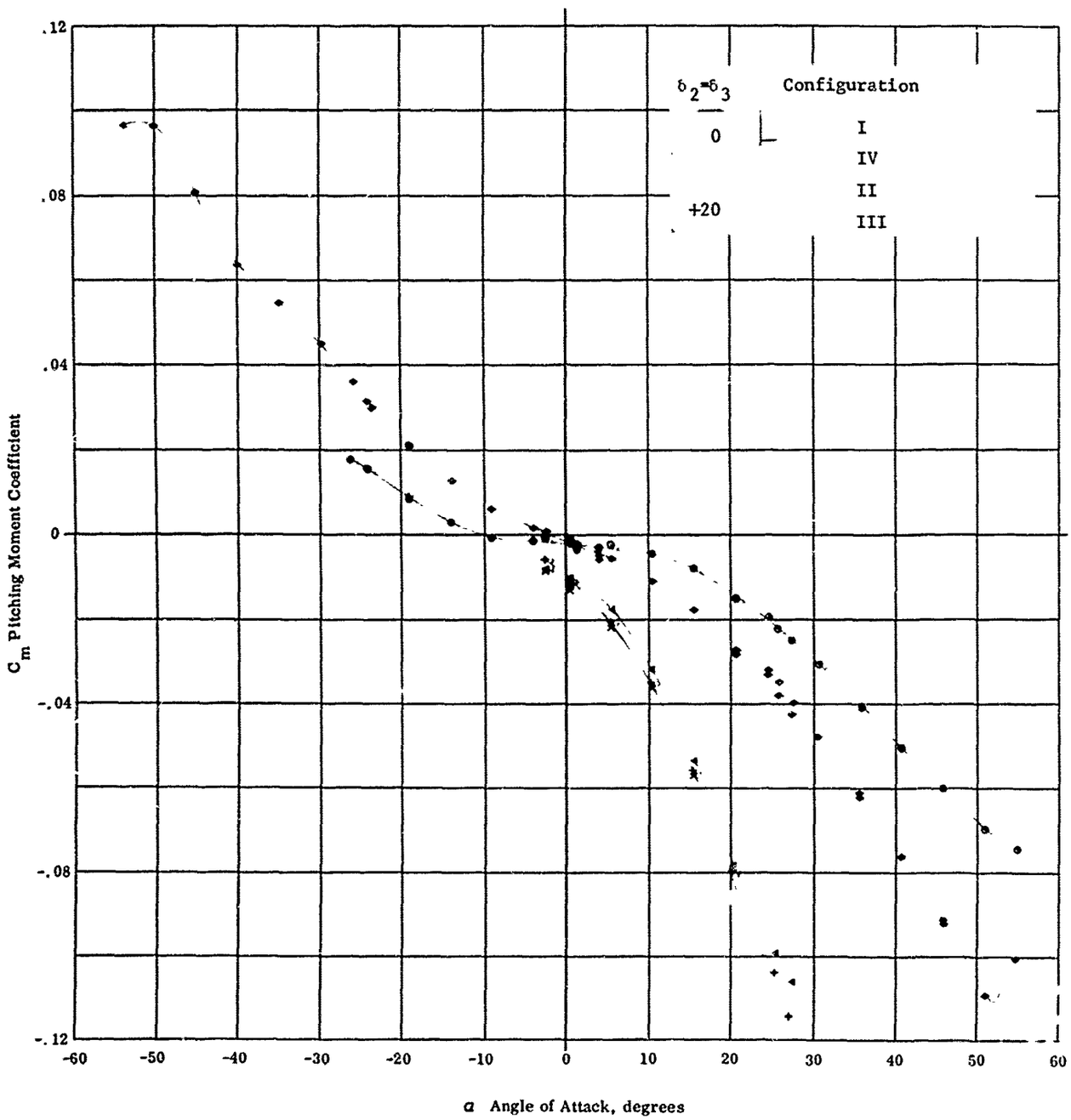

Fig. 17b Configuration II & III - M_∞=8.08, C_m vs. α
$Re_\infty/ft \times 10^{-6}$ = 2.26 δ_1=0 $\delta_c=\delta_2=\delta_3$=0, +20

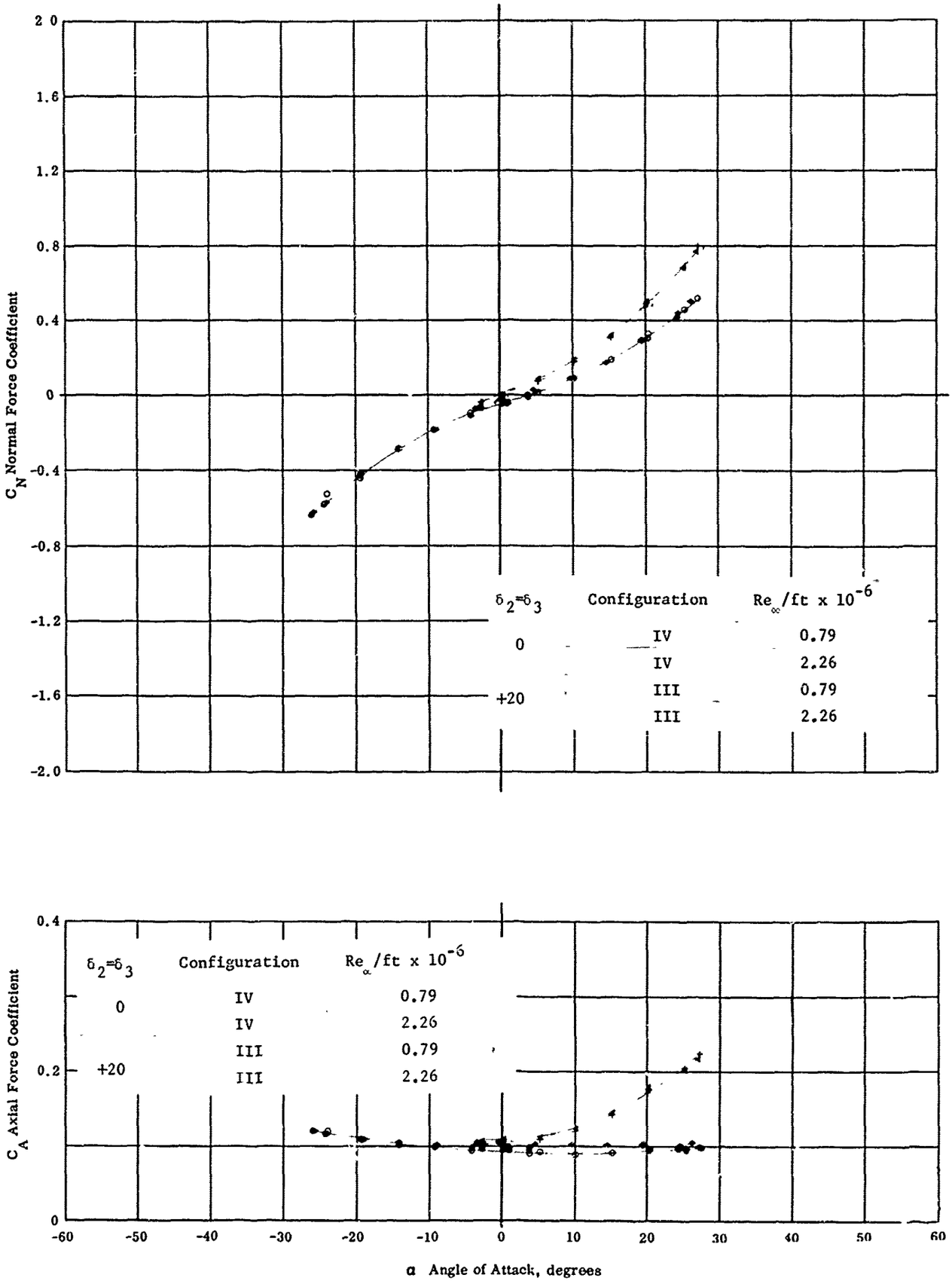

Fig. 18a Configuration III - M_∞=8.08, C_N & C_A vs. α
Re_∞/ft x 10^{-6} = 0.79, 2.26 δ_1=0 $\delta_c=\delta_2=\delta_3$=0, +20

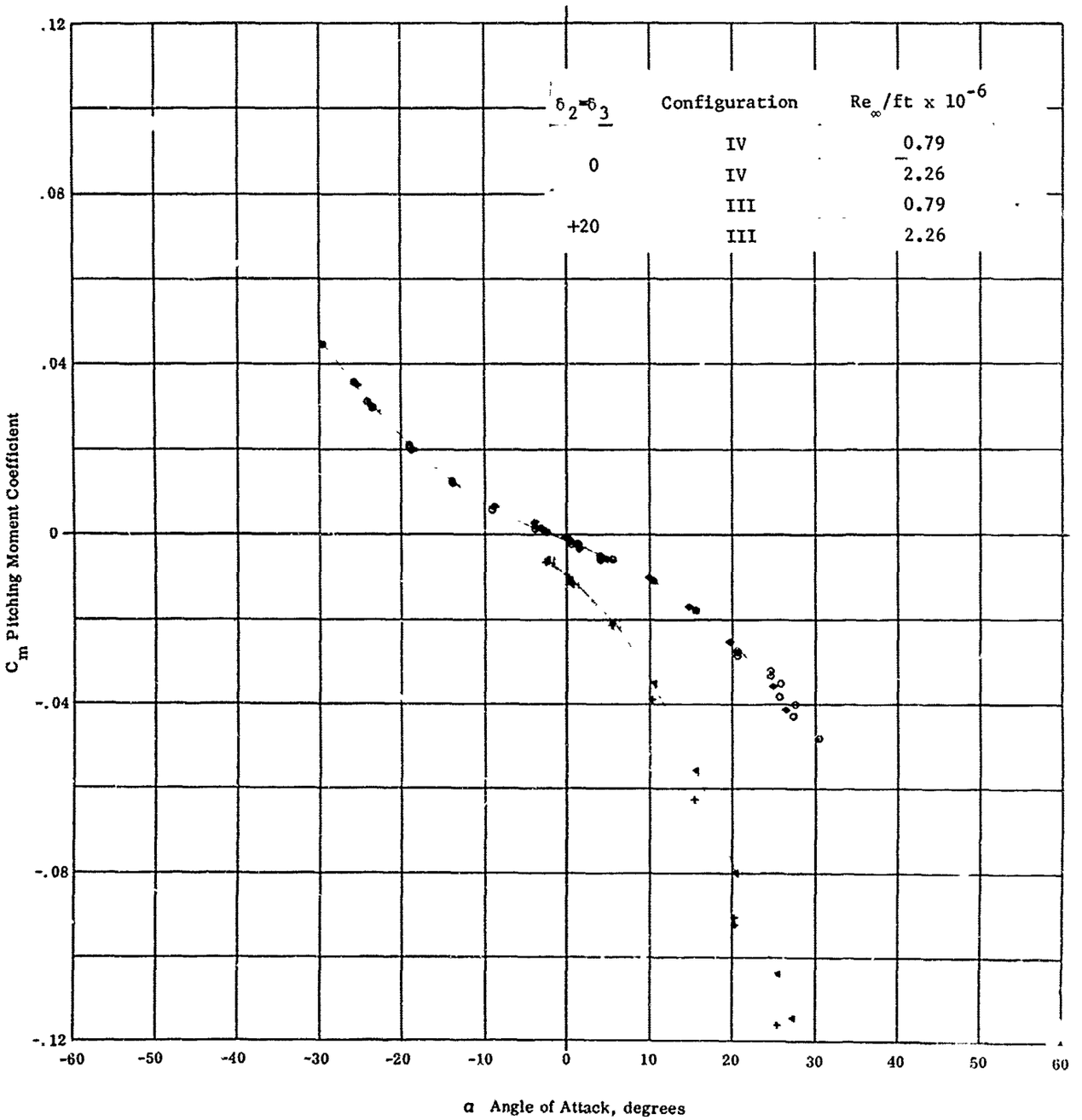

Fig. 18b Configuration III - M_∞=8.08, C_m vs. α
$Re_\infty/ft \times 10^{-6}$ = 0.79, 2.26 δ_1=0 $\delta_c=\delta_2=\delta_3$=0, +20

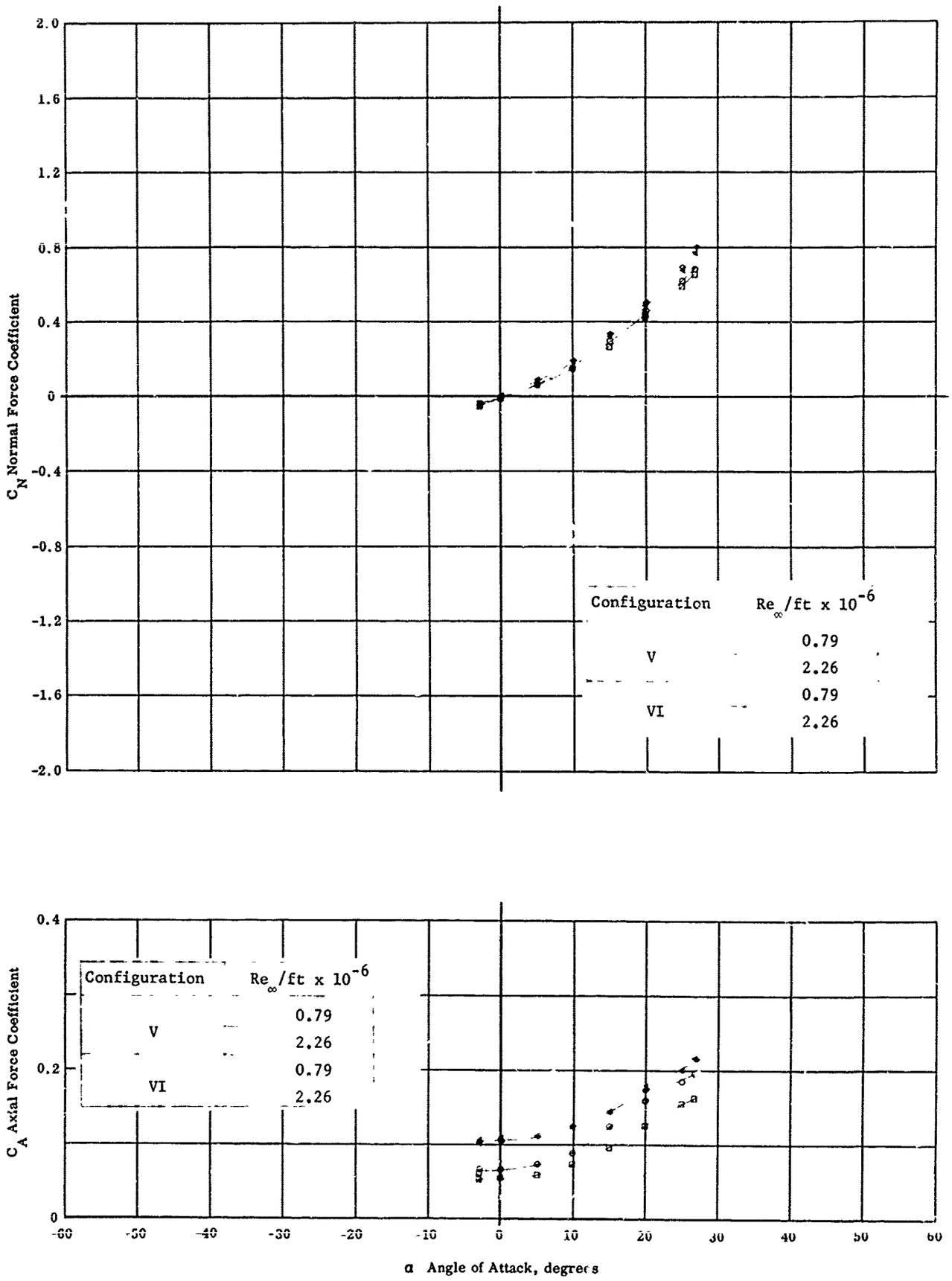

Fig. 19a Configuration V & VI - M_∞=8.08, C_N & C_A vs. α
Re_∞/ft x 10^{-6} = 0.79, 2.26 $\delta_1=\delta_2=\delta_3=0$ Spoiler On

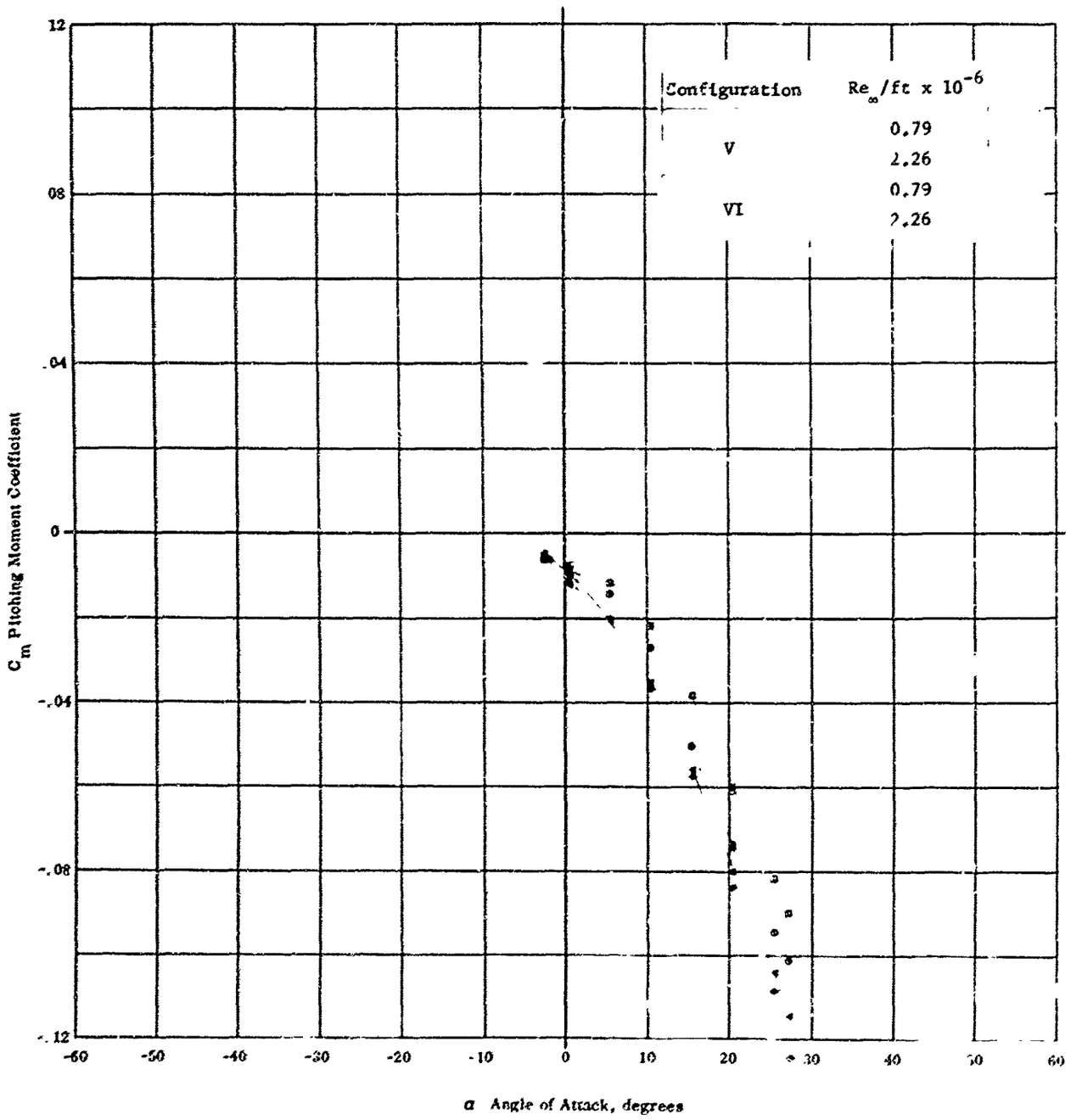

Fig. 19b Configuration V & VI - M_∞=8.03, C_m vs. α
Re_∞/ft x 10^{-6} = 0.79, 2.26, δ_1=0, δ_2=0, δ_3=0 Spoiler On

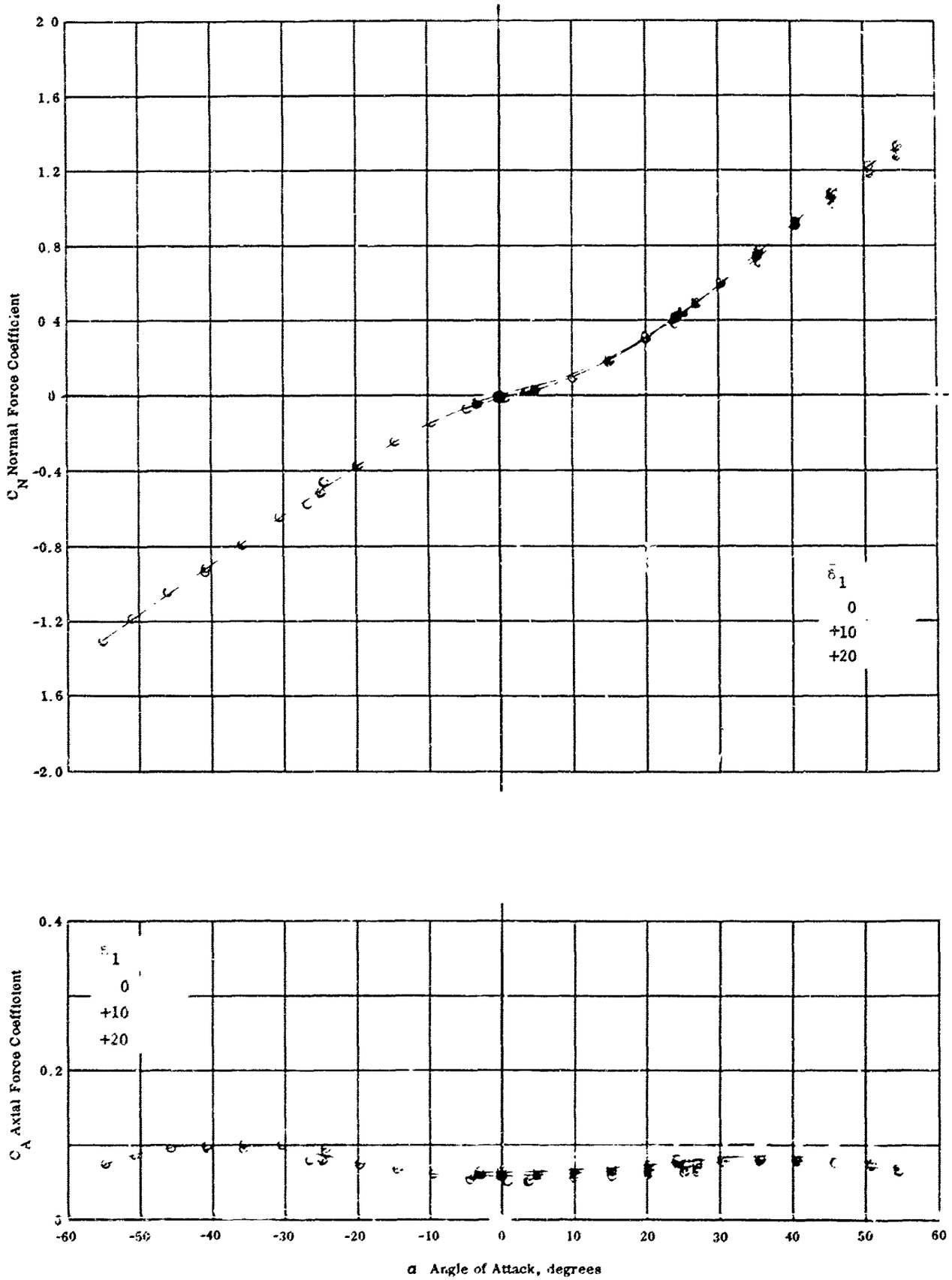

Fig. 20a Configuration I - M_∞=3.00, C_N & C_A vs. α
$Re_\infty/ft \times 10^{-6}$ = 2.25 $\bar{\delta}_1$=0, +10, +20 $\bar{\delta}_3$=0

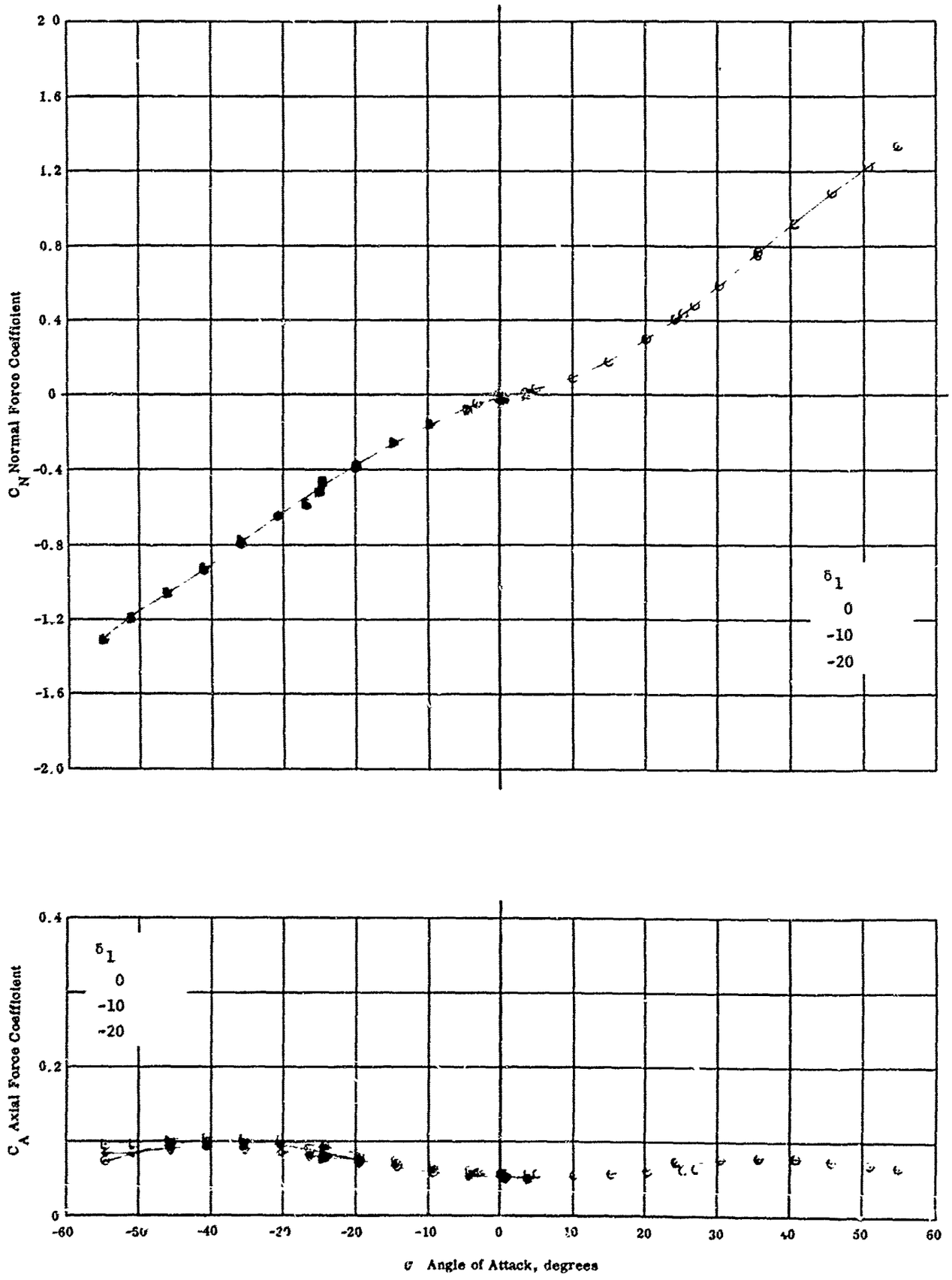

Fig. 20b Configuration 1 - M_∞=8.08, C_N & C_A vs. σ
$Re_\infty/ft \times 10^{-6}$ = 2.26 δ_1=0, -10, -20 δ_2=δ_3=0

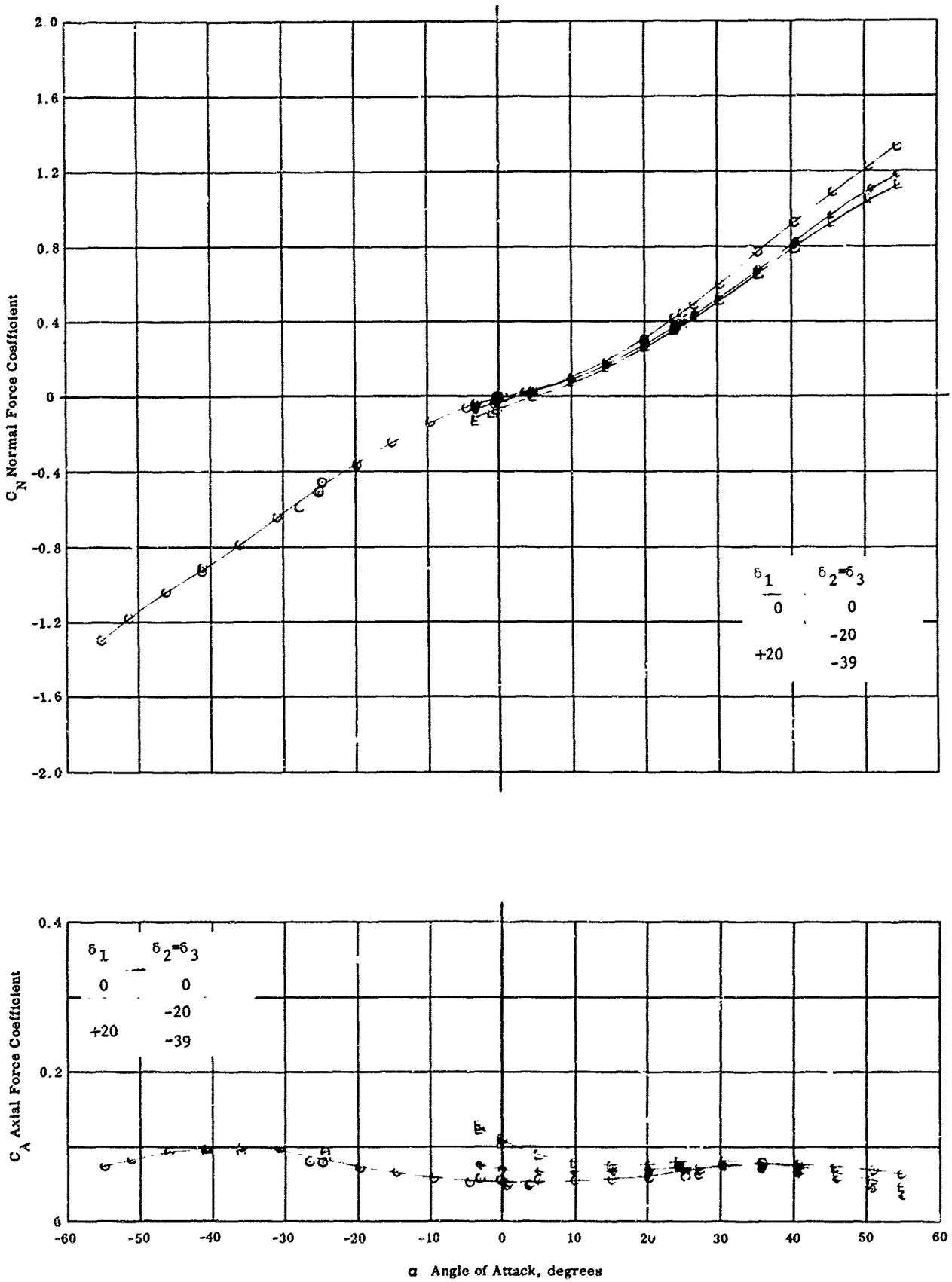

Fig. 20c Configuration I - M_∞=8.08, C_N & C_A vs. ,
$Re_\infty/ft \times 10^{-6}$ = 2.26 $\delta_1=\delta_2=\delta_3=0$, $\delta_1=+20$ $\delta_2=\delta_3=-20, -39$

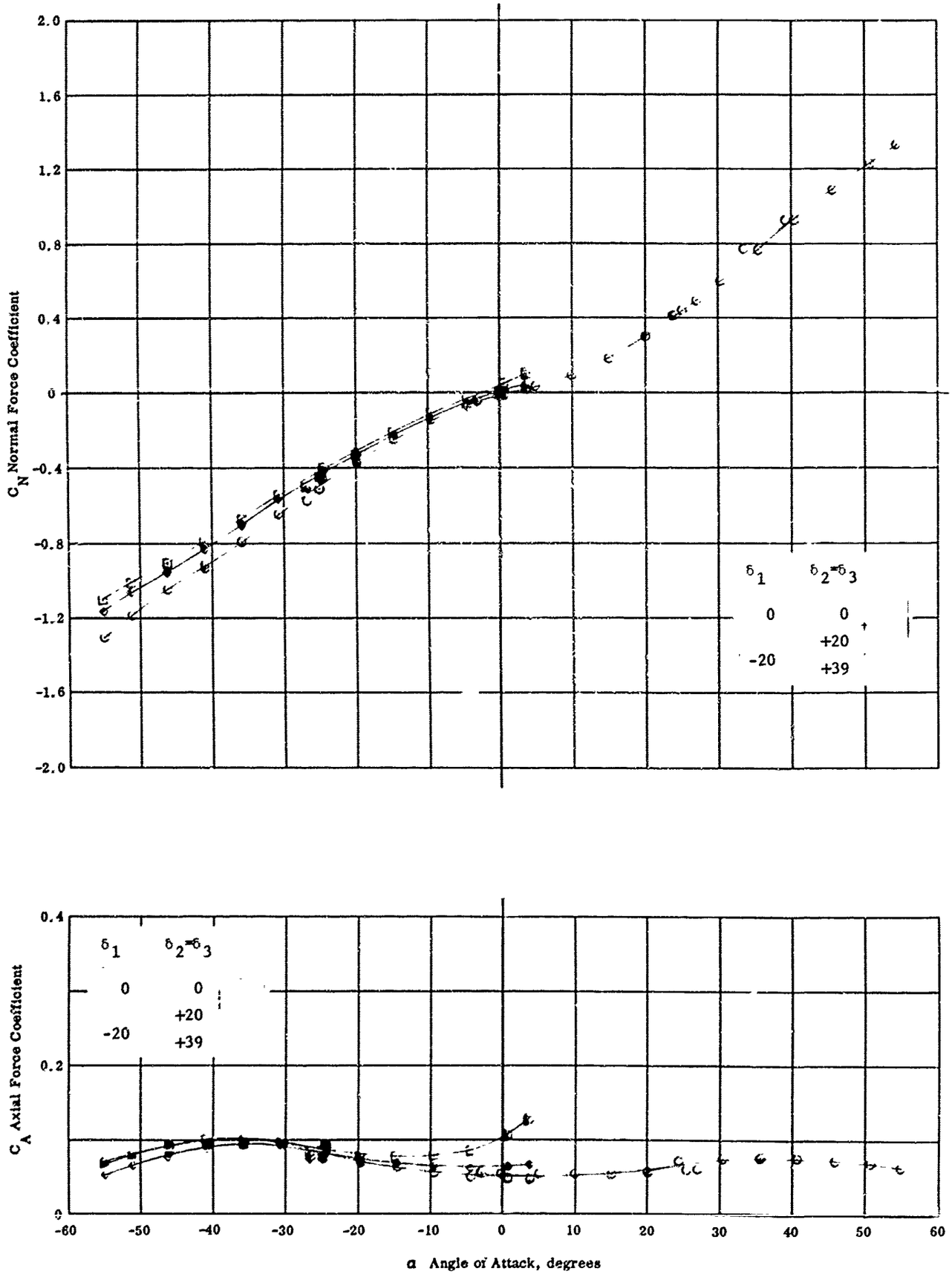

Fig. 20d Configuration I - M_∞=8.08, C_N & C_A vs. α
$Re_\infty/ft \times 10^{-6}$ = 2.26 $\delta_1=\delta_2=\delta_3=0$, $\delta_1=-20$ $\delta_2=\delta_3=+20$, +39

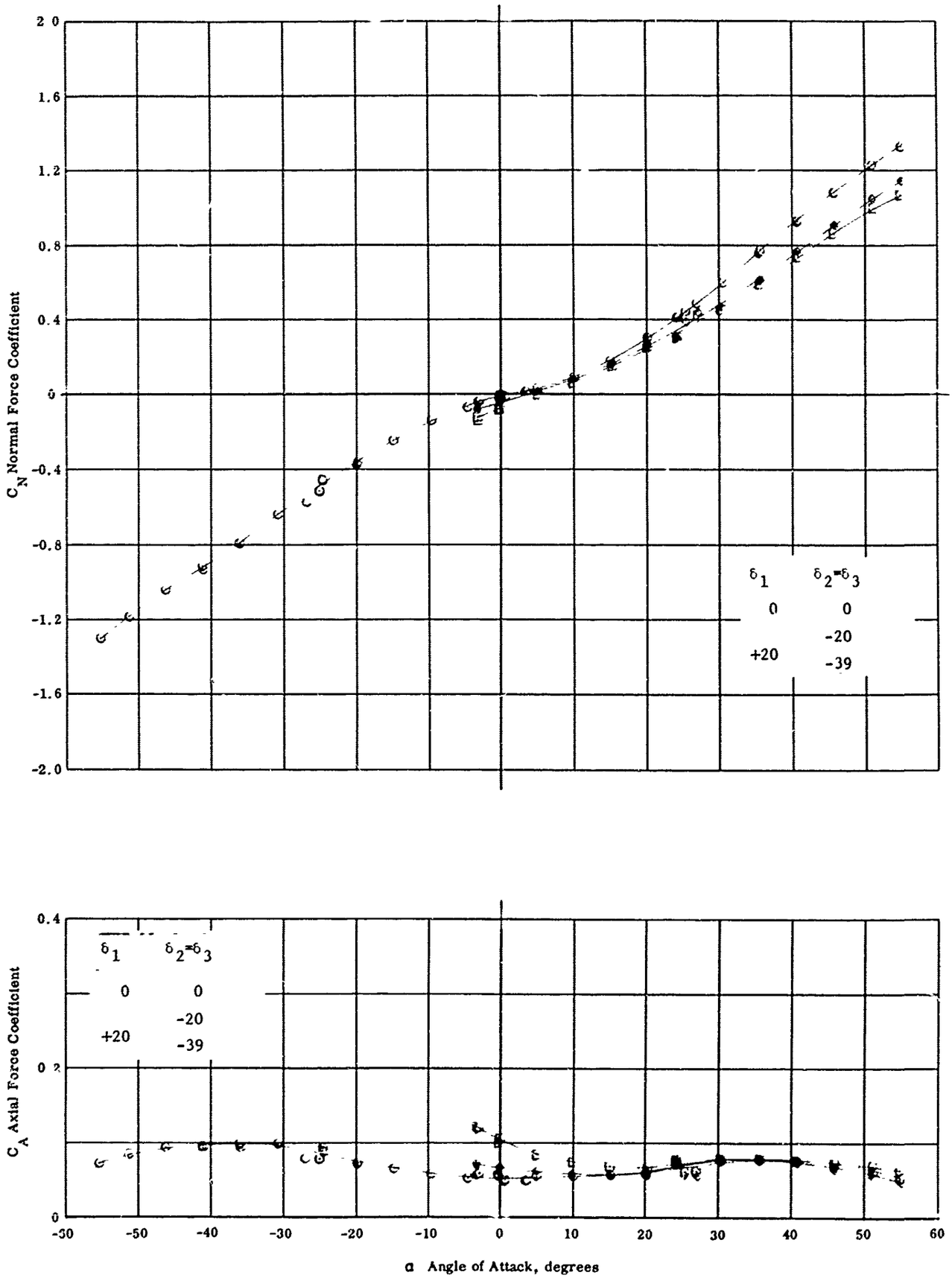

Fig. 20e Configuration I - M_∞=8.08, C_N & C_A vs. α
Re_∞/ft x 10^{-6} = 2.26 $\delta_1=\delta_2=\delta_3=0$, $\delta_1=+10$ $\delta_2=\delta_3=-20,-39$

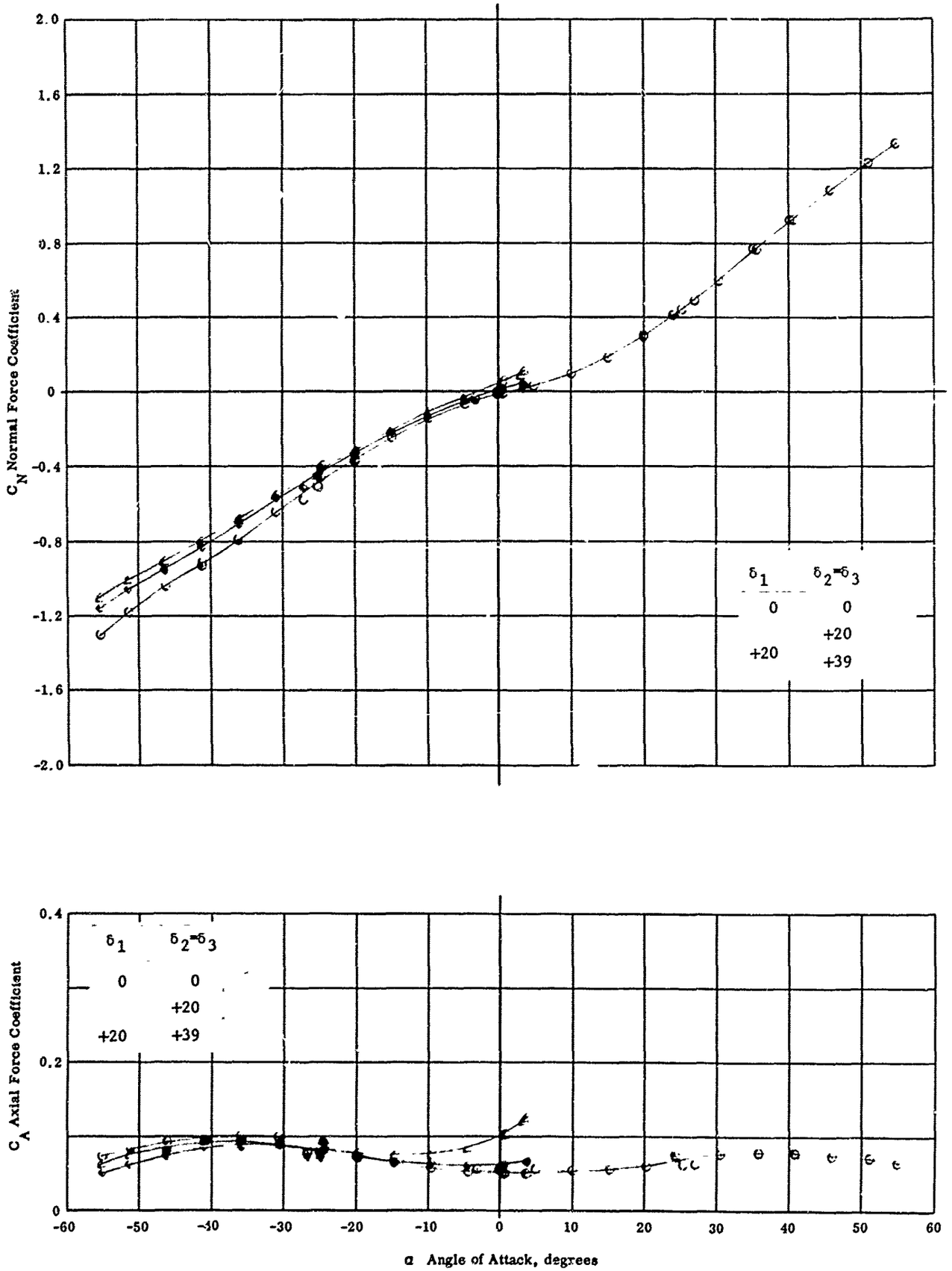

Fig. 20f Configuration I - M_∞=8.08, C_N & C_A vs. α
Re_∞/ft x 10^{-6} = 2.26 $\delta_1=\delta_2=\delta_3=0$ δ_1=+20 $\delta_2=\delta_3$=+20,+39

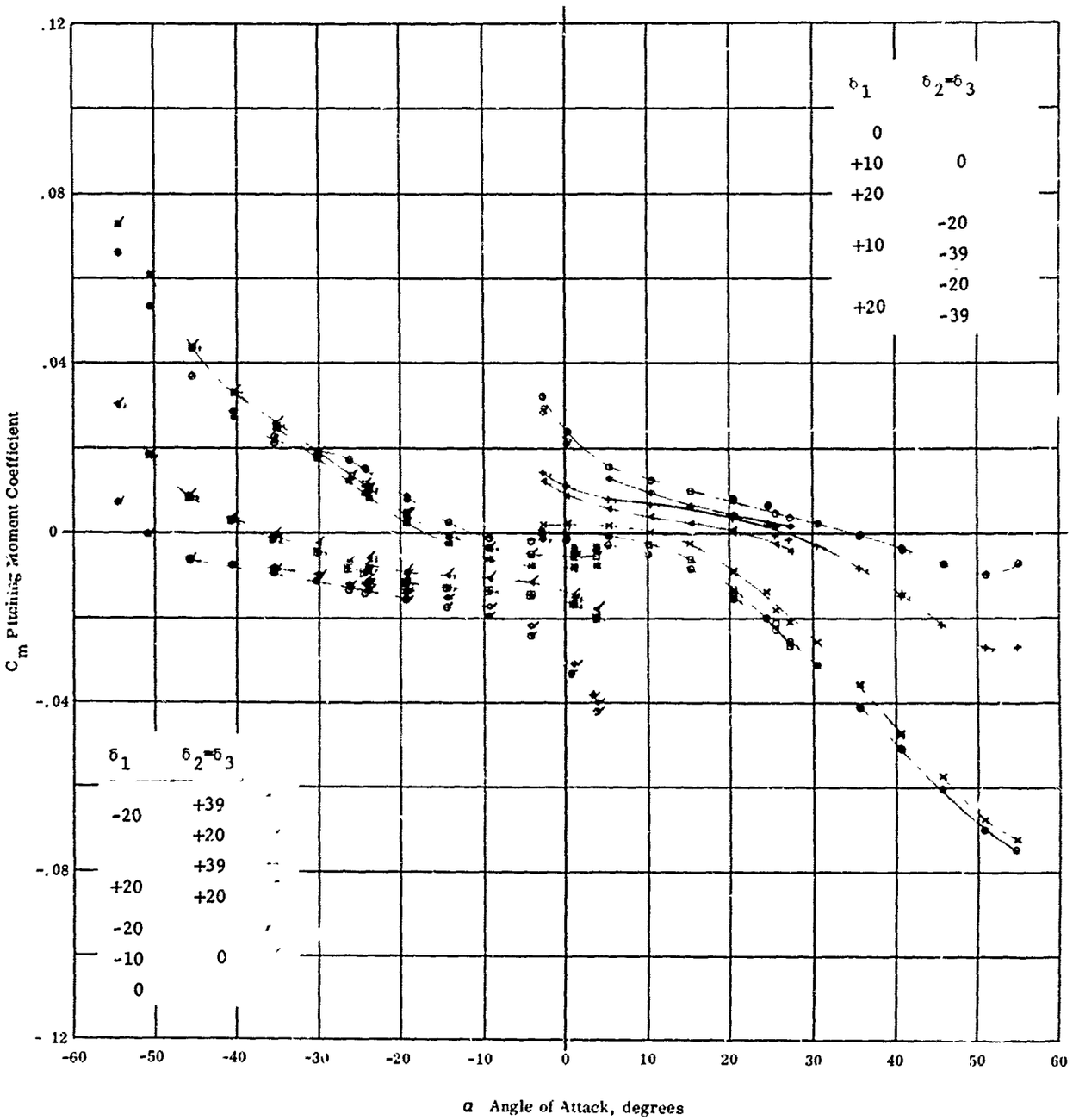

Fig. 20g Configuration 1 - M_∞=8.08, C_m vs. α
Re_∞/ft x 10^{-6} = 2.26 δ_1=0,±10,±20 δ_2=δ_3=0
δ_1=+20 δ_2=δ_3=±20, ±39
δ_1=+10 δ_2=δ_3=-20, -39
δ_1=-20 δ_2=δ_3=+20, +39

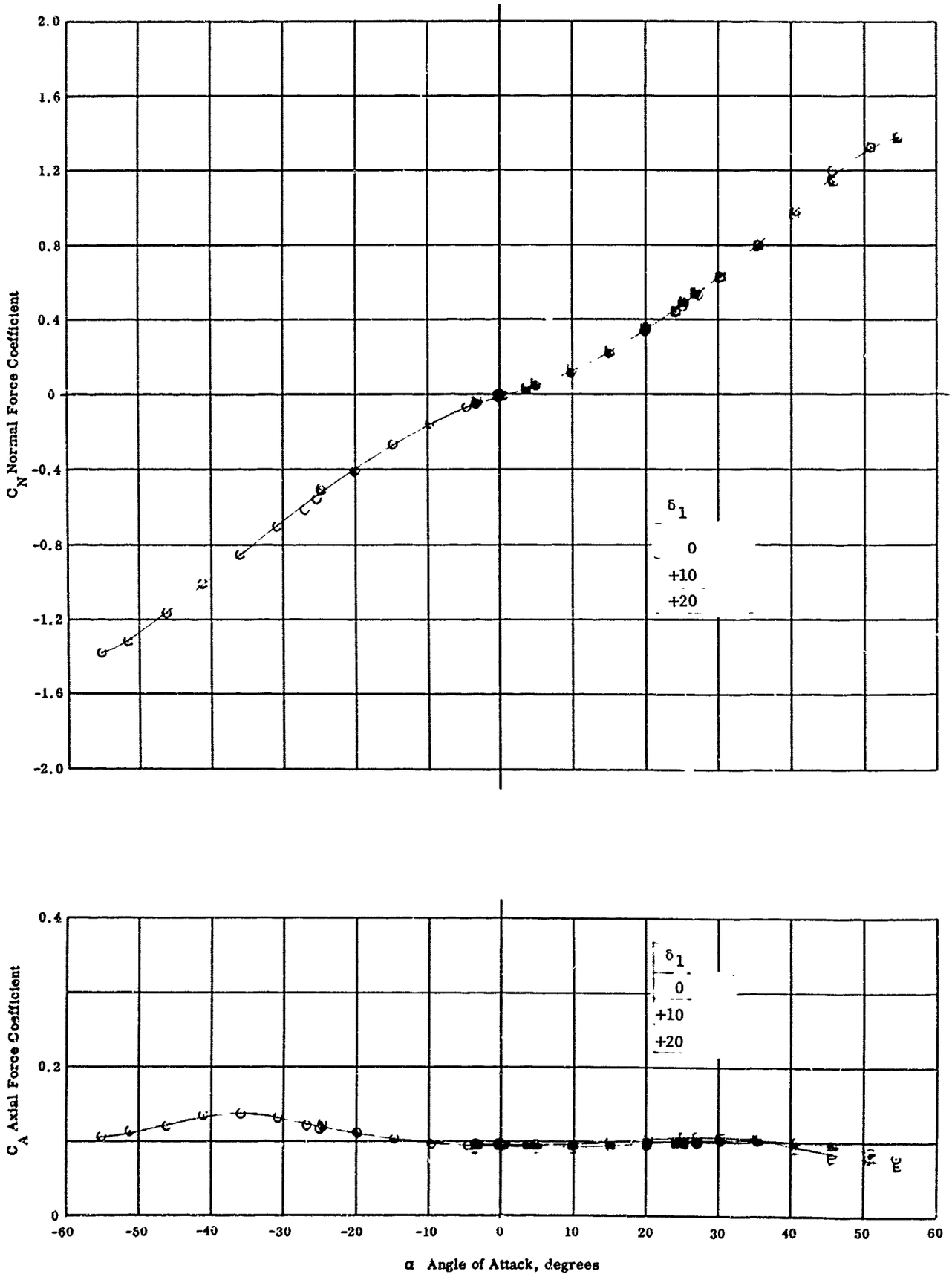

Fig. 21a Configuration IV - M_∞=8.08, C_N & C_A vs. α
Re_∞/ft x 10^{-6} = 2.26 δ_1=0, +10, +20 δ_2=δ_3=0

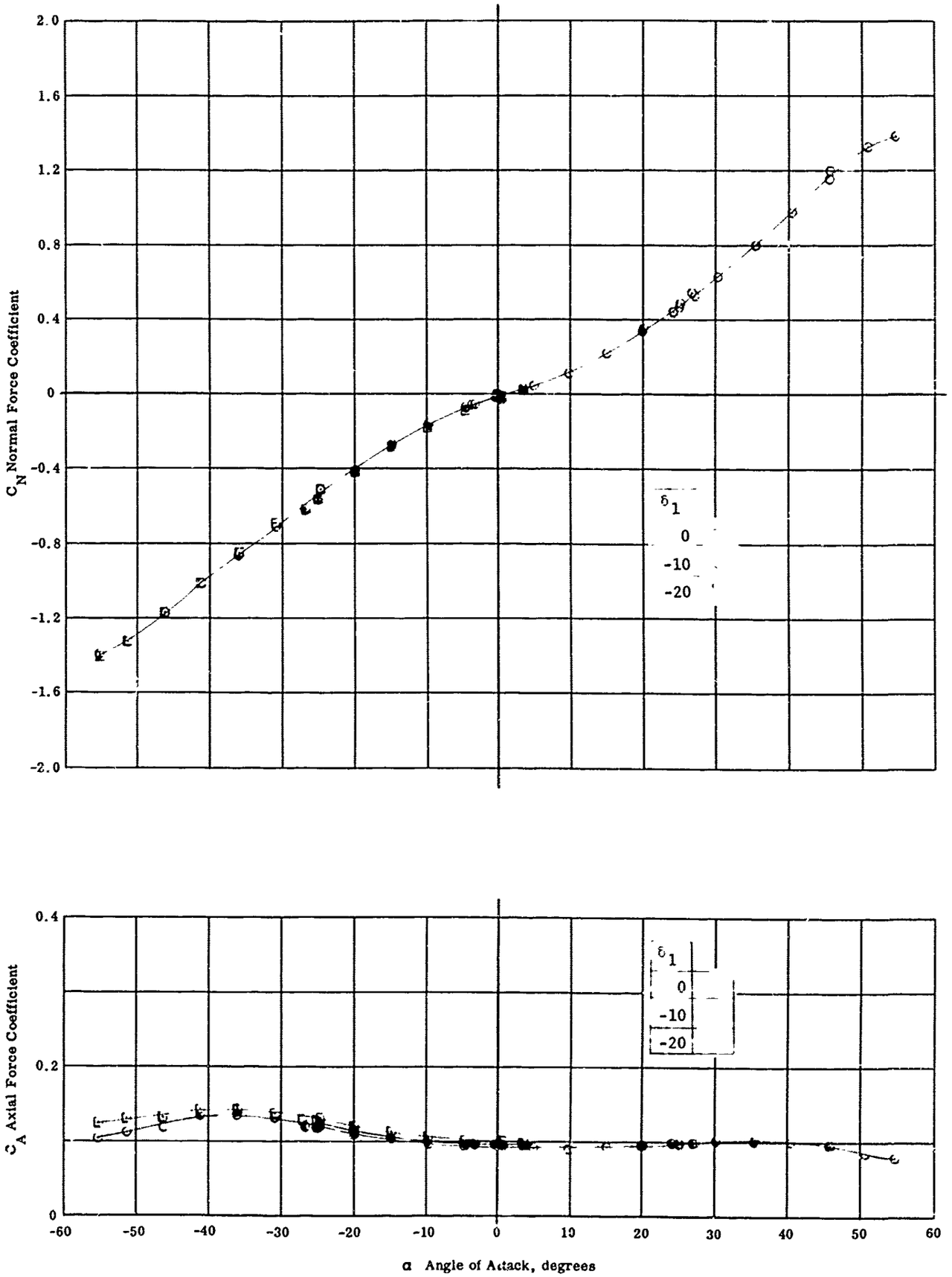

Fig. 21b Configuration IV - M_∞=8.08, C_N & C_A vs. α
$Re_\infty/ft \times 10^{-6}$ = 2.26 δ_1=0, -10, -20 δ_2=δ_3=0

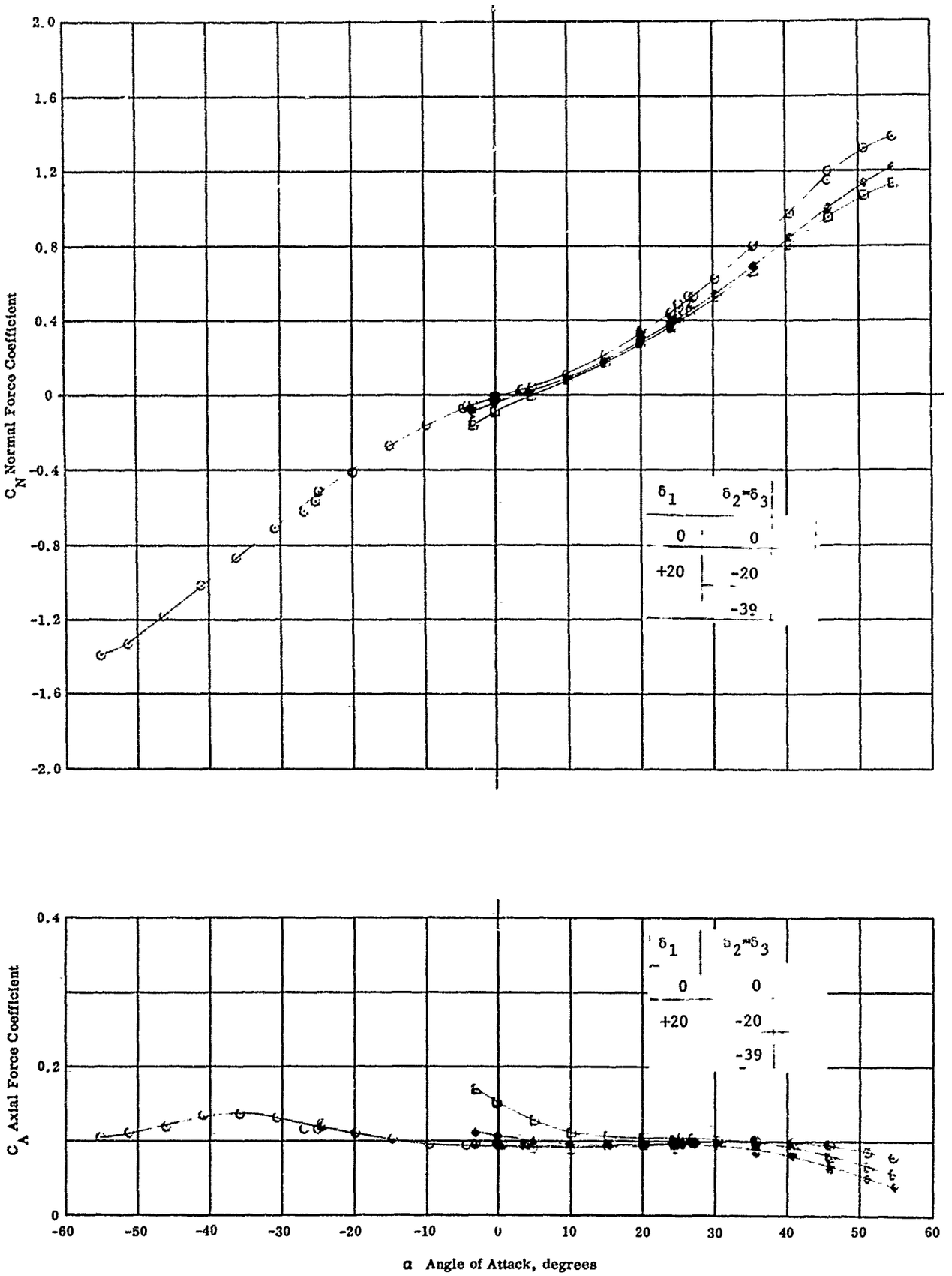

Fig. 21c Configuration IV - M_∞=8.08, C_N & C_A vs. α
$Re_\infty/ft \times 10^{-6}$ = 2.26 $\delta_1=\delta_2=\delta_3=0$, $\delta_1=+20$ $\delta_2=\delta_3=-20,-39$

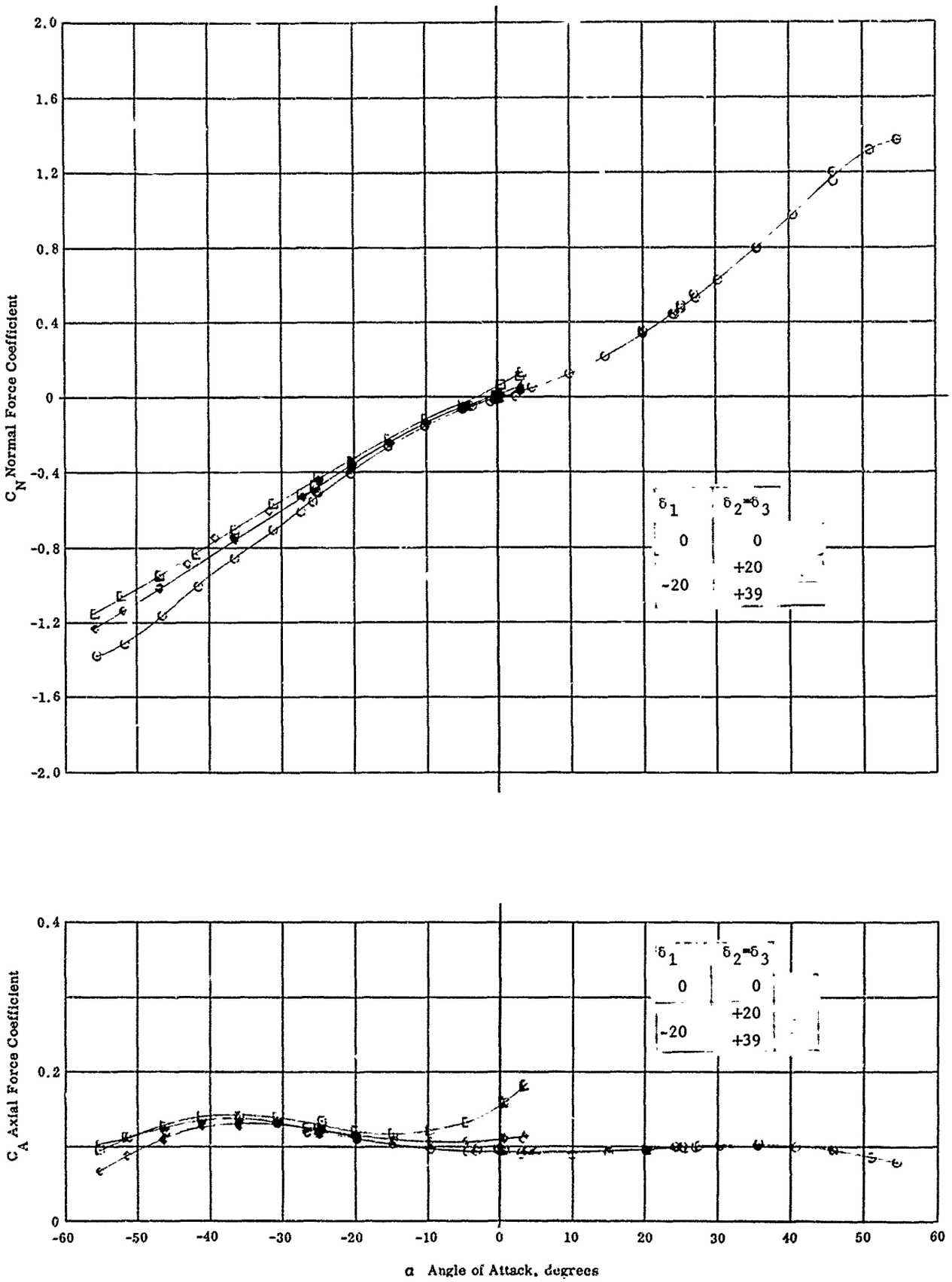

Fig. 21d Configuration IV - M_∞=8.08, C_N & C_A vs. α
Re_∞/ft x 10^{-6} = 2.26 $\delta_1=\delta_2=\delta_3=0$, δ_1=-20 $\delta_2=\delta_3$+20, +39

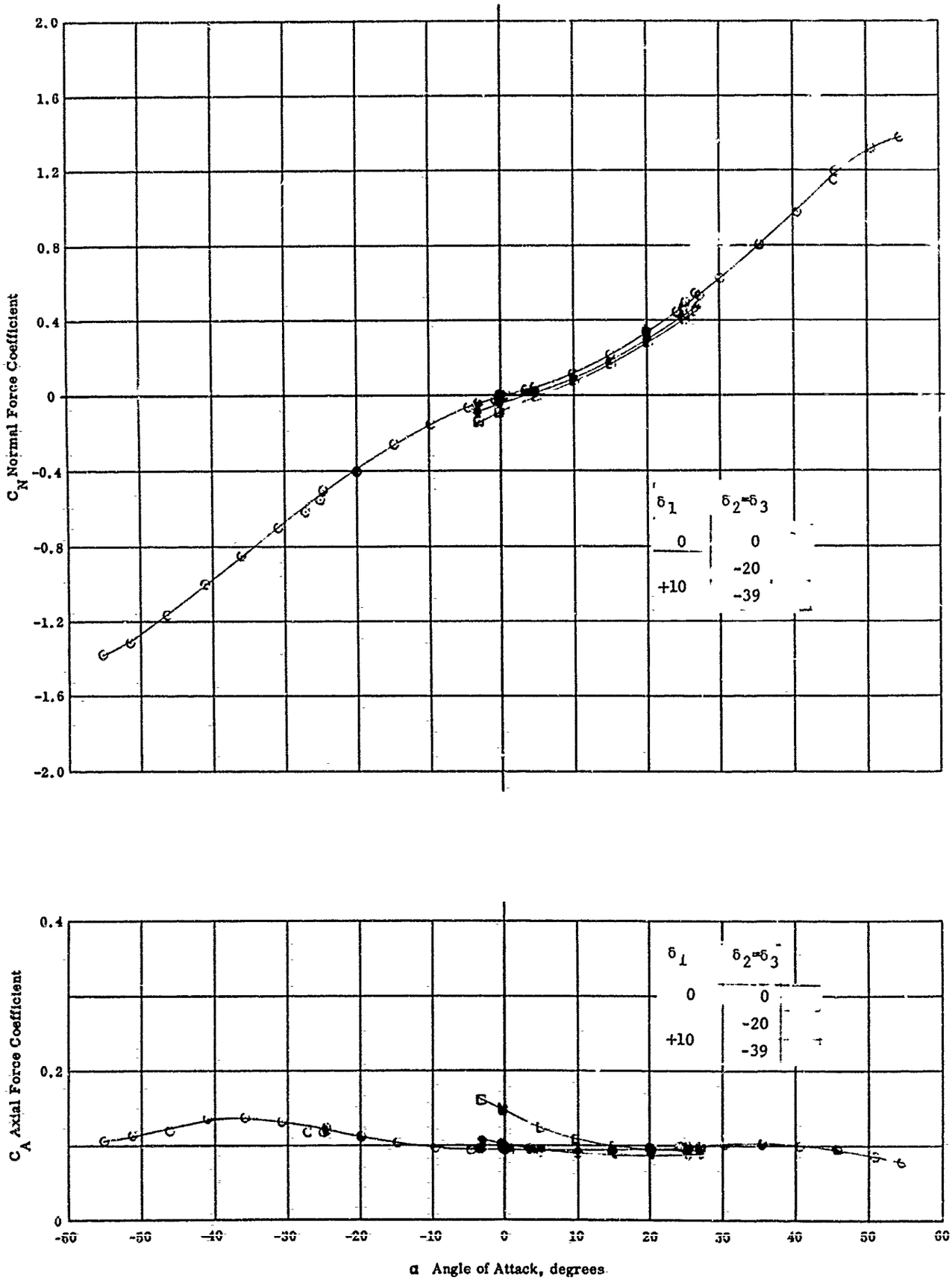

Fig. 21e Configuration IV - M_∞=8.08 C_N & C_A vs. α
$Re_\infty/ft \times 10^{-6}$ = 2.26 $\delta_1=\delta_2=\delta_3=0$, δ_1=+10 $\delta_2=\delta_3$=-20,-39

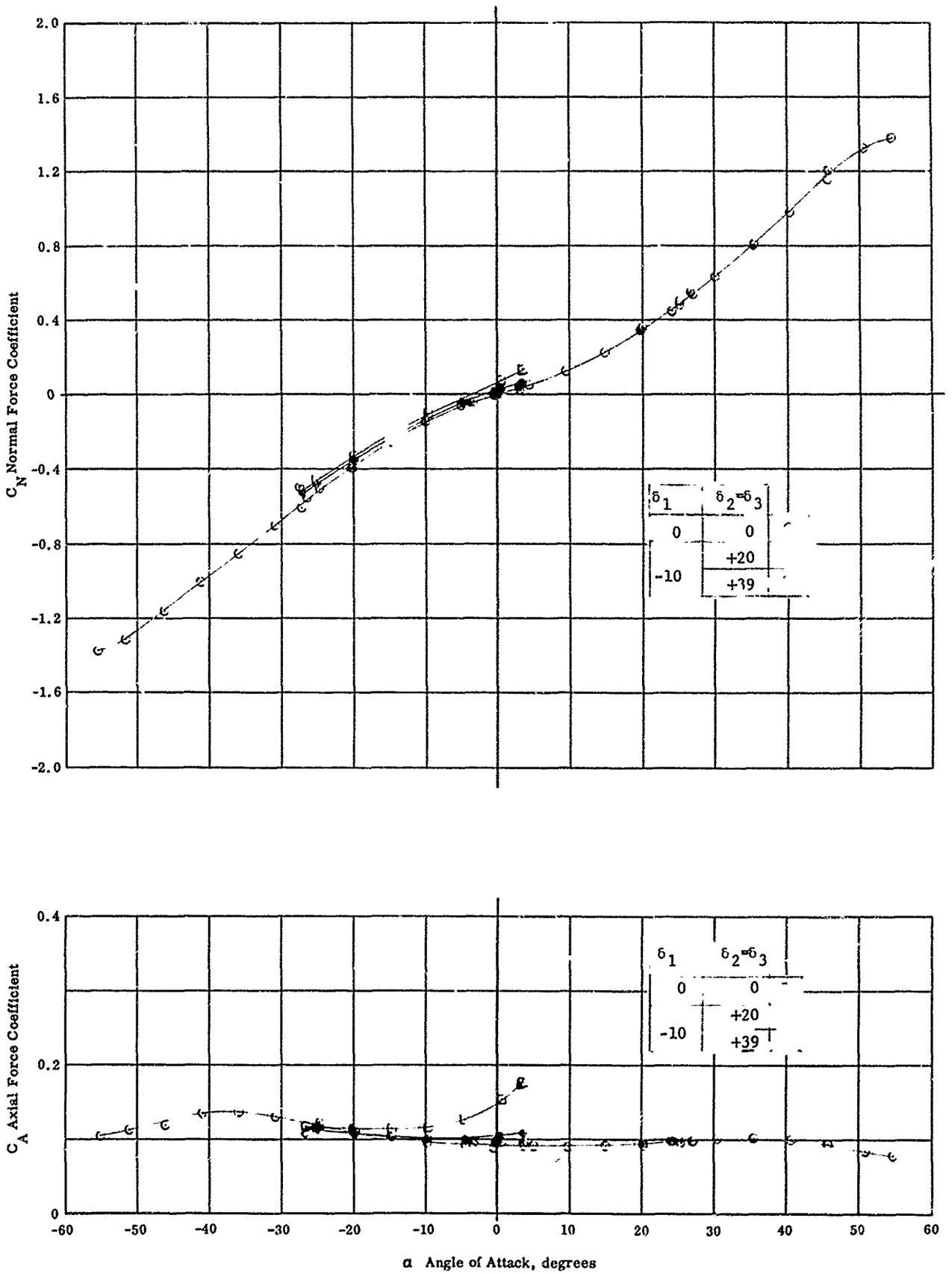

Fig. 21f Configuration IV - M_∞=8.08, C_N & C_A vs. α
$Re_\infty/ft \times 10^{-6}$ = 2.26 $\delta_1=\delta_2=\delta_3=0$, $\delta_1=-10$ $\delta_2=\delta_3=+20,+39$

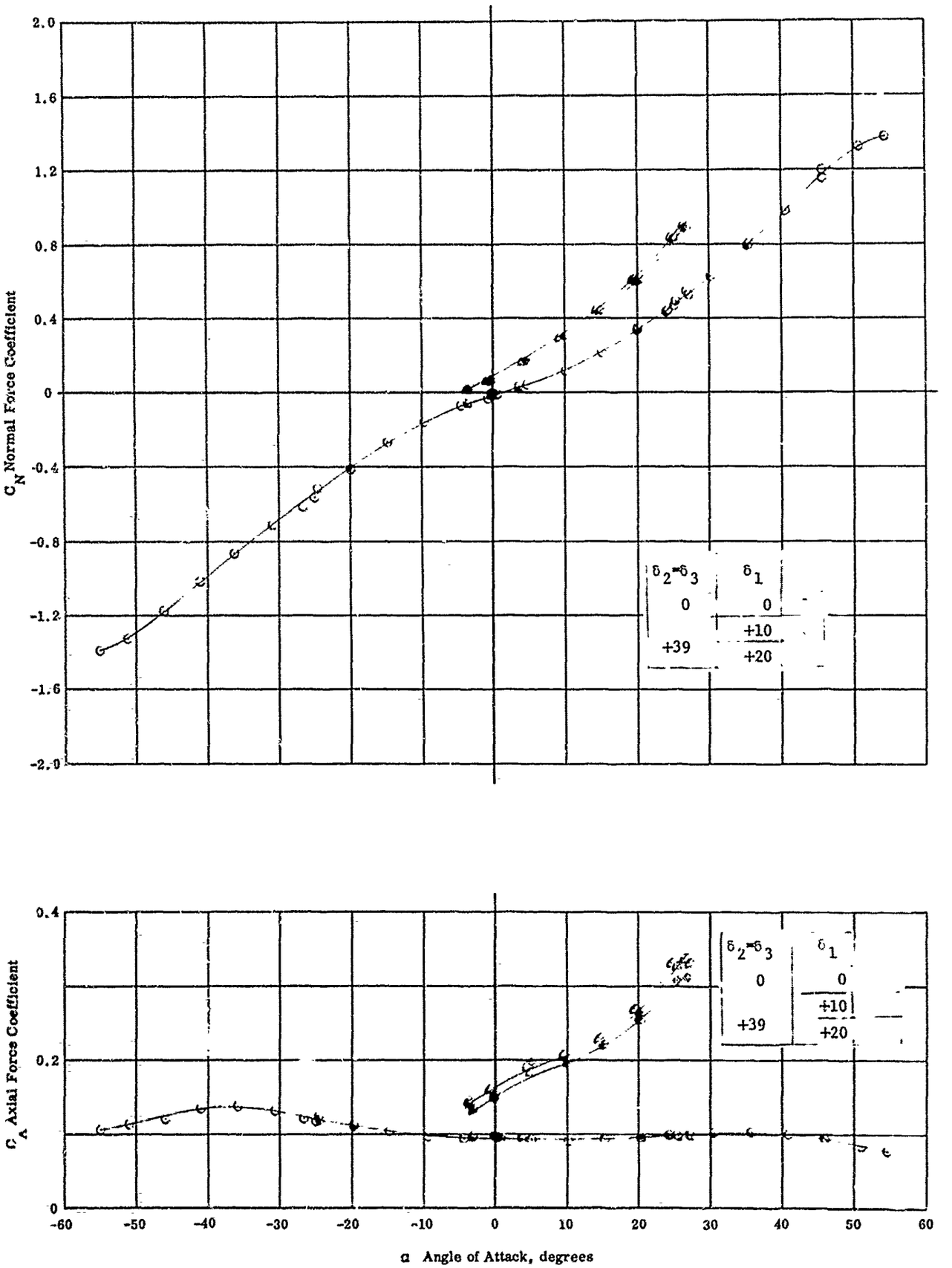

Fig. 21g Configuration IV - M_∞=8.08, C_N & C_A vs. α
$Re_\infty/ft \times 10^{-6}$ = 2.26 $\delta_1=\delta_2=\delta_3=0$, δ_1=+10,+20 $\delta_2=\delta_3$=+39

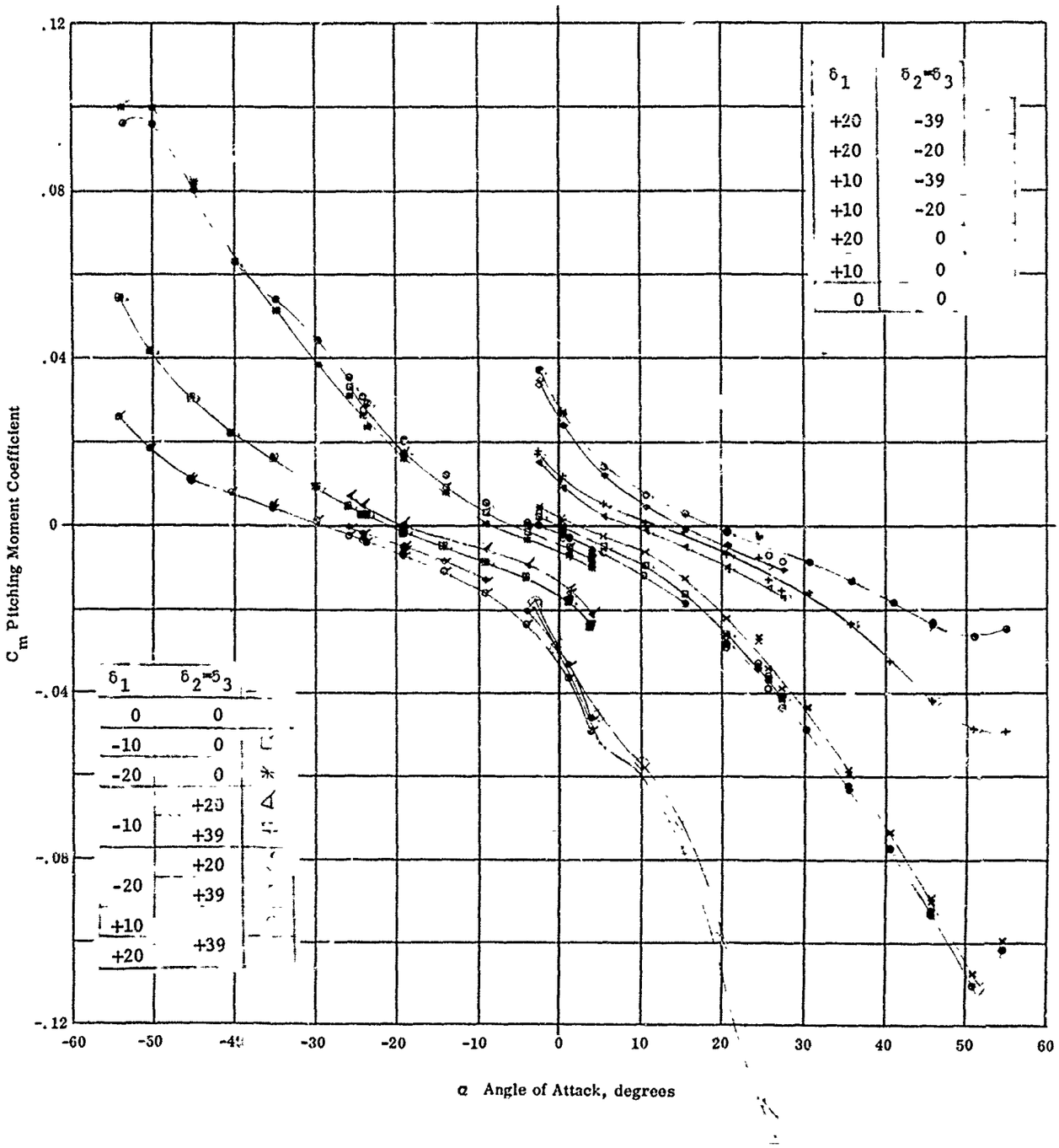

Fig. 21h Configuration IV - M_∞=8.08, C_m vs. α
$Re_\infty/ft \times 10^{-6}$ = 2.26 δ_1=0,±10,±20 $\delta_2=\delta_3$=0
δ_1=+10,+20 $\delta_2=\delta_3$=-20, ∓39
δ_1=-10,-20 $\delta_2=\delta_3$=+20,+39

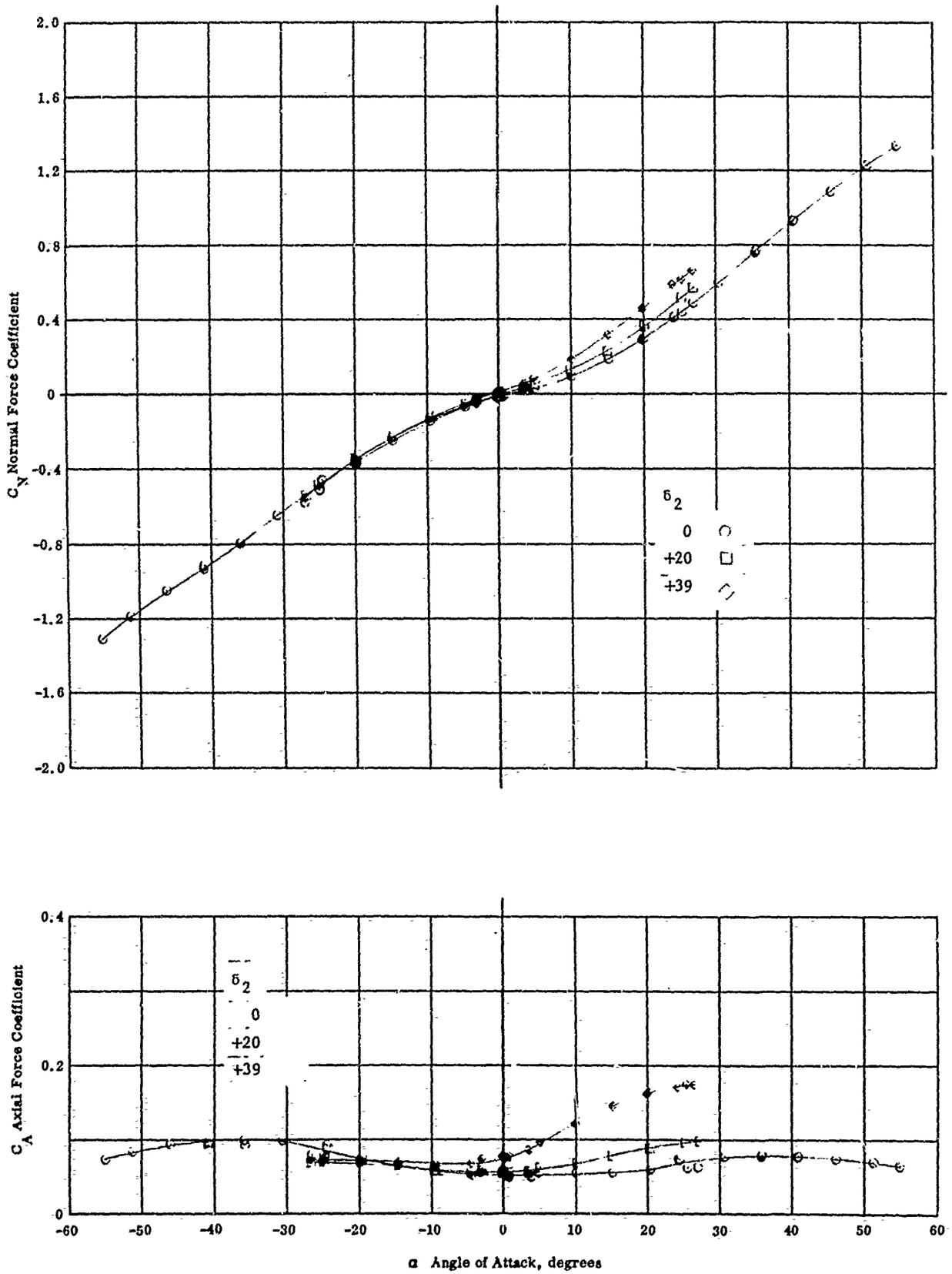

Fig. 22a Configuration I - M_∞=8.08, C_N & C_A vs. α
$Re_\infty/ft \times 10^{-6}$ = 2.26 $\delta_1=\delta_3=0$ δ_2=0, +20,+39

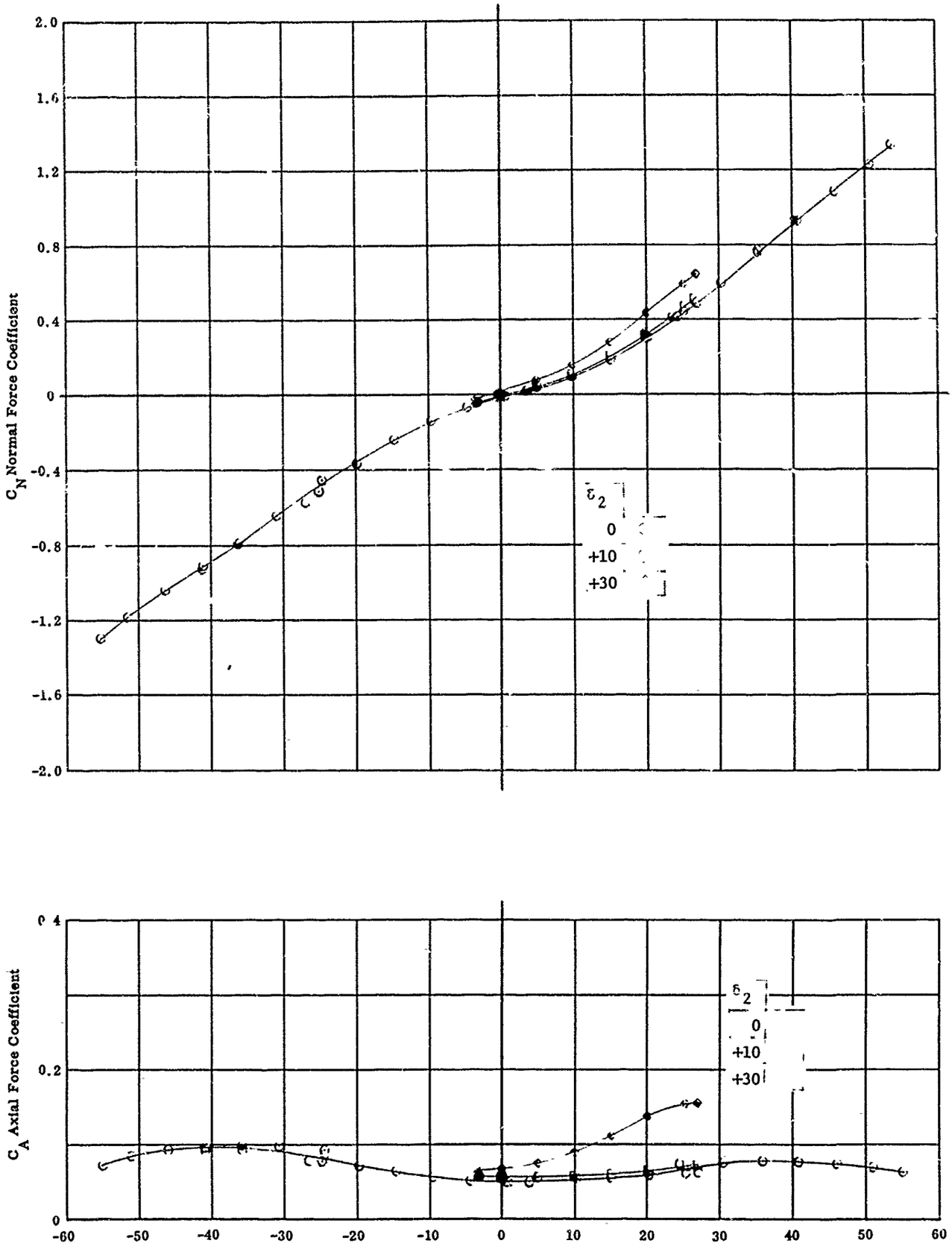

Fig. 22b Configuration I - M_∞=8.08, C_N & C_A vs. α
Re_∞/ft x 10^{-6} = 2.26 $\delta_1=\delta_3=0$ δ_2=0,+10,+30

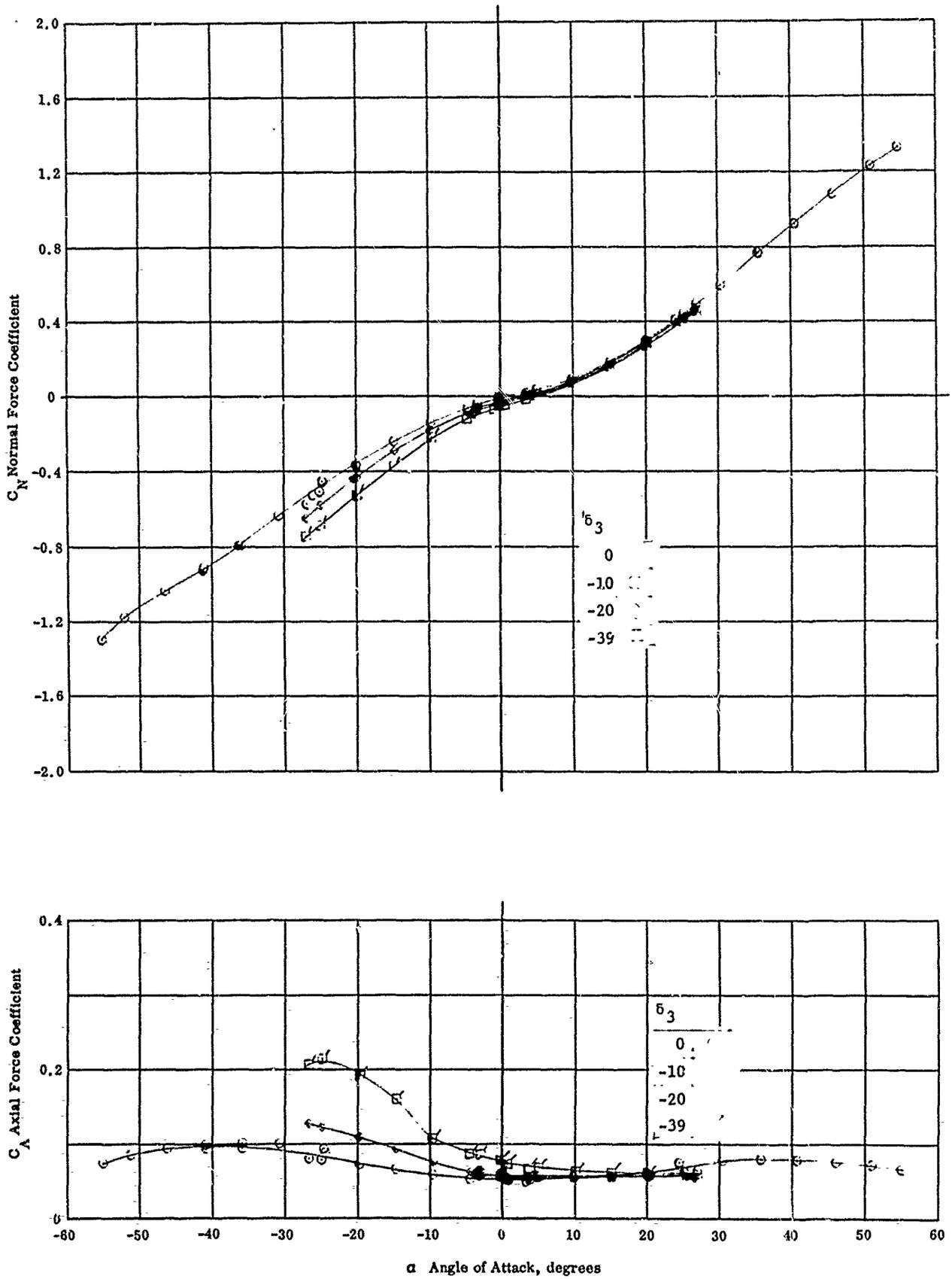

Fig. 22c Configuration I - M_∞=8.08, C_N & C_A vs. α
$Re_\infty/ft \times 10^{-6}$ = 2.26 $\delta_1=\delta_2=0$ δ_3=0,-10,-20,-39

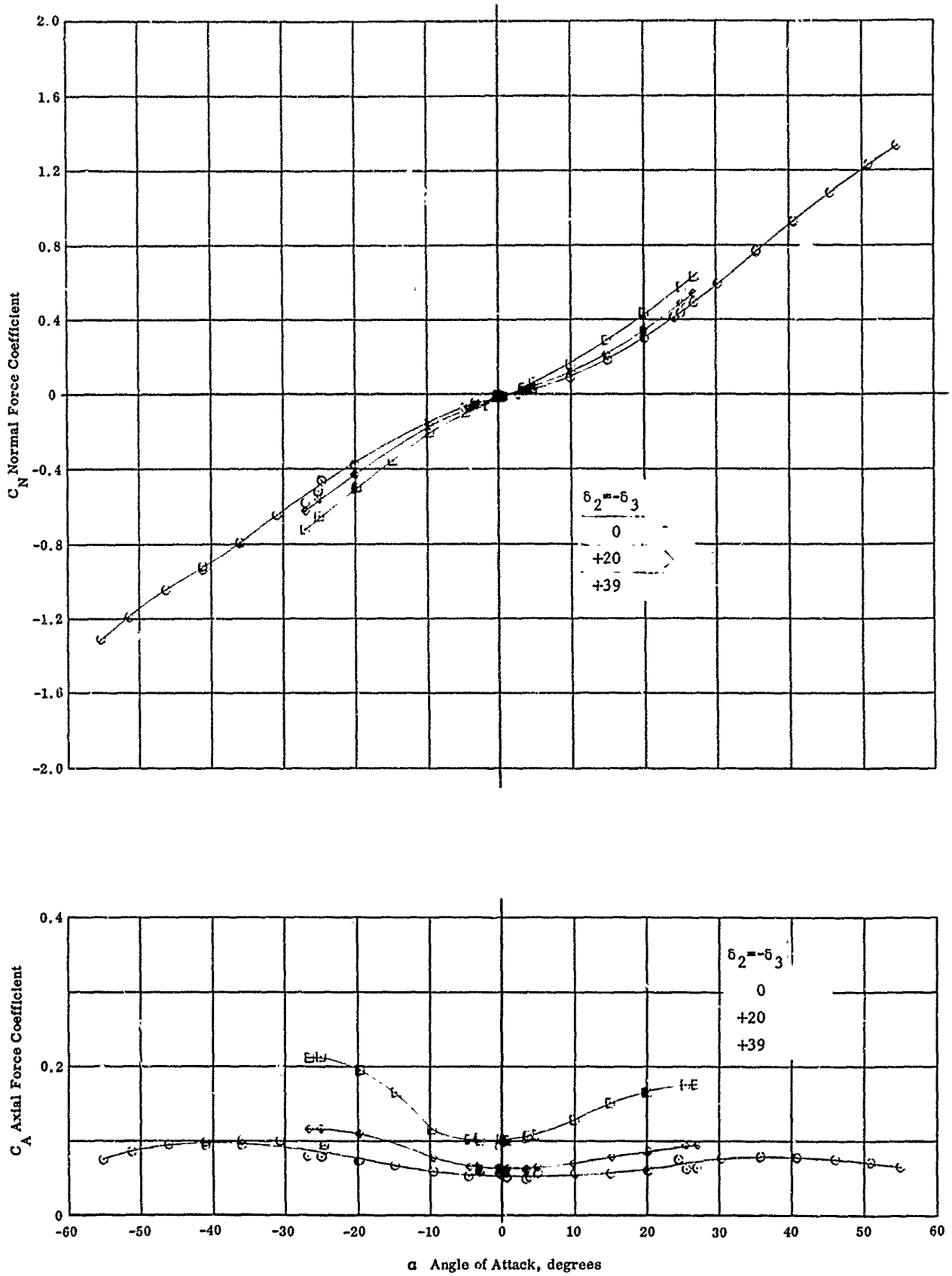

Fig. 22d Configuration I - M_∞=8.08, C_N & C_A vs. α
Re_∞/ft x 10^{-6}= 2.26 δ_1=0 $\delta_2=-\delta_3$=0,+20,+39

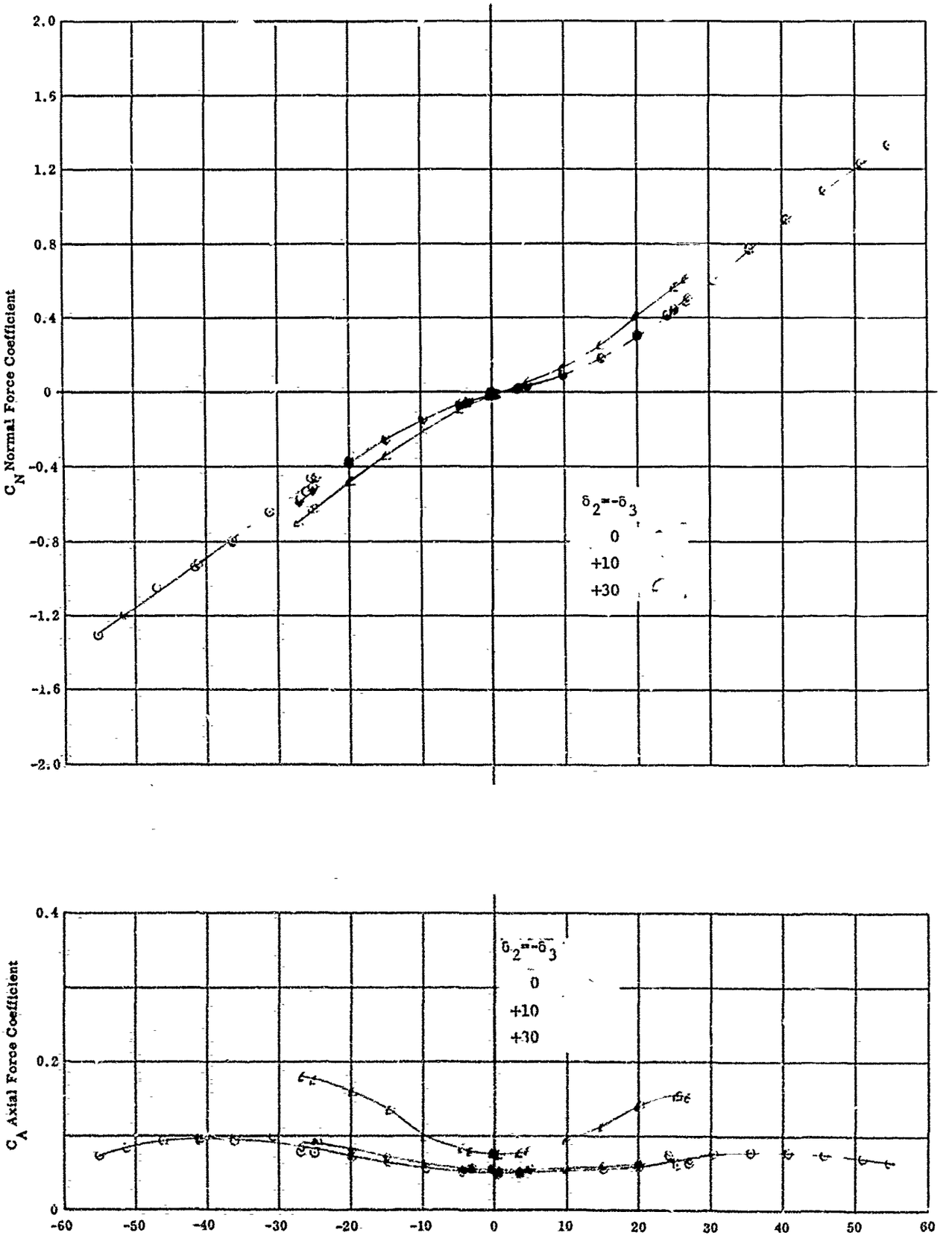

Fig. 22e Configuration I - M_∞=8.08, C_N & C_A vs. α
$Re_\infty/ft \times 10^{-6}$ = 2.26 δ_1=0 $\delta_2=-\delta_3$=0,+10,+30

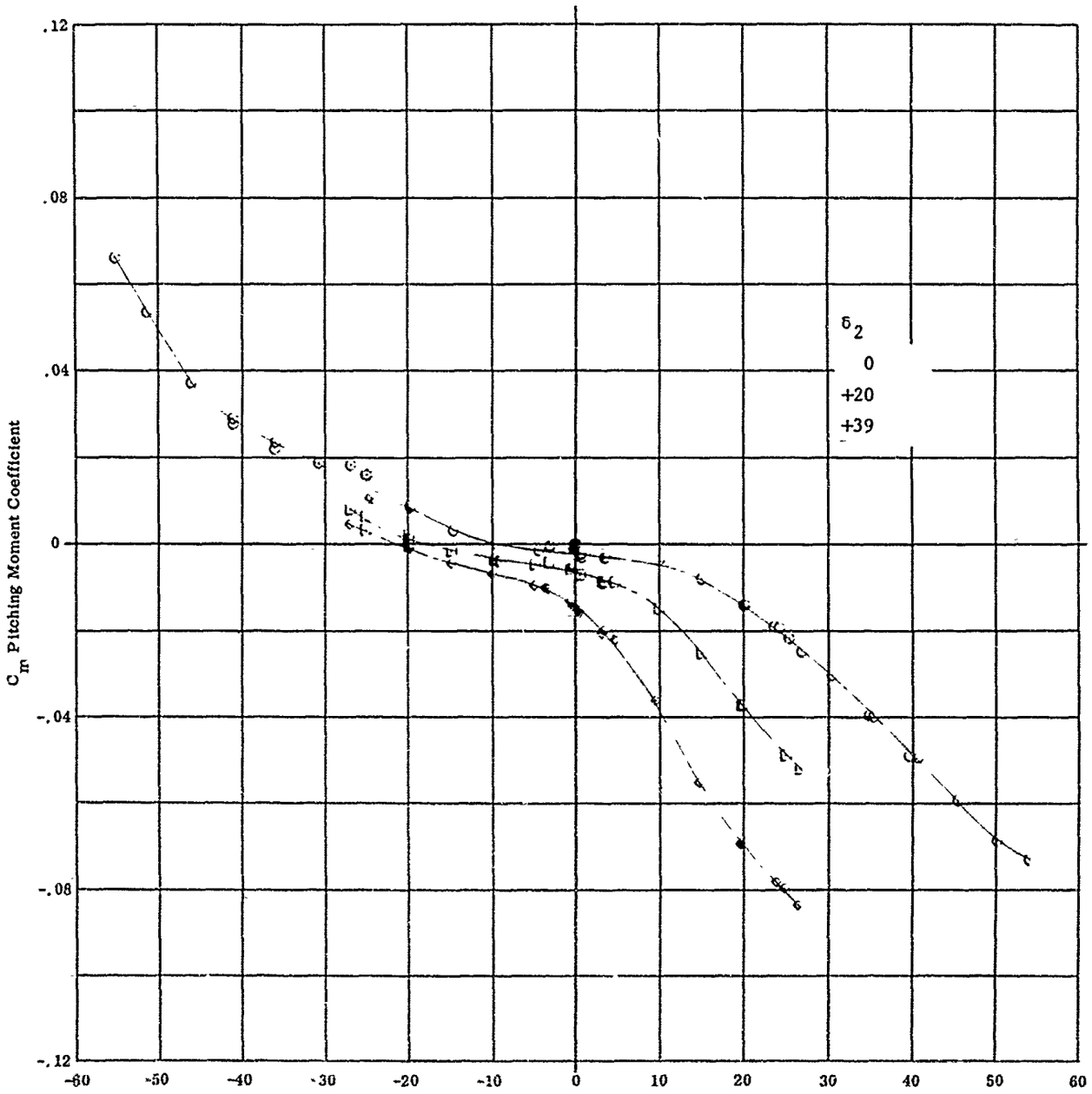

Fig. 22f Configuration I - M_∞=8.08, C_m vs. α
$Re_\infty/ft \times 10^{-6}$ = 2.26 $\delta_1=\delta_3=0$ δ_2=0,+20,+39

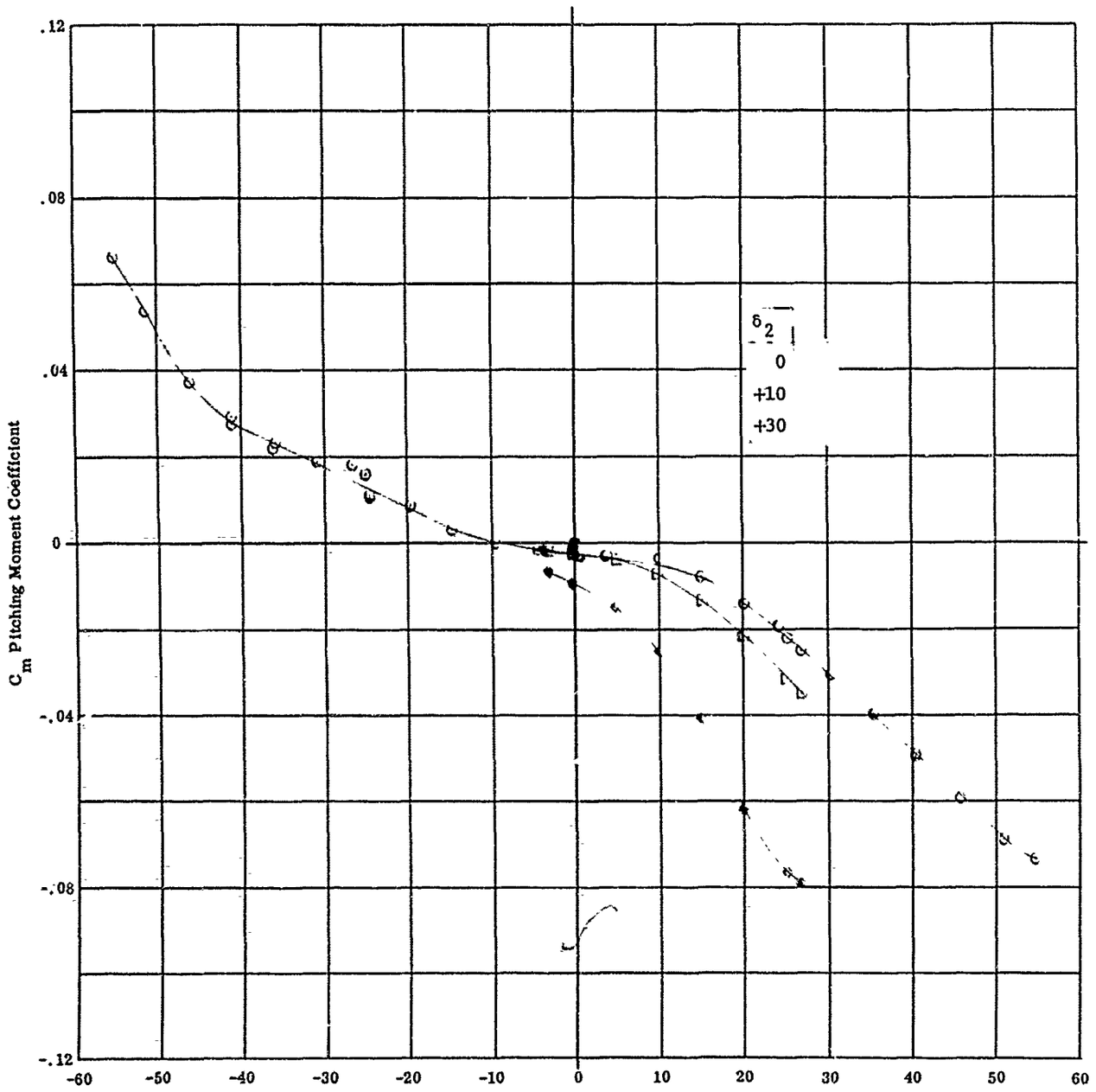

Fig. 22g Configuration I - M_∞=8.08, C_m vs. α
$Re_\infty/ft \times 10^{-6}$ = 2.26 $\delta_1=\delta_3=0$ δ_2=0,+10,+30

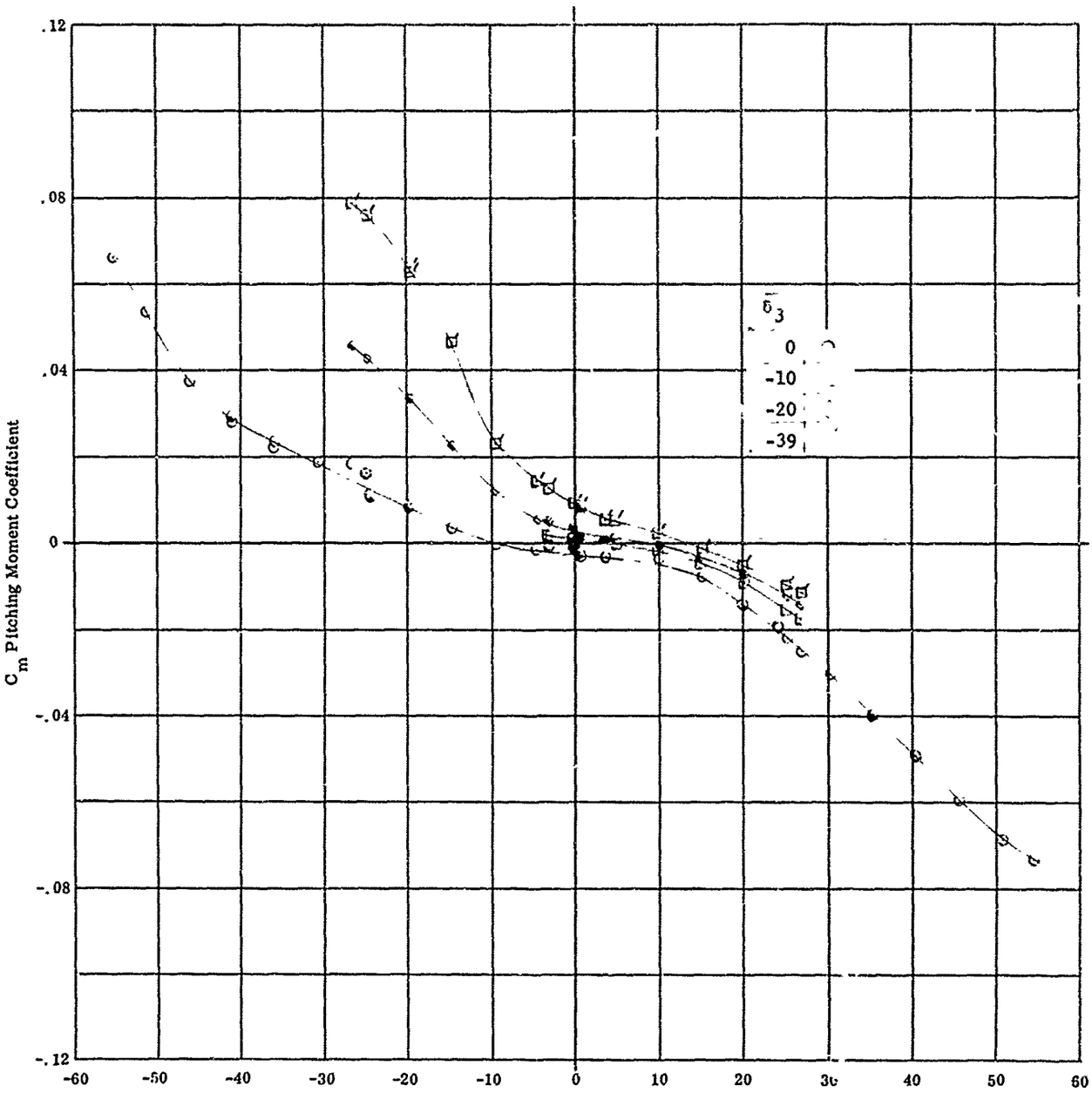

Fig. 22h Configuration I - M_∞=8.08, C_m vs. α
$Re_\infty/ft \times 10^{-6}$ = 2.26 $\delta_1=\delta_2=0$ δ_3=0,-10,-20,-39

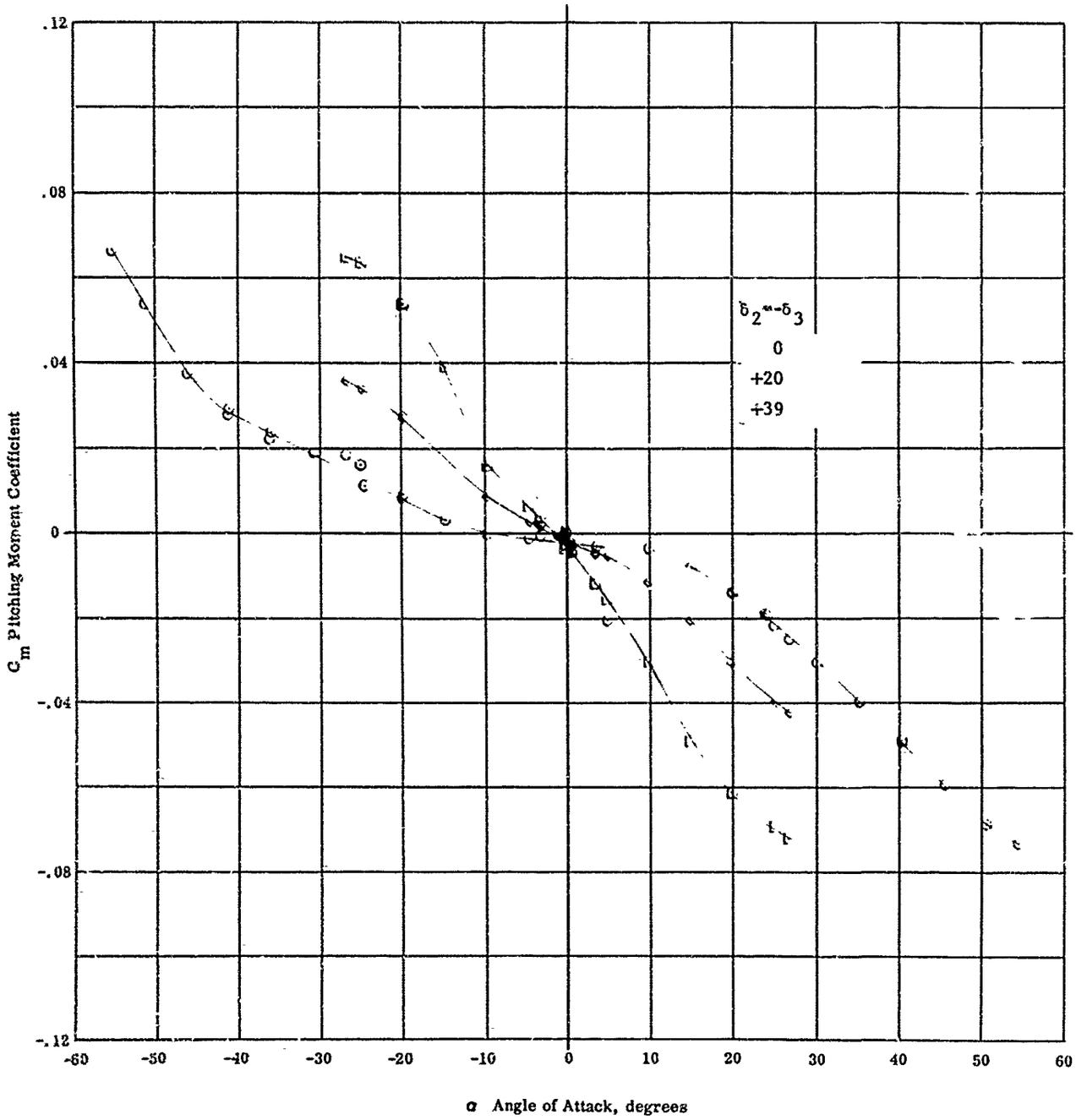

Fig. 22i Configuration I - M_∞=8.08, C_m vs. α
Re_∞/ft x 10^{-6} = 2.26 δ_1=0 δ_2=-δ_3=0,+20,+39

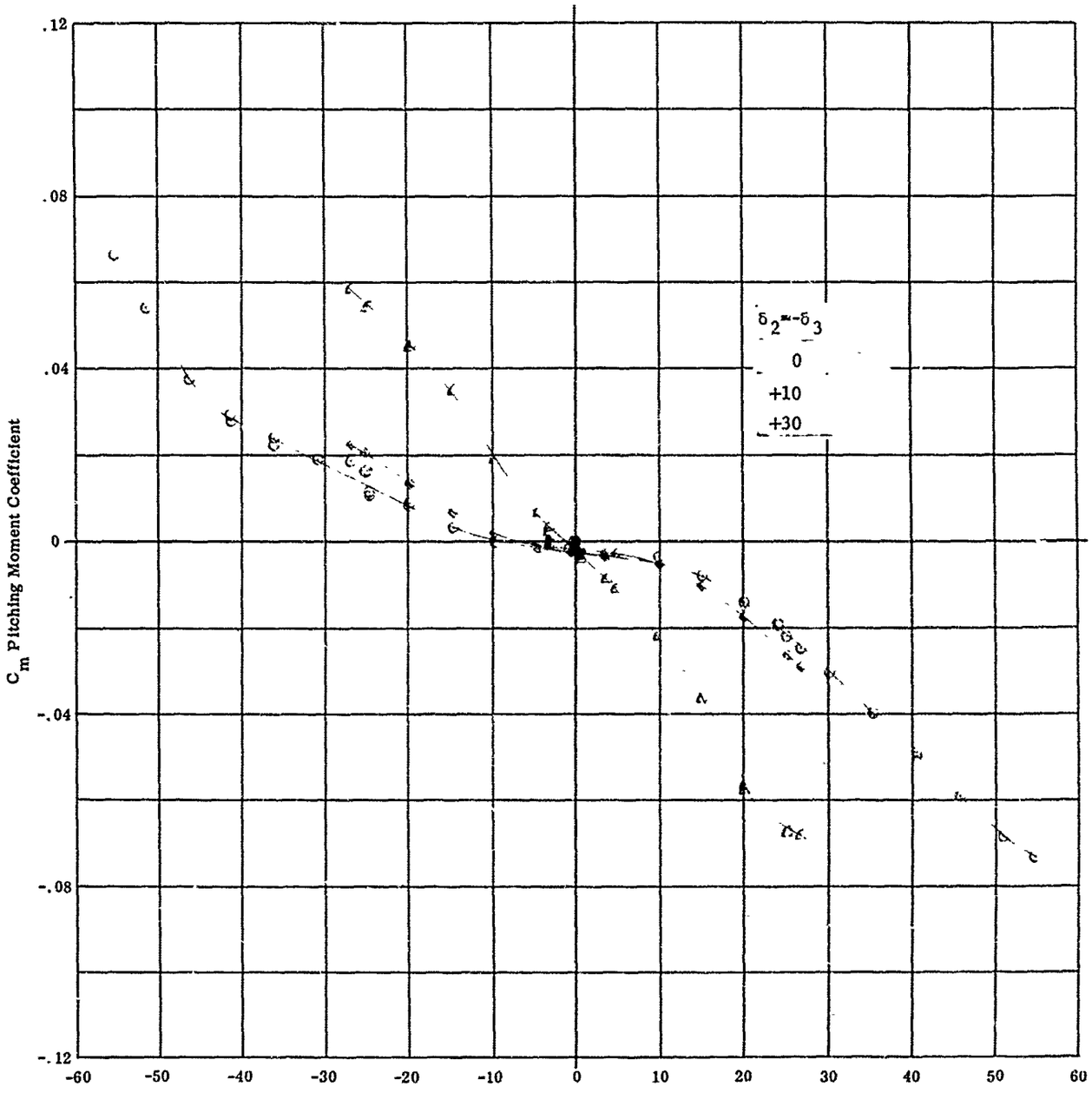

Fig. 22j Configuration I - M_∞=8.08, C_m vs. α
$Re_\infty/ft \times 10^{-6}$ = 2.26 δ_1=0 $\delta_2=-\delta_3$=0,+10,+30

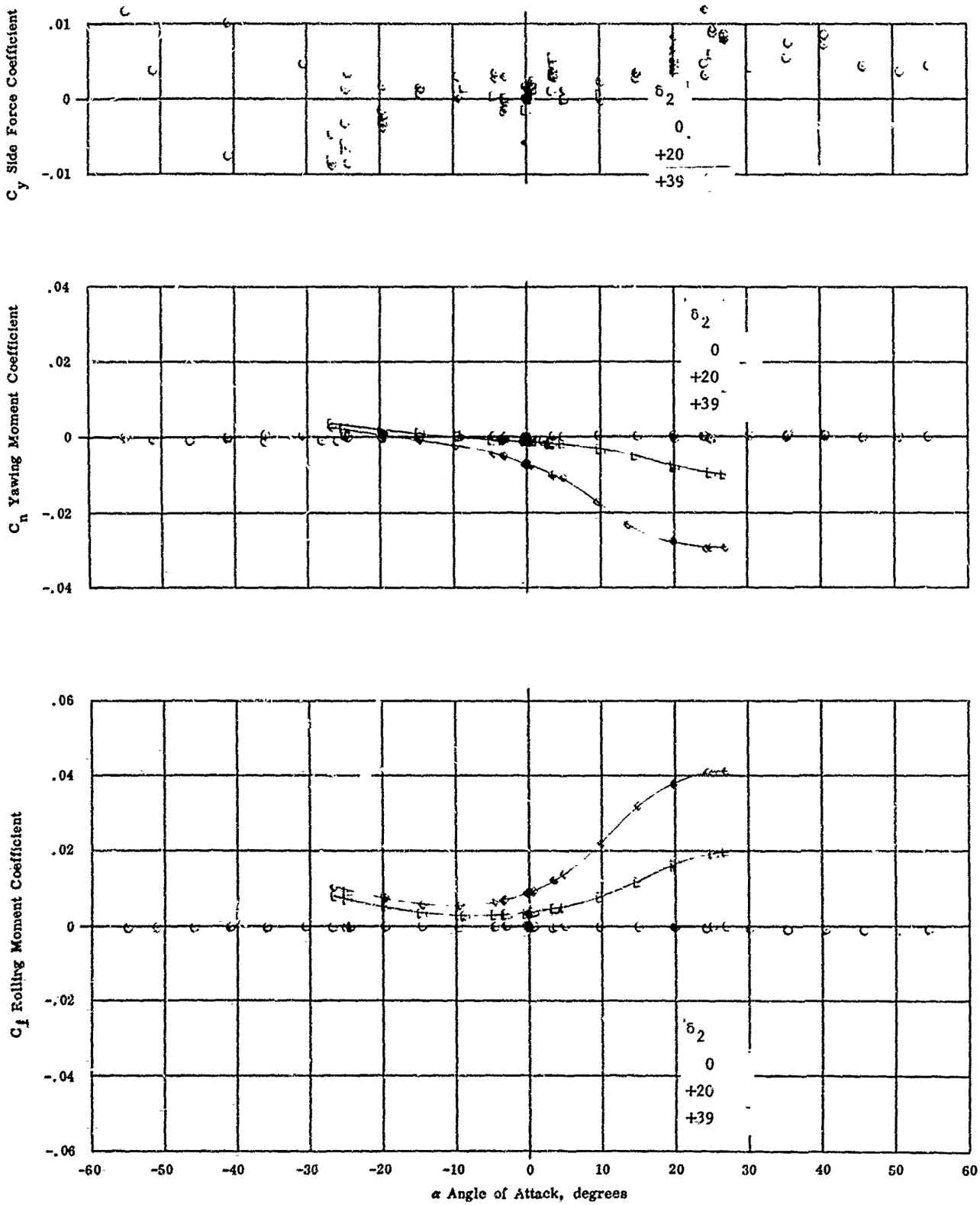

Fig. 22k Configuration I - M_∞=8.08, C_y, C_n, C_ℓ vs. α
Re_∞/ft x 10^{-6} = 2.26 $\delta_1=\delta_3=0$ $\delta_2=0,+20,+39$

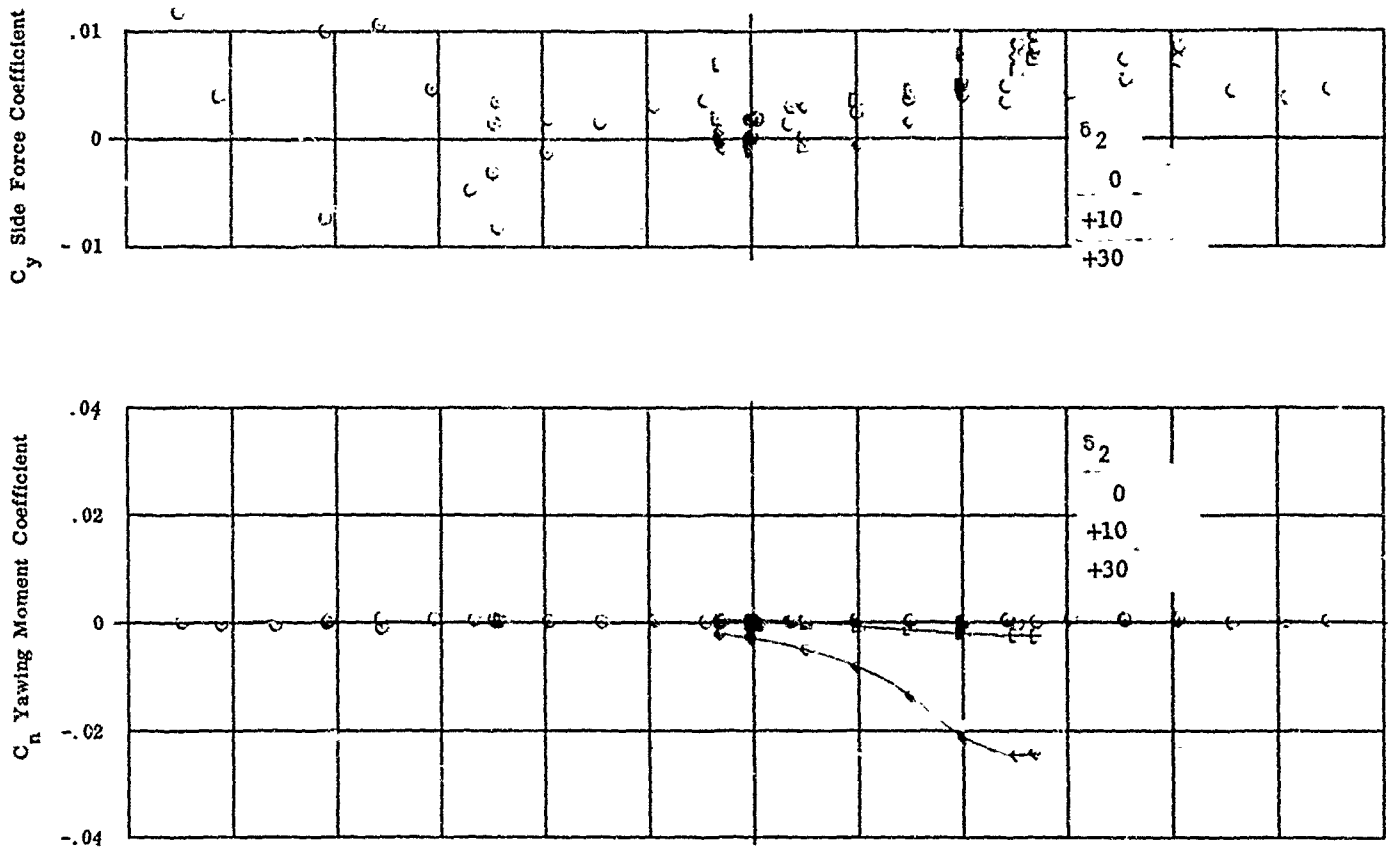

Fig. 22ℓ Configuration I - M_∞=8.08, C_y, C_n, C_ℓ vs. α
$Re_\infty/ft \times 10^{-6}$ = 2.26 $\delta_1=\delta_3=0$ δ_2=0,+10,+30

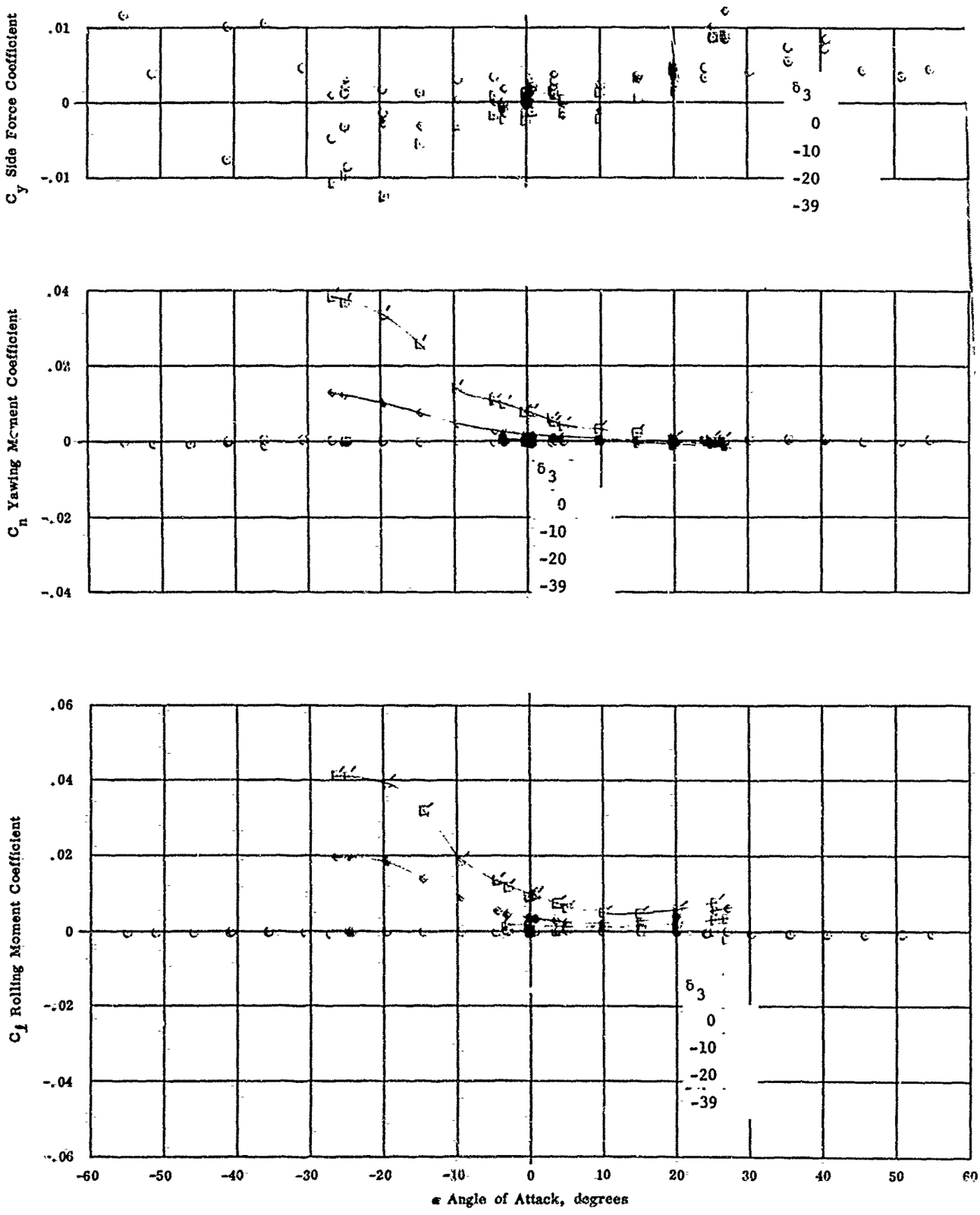

Fig. 22m Configuration I - M_∞=8.08, C_y, C_n, C_ℓ vs. α
$Re_\infty/ft \times 10^{-6}$ = 2.26 $\delta_1=\delta_2=0$ δ_3=0,-10,-20,-39

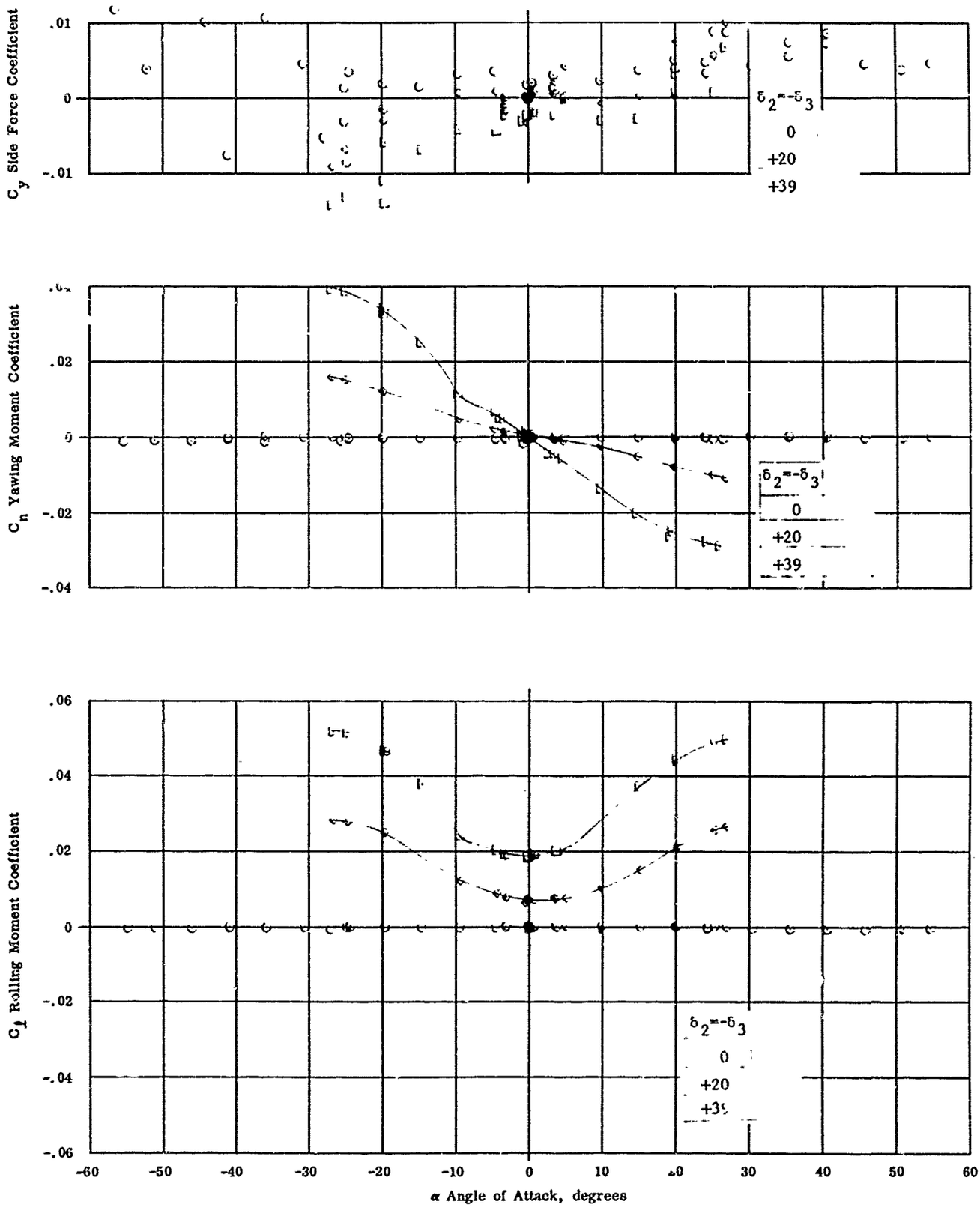

Fig. 22n Configuration I - M_∞=8.08, C_y, C_n, C_ℓ vs. α
$Re_\infty/ft \times 10^{-6}$ = 2.26 $\delta_1=\infty$ $\delta_2=-\delta_3$=0,+20,+39

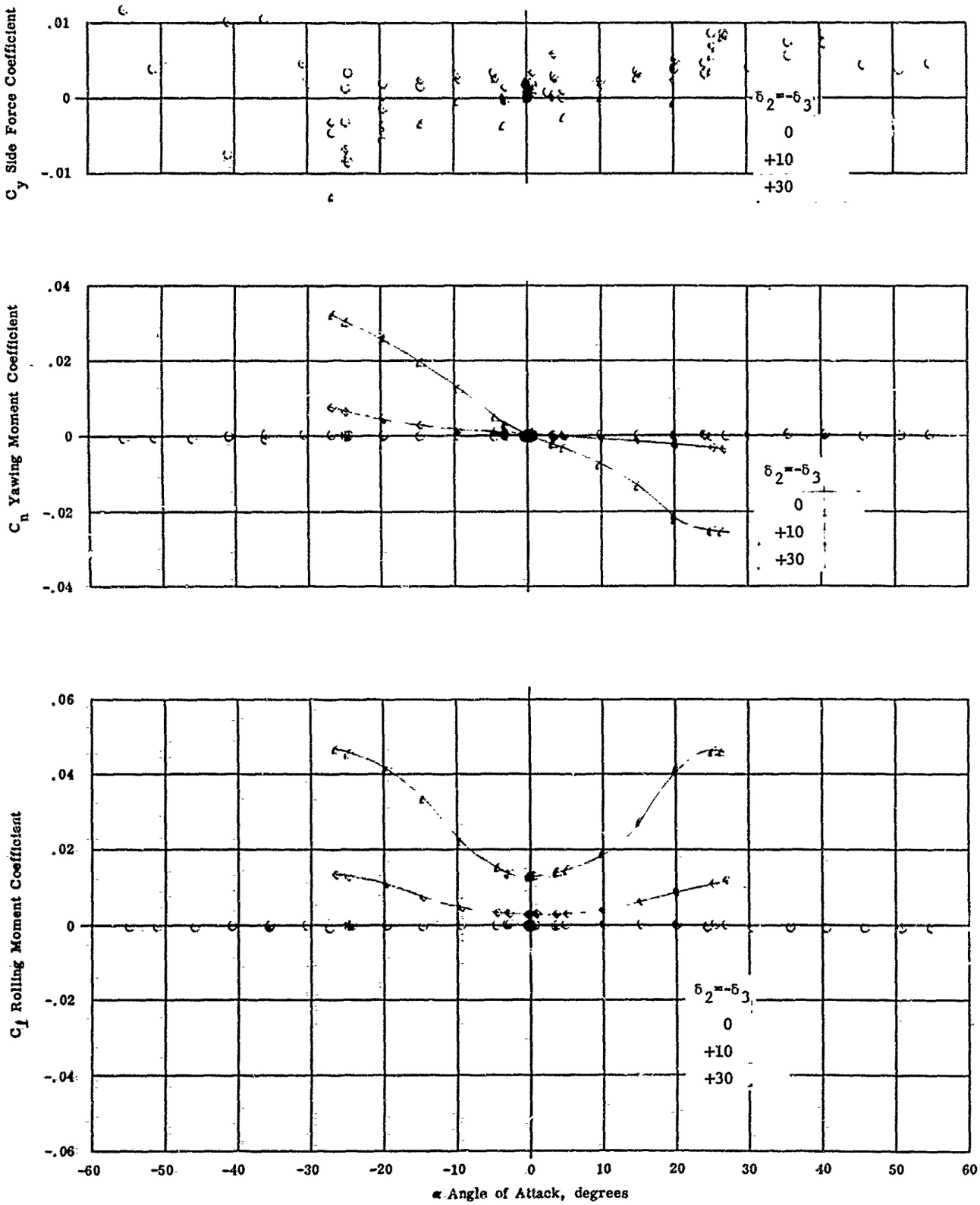

Fig. 22o Configuration I - M_∞=8.08, C_y, C_n, C_ℓ vs. α
$Re_\infty/ft \times 10^{-6}$ = 2.26 δ_1=0 $\delta_2=-\delta_3$=0,+10,+30

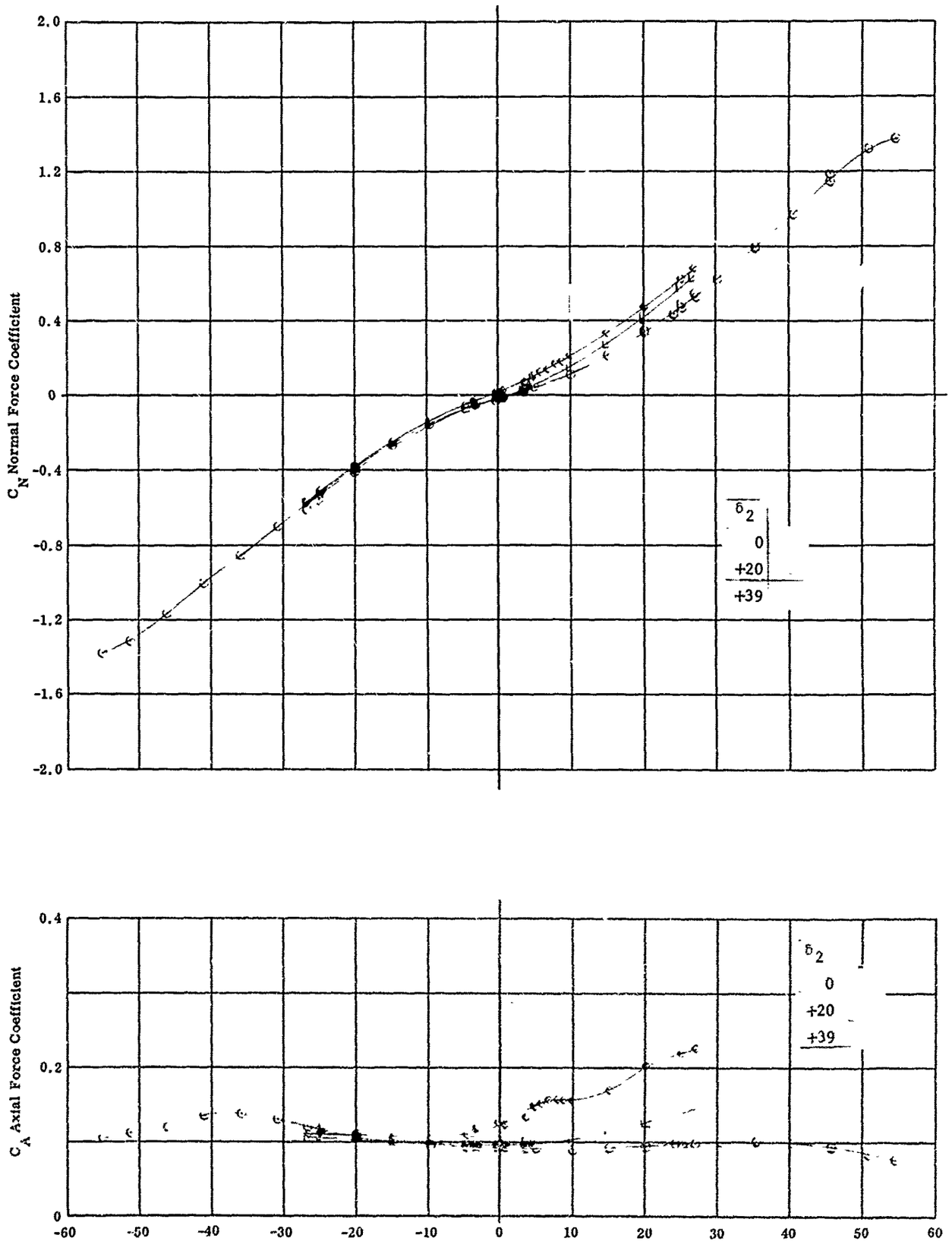

Fig. 23a Configuration IV - M_∞=8.08, C_N & C_A vs. $Re_\infty/ft \times 10^{-6}$ = 2.26 $\delta_1=\delta_3=0$ $\delta_2=0,+20,+39$

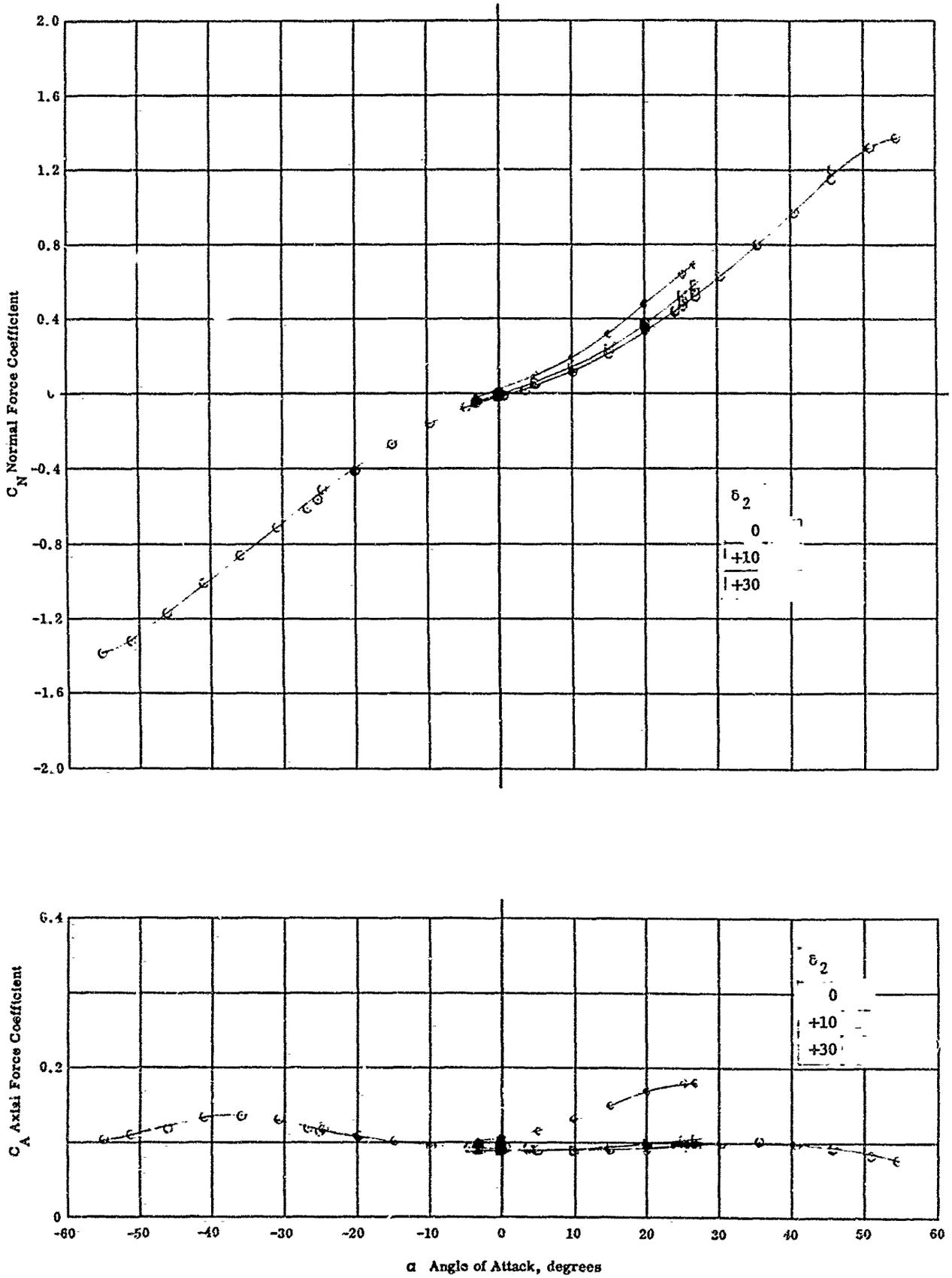

Fig. 23b Configuration IV - M_∞=8.08, C_N & C_A vs. α
$Re_\infty/ft \times 10^{-6}$ = 2.26 $\delta_1=\delta_3=0$ δ_2=0,+10,+30

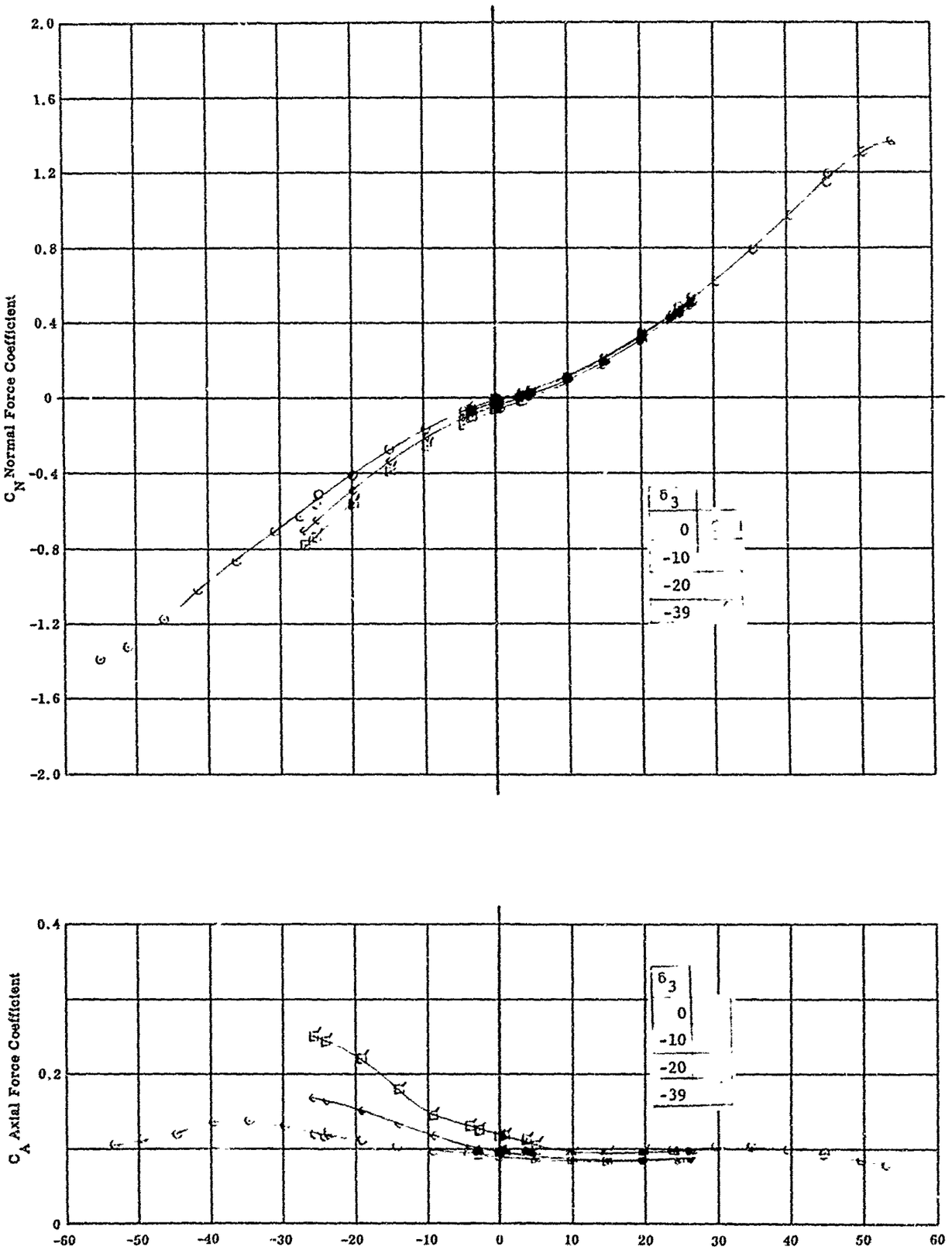

Fig. 23c Configuration IV - $M_\infty = 8.00$, C_N & C_A vs. α
$Re_\infty/ft \times 10^{-6} = 2.26$ $\delta_1 = \delta_2 = 0$ $\delta_3 = 0, -10, -20, -39$

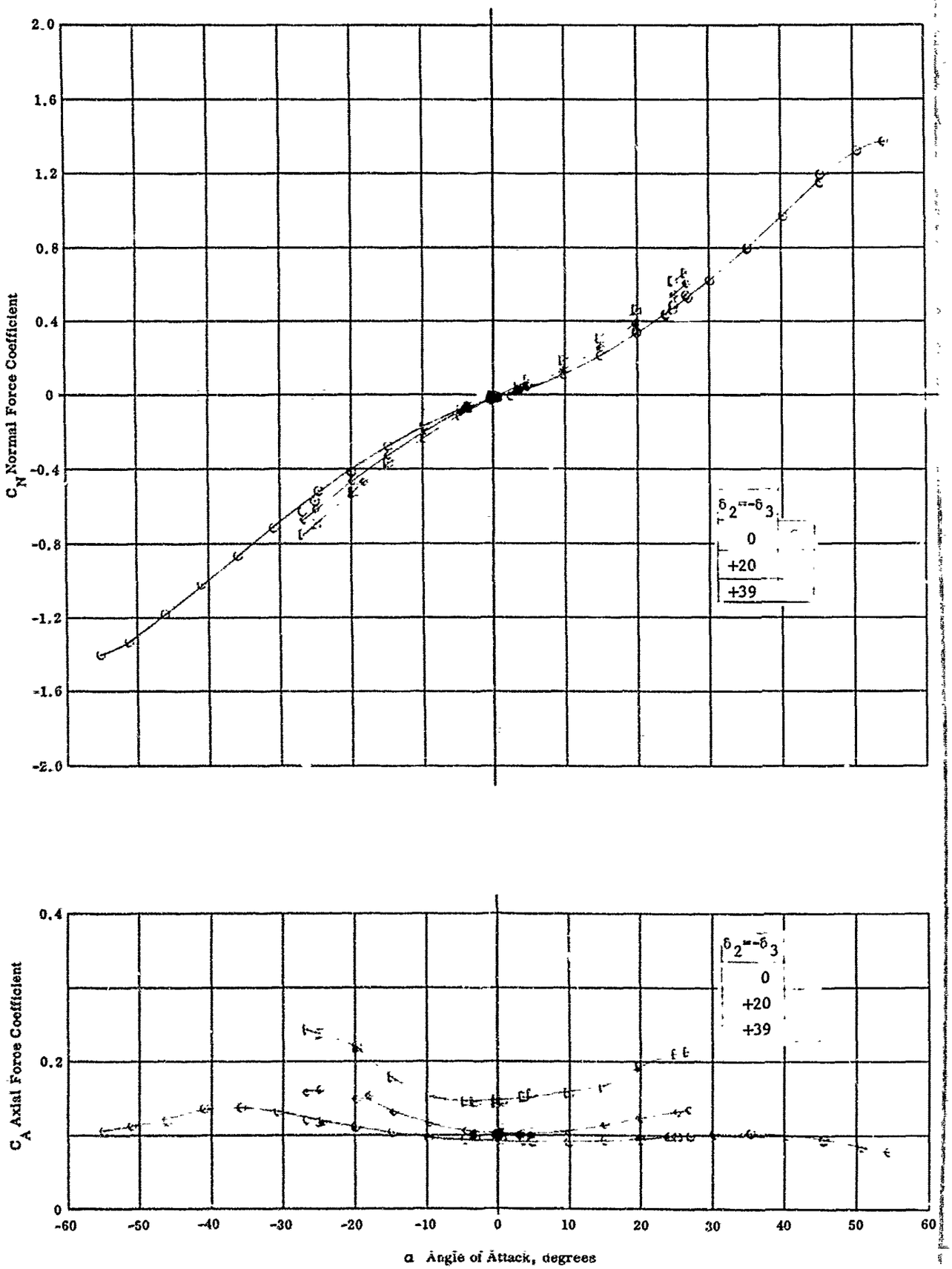

Fig. 23d Configuration IV - M_∞=8.08, C_N & C_A vs. α
$Re_\infty/ft \times 10^{-6}$ = 2.26 $\delta_1=0$ $\delta_2=-\delta_3=0,+20,+39$

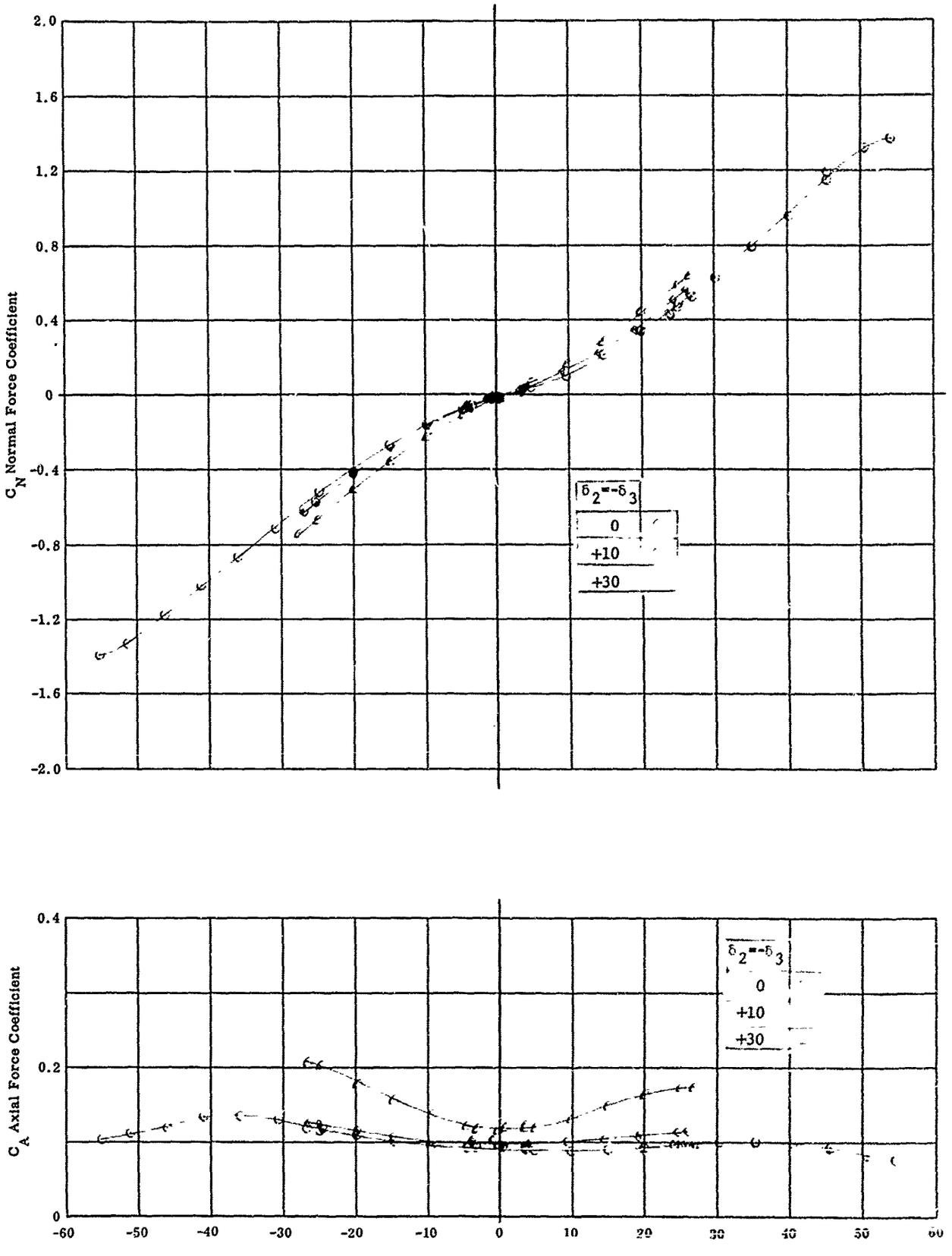

Fig. 23e Configuration IV - M_∞=8.08, C_N & C_A vs. α
$Re_\infty/ft \times 10^{-6}$ = 2.26 δ_1=0 $\delta_2=-\delta_3$=0,+10,+30

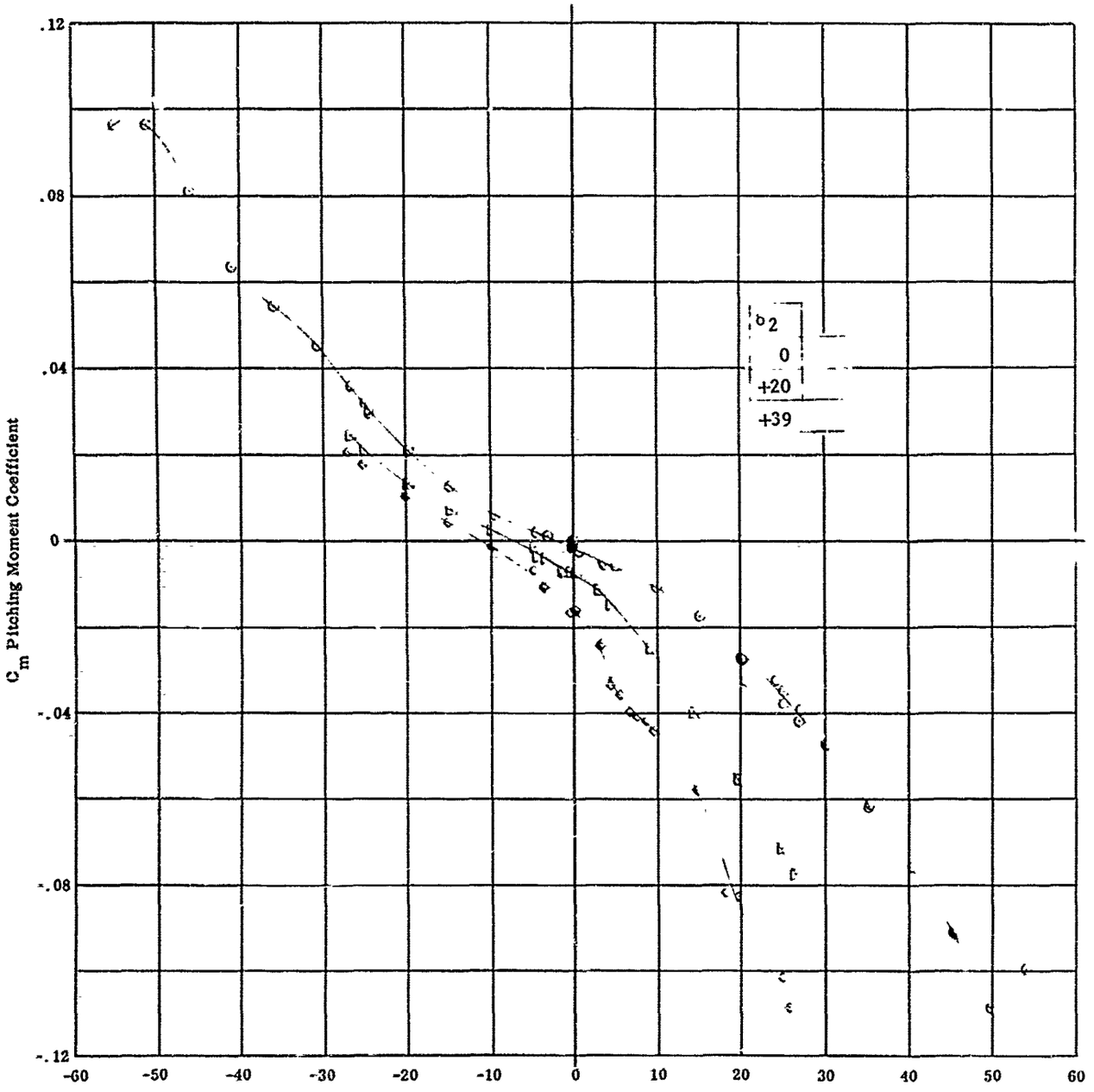

Fig. 23f Configuration IV - M_∞=8.08, C_m vs. α
$Re_\infty/ft \times 10^{-6}$ = 2.26 $\delta_1=\delta_3=0$ δ_2=0,+20,+39

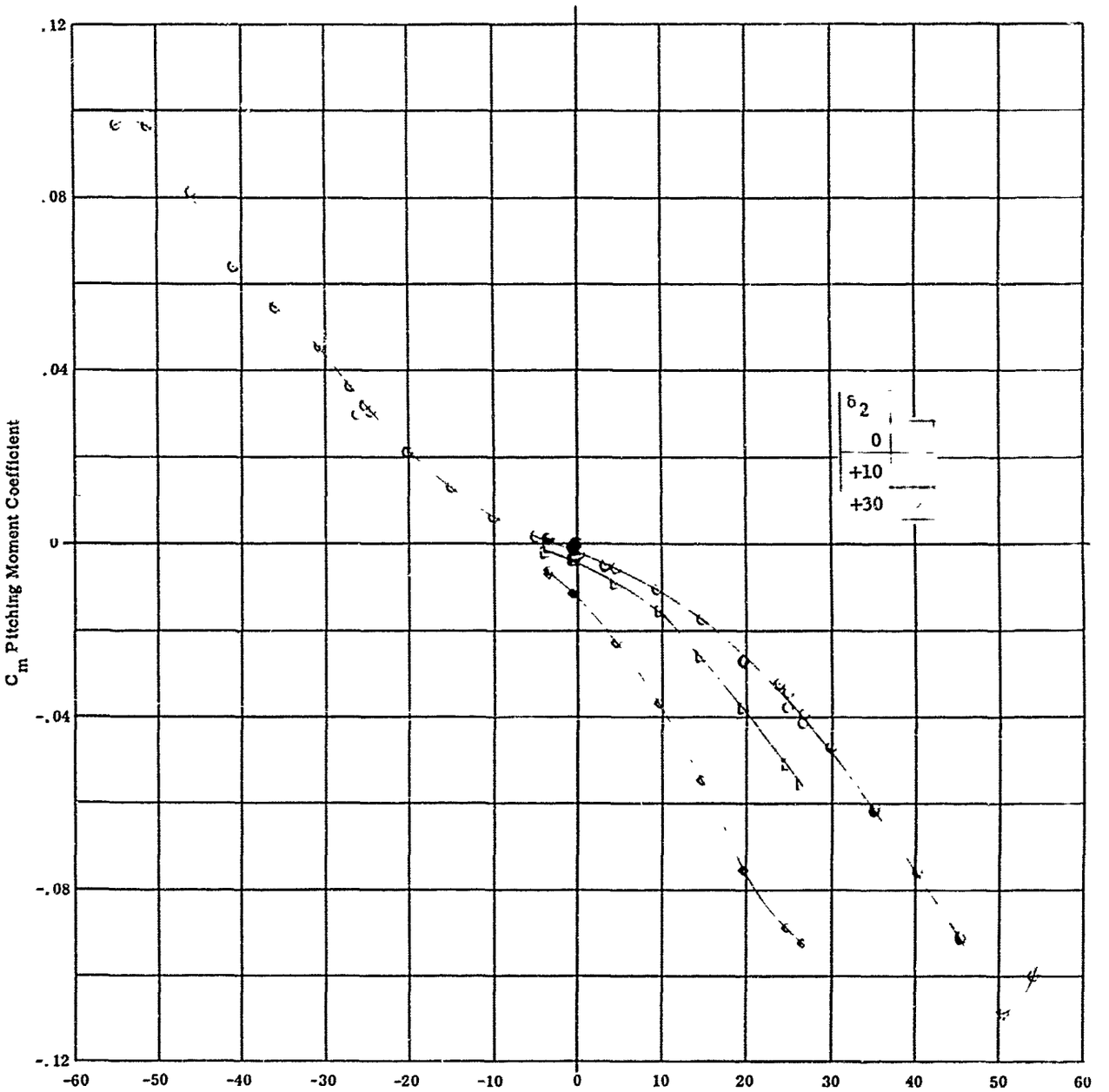

Fig. 23g Configuration IV - M_∞=8.08, C_m vs. α
$Re_\infty/ft \times 10^{-6}$ = 2.26 $\delta_1=\delta_3=0$ δ_2=0,+10,+30

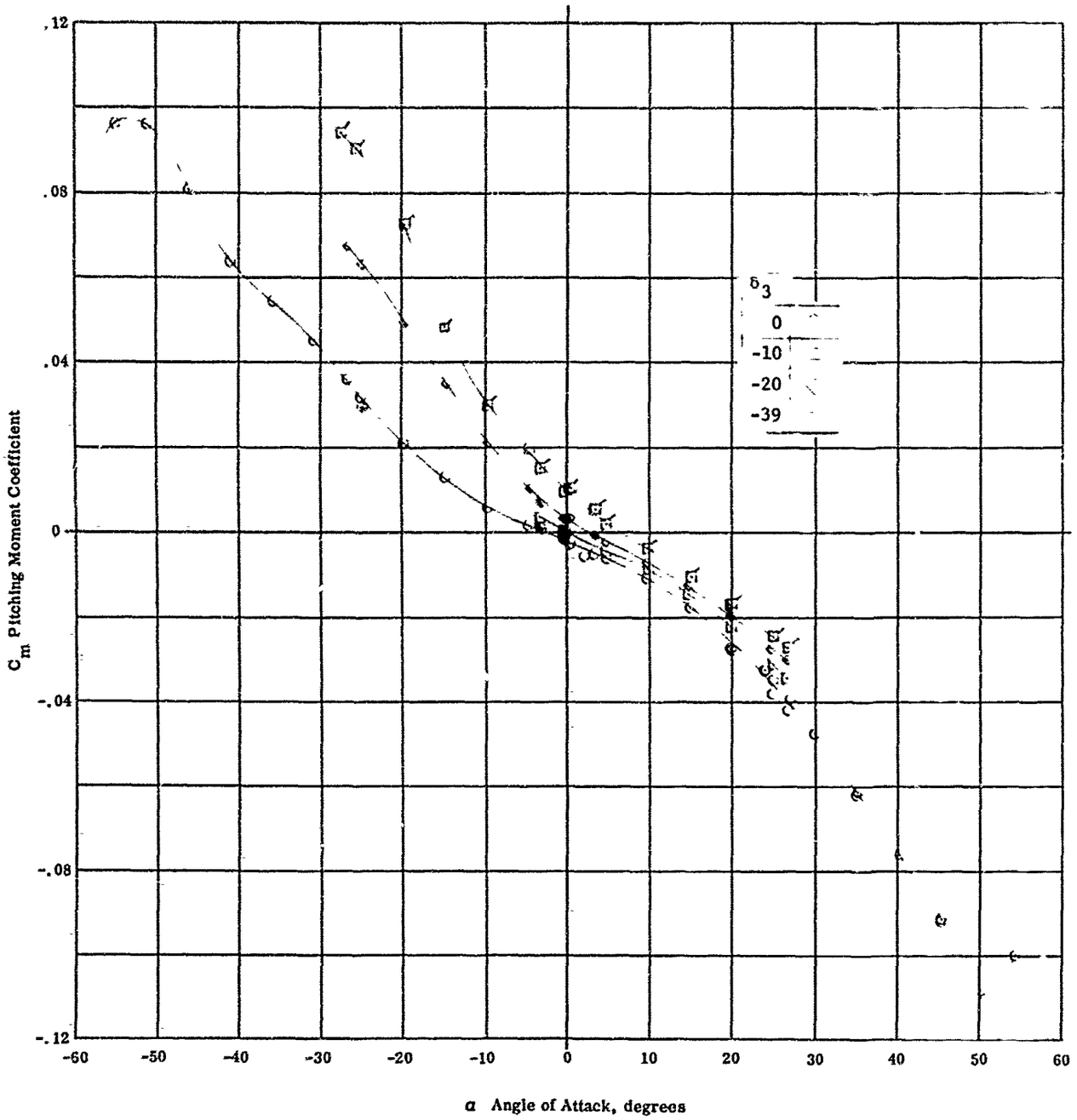

Fig. 23h Configuration IV - M_∞=8.08, C_m vs. α
$Re_\infty/ft \times 10^{-6}$ = 2.26 $\delta_1=\delta_2=0$ δ_3=0,-10,-20,-39

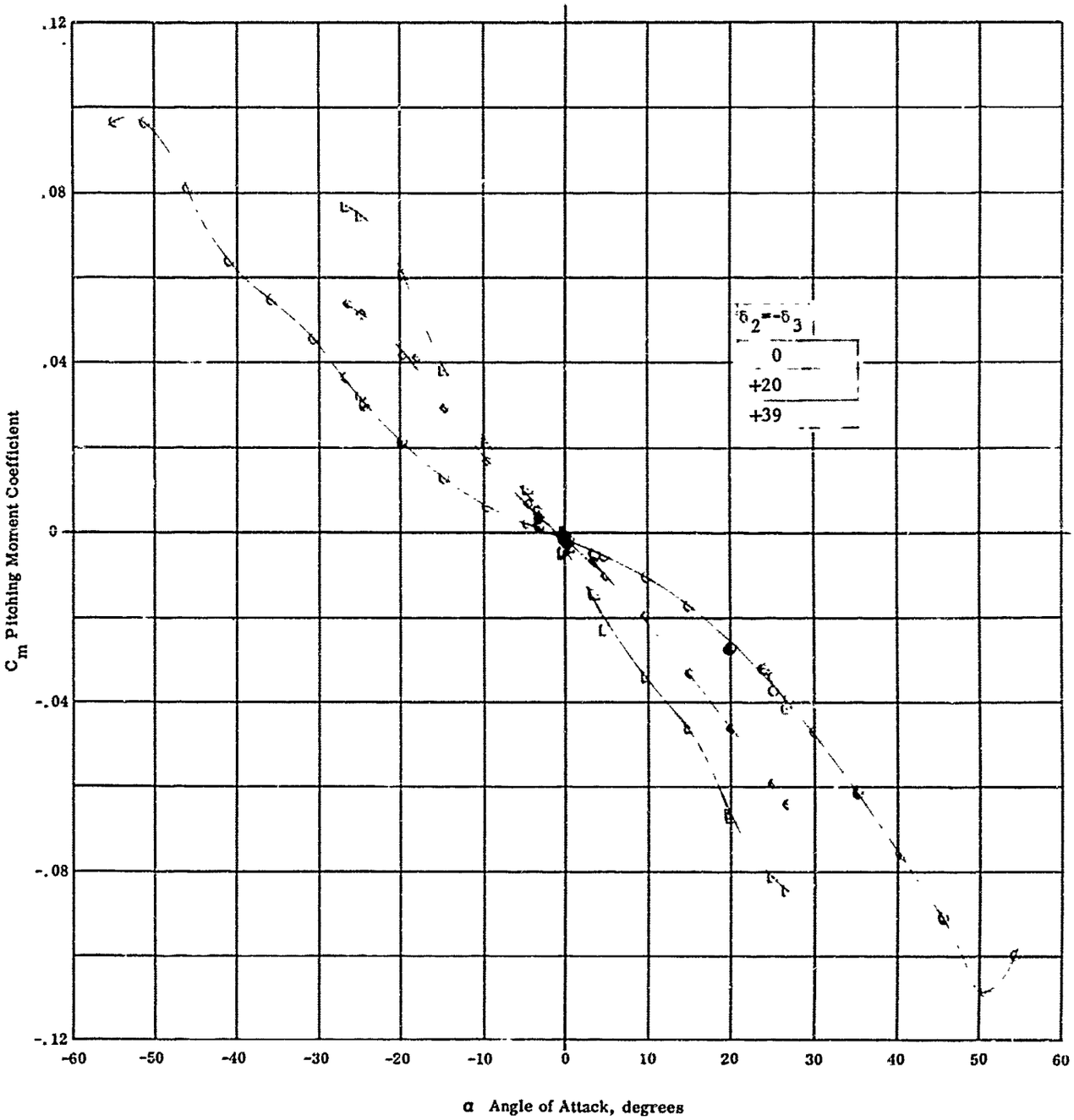

Fig. 23i Configuration IV - M_∞=8.08, C_m vs. α
$Re_\infty/ft \times 10^{-6}$ = 2.26 δ_1=0 $\delta_2=-\delta_3$=0,+20,+39

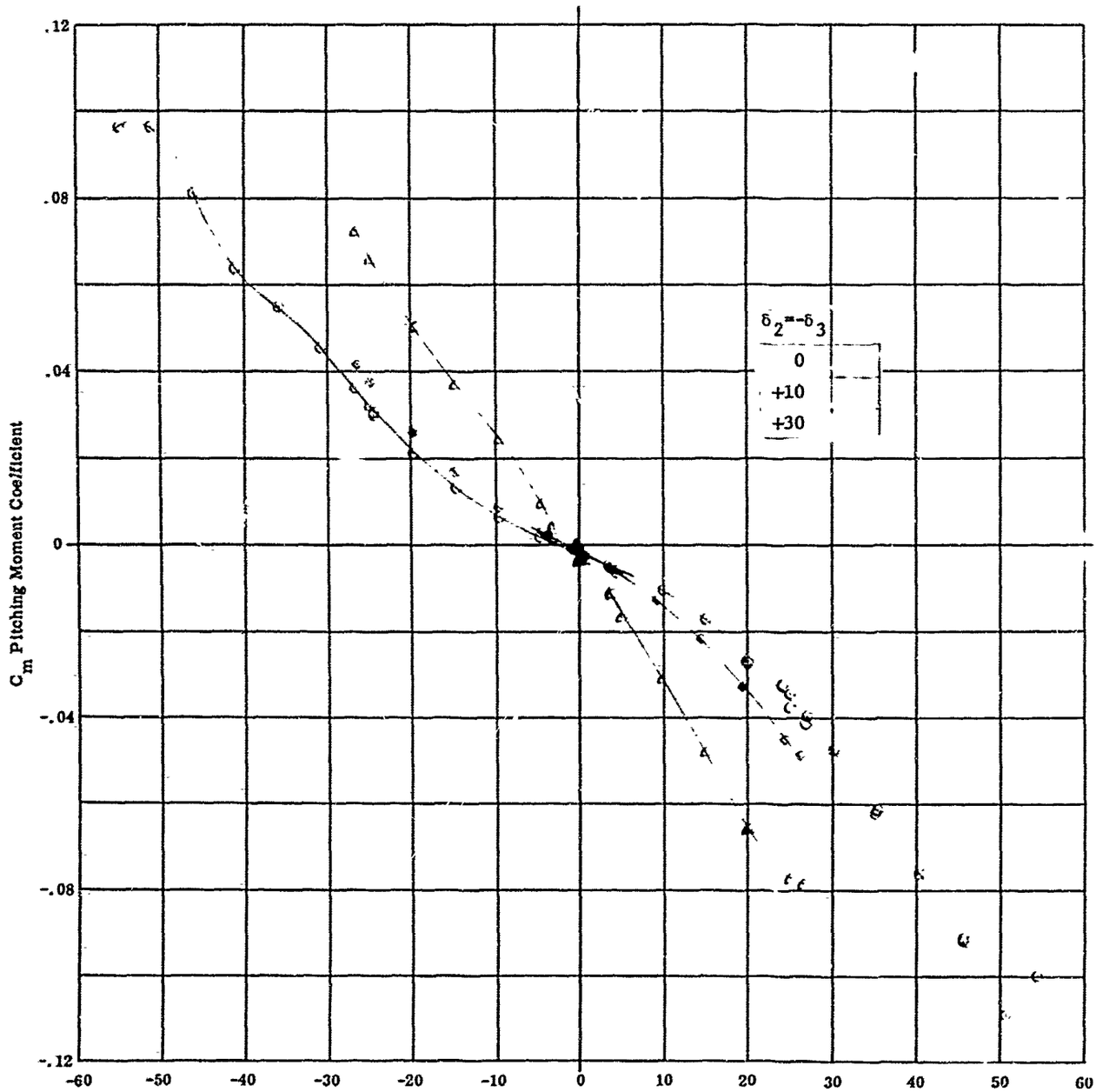

Fig. 23j Configuration IV - M_∞=8.08, C_m vs. α
$Re_\infty/ft \times 10^{-6}$ = 2.26 δ_1=0 $\delta_2=-\delta_3$=0,+10,+30

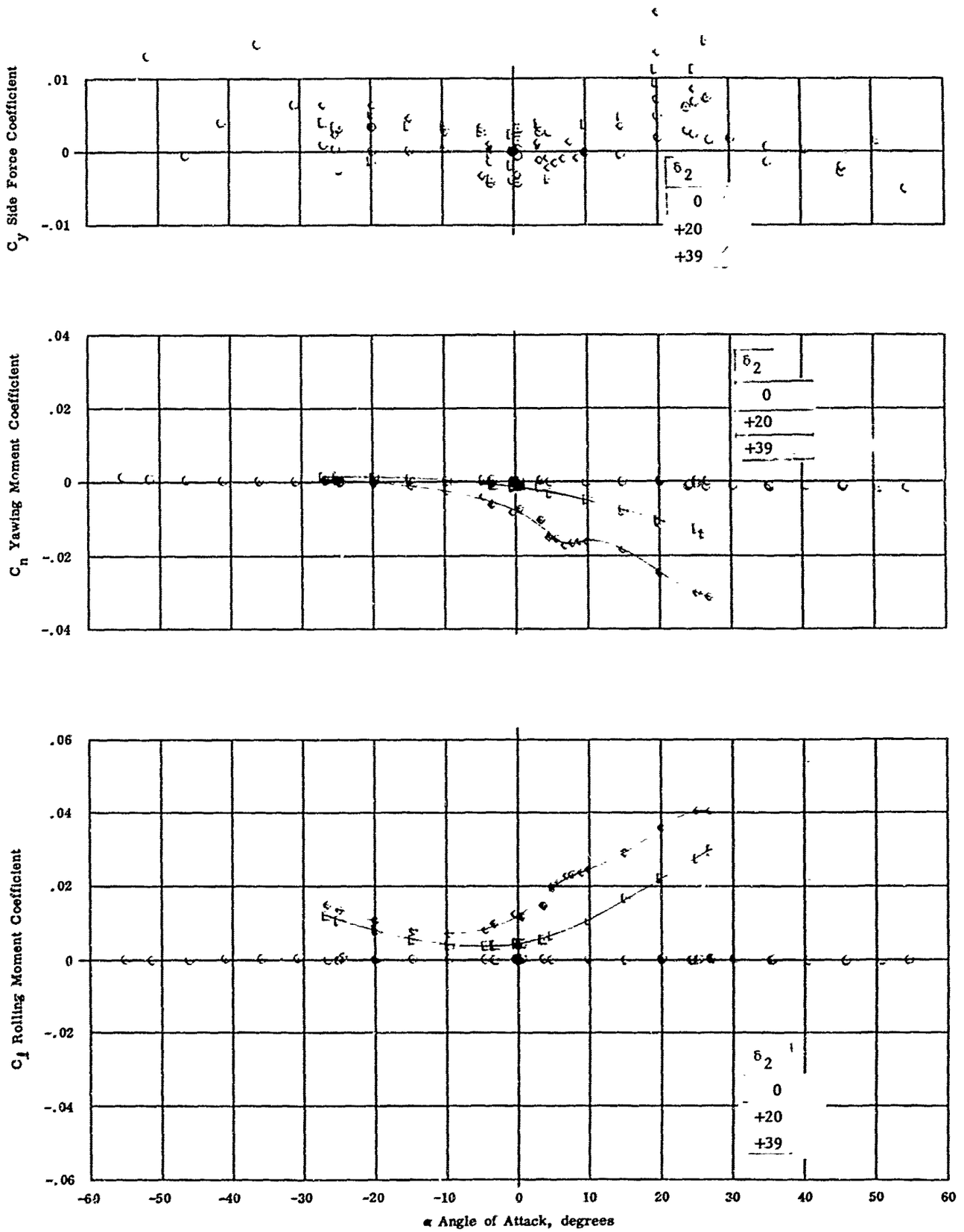

Fig. 23k Configuration IV - M_∞=8.08, C_y, C_n, C_ℓ vs. α
$Re_\infty/ft \times 10^{-6}$ = 2.26 $\delta_1=\delta_3=0$ δ_2=0,+20,+39

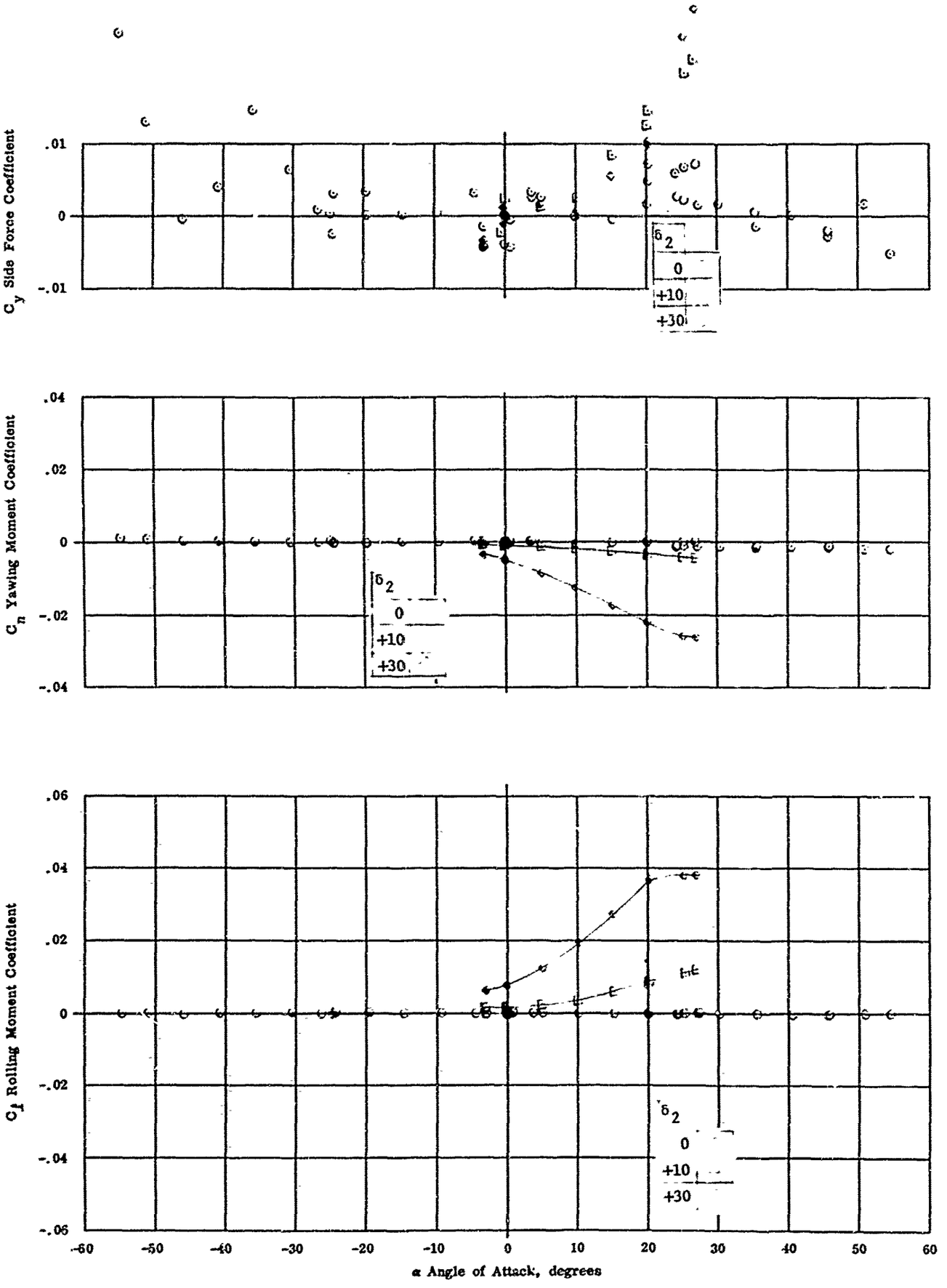

Fig. 23ℓ Configuration IV - M_∞=8.08, C_y, C_n, C_ℓ vs. α
$Re_\infty/ft \times 10^{-6} = 2.26$ $\delta_1=\delta_3=0$ $\delta_2=0,+10,+30$

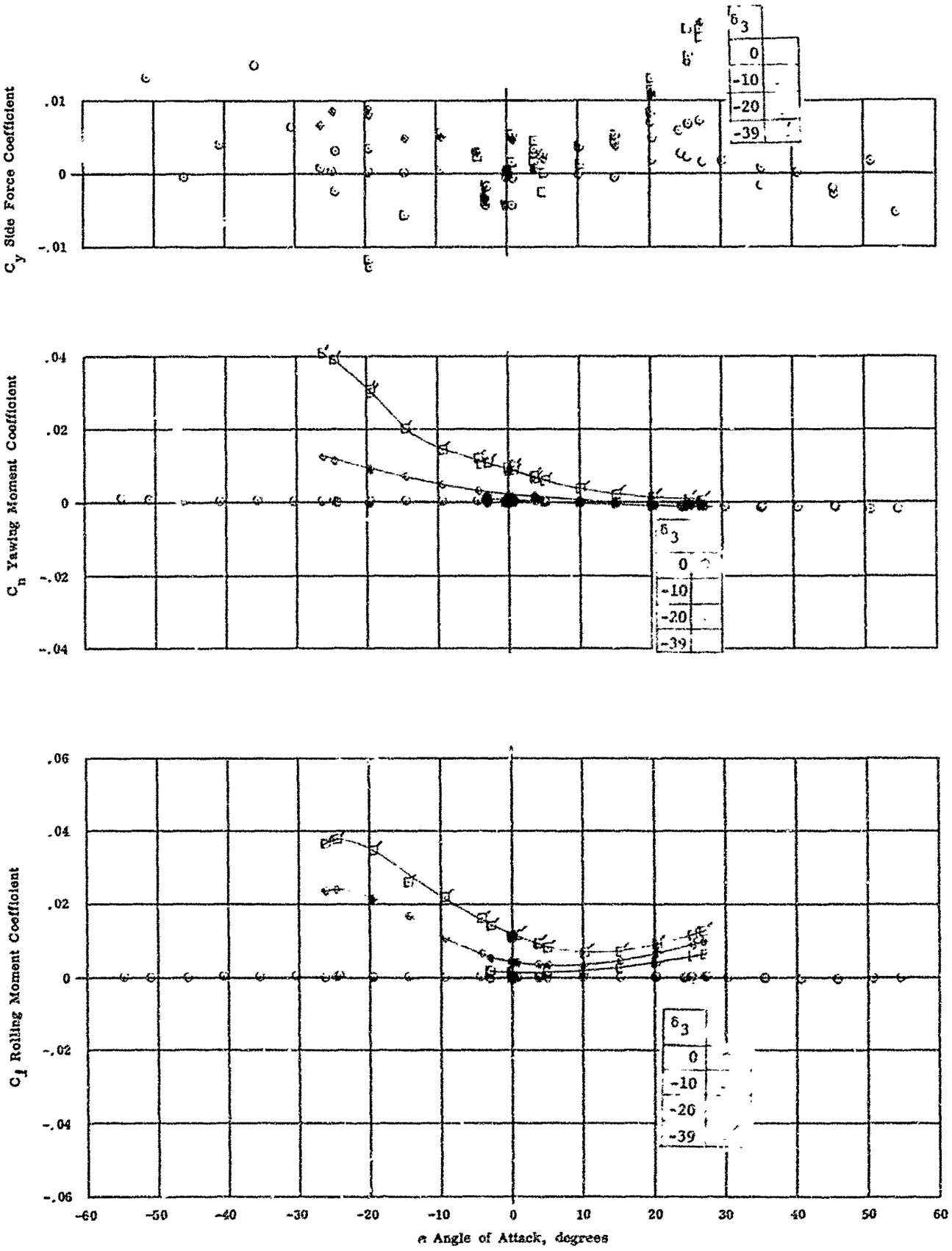

Fig. 23m Configuration IV - M_∞=8.08, C_y, C_n, C_ℓ vs. α
$Re_\infty/ft \times 10^{-6}$ $\delta_1=\delta_2=0$ $\delta_3=0,-10,-20,-39$

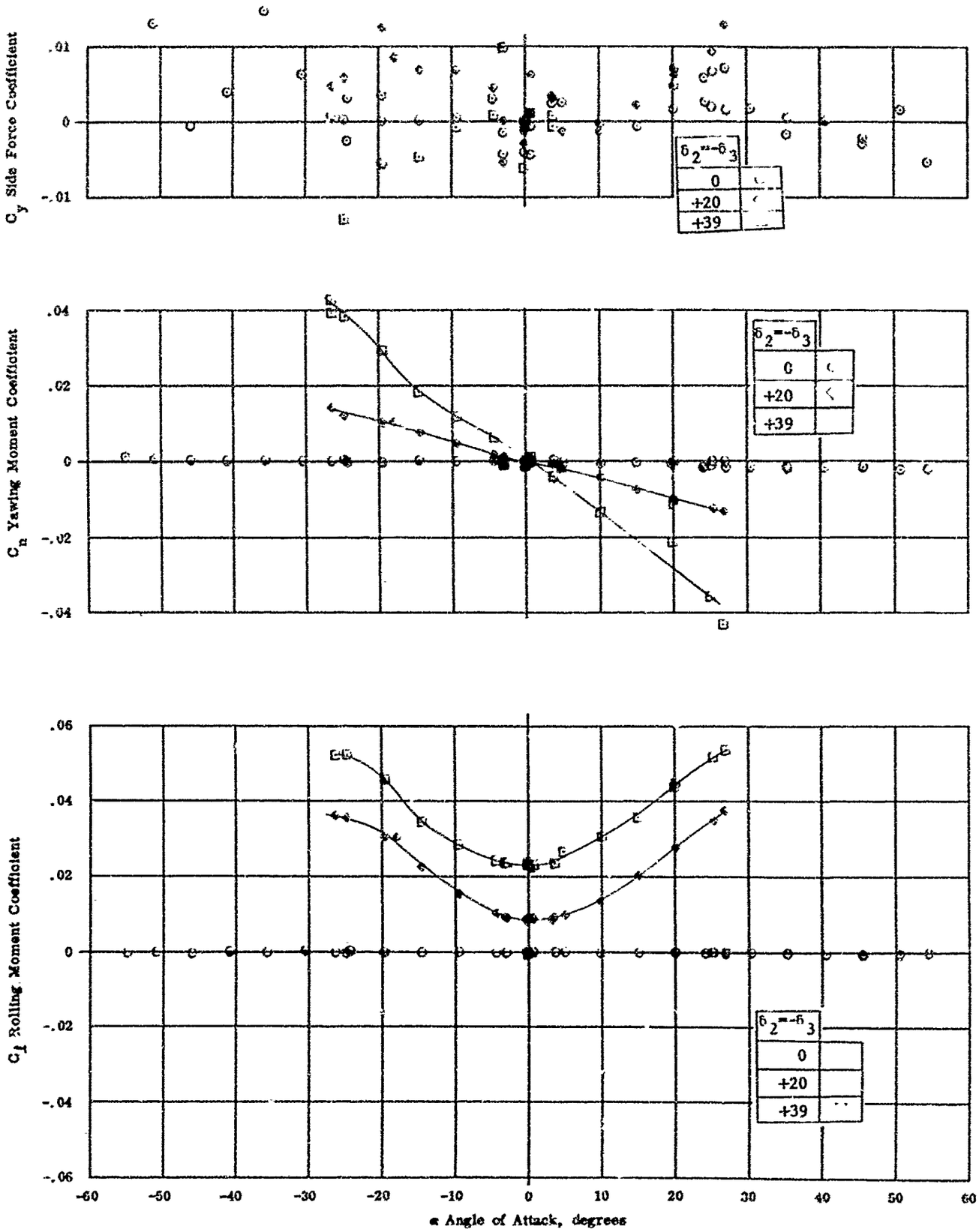

Fig. 23n Configuration IV M_∞=8.08, C_y, C_n, C_l vs. α
$Re_\infty/ft \times 10^{-6}$ = 2.26 δ_1=0 $\delta_2=-\delta_3$=0,+20,+39

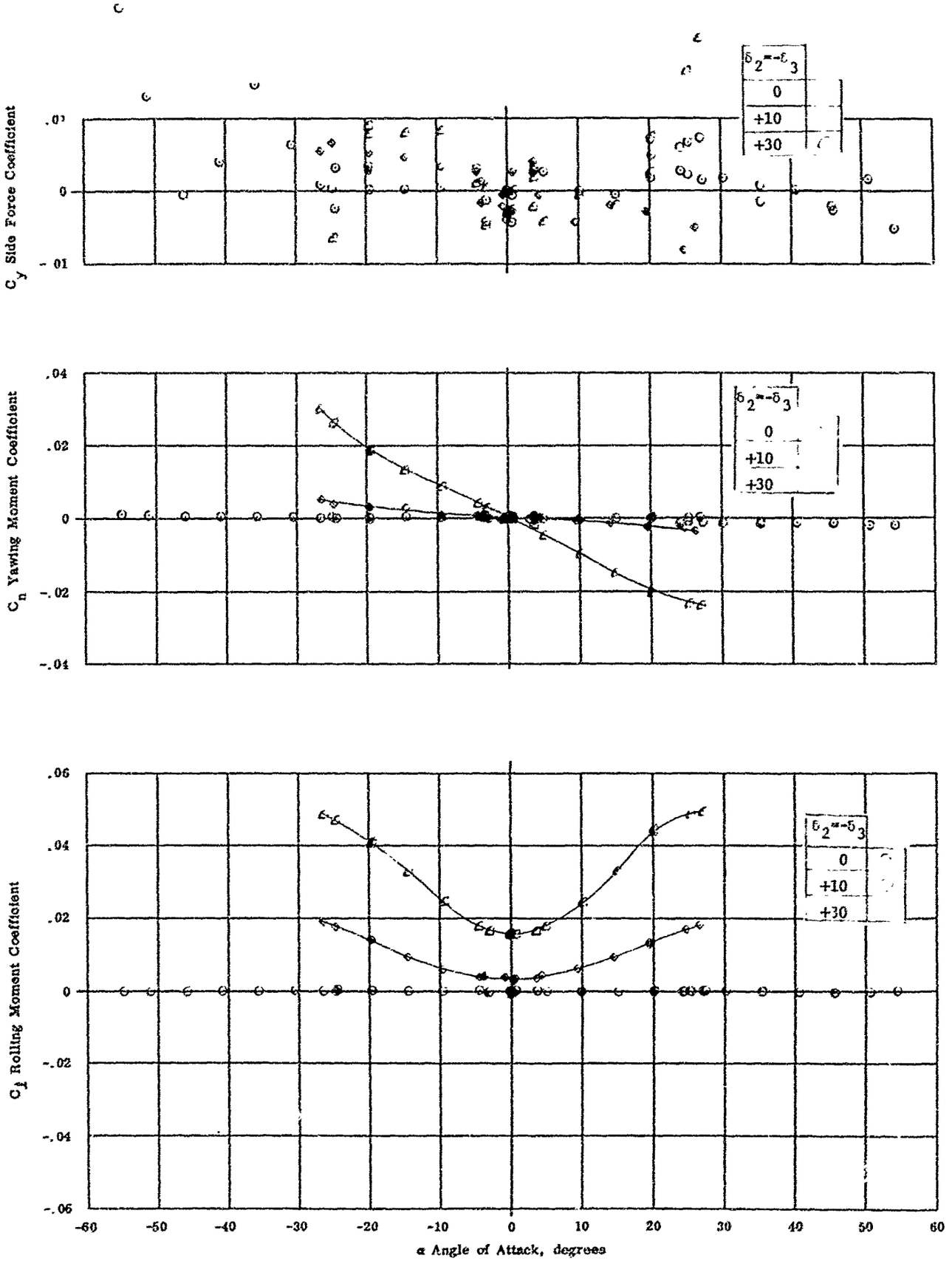

Fig. 2:o Configuration IV - M_∞=8.08, C_y, C_n, C_ℓ vs. α
$Re_\infty/ft \times 10^{-6}$ = 2.26 $\delta_1=0$ $\delta_2=-\delta_3=0,+10,+30$